

EPA-650/2-74-075

August 1974

Environmental Protection Technology Series

# CHARGED DROPLET SCRUBBING OF SUBMICRON PARTICULATE



Office of Research and Development  
U.S. Environmental Protection Agency  
Washington, DC 20460



EPA-650/2-74-075

# **CHARGED DROPLET SCRUBBING OF SUBMICRON PARTICULATE**

by

J. R. Melcher and K. S. Sachar

Massachusetts Institute of Technology  
Department of Electrical Engineering  
Cambridge, Massachusetts 02139

Contract No. 68-02-0250  
ROAP No. 21ADL-003  
Program Element No. 1AB012

EPA Project Officer: D. C. Drechsel

Control Systems Laboratory  
National Environmental Research Center  
Research Triangle Park, North Carolina 27711

Prepared for

OFFICE OF RESEARCH AND DEVELOPMENT  
U.S. ENVIRONMENTAL PROTECTION AGENCY  
WASHINGTON, D.C. 20460

August 1974

This report has been reviewed by the Environmental Protection Agency and approved for publication. Approval does not signify that the contents necessarily reflect the views and policies of the Agency, nor does mention of trade names or commercial products constitute endorsement or recommendation for use.

## ABSTRACT

The report gives results of an investigation of the collection of charged submicron particles, through a sequence of interrelated experiments and theoretical models; by oppositely charged supermicron drops; by bicharged drops; and by drops charged to the same polarity as the particles. It provides experimentally verified laws of collection for a system with different effective drop and gas residence times. The report shows, experimentally and through theoretical models, that all three of the above configurations have the same collection characteristics. Charging of the drops in any of these cases: results in dramatically improved efficiency, compared to inertial scrubbers; and approaches the efficiency of high-efficiency electrostatic precipitators. For example, in experiments typical of each configuration, inertial scrubbing by 50  $\mu\text{m}$  water drops of 0.6  $\mu\text{m}$  DOP aerosol particles gives 25% efficiency; self-precipitation of the particles with charging (but without charging of the drops) results in 85-87% efficiency; and drop and particle charging (regardless of configuration) results in 92-95% efficiency. Charged-drop scrubbers and precipitators have the operating costs and capital investment profiles of wet scrubbers, and submicron particle removal efficiencies approaching those of high-efficiency electrostatic precipitators.



## TABLE OF CONTENTS

Abstract	iii
Table of Contents	iv
Figures	viii
Tables	xvi
Acknowledgement	xvii
Conclusions	1
Recommendations	4
1 Introduction	6
1.1 Submicron Particulate as an Environmental Control Problem	6
1.2 Incentives for Developing Charged Droplet Scrubbers	7
1.3 Scope and Objectives	10
2 Conventional and Charged-Drop Submicron Particle Control in Perspective	13
2.1 Residence Time as a Basis for Comparisons	13
2.2 The Inertial Impact Wet Scrubber	14
2.3 The Electrostatic Precipitator	19
2.4 Hierarchy of Characteristic Times for Systems of Charged Particles and Drops	23
2.5 Classification and Comparison of Basic Collection Configurations	32
3 Survey of Devices and Studies	48
3.1 Charged Drop Control Systems	48
3.2 Patents	50
3.3 Literature	57
4 Electrically Induced Self-Precipitation and Self-Discharge	64

4.1	Objectives	64
4.2	Theory of Self-Precipitation Systems	65
4.2.1	General Equations	65
4.2.2	Laminar Flow Systems	68
4.2.3	Turbulent Flow Systems	72
4.3	Analysis of Self-Discharge Systems (SAG)	74
4.3.1	Mechanisms for Self-Discharge	74
4.3.2	Self-Discharge Dynamics	80
4.4	Generation of Monodisperse Submicron Aerosols	84
4.4.1	Classification of Techniques	84
4.4.2	Liu-Whitby Generator	85
4.5.1	Light Scattering by Small Particles	89
4.5.2	Higher Order Tyndall Spectra	91
4.5.3	90° Scattering Ratio	94
4.5.4	Extinction	96
4.6	Ionic Charging of Submicron Aerosols	100
4.6.1	Diffusion and Impact Charging	100
4.6.2	High Efficiency Charger for Submicron Aerosols	102
4.7	Analysis of Submicron Aerosols for Charge Density and Mobility	105
4.7.1	Imposed Field Analyzers	105
4.7.2	Space-Charge Effects	109
4.8	Self-Precipitation Experiments (SCP)	113
4.8.1	Laminar Flow Experiment	113
4.8.2	Turbulent Flow Experiment	116
4.9	Self-Discharge Experiments (SAG)	117
5	Electrically Induced Self-Discharge and Self-Precipitation of Supermicron Drops	124

5.1	Objectives	124
5.2	Self-Precipitation in Systems of Unipolar Drops	125
5.2.1	Mechanisms for Deposition	125
5.2.2	Self-Precipitation Model for a Channel Flow	129
5.3	Analysis of Self-Discharge Systems	131
5.3.1	Mechanisms for Discharge	131
5.3.2	Self-Discharge Model for a Turbulent (Slug-Flow) Channel Flow	139
5.4	Techniques for Generation of Charged Drops	141
5.4.1	Fundamental Limits on Charging and Polarization of Isolated Drops	142
5.4.2	Pressure Nozzles and Orifice Plate Generators With Charge Induction	144
5.4.3	Pneumatic Atomization With Induction Charging	149
5.4.4	Ion-Impact Charging	153
5.5	Charged Drop Self-Precipitation Experiments	156
5.5.1	Experimental System	158
5.5.2	Drop Velocity Measurements	158
5.5.3	Measurements of Self-Precipitation of Charged Drops	165
5.6	Experimental Investigation of Self-Discharge of Bicharged Drops	170
5.6.1	Experimental Apparatus	172
5.6.2	Measurement of Drop Velocity	172
5.6.3	Drop Discharge Process	175
6	Scrubbing and Precipitation of Charged Submicron Aerosols by Charged Supermicron Drops	178
6.1	Objectives	178
6.2	Models for Particle Collection on Isolated Drops	179



6.2.1	Laminar Theory of Whipple and Chalmers	179
6.2.2	Collection With Complete Turbulent Mixing	193
6.3	Multipass System	198
6.4	Model for Scrubbing With Unipolar Drops and Particles of Opposite Sign (CDS-I)	201
6.5	Model for Scrubbing With Bicharged Drops and Charged Particles (CDS-II)	207
6.6	Model for Precipitation by Unipolar Drops and Particles of the Same Polarity (CDP)	209
6.7	Experiments With Unipolar Drops and Particles of Opposite Sign	210
6.7.1	Experimental System	210
6.7.2	Experimental Diagnostics	211
6.7.3	Scrubbing Efficiency	214
6.8	Experiments With Bicharged Drops and Charged Particles	215
6.9	Experiments With Unipolar Drops and Particles of the Same Polarity	217
6.10	Summary of Measured Efficiencies	217
7	Summary	
7.1	State of Fundamentals	221
7.2	Charged Drop Devices Compared to Conventional Devices	222
7.3	Practical Application	225
7.4	Summary of Calculations Estimating CDS-I, CDS-II and CDP Performance	227
	References	229
	Glossary of Symbols	234

## FIGURES

<u>No.</u>		<u>Page</u>
2.2.1	Inertial impact scrubbing viewed from drop frame of reference. Gas entrained particles approaching the drop within the cross-section $\pi y^2$ impact the drop.	15
2.3.1	A conventional (imposed-field) electrostatic precipitator configurations. a) plane parallel geometry b) generalized geometry	21
2.4.1	Two-"particle" model for electrical discharge and possible agglomeration due to micro-fields	26
2.4.2	Limits of collection time for two particle model that give the three time constants when these are interpreted as self-discharge and drop-particle agglomeration times.	28
2.4.3	Simple model used to illustrate roles of $\tau_a$ and $\tau_R$ as self-precipitation times for like-charged particles and like-charged drops respectively	29
2.5.1	Collection particles polarized by means of ambient electric field imposed by means of external electrodes.	43
3.1	Overall charged drop scrubbing system	48
4.2.1	Self-precipitation in a cylindrical channel with radius 0.95cm carrying a flow with $F = 1.08 \times 10^{-4} \text{ m}^3/\text{sec}$ .	71

4.2.2	Comparison of typical decay laws for self-precipitation and "imposed" field types of devices.	72
4.3.1	Self-discharge model consisting of a pair of oppositely charged particles.	75
4.4.1	Monodispersed aerosol generating system (Liu, Whitby and Yu, 1966).	86
4.4.2	Collision atomizer (Liu, Whitby and Yu, 1966)	87
4.4.3	Calibration curve showing the variation of the number median diameter of the aerosol with the volumetric concentration of DOP in the atomizer.	88
4.5.1	Light scattering from a single sphere.	90
4.5.2	Tyndall red angular positions for DOP. Each point is numerically calculated. Circled points indicate a peak, but for which the ratio of red to green is less than unity.	92
4.5.3	Tyndall spectra observation device ("Owl").	93
4.5.4.	90° scattering ratio for DOP.	95
4.5.5	90° scattering apparatus	97
4.5.6	Extinction coefficient for DOP spheres as a function of $\alpha_\lambda$ .	98
4.5.7	Light extinction system for a divergent light source	99
4.5.8	Light extinction system for a laser light source and a detector aperture determined by cell dimensions.	101



4.6.1	Aerosol charger showing alternative resistors for positive and negative charging.	104
4.7.1	Analyzer configurations (a) plane flow with multiple parallel electrodes (b) radial flow with air injection to prevent leakage current.	107
4.7.2	Ideal imposed-field analyzer volt-ampere characteristic for either of configurations in Fig. 4.7.1.	108
4.7.3	Typical analyzer V-I characteristic determined using the radial flow air injection configuration of Fig. 4.7.1b. $F = 1.08 \times 10^{-4} \text{ m}^3/\text{sec}$ . Hence from data $b = 1.45 \times 10^{-7} \text{ m/sec/V/m}$ , $nq = 4.63 \times 10^{-5} \text{ coul/m}^3$ .	110
4.7.4	Self-precipitation for a radial flow: comparison of exact solution for Poiseuille flow with one from slug model.	112
4.8.1	Laminar flow self-precipitation experiment. Aerosol generator, charger and analyzer respectively described in Secs. 4.4, 4.6 and 4.7.	114
4.8.2	Self-precipitation of aerosol from experiment of Fig. 4.8.1. Broken curve is based on slug flow model, Eq. (4.2.12), while solid curve is result of theory including effect of parabolic velocity profile (Sec. 4.2).	115
4.8.3	Self-precipitation experiment with mixing. Aerosol generator, charger and analyzer respectively described in Secs. 4.4, 4.6 and 4.7.	116

4.8.4	Self-precipitation with mixing. Solid curve is predicted by Eq. (4.2.20). Data points are experiments performed using three different flasks having different volumes $V$ so that residence time $\tau_{res}$ is varied while holding $\tau_a$ fixed.	118
4.9.1	Charged aerosol experimental system	119
4.9.2	Analyzer curves for self-discharge experiments with bicharged aerosols $F = 1.1 \times 10^{-4} \text{ m}^3/\text{sec} \dots$	120
4.9.3	Experimental self-discharge of bicharged aerosol in laminar flow as a function of distance down the duct. Solid curve is theory based on Eq. (4.3.22) with the initial condition found by extrapolation back from the first data point. Inset defines analyzer currents.	121
5.3.1	Geometry for two-particle model of discharge process between two drops.	135
5.3.2	Maximum discharge velocity occurring at instant of impact.	137
5.3.3	Normalized discharge time $\tau_R$ .	140
5.4.1	Cross-sectional view of acoustically excited pressure nozzle with induction type charging electrodes.	144
5.4.2	Growth rates of instabilities on convecting liquid streams.	145
5.4.3	Coefficient of discharge for a circular orifice as a function of Reynolds number.	147

5.4.4	Geometry of inducer bar relative to one of the two sheets of drops.	150
5.4.5	Drops charge and mobility as a function of inducer bar voltage. $V_D = v_a = v_b$ , $Q$ in units of $10^{-14}$ coul, $B$ in units of $10^{-6}$ m/sec/V/m.	151
5.4.6	Pneumatic nozzles with induction chargers (a) commercial nozzle with inducer electrode added (b) multi-nozzle unit with built in chargers.	152
5.4.7	Current carried by drops generated using 60Hz inducer voltage. Solid curve is multi-nozzle unit with 40 psi air pressure while broken line is single commercial nozzle.	154
5.5.1	Jet of 50 $\mu$ m diameter drops ejected into open volume between plane parallel electrodes with 10cm spacing. Residence time for a drop in 40cm length of system is about $5 \times 10^{-2}$ sec.	157
5.5.2	Schematic of experimental system used to study dynamics of unipolar drops and CDS-I, CDS-II and CDP collection of aerosol. All dimensions in cm.	
5.5.3	Current probe used to measure unipolar drop current impinging from above.	161
5.5.4	Delay time as a function of distance downstream of charging bars.	161
5.5.5	Positions 90° out of phase with voltage applied to charging bars for $f = 20$ Hz and the implied velocities.	162



5.5.6	Spatial decay of probe current normalized to value at $z = z_r = 11\text{cm}$ , where $z$ is the position of the probe relative to charging bars.	167
5.5.7	Decay of current to probe normalized to value $z_r = 16\text{cm}$ downstream of charging bars, beyond which drop velocity is constant (4m/sec). Downstream position $z$ is normalized to decay length appropriate to particular charging voltage. Note that as voltage is raised decay rate approaches that predicted by theory assuming dominance of electric self-precipitation.	169
5.5.8	Measured drop-probe current as function of $V_D$ (which is proportional to the drop charge $Q$ ) at four different positions $z$ from charging bars.	171
5.6.1	Bicharged drop stream with variable position analyzer to deflect drops that remain charged at a given position $z$ . Dimensions in cm.	173
5.6.2	Bicharged drop jet in configuration of Fig. 5.6.1. Note increase in discharged drops as analyzer field is imposed increasingly further downstream.	174
6.2.1	Spherical conducting drop in imposed electric field $E_0$ and relative flow $w_0$ that are uniform at infinity. $E_0$ and $w_0$ are positive if directed as shown; in general, the electric field intensity $E_0$ can be either positive or negative.	180

6.2.2	Positive particle charging diagram.	185
6.2.3	Negative particle charging diagram.	186
6.2.4	Force lines in detail for regimes (e) for the positive ions and (h) for the negative ions. Here, all of the force lines terminating on the particle, also originate on the particle; hence, there is no charging. For the case shown, $w_o = \pm 2bE_o$ , $Q = \pm Q_c/2$ .	192
6.2.5	Regimes (h) for the positive ion and (e) for the negative. Some of the force lines extend to where the charge enters. $w_o = \pm 2b_{\pm}E_o$ , $Q = \pm Q_c/2$ .	194
6.2.6	Charging trajectories for a drop having total charge $Q$ in an ambient field $E_o$ as it collects positive and negative particles with complete mixing...	197
6.3.1	Schematic cross-sectional view of cleaning volume. Drops are injected at top to form turbulent jet that drives gas downward in the central interaction region. Drops are removed by impaction at the bottom, while the baffles provide a controlled recirculation of gas and particles.	200
6.7.1	Drop-particle interaction experiment showing system for controlled generation of charged particles and measurement of essential parameters.	211
6.7.2	Calculated and measured collection of positively charged aerosol particles upon negatively charged drops as a function of drop charging voltage.	214

6.8.1	For bi-charged drops, calculated and measured efficiencies for collection of positively charged aerosol particles.	216
6.9.1	Theoretical and measured particle collection for drop-precipitation of positively charged aerosol particles by positively charged drops as a function of drop charging voltage.	218
6.10.1	Stages of concentration attenuation through system as a whole.	220

## TABLES

<u>No.</u>		<u>Page</u>
2.4.1	Summary of times characterizing systems of charged drops and particles.	24
2.5.1	Summary of basic configurations for collecting sub-micron particles. Characteristic times $\tau_a, \tau_c, \tau_R$ are summarized in Table 2.4.1	33
3.2.1	Summary of patents relating directly to electrically-induced collection of particles on drops...	51-53
3.2.2	Certain patents relating to the use of electrically induced agglomeration in the control of particle pollutants.	55-56
5.4.1	Rayleigh's limiting charge $Q_{Ray}$ , Taylor's limiting electric field intensity $E_{Tay}$ and the saturation charge as a function of drop radius $R$ .	143
5.6.1	Typical drop velocity as a function of $z$ as measured by observing phase of traveling charge wave.	175
6.10.1	Efficiency of system as a whole.	219
7.2.1	Estimates of average parameters in Pilat's CDS-I experiments.	223

## Acknowledgements

Our initial interest in the use of charged collection sites in the control of submicron particles resulted from discussions with Bob Lorentz of the Environmental Protection Agency in 1970. Three related programs, sponsored by EPA, have contributed to what is summarized in the following chapters. The first, on self-agglomeration processes in oil ash, and the second, a general study of the charged drop approach to collecting particulate, led to a third, which is the development of models and experiments for the charged drop family of devices, for which this is a final report. This most recent project has been overseen by Dennis Drehmel on behalf of EPA, and for his active participation, encouragement and patience, we are indebted. Contributions to the laboratory tests were made by Messrs. E. Paul Warren and Karim Zahedi. Portions of the work constituted a Ph.D. Thesis for one of the authors (K.S.S.) in the Department of Electrical Engineering at M.I.T. Members of his committee were Ain A. Sonin and David H. Staelin. Valuable conversations with M.J. Pilat and L.E. Sparks helped to mature our thinking on the relative merits of charged drop scrubbers.

## CONCLUSIONS

Although primarily concerned with systems in which charged droplets are used to promote the collection of submicron charged particles, because they are inherent to these systems and to place matters in perspective, this report also considers collection processes based on the charging of the particulate alone. Collection mechanisms considered are space charge precipitation (SCP) (where the electric precipitation field is generated by the particles to be collected), self-agglomeration (SAG) (where oppositely charged particles are induced to agglomerate by an electrical force of attraction), charged-droplet scrubbers (CDS-I) (where drops charged to one polarity collect particulate charged to the opposite polarity), charged droplet scrubbers (CDS-II) (where bi-charged drops collect oppositely charged particulate) and charged drop precipitators (CDP) where the fields generated by charged drops are used to precipitate particles charged to the same polarity as the drops.

Experiments and correlated theoretical models support the contentions that:

- (1) Both SCP and SAG interactions among submicron particles ( $0.6\mu\text{m}$ ) are governed by the characteristic time  $\tau_a = \epsilon_o / nqb$  ( $\epsilon_o = 8.854 \times 10^{-12}$  farads/m). For SCP interactions,  $n, q$ , and  $b$  are respectively the particle number density, charge and mobility (in MKS units). For SAG, these quantities are based on one or the other of the two families of charged particles.
- (2) Unipolar drops self-precipitate with the characteristic time  $\tau_R = \epsilon_o / NQB$ . Here  $N$  is the droplet number density,  $Q$  is the droplet charge and  $B$  is the droplet mobility. Hence, this time characterizes the effective lifetime of a drop in the CDS-I configuration.
- (3) Bi-charged drops tend to self-discharge in the characteristic time  $\tau_R$ , where  $N, Q$  and  $B$  are based on one or the other of the drop families. Hence, this time characterizes the effective lifetime of drops in the CDS-II system.

- (4) A simple model for the electrically induced collection of submicron particles on charged drops, based on complete mixing in the air surrounding the drops, appears to give a meaningful estimate of the collection process. This model is consistent with the notion that  $\tau_c = \epsilon_0 / NQb$  characterizes the time required for removal of charged particles by charged drops.
- (5) In terms of residence time required for achieving a given efficiency, systems based on the CDS-I, CDS-II and CDP interactions have essentially the same performance characteristics. Of course, in the CDP interactions, the particles immediately agglomerate with the drops while in the CDS interaction, the particles are precipitated on the walls. However, because the drops are also precipitated on the walls in either the CDS-I or CDP interactions, the entrainment of the particles in the liquid is the end result in either of these cases.
- (6) Because of the dominant role of self-discharge and self-precipitation of the drops in the CDS-I, CDS-II and CDP interactions, there is an optimum droplet charge for achieving the best efficiency. This charge is given by  $Q_{opt} \propto [24\pi\eta R\epsilon_0 (U/l)N(0)]^{1/2}$  where  $\eta$  is the gas viscosity,  $R$  is the droplet radius,  $(U/l)$  is the droplet residence time in the absence of charging and  $N(0)$  is the inlet droplet number density. This optimum would be somewhat increased by effects of droplet inertia which come into play for drops exceeding about 100 $\mu$ m diameter.

It is evident from both the theoretical models and experimental results that regardless of which of the three types of interactions is used in the submicron range, charging of drops and particulate (CDS-I, CDS-II and CDP) dramatically improve the performance relative to that of an inertial scrubber.

That it makes little difference whether the drops and particles have opposite signs, the same signs or there is a mixture of both positive and negative drops, points to the fact that the charged droplet devices are more nearly typified as being precipitators than as being scrubbers. This is most obvious for the charged droplet precipitator (CDP) which is essentially an electrostatic precipitator with half of the electrodes replaced by the mobile drops. Thus it is clear that, in terms of residence time required for gas cleaning, the charged drop devices are not likely to outperform the electrostatic precipitator. They are in fact similar in nature to the wet-wall precipitator. By contrast with these wet-wall precipitators, however, they are akin to the wet-scrubber in terms of capital investment and operating cost. For this reason the charged drop devices are most viable in applications where wet-scrubbers are attractive. If a wet-scrubber is marginally competitive because it lacks desired performance in the submicron range, the use of charged drops in the CDS-I, CDS-II or CDP configurations is highly attractive.



## RECOMMENDATIONS

Further development of the charged droplet system is recommended provided that it is recognized that such an effort is justified only because of operational advantages of using a scrubber-like system instead of an ESP. Whether the configuration is CDS-I, CDS-II or CDP, the residence time for removal of submicron particulate at best only approaches that of the wet-wall ESP. But, in those applications where improved wet-scrubber performance in the submicron range is required, the use of charged drops and particulate appears warranted. The following are specific issues that should be faced by future work.

- 1) Because practical systems will incorporate drops and particles having very different residence times, and because the drops interact with the gas as a turbulent jet, the modeling of the large scale drop-gas mixing is necessary to further refinement of the performance model. In the CDS-I and CDP configurations, the interaction is further complicated by electrohydrodynamic contributions to the mechanics.
- 2) Prediction of the performance taking into account polydispersity of particulate is necessary if the models are to be seriously used in predicting performance in some practical applications. Developments of the model in this regard could follow the same lines as being presently used in connection with ESP's by Nichols of the Southern Research Institute.
- 3) This work suggests that a "complete" mixing model for the particulate collection at the inter-drop scale is meaningful. Although perhaps not a first priority in the development of charged drop scrubbers, it is important that at some point the true nature of the drop-particle interaction, especially when collection is dominated by the electrical forces, be studied in a fundamental way. Clearly, models that represent that collection process in the CDS configurations as involving a laminar

particle trajectory are not consistent with what is actually taking place in a practical system.

- 4) The experimental tests reported here indicate that although the self-discharge of drops in the CDS-II configuration does take place with a typical characteristic time  $\tau_R$ , the observed decay is several times slower than expected. The implication of this finding is that the CDS-II system may have merits over the CDS-I system, where the loss of drops by self-precipitation is at the rate expected and characterized by  $\tau_R$ . Of the three charged drop configurations, the CDS-II is the most poorly understood apparently because of some shortcomings in the self-discharge model. For these reasons, the model for self-discharge of bi-charged systems of drops deserves further scrutiny.

With the objective of greatly improving on the residence time of an ESP required for collection of submicron particulate, it is clear from this study that the most promising avenue for further development is in the direction of using EPB's or EFB's. For industrial applications, where large amounts of material must be extracted from the gas, the EFB appears preferable to the EPB because of the convenience readily incorporated into a system for handling the particulate collected on bed particles in a fluidized state.

## 1 Introduction

### 1.1 Submicron Particulate as an Environmental Control Problem

In terms of being a threat to human health, all particles inhaled are not equally dangerous. According to Drinker and Hatch (1954) and Brown, et al. (1950), the pulmonary system acts as a size-selective filter. The air is delivered to the lungs at first through relatively open channels. These branch into progressively narrower passages before reaching the regions where the actual exchange of oxygen and carbon dioxide takes place. Relatively large particles, diameters exceeding perhaps 5 micron, have a sufficiently high inertia that they can impact on the walls of the upper respiratory system. In the mucous lining of this region the particles can be transported outward through mechanisms available in the nose and mouth. A greater fraction of smaller particles find their way into the lungs. Of these, those that are extremely small tend to be in a state of Brownian diffusion with the gas molecules themselves. Hence, they tend to be retained in the air and eventually exhaled. Particles in the intermediate diameter range from .8 to 1.6 micron tend to be retained in the walls of the lungs. They tend to be neither caught through impact in the upper respiratory system nor permanently entrained in the gas so that they are removed in the exhaling process. By many, all particles less than 5 micron are considered hazardous to health, and this is one reason for a growing interest in particulate control systems that are effective in the submicron range.

Further incentive to develop more effective means for collecting sub-micron particulate comes from recent studies by Natusch (1974) which indicate the tendency for the most dangerous pollutants to concentrate on particle

sizes in this same range. Submicron particles of fly-ash have been shown to exhibit concentrations of such trace elements as cadmium and arsenic that increase with decreasing particle size. Evidence tends to support the hypothesis that the predominance of these elements on the smaller particles results because the trace elements are volatilized in the combustion process and reabsorbed or condensed on the fly-ash particles after leaving the combustion zone. Because the surface area per unit mass for the smaller particles is the greatest, the amount of the trace elements on the smaller particles per unit mass is greater.

In a way, these submicron particles that pose the most difficulty to the respiratory system, are a catalyst for inducing absorption of objectionable materials into the body.

## 1.2 Incentives for Developing Charged Droplet Scrubbers

With the exception of fabric filters, conventional dust collection equipment exhibits poor efficiencies in this submicron range (Sargent, 1969). Commonly installed types of equipment rely directly on the inertia of the particulate to effect its removal. In the cyclone, the gas stream flows rapidly around an annulus, resulting in a centrifugal force that causes the particles to move to the outside and be sedimented. In scrubbers, water drops are either injected into the flow at a relatively high speed, as in the spray design, or are accelerated from rest by a rapidly moving gas stream, as in the venturi design. Particles of sufficient mass are unable to follow the gas as it diverges around the drop, and hence are collected. In fabric filters, the gas follows a tortuous path through the medium and deposits particulate first on the fibers, and then, as the filter is used, upon agglomerates. Especially for extremely fine particles,

diffusion is also an important collection mechanism. In the electrostatic precipitator, the particle in passing through the device is first charged by an ion flux and then precipitated upon plates by the same field that charged it. Although not exactly inertia dependent, this process is also sensitive to the particle size. Except for the filters, typical devices based on these processes allow a major fraction of the submicron particles to pass through uncollected. In addition, the filters are often unable to withstand the necessary operating conditions. Electrostatic precipitators are certainly superior to cyclones and scrubbers in the submicron range and can be designed to achieve high efficiency in this range.

This report is concerned with a class of devices that is hybrid between inertial wet scrubbers and electrostatic precipitators. As in the conventional wet scrubber, drops are used as collection sites for the fine particles. However, rather than depending solely on inertial forces to cause impact between the fine particles and the drops, electrical forces are used. For this reason charged droplet scrubbers are also closely related to the conventional electrostatic precipitator, with the drop surface playing the role conventionally played by electrodes.

Although our primary concern is with collection sites which are water drops, it should be recognized that the investigations more generally relate to a wide class of devices that make use of particles of all sorts as collection sites for other particles. Many of the principles developed in the following chapters are as applicable to systems of solid particles used as collection sites as to those using liquid drops.

Of the many reasons that can be given for efforts to develop a technology of charged droplet scrubbers, two are consistent with the actual nature of these devices. First, in the general area of air pollution control the inertial wet scrubber has a well-established position.

The scrubbers are used not only to control particulates, but for control of gaseous effluents as well. It is a well-known fact that the efficiency of inertial scrubbers in the removal of particles much below a five micron diameter range is poor. The use of electrical forces in improving this efficiency so that such devices function as charged droplet scrubbers in the range of one micron and less is attractive, since the capital investment associated with additions to existing equipment have the potential of being relatively small.

The second incentive comes from the fact that the conventional electrostatic precipitator is a capital intensive device. At least for submicron particles having reasonable electrical characteristics, the electrostatic precipitator can be made to function effectively provided that devices are scaled to provide the required residence time. In the engineering of environmental control systems, greater flexibility would be available if devices were developed having the collection efficiency of an electrostatic precipitator but by contrast representing a greater investment in operating costs as compared to capital costs.

Of course the use of charged droplets implies that the system is "wet". This is by contrast with the systems involving a conventional electrostatic precipitator. There is however a current increase in the use of wet-wall electrostatic precipitators, and this fact tends to underscore the increasing market for devices that have many of the characteristics of the electrostatic precipitator but the capital investment characteristics of a wet inertial scrubber.

### 1.3 Scope and Objectives

Nature gives examples of how drops can scavenge particulate from the atmosphere. McCully et al. (1956) describe how falling raindrops effectively reduce the number density of particulates in the range of 1 - 50 $\mu$ m. Further, the existence of atmospheric electric fields has encouraged investigations, such as those of Zebel (1968), of possible influences of particle and drop charging on the collection of particulate by the drop. Because of these meteorologically oriented interests alone, it is not surprising that the idea of using electric fields to enhance collection of particulate on drops is often suggested as an approach to controlling particle emissions in industrial gasses.

One of the objectives in the following chapters is to key on what is unique in the use of drops and electric fields in collecting fine particles by providing a classification based upon the fundamental mechanism for the electrically induced collection of particle on drops. In Chapter 2 an overview of the basic significant collection mechanisms is used to compare and relate various charged droplet systems and conventional wet scrubbers and electrostatic precipitators. This chapter is intended not only to provide a classification for devices, but to promote comparisons as well. Primarily in the patent literature, but also in the formal literature, there are described a collection of seemingly widely different devices. Chapter 3 is a review of relevant literature based upon the classifications available from Chapter 2.

There have been remarkably few research efforts into charged droplet scrubbing with a) sufficiently high charged-drop densities to be of industrial interest and b) experimental parameters carefully enough controlled

that comparisons could be made between theoretical models and experimental results. Research oriented toward meteorological phenomena does not recognize the dominant role of collective effects that occur at practical drop densities. Configurations having practical air-pollution-control objectives have generally incorporated many collection mechanisms and failed to control and identify parameters so that meaningful scaling laws could be verified. The primary objectives in Chapters 4,5, and 6 are experiments that can be used to test knowledge of the electromechanical dynamics of a) systems of charged submicron particles, b) charged super-micron systems of droplets and c) systems involving both charged droplets and charged fine particles in charged droplet scrubbing configurations. These experiments show in specific terms how the characteristic times enunciated in Chapter 2 come into play.

The theoretical models developed in these later chapters not only are sufficiently refined to relate the basic theoretical models to the actual experimental systems, but also can be used to project the performance characteristics of devices scaled to industrial sizes. Considering the relatively small scale of the experiments, this will seem to some, well acquainted with the realities of scaling process control systems, to be a presumptive statement. But the dominant feature of the charged-drop scrubber is the collective interaction of drops and particles through the electrical forces. If the essential scaling parameters are not recognized, a large experiment can easily fail to confront the scaling question, while a properly designed smaller experiment can be successful.

In Chapter 7, the implications of the experimental and theoretical findings for full scale industrial applications are summarized. Finally,



in Chapter 7, there is a summary of the "state of affairs" for charged drop scrubbers, and some views as to how efforts should proceed toward control of particle pollutants on an industrial scale.

## 2 Conventional and Charged-Drop Submicron Particle Control in Perspective

### 2.1 Residence Time as a Basis for Comparisons

The objective in this chapter is the identification of fundamental factors determining the performance of submicron particle control devices in simple enough terms that a comparison can be made easily between alternative approaches. For this comparison, the key performance characteristic is taken to be the gas residence time required to achieve the desired cleaning. A total active volume  $V$  handling a gas rate of flow  $F$  would have an average residence time

$$\tau_{\text{res}} = \frac{V}{F} \quad (1)$$

The residence time is indeed a way of representing the required device volume and hence at least to some degree reflects the "cost" of the device. Of course this is an over-simplification. A refined comparison of systems would translate this volume into capital investment and operating costs. It would consider the materials within the volume on the one hand and the energy requirements for operation on the other. However, the more refined the evaluation, the more difficult it becomes to achieve the perspective required to make preliminary judgements.

The point in this chapter is the overview that follows from relatively simple comparisons. To be practical, devices must incorporate a collection mechanism characterized by time "constants" that are shorter than the residence times. In the following sections, these times are identified and used as a basis for comparing charged-drop devices to each other and to conventional devices. In the next chapter, the basic mechanisms outlined

here are further used to classify and organize the variety of patents and literature related to charge-drop scrubbing. Then, in the remaining chapters, the characteristic times identified here are quantitatively incorporated into detailed descriptions of device performance which are related to critical experiments.

The "conventional" competition to charge-drop devices is considered first in the following sections on wet-scrubbers and electrostatic precipitators. Charged-drop scrubbers, which are the subject of the remaining sections, are a hybrid of these devices. In the configurations of most interest in these sections, charged drops (typically exceeding 20 microns in diameter) are used as collection sites for oppositely charged submicron particles. If compared to a wet-scrubber, the effects of fine particle inertia conventionally responsible for causing impaction, are replaced by an electric force of attraction. If compared to an electrostatic precipitator, the charged-drop scrubber replaces the electrodes with drops.

## 2.2 The Inertial Impact Wet Scrubber

The collection of particles on drops through inertial impaction, pictured in Fig. 2.2.1, depends on there being a relative velocity  $w$  between the gas and a drop. Because of viscous drag, particles entrained in the gas tend to follow the gas around the drop. But because of their inertia, a fraction of those particles that would, in the absence of the gas, be intercepted by the geometric cross-section  $\pi R^2$  of the drop, have sufficient inertia to impact the drop surface. By definition, those particles approaching the drop through the cross-section  $\pi y^2$  shown in Fig. 2.2.1, impact the drop surface.

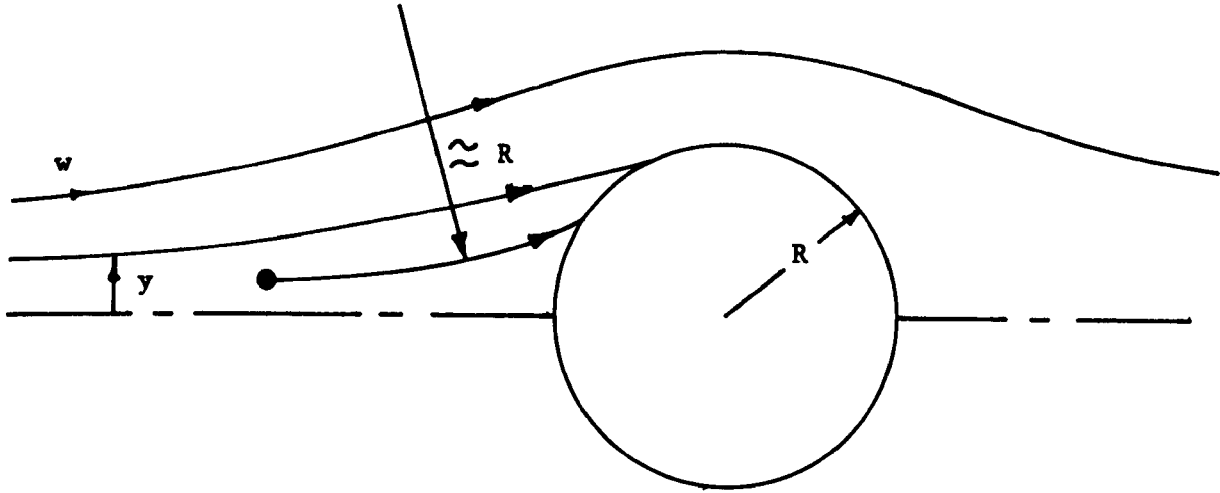


Fig. 2.2.1 Inertial impact scrubbing viewed from drop frame of reference. Gas entrained particles approaching the drop within the cross-section  $\pi y^2$  impact the drop.

Particle-Scrubbing Time  $\tau_{sc}$  The effectiveness of inertial impaction in the removal of a particle depends upon the importance of the inertial force acting on the particle, as it accelerates to avoid colliding with the drop, relative to the viscous drag force tending to make the particle follow the gas around the drop. Based on the mass of a spherical particle having radius (a) and mass density  $\rho_a$ , and on an acceleration  $w^2/R$ , the typical inertial force is  $\frac{4}{3}\pi a^3 \rho_a w^2/R$ . Based on a Stoke's drag model with  $\eta_c$  the gas velocity corrected by the Cunningham factor, the viscous drag force tending to divert the particle around the drop is  $6\pi\eta_c a w$ . The impaction parameter  $K_s$ , which is the ratio of inertial to viscous drag force

$$K_s \equiv \frac{2}{9} \frac{a^2 \rho_a w}{\eta_c R} \quad (1)$$

therefore characterizes the fraction of the geometric cross-section of the drop that is successful in collecting particles. Walton and Woodcock (1960) and Calvert (1970) show that to a useful approximation

$$\left(\frac{y}{R}\right)^2 = \left(1 + \frac{0.7}{K_s}\right)^{-2} \quad (2)$$

This expression correlates data measured in actual scrubbing situations for  $K_s > 70.1$ . As an example, for  $w = 10\text{m/sec}$ ,  $a = 0.5\mu\text{m}$ ,  $R = 50\mu\text{m}$ ,  $K_s = 0.7$ . For smaller values of the impact parameter, collection increasingly depends upon the Reynolds's number of the flow. This is a consequence of impaction on the downstream side of the obstacle resulting from the eddies established there.

As it travels with velocity  $w$  relative to the gas, one drop cleans a gas volume  $\pi w(y)^2$  each second. Hence, with  $n$  particles per unit volume, a drop removes  $n\pi w(y)^2$  particles from the gas each second. The number of particles removed per unit time from a unit volume in which there are  $N$  drops is therefore  $N(n\pi w y^2)$  so that

$$\frac{dn}{dt} = N(n\pi w y^2) \quad (3)$$

By rewriting the right hand side as  $n/[1/\pi w N y^2]$ , the characteristic time can be identified in Eq. (3) as  $(1/\pi w N y^2)$  and from Eq. (2) it follows that

$$\tau_{sc} = \left(1 + \frac{0.7}{K_s}\right)^2 / \pi w N R^2 \quad (4)$$

This is a time typical of that required to appreciably reduce the original density of particles. If  $\tau_{sc}$  were constant in Eq. (3), it would be the time

to reduce  $n$  by the factor  $e^{-1}$ . Usually, the drop velocity is continually changing as a result of the drag of the gas. In general, the details of the collection law are a matter for refined analysis, but the minimum collection time expected from such a system results from substitution of the drop injection velocity for  $w$ . To be practical, a device must have a collection time that is short compared to the gas residence time.

For purposes of comparison with other devices, it is convenient to limit discussion to collection of submicron particulate, hence  $K_s < 1$ , and approximate Eq. (4) by

$$\tau_{sc} \approx \frac{3\eta_c^2}{w^3 Na^4 \rho_a^2} \quad (5)$$

To be practical in removing submicron particles, an inertial impact device must have  $\tau_{sc} < \tau_{res}$ .

Drop Scrubbing Life-Time  $\tau_{SR}$  A second time that is critical to the performance of an inertial scrubber characterizes the tendency of the drops to decelerate to the gas velocity as in a spray scrubber, or accelerate to the gas velocity, as in a venturi scrubber. The fact that  $w$  appears to the third power in Eq. (5) suggests that this time, during which the drop retains sufficient velocity to effectively clean the gas, is also a critical parameter.

The tendency of the drop to approach the velocity of the gas is represented by the balance of drop inertial force with viscous drag

$$\frac{4}{3}\pi\rho_R R^3 \frac{dw}{dt} = 6\pi R\eta w \quad (6)$$

For the present purposes, where drop radii are in the range 25–200 $\mu$ m

and  $w$  is typically 10m/sec, the drop Reynolds number  $\frac{w\rho_g R}{\eta}$  ( $\rho_g$  = gas mass density,  $\eta$  = gas viscosity) is in the range 10-40, and the use of Stoke's drag is consistent with the order of approximation of interest.

It follows from Eq. (6) that the time characterizing the slowing of the drop to the gas velocity is

$$\tau_{sR} = \frac{2}{9} \frac{\rho_R R^2}{\eta} \quad (7)$$

In identifying  $\tau_{sR}$ , collective interactions of the drops with the gas flow have been ignored. That is, it is assumed that in the gas stream the drops are sufficiently separated that their mutual hydrodynamic interactions are not a factor in determining the transfer of momentum between gas and drops. Thus it is that the drop number density does not appear in Eq. (7).

If the scrubbing life-time of a drop  $\tau_{sR}$  falls short of the residence time required of the gas, then drops must be supplied in such a way that their life-times in the cleaning volume are short compared to the residence time. In this mode of operation, the gas recirculates through the drop injection volume or is held up by pressure forces in this volume. In either case, a given volume of gas is subject to many "passes" by the drops.

Characteristics of Submicron Inertial Scrubbing With the relevant time constants in view, the following observations can be made:

a) In the sub-micron range, the efficiency of the inertial scrubber decreases dramatically with decreasing particle size:  $\tau_{sc} \propto a^{-4}$ . For example, using as representative scrubbing conditions  $w = 10\text{m/sec}$ ,  $N = 10^9\text{drops/m}^3$ ,  $\rho_a = 10^3\text{kg/m}^3$ ,  $\eta_c \sim 2 \times 10^{-5}\text{nt-sec/m}^2$ , 1 micron diameter particles have a particle scrubbing time  $\tau_{sc} = 2 \times 10^{-2}\text{sec}$ . Under the same conditions,

0.3 micron particles have  $\tau_{sc} \sim 2.5$  sec.

b) The drop scrubbing time,  $\tau_{sR}$ , acts in parallel with the particle scrubbing time,  $\tau_{sc}$ , to limit the performance of a system. Normally, the gas must interact with the drops for several  $\tau_{sc}$ 's to be reasonably cleansed. This time, however, is based upon the maximum difference in velocity between the drop and particles, occurring at injection. If  $\tau_{sR}$  is much greater than  $\tau_{sc}$ , then the relative velocity between the two species is approximately  $w$  over a period sufficient to remove most of the particles. If the opposite is true, then the relative velocity over most of the drop trajectories is much less than  $w$ , and collection practically vanishes. This condition sets a lower limit on the particle size that can be effectively cleaned by inertial scrubbing.

$$\tau_{sc} \ll \tau_{sR}$$

$$a \gg \left( \frac{27\eta \eta_c^2}{2 w^3 N \rho_a^2 \rho_R R^2} \right)^{\frac{1}{4}} \quad (8)$$

For the system parameters  $w = 10\text{m/sec}$ ,  $N = 10^9\text{drops/m}^3$ ,  $\rho_a \approx \rho_R = 10^3\text{kg/m}^3$ ,  $\eta_c \approx \eta = 2 \times 10^{-5}\text{nt-sec}$ ,  $R = 25\mu\text{m}$ , the radius given by Eq. (8) is  $0.7\mu\text{m}$ . To collect particles smaller than this, a given gas volume must be subjected to multiple passes through the drops.

### 2.3 The Electrostatic Precipitator

In an electrostatic precipitator, particles are removed from the gas in three steps. First, they are charged (usually by means of the ion flux associated with a corona discharge). They are then precipitated onto collecting electrodes and finally rapped in the form of agglomerates from



the electrodes into a hopper. By a "conventional" electrostatic precipitator, it is meant that particles are precipitated onto electrodes by means of an imposed electric field. That is, the charges responsible for the precipitating field largely reside on the electrodes, and not on the particles themselves.

The crucial time in an imposed field precipitator is that necessary to remove a particle, having mobility  $b$  and an associated velocity  $bE$  in the direction of the imposed electric field  $E$ . For example, in the plane parallel geometry of Fig. 2.3.1a with the distance between the charging region and the collecting electrode defined as  $s$ , the precipitator collection time is characteristically

$$\tau_{pc} = \frac{s}{bE_w} \quad (1)$$

For successful operation,  $\tau_{pc}$  must be short compared to the gas residence time.

Of course, it would be entirely possible to design a highly inefficient precipitator having a residence time long compared to  $\tau_{pc}$ ....one incorporating by-passing paths for the gas or having reentrainment problems. Because of the mobility  $b$ , the precipitation time  $\tau_{pc}$  clearly depends on particle size and so there are a spectrum of such characteristic times relating to the performance of a device in removing polydisperse particulate. In the turbulent flows of practical precipitators the collection process even for a monodisperse particulate is far more complex than portrayed in writing Eq. (1). But, more realistic models turn out to also be characterized by  $\tau_{pc}$  and it will be used for the rough comparisons which are the point of this chapter.

More generally, electrostatic precipitators are described in terms of an effective precipitation perimeter  $S$  and a flow cross-section  $A$ , as sketched in Fig. 2.3.1b (White, 1963). The precipitation time is still the

essence of the matter, as is seen by writing the particle conservation equation expressing the loss of particles from an incremental length  $\Delta x$  of the precipitator section in terms of the particles removed from the gas to the electrodes. The particle concentration is assumed to remain uniform at every cross-section.

$$AU [n(x + \Delta x) - n(x)] = -SE_w bn \Delta x \quad (2)$$

Here,  $E_w$  is the electric field at the precipitation surface,  $U$  is the mean gas velocity and  $n$  is the particle density. The particle removal is

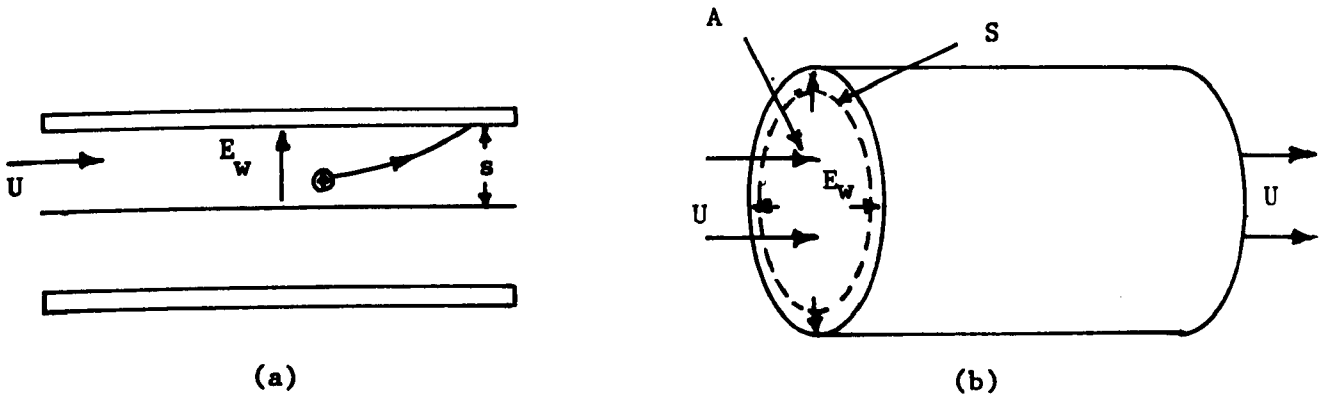


Fig. 2.3.1 A conventional (imposed-field) electrostatic precipitator configurations. a) plane parallel geometry b) generalized geometry

described by Eq. (2) in the limit  $\Delta x \rightarrow 0$ .

That the essence of the device performance is determined by the precipitation time relative to a residence time can be seen by writing this expression with  $x$  normalized to the length  $\ell$  of the precipitator.

$$\frac{dn}{d(x/\ell)} = \left[ -\frac{SE_w b \ell}{AU} \right] n \quad (3)$$

Specifically, Eq. (3) shows that the particle density decays exponentially as the gas passes through the device. The efficiency of removal is determined by the parameter  $AU/SE_w b \ell$ , which will be recognized as the ratio

of a generalized precipitation time

$$\tau_{pc} = \frac{A}{SE_w b} \quad (4)$$

to the gas residence time  $\tau_{res} = l/U$ . Note that for plane parallel geometry of depth  $d$  (into paper)  $S = 2d$  and  $A = 2sd$ . Thus, Eqs. (1) and (4) are consistent. For high efficiency, a device must be designed to make  $\tau_{pc} \ll \tau_{res}$ . Detailed models add refinement to the picture but are nevertheless in agreement that  $\tau_{pc}$  is the time characterizing the electrostatic precipitation process in a well designed device.

In the inertial scrubber, and in the charged drop devices to be considered in the following section, a time constant in addition to the collection time is necessary to properly characterize a device. In the inertial scrubber it is a life-time  $\tau_{SR}$  for the decay of relative drop gas velocity, while in the charged drop devices it is the time that a drop retains its capacity to attract particles. Is there an analogous "second characteristic time" required to place the conventional precipitator in perspective? Consider some possibilities:

One process that brings into play another characteristic time is the ion-impact and diffusion charging of the particles as they pass through the corona flux prior to the collection process. However, the ions are of relatively high mobility ( $b_i \sim 2 \times 10^{-4}$ ) so that this charging time is usually very short compared to the residence time. Hence, the charging time is not an important factor in making comparisons.

However, the charge relaxation time of the particles (effectively, the resistivity) is an important factor in the collection of highly resistive particles. Because insulating particles tend to retain their

charge even after contacting the electrode, fields produced by build up of charge in the collected dust on the electrodes compete with the imposed field tending to turn off the corona and even establish "back-corona". But the particle relaxation time pertains to the processing of particles once collected and not to the collection process itself. For example, the wet-wall precipitator characterized by the same typical collection time  $\tau_{pc}$  derived here, has little problem with highly resistive particles.

In comparing the electrostatic precipitator to other devices, only one characteristic time will be used.

#### 2.4 Hierarchy of Characteristic Times for Systems of Charged Particles and Drops

Three ubiquitous characteristic times are basic to the dynamics of systems of charged particles and drops. They pertain to seemingly very different configurations. Nomenclature is summarized in Table 2.4.1. The particles are of number density  $n$ , charge per particle  $\pm q$ , mobility  $B$  and radius  $R$ . Table 2.4.1 summarizes the three time constants  $\tau_a$ ,  $\tau_c$  and  $\tau_R$  discussed in this section.

Unless otherwise specified, the interaction between drops and particles is assumed to occur in a volume bounded by equipotentials. That is, external electrodes are not used to produce even a part of any possible ambient field. The submicron particulate is termed the "particle" system while the collection sites are called "drops".

If a volume is filled with submicron particles charged to the same polarity, then  $\tau_a$  typifies the time required for these particles to self-precipitate on the walls. This time is based on the system parameters of particle number density  $n$ , particle charge  $q$ , and mobility  $b$ . Note that it

Table 2.4.1

Summary of times characterizing systems of charged drops and particles

Designation	Description	Schematic	
$\tau_a \equiv \frac{\epsilon_0}{bqn}$	Particle self-discharge or self-precipitation time.		
$\tau_c \equiv \frac{\epsilon_0}{bQN}$	Drop-particle collection time or time for precipitation of particles due to space-charge of drops		
$\tau_R \equiv \frac{\epsilon_0}{BQN}$	Drop self-discharge or self-precipitation time		

Summary of Nomenclature ( $\epsilon_0 \equiv 8.85 \times 10^{-12}$ )

	number density	charge	mobility	radius	mass density
drop	N	Q	B	R	$\rho_R$
particle	n	q	b	a	$\rho_a$

does not involve the dimensions of the device. As a variation of this configuration, if a similar volume is filled with regions of positively charged particles and other regions of negatively charged particles, then  $\tau_a$  typifies the time required for the oppositely charged particles to intermingle. If, to prevent space-charge fields, positively and negatively charged particles are mixed, then  $\tau_a$  (based on the density of one or the other of the species) is the time required for self-discharge and perhaps self-agglomeration of the particles.

The time required for collection of fine particles on oppositely charged drops is typically  $\tau_c$ . This collection time is also based on the mobility of the fine particles, but the charge-density  $NQ$  of the drops rather than that of the particles ( $nq$ ). The residence time of the gas must be at least of this order for the device to be practical. Provided that the charge density of the drops exceeds that of the particles, this same time constant  $\tau_c$  characterizes particle precipitation onto the walls of a volume filled with drops and particles having the same polarity.

For a system of charged drops,  $\tau_R$  plays the role that  $\tau_a$  does with respect to the particles. Thus, in a system of like-charged drops,  $\tau_R$  is the self-precipitation time of the drops, while in a system of oppositely charged drops where there is no space-charge due to the drops, this same time-constant governs how long the drops retain their charge before discharging each other and perhaps agglomerating.

A simple model that motivates the physical significance of  $\tau_a$ ,  $\tau_R$  and  $\tau_c$  in the role of inducing self-discharge among oppositely charged particles, among oppositely charged drops or particle collection on drops is shown in Fig. 2.4.1.

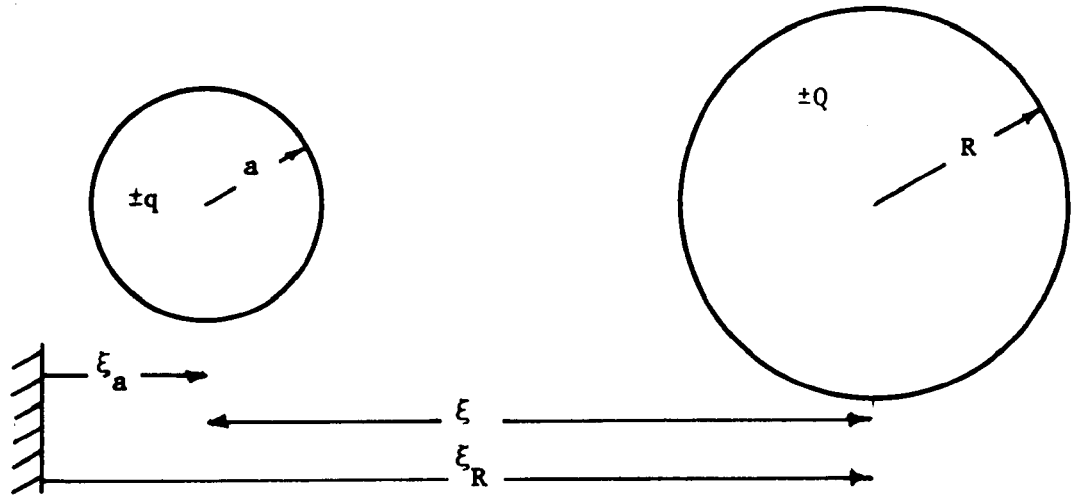


Fig. 2.4.1 Two-"particle" model for electrical discharge and possible agglomeration due to micro-fields.

If the effects of inertia are ignored, the equations of motion for the two charged spheres are:

$$\frac{d\xi_a}{dt} = \frac{Qb}{4\pi\epsilon_0\xi^2} \quad (1)$$

$$\frac{d\xi_R}{dt} = \frac{-qB}{4\pi\epsilon_0\xi^2} \quad (2)$$

Strictly, these expressions are valid when the spacing  $\xi$  is large compared to  $R + a$ . However, as the spheres are drawn together most of the time is spent when they are relatively far apart. Hence, for systems of

relatively tenuous particles (of main interest here) Eqs. (1) and (2) are adequate.

Subtraction of Eq. (1) from Eq. (2) gives an expression for the relative velocity ( $\xi = \xi_R - \xi_a$ )

$$\frac{d\xi}{dt} = -\frac{1}{3\tau\xi^2}$$

where

$$\xi = \frac{\xi}{\xi_0} \quad (3)$$

and

$$\tau = \frac{4\pi\epsilon_0\xi_0^3}{3(qB+Qb)}$$

With the initial spacing taken as  $\xi_0$ , and provided  $\xi_0 \gg R+a$ , integration of Eq. (3) gives a time  $\tau$  for collision. Three limiting cases are summarized in Fig. 2.4.2. First, consider a system of oppositely charged particles alone. Then using as the number density  $n$  the particle density of one of the species,  $n \approx \frac{1}{2}(\xi_0)^3$ , and the time for collision  $\tau$  becomes  $\frac{\pi}{3}\tau_a$ .

Second, consider the collection of particles charged to one sign by drops charged to the opposite sign. In an array of drops, the "last" particle to be collected is midway between two drops. Hence an estimate of the collection time for this worst case is given by making  $N \sim 1/(2\xi_0)^3$ . Also, note that typically  $qB \ll bQ$ . This can be seen by estimating the respective mobilities using a Stoke's drag model ( $b \approx q/6\pi\eta a$ ,  $B = Q/6\pi\eta R$ ) and taking the respective charges as being the saturation values due to impact charging in a field  $E_c$  ( $q \sim 12\pi\epsilon_0 a^2 E_c$ ,  $Q \sim 12\pi\epsilon_0 R^2 E_c$ ). Then,



$$\frac{qB}{Qb} = \frac{a}{R} \quad (4)$$

It follows from this limit that the collection time is characterized by

$\tau_c$ .

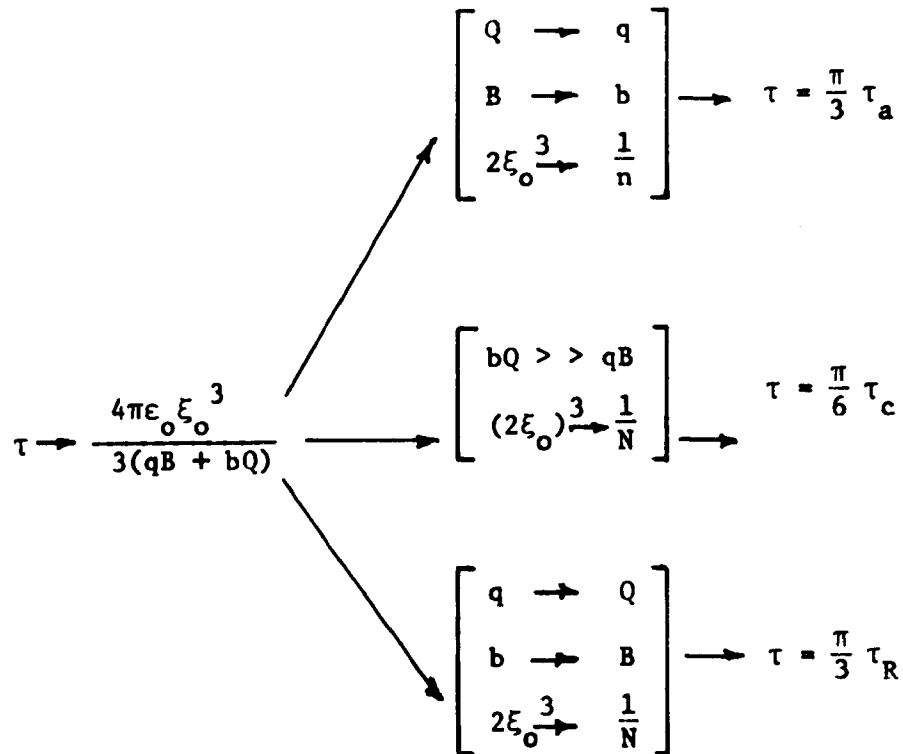


Fig. 2.4.2 Limits of collection time for two particle model that give the three time constants when these are interpreted as self-discharge and drop-particle agglomeration times.

Third, consider the case of a system of oppositely charged drops having total number density  $N$ . Using the same limiting arguments as for the particles, it follows that the time that they will retain their charge is approximated by  $\tau_R$ .

That the same characteristic times  $\tau_a$  and  $\tau_R$  also respectively typify

the self-precipitation of systems of like-charged particles alone or like-charged drops alone follows using the planar geometry of Fig. 2.4.3. For example, for particles, Gauss' Law requires that the electric field intensity  $E_w$  at the walls is

$$E_w = \frac{nqs}{2\epsilon_0} \quad (5)$$

Conservation of the charge within the control volume shown requires that the net charge decrease at a rate determined by the electrical current  $nqbE_w$  caused by the migration of particles to the walls.

$$\frac{d}{dt} (nqs) = -2nqbE_w \quad (6)$$

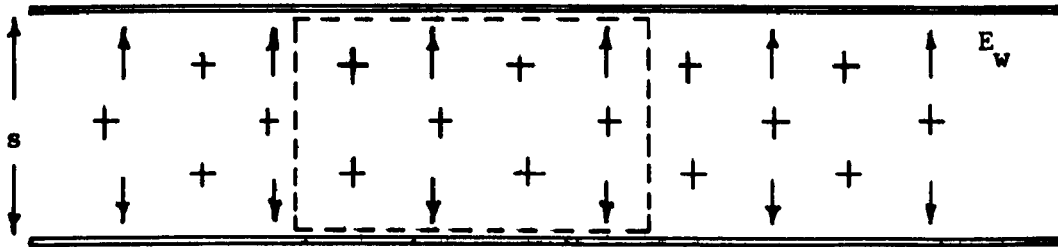


Fig. 2.4.3 Simple model used to illustrate roles of  $\tau_a$  and  $\tau_R$  as self-precipitation times for like-charged particles and like-charged drops respectively.

Combined, these two laws show that the particle density decreases at a rate determined by the equation

$$\frac{n}{n_o} = (1 + \frac{\tau}{\tau_a})^{-1}; \tau_a \equiv \frac{\epsilon_o}{n_o q b} \quad (7)$$

and so it follows that the self-precipitation of unipolar particles is typified by  $\tau_a$ .

The same arguments can be applied to the dynamics of a system of like charged drops. In Eq. (7),  $n \rightarrow N$  and  $\tau_a \rightarrow \tau_R$ . Hence,  $\tau_R$  typifies the rate at which unipolar drops are self-precipitated from a volume.

From several points of view, it is of course possible to criticize the simple models used to motivate the three characteristic times  $\tau_a$ ,  $\tau_c$ ,  $\tau_R$ . For example, in a bicharged system of drops or particles, a given particle or drop is subject to attractive or repulsive forces from more than just its nearest neighbor. In an extreme case, the positive and negative particles or drops might form a cubical lattice of alternately positive and negative polarity. Then the net electric force on a given particle and drop would vanish. Even so, the given drop or particle would be in an unstable equilibrium. Given initiating noise, the rate of growth of the instability representing its departure from the equilibrium is characterized by  $\tau_a$  or  $\tau_R$ , as the case may be.

The appropriateness of  $\tau_c$  for the characteristic time for collection of particles on drops can be further supported by a more refined laminar flow model that gives a detailed description of the collection of a continuum of charged particles on a drop having net charge  $Q$  in an ambient electric field  $E_o$  and with a relative gas velocity  $w$ . (This model is taken up in detail in Sec. 6.2.b) There are in fact 12 possible collection

regimes, determined by the drop charge, the ambient field, and the slip velocity. Of most importance are those regimes in which the drop carries a charge exceeding the saturation charge  $12\pi\epsilon_0 R^2 E_0$  in whatever ambient field  $E_0$  may exist. Then, the electrical current caused by the collection of particles is  $i_2 = -bnqQ/\epsilon_0$  and the rate at which particles are collected is this current per drop multiplied by the number of drops per unit volume and divided by the charge per particle.

$$\frac{dn}{dt} = -\frac{i_2}{q} N = \frac{n}{\tau_c} \quad ; \quad \tau_c = \frac{\epsilon_0}{bNQ} \quad (8)$$

From Eq. (8), it is clear that this more refined laminar flow picture of the particle collection agrees that the characteristic time is still  $\tau_c$ . The details of the collection transient depend on the regime, but, so long as the drops are charged significantly, the characteristic collection time is  $\tau_c$ .

Yet another approach to the drop collection of submicron particles pictures the particle distribution in the void region between drops as determined by turbulent mixing. According to this model, which is similar to the Deutsch model for the precipitator (White, 1963), mixing supplies the particles to the immediate neighborhood of the drop where electrical forces then dominate in depositing the particles onto the surface. This model, taken up in Sec. 6.2.2, also results in a time for significant collection characterized by  $\tau_c$ .

Devices can be envisioned that make use of drops as collection sites in an ambient electric field imposed by means of external electrodes. The drops are in this case "polarized" by the field. For purposes of comparison, it is useful to recognize that even if the drops have no net charge, but are polarized by the ambient field so that they collect particles over a

hemisphere of their surface,  $\tau_c$  remains the basic collection time. However,  $Q$  is interpreted as the charge on the collecting hemisphere.

For the self-discharge of oppositely charged drops, it is possible that drop inertia can become an important factor. This has not been included here because in systems of relatively tenuous drops the inertia is usually not an important factor. However, in specific instances it is convenient to have a ready means of determining the relative importance of inertia in increasing  $\tau_R$ , and this is provided in Sec. 5.3.1.

## 2.5 Classification and Comparison of Basic Collection Configurations

A summary of configurations representing the basis for devices that collect submicron particles is given in Table 2.5.1. It is natural to include the two representatives of conventional technology that are nearest relatives of devices that make use of charged drops: the inertial scrubber and the electrostatic precipitator. In the table, the collection process is characterized by whether or not the particles to be collected are charged, and whether or not the drops, if present, are charged. In addition, a distinction is made between devices that involve an ambient electric field (one associated with many charged particles and hence having an average value over distances that are large compared to the interparticle spacing), and those that primarily involve only a microscopic field (having essentially no space - average value over distances greatly exceeding the interdrop or interparticle spacing). A further distinction is made between ambient field configurations in which the fields are "imposed" by means of charges on electrodes bounding the active volume or are "self-fields" induced by the net charge on particles and drops within the active volume itself.

INS & ESP The characteristic times also included in Table 2.5.1 are

Table 2.5.1 Summary of Basic Configurations for Collecting Submicron Particles  
 Characteristic times  $\tau_a$ ,  $\tau_c$ ,  $\tau_R$  are summarized in Table 2.4.1

Designation	System	Particle Charge	Drop Charge	Ambient Field	Characteristic Times
INS	Inertial Scrubber	none	none	none	$\tau_{sc}$ , $\tau_{sR}$ (Eqs. 2.2.5, 2.2.7)
ESP	Electrostatic Precipitator	unipolar	-	imposed	$\tau_{pc}$ (Eq. 2.3.1)
SCP	Space-charge Precipitator	unipolar	-	self	$\tau_a$
SAG	Self-agglomerator	bipolar	-	none	$\tau_a$
CDS-I	Charged Droplet Scrubber	unipolar (+ or -)	unipolar (+ or -)	( $nq < NQ$ ) self	$\tau_c$ , $\tau_R$
	"	"	"	( $nq = NQ$ ) none	$\tau_c = \tau_a$
CDS-II	"	unipolar or bipolar	bipolar	( $N_+Q_+ = N_-Q_-$ ) none	$\tau_c$ , $\tau_R$
CDP	Charged Drop Precipitator	unipolar	unipolar	( $nq < NQ$ ) self	$\tau_c$ , $\tau_R$
EIS	Electric Inertial Scrubber	none "	a)uni- polar b)bipolar	imposed or "self" imposed	$\tau_{sce}$ (Eqs. 2.2.5 & 2.5.4) Eq. (2.5.9)
EFB & EPB	Electrofluidized and Electro-Packed Beds	unipolar or bipolar	none or bipolar	imposed	$\tau_c$ (Q based on "half-charge")

the basis for making comparisons between systems. With the understanding that the collection lifetime of a drop is typified by a second time constant  $\tau_{SR}$ , inertial scrubber (INS) technology is represented by the collection time  $\tau_{sc}$ . Further conventional competition comes from the side of the electrostatic precipitator (ESP), which has a characteristic collection time  $\tau_{pc}$ .

SCP The space-charge precipitator relies on precipitation on the walls caused by the self-fields induced by charge on the particles themselves. As discussed in Sec. 2.4, the characteristic time for this type of particle collection is  $\tau_a = \epsilon_0 / nqb$ . Note that according to Gauss' Law the electric field at the wall is of the order  $nqs/\epsilon_0$ , where  $s$  is a typical dimension of the active volume. Thus,  $\tau_a$  is equivalent to the collection time  $\tau_{pc}$  in a conventional precipitator provided that  $nqs/\epsilon_0 \rightarrow E_w$ . Clearly, to be competitive, the self-field must be on the order of the electric field intensity that can be imposed by means of electrodes. This places a lower limit on the range of particle densities that can be practically used in a space-charge precipitator. At high particle densities it is indeed possible to make  $nqs/\epsilon_0$  approach the breakdown limitation encountered in the conventional precipitator, but for refined cleaning, the collection time  $\tau_a$  is far too long to be of practical significance.

SAG With the particles charged to both polarities, so that there is no ambient self-field, there is electrically induced self-agglomeration also characterized by the typical time  $\tau_a$ . (Sec. 2.4.). Agglomeration results in electrical discharge between the particles of opposite polarity. Hence, to be useful as a mechanism for increasing particle size prior to collection

by some other means, the agglomeration must be combined with a continual bipolar recharging of the particles. Because an agglomeration event only results in a doubling of the particle volume, self-agglomeration has been generally regarded as too slow a process to be of practical interest. That it is characterized by the same time  $\tau_a$  as the self-precipitator further dampens enthusiasm for making use of electrically induced agglomeration. In a way, the self-precipitator is a self-agglomerator with the agglomeration event one between a particle and an electrode. But the result of this event in the self-precipitator is the removal of the particle from the volume rather than simply a doubling of the particle volume.

With the first four configurations of Table 2.5.1 as a background, consider now the heart of the discussion....the configurations CDS-I and CDS-II exploiting Charged Droplet Scrubbing. Charged drops are used as collection sites for oppositely charged particles.

CDS-I First, consider charged drop scrubbers in which unipolar drops are used. For example, the drops are charged to positive polarity and the particles charged to negative polarity. If the drop charge density dominates ( $|NQ| > |nq|$ ), as would be the case with gas containing relatively little particulate, there is an ambient self-field associated with the drops. This field results in a self-precipitation of the drops with the characteristic time  $\tau_R$ . The situation is analogous to inertial scrubbing. The collection process is limited in this case by loss of collection sites by self-precipitation. However, for an inertial scrubber, the limiting time  $\tau_{SR}$ , can be considered to be constant if the drop size is fixed. Thus, its influence can be circumvented by injecting the drops at a higher velocity. In the case of a charged drop scrubber, this is not true. Increasing the



charge on the drops decreases both  $\tau_c$  and  $\tau_R$  in such a manner that their ratio decreases. In fact, if particles and drops are both charged to saturation in a field  $E_0$  (meaning the largest charge possible by ion impact charging, (see Sec. 5.4.4) ( $Q = 12\pi\epsilon_0 R^2 E_0$  and  $q = 12\pi\epsilon_0 a^2 E_0$ ) and if Stoke's law is used to approximate both mobilities, the collection time and drop self-precipitation time are simply related

$$\frac{\tau_R}{\tau_c} = \frac{b}{B} \approx \frac{a}{R} \quad (1)$$

The ratio of the effective life time  $\tau_R$  of a drop to the cleaning time  $\tau_c$  is essentially the ratio of particle to drop size. This emphasizes the point that to be practical, the charged droplet scrubber using unipolar drops must incorporate a sufficient supply of charged drops that the effective drop lifetime can be much shorter than the gas residence time. This means that a drop is removed by its own field long before its capacity to collect particles is significantly reduced.

As a limiting case, in Table 2.5.1, that CDS-I charged droplet scrubber configuration is identified in which space charge associated with the particles just cancels that due to the drops. That is, the particle loading is sufficiently high that  $|NQ| = |nq|$ . In this case there is no ambient field and hence no self-precipitation of the drops. Thus,  $\tau_R$  is no longer a limiting lifetime of the drops. But, note that the collection time is then  $\tau_c = \tau_a$ , or the same as would be obtained in the space-charge precipitator that would be realized in the absence of the drops.

The picture that now begins to unfold is one in which the performance based on the collection time of the charged-drop scrubber approaches but

does not surpass that of an electrostatic precipitator. To see this directly, assume that there is no limit on the supply of charged drops, so that  $\tau_R$  is not a limiting time. Then, for the charged drop scrubber to compete favorably with the electrostatic precipitator, the ratio

$$\frac{\tau_c}{\tau_{pc}} = \frac{E_w}{(NQs/\epsilon_o)} \quad (2)$$

must be unity or less. Because  $NQs/\epsilon_o$  is the self-field induced by the net charge on the drops at the walls of the active volume (assuming again that  $NQ \gg nq$ ), Eq. (2) makes it clear that for the charged drop scrubber to compete favorably with the electrostatic precipitator, this self-field must exceed that imposed in the conventional device by the electrodes. In the electrostatic precipitator, the maximum  $E_w$  is usually determined by electrical breakdown and this also imposes one upper limit on  $NQ$  in the charged drop scrubber.

In practice it is difficult to generate charged drops with sufficient density that the limit on  $NQ$  is set by electrical breakdown. Rather, the loss of drops due to self-precipitation, reflected by Eq. (1), is the dominant factor in limiting the effective field  $NQs/\epsilon_o$ .

The charged drop scrubber at least requires the same residence time as the conventional precipitator. In fact, the drop loss represented by  $\tau_R$  is likely to make the performance fall short of that for an electrostatic precipitator. However, it must also be understood that in terms of residence time, the conventional electrostatic precipitator, with which the comparison is being made in Eq. (2), is (short of fabric filters) the most viable class of devices for removing submicron particles. The fact that inertial

scrubbers are viewed as competitors of the electrostatic precipitator in collecting particles even below  $10\mu$  suggests that there is more to making a choice of systems than is simply represented by the residence time.

A comparison of the charged drop scrubber with its other "relative"... the inertial scrubber...would tend to cast the charged drop scrubber in a somewhat more favorable light. To make this second comparison, again ignore consideration of the effective lifetime of the drop in either an inertial scrubber ( $\tau_{sc}$ ) or charged drop scrubber ( $\tau_c$ ) and compare the collection times. Using  $\tau_{sc}$  from Eq. (2.2.5) and  $\tau_c = \epsilon_o / NQb$ ,  $\eta \sim \eta_c$ , and saturation charging of particles and drops in a charging field  $E_c$ , ( $Q = 12\pi\epsilon_o R^2 E_c$ )

$$\frac{\tau_c}{\tau_{sc}} = \frac{w^3 \rho_a^2 a^3}{226\eta\epsilon_o R^2 E_c^2} \quad (3)$$

For charging of the drops and particles to improve the performance of the inertial scrubber, the ratio of Eq. (3) must be in the range of unity or less. Note the dramatic dependence on the particle radius  $a$ . Typically, the ratio is unity for particles somewhere under a micron diameter. This is the range where the inertial scrubber usually loses its particle collection performance. For example, let  $2a = 0.4\mu$ ,  $w = 10\text{m/sec}$ ,  $\rho_a = 2 \times 10^3 \text{kg/m}^3$ ,  $\eta = 2 \times 10^{-5} \text{kg/m-sec}$ ,  $R = 50\mu\text{m}$  and  $E_o = 10^6 \text{v/m}$  and Eq. (3) gives  $(\tau_c / \tau_{sc}) \approx 0.3$ . Thus, for particles of this size the charging of the drops and particles would be expected to significantly improve the performance of a conventional scrubber.

CDS-II One way to seemingly avoid the extremely short effective lifetime of charged drops caused by self-precipitation is to employ a mixture of oppositely charged drops. In the charged drop scrubber with bi-charged drops, a short collection time  $\tau_c$  is obtained while space charge neutrality is preserved even at low particle loadings. The basic limitations remain for this second class of configurations, as can be seen by recognizing the dual significance of the characteristic time  $\tau_R$ . In the context of bipolar drops, it represents the typical lifetime of a charged drop before it is discharged by an electromechanically induced encounter with another drop having the opposite polarity. Because of this dual role of  $\tau_R$ , the basic limitations on the CDS-I and CDS-II systems are the same.

CDP In the Charged Drop Precipitator, particles and drops are charged to the same polarity. In the case of most practical interest, the charge density of the drops dominates that of the particles ( $NQ \gg nq$ ). (If  $nq \gg NQ$  the drops do not participate in removal of particles from the gas.) Then, the electric field intensity  $E_w$  at the walls where the particles are precipitated is determined by Gauss' Law to be  $E_w = NQs/2\epsilon_0$ . This deduction follows from the same reasoning as in Eq.(2.4.2) with the field induced by drops rather than particles. In turn, Eqs. (2.4.6) and (2.4.7) describe the particle collection, with the only alteration being that  $E_w = NQs/2\epsilon_0$ . Hence, just as for the CDS interactions, the removal of particles is governed by the collection time  $\tau_c$ . But rather than being scrubbed by the drops, the particles are precipitated on the walls by means of the drop's self-fields. Unlike the SCP, however, the CDP has an all important second characteristic time  $\tau_R$  typifying the lifetime of a charged drop in the volume. Because  $\tau_R < \tau_c$ , the time varying nature of  $N$  plays an essential

limiting role in the collection process.

EIS Yet another collection configuration relies on inertial impact for collection and only makes use of the electric field to drive the charged drops through to the gas. Hence, in the electric inertial scrubber, the particles are not charged. This variation of the inertial scrubber has a collection time  $\tau_{sc}$  that is given by Eq. (2.2.5), with the relative velocity  $w$  approximated by

$$w = BE \quad (4)$$

where  $E$  is the ambient electric field intensity. If the drops are assumed charged to saturation in a field  $E_c$  and if Stoke's drag is used to evaluate  $B$ , then the relative velocity of Eq. (4) becomes

$$w = \frac{2R}{(\eta/\epsilon_o E_c E)} \quad (5)$$

Both the inertia of the gas (finite Reynolds number) and of the drop have been ignored. But Eq. (5) serves to illustrate that typically  $w$  is on the order of 10m/sec. The quantity  $\eta/\epsilon_o E_c E$  is itself a characteristic time which in air and for  $E = 5 \times 10^5$  V/m is not likely to be less than  $10^{-5}$  sec. Thus, for 100 $\mu$ m diameter drops, Eq. (5) gives 10m/sec. Relative velocities achieved using the electric field will be in the same range as those obtained by mechanical means. One limit on  $w$  resulting from an electric drive is set by the breakdown strength of the gas and device insulation. But, it is important to keep in mind limits encountered because of space charge as well. This is particularly true because one incentive for considering the electrically driven inertial scrubber is the possibility of extending the time that the drop retains a velocity relative to the gas. If drops of a single polarity are injected, then the dimensions of the interaction region

are limited by the requirement that the self-field from the drops at the walls not exceed the imposed field. For a region having a typical dimension  $s$ , this means that the imposed field must be greater than  $NQs/\epsilon_0$ . Because the lifetime of a drop in the volume is of the order  $s/BE$ , it follows that this lifetime is less than  $\tau_R = \epsilon_0/NQB$ . If, to avoid the space charge field associated with unipolar drops, a system is envisioned that uses counter-streaming drops of opposite polarity, a similar limitation on the lifetime is encountered. In this case, the drops tend to discharge each other in the characteristic time  $\tau_R$ .

Electrically driven inertial scrubbing is a likely contributor to the performance of any system of charged drops in an ambient electric field. However, for the reasons outlined, it does not appear sufficiently attractive relative to the charged drop scrubbers to merit development in its own right.

EFB & EPB As a last configuration, consider a broad class of systems composed of "sites" that are not charged prior to being injected into the active volume. Rather, because an electric field is imposed they are either charged or polarized within the active volume. Various mechanisms lead to devices having essentially the same engineering characteristics. Although the collection sites have been regarded as drops, in these configurations practical considerations make it more likely that the sites are solid particles. The fact that the active volume must be filled by ambient field makes it necessary that the collection sites be dense if there is to be any merit relative to the ESP.

First, suppose that the collection sites are perfectly insulating. Application of an ambient electric field results in polarization of the

site, with electric field lines tending to be drawn into the site, as sketched in Fig. 2.5.1. Typically, this induced polarization is represented by a relative permittivity reflecting volume polarization at the molecular scale. Positively charged particulate will be collected by the hemisphere of the collection site that terminates field lines directed into the site, while negatively charged ones will be collected over the hemisphere exposed to the outward directed field. The poles of the site play the same role for oppositely charged particles as do the electrodes of the electrostatic precipitator. Particles to be collected can therefore be unipolar or bipolar. In addition to the polarization associated with molecular scale dipoles, it is possible that solid particle sites are permanently polarized or become polarized because of surface charges created by frictional electrification. Polarization of this type is essentially independent of the applied field, and hence can result in collection even in the absence of an applied field.

Second, suppose that the sites are sufficiently conducting that the charge relaxation time based on the site properties ( $\epsilon/\sigma$ , where  $\epsilon$  is the site permittivity and  $\sigma$  is its conductivity) is short compared to the mean time for collision between the sites. In a fixed bed, this collision time is essentially zero, whereas in a fluidized bed, at low electric field strengths, it is determined by the turbulence of the bed. At higher field strengths it can be influenced by the electric field itself. In any case, with each encounter between the sites there is a polarization of the contacting pair induced by the imposed field which tends to make them separate with a net charge. This process results in a continual recharging

of the sites at the expense of an electrical current carried between the electrodes used to impose the ambient field. At any instant the net charge in a volume enclosing many particles tends to be zero. In a sense, the fluidized bed in this state, or the fixed bed in a state where the particles are continually in contact and the field distribution determined by electrical conduction between sites, uses the electrical current to keep the sites active as collection sites. The limitation on effective lifetime of the particles for collection (represented by  $\tau_R$  as in the cases where the collection fields are associated primarily with the charge initially placed on the site) is therefore obviated. Of course, in addition to the net charge on each particle there is an induced polarization of the site, again much as depicted by Fig. 2.5.1

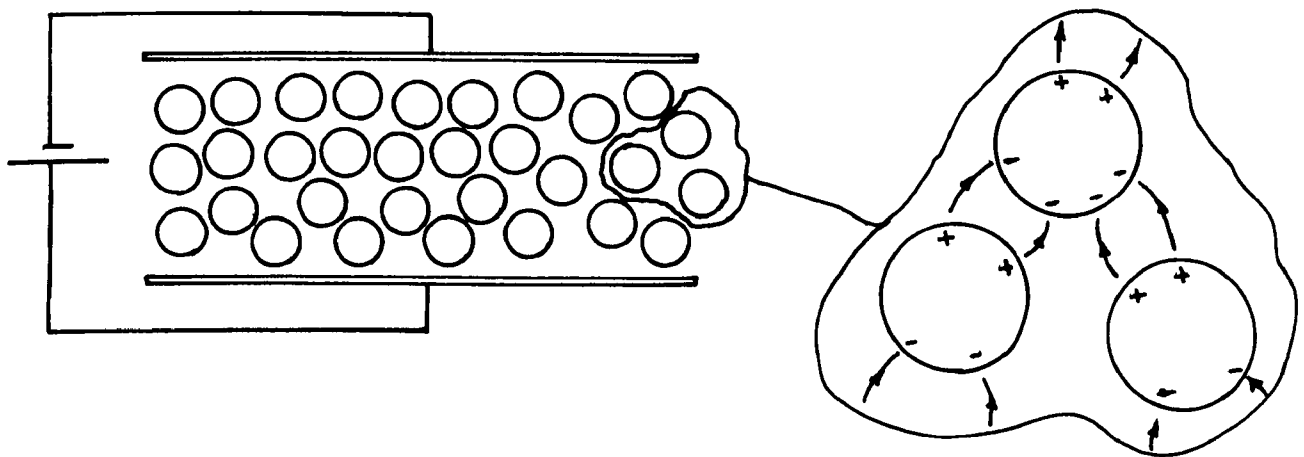


Fig. 2.5.1 Collection particles polarized by means of ambient electric field imposed by means of external electrodes.



Regardless of the detailed mechanisms for establishing an electric field over part or all of the collection site, each of these configurations, whether in the form of a fluidized bed or a packed bed, is typified by the same considerations. The site surfaces play the same role as the electrostatic precipitator electrodes. Hence, the collection time is of the form given by Eq. (2.3.4) for the conventional precipitator. However, the precipitation perimeter  $S$  is replaced by an effective collection surface area of the sites per unit length in the flow direction, and  $A$  can be approximated by the effective flow cross-section through the device.

For spherical collection sites having radius  $R$ , a device having the overall cross-sectional area  $A_{\text{syst}}$  will have approximately

$$S \approx A_{\text{syst}} \left[ 2\pi R^2 \left( \frac{1}{\alpha R} \right)^3 \right] \quad (7)$$

where the mean distance between site centers is taken as  $\alpha R$ . Here the particles are assumed to be unipolar and hence are collected over only half of the site surfaces. Bipolar particle charging would exploit the full site surface but would result in essentially the same collection time. It would, however, avoid the problem of charge build-up within the bed. The effective flow cross-section is essentially that of the system reduced by the geometric cross-section of the sites.

$$A = A_{\text{syst}} \left[ 1 - \frac{(\pi R^2)}{(\alpha R)^2} \right] = A_{\text{syst}} \left[ 1 - \frac{\pi}{\alpha^2} \right] \quad (8)$$

and hence it follows from Eq. (2.3.4) that the collection time is approximately

$$\tau_{bc} \approx \frac{\alpha^3 R}{2\pi E_w b} \quad (9)$$

where  $E_w$  is the average electric field intensity on that part of the site

collecting particles. To be consistent with other approximations inherent in writing Eq. (9),  $\pi/\alpha^2$  is assumed small compared to unity. It is worthwhile to observe that the collection time  $\tau_{bc}$  takes the same form as for devices having sites that carry net charge, provided the charge on a hemisphere is used to replace  $Q$ . This charge is  $Q_{1/2} \equiv 3\pi\epsilon R^2 E_o$ , where  $E_o$  is the ambient electric field. Because  $E_w = \frac{3}{2}E_o$ , Eq. (9) can also be written as

$$\tau_{bc} = \frac{\epsilon_o}{NQ_{1/2}b} \quad (10)$$

A comparison of the collection time for the sites in an ambient field to the collection time of the electrostatic precipitator is made by taking the ratio of the respective collection times. For purposes of comparison consider an electrostatic precipitator with cylindrical electrodes having radius  $r$ . Then, if the limiting values of  $E_w$  are the same in both cases,

$$\frac{\tau_{bc}}{\tau_{pc}} = \alpha^3 \left( \frac{R}{r} \right) \quad (11)$$

As is clear from the derivations of the time constants, this amounts to a ratio of effective collection areas in the two configurations.

From the comparison afforded by Eq. (11), it is clear why the use of collection sites in an ambient field has been considered in the context of packed or fluidized beds. One of the main advantages gained from using the particles as collection sites is lost once external electrodes are used to produce an ambient field throughout the active volume. Unless the collection time using the "drops" is short compared to that for a conventional precipitator, it is difficult to argue for the use of "drops" rather than electrodes. In fact, to produce drops with sufficient density to be competitive is difficult.

However, in the packed and fluidized bed configurations the density of collection sites can be made sufficiently high that the effective surface area is greatly increased over that of a conventional precipitator. Sites in these cases are more likely to be solids than drops. It follows from Eq. (11) that to compete with a conventional electrostatic precipitator, the fluidized bed must have an  $\alpha$  of approximately

$$\alpha \leq \left(\frac{r}{R}\right)^{1/3} \quad (12)$$

For example, using sites having radius  $100\mu\text{m}$ , the collection time in the EFB types of configurations competes favorably with an electrostatic precipitator having  $r = 0.1\text{m}$  if  $\alpha < 10$ . As a second example, suppose that  $r = 0.1\text{m}$  and  $\alpha = 3$  in a bed composed of sites having  $R = 300\mu$ . Then, from Eq. (11)  $\tau_{bc}/\tau_{pc} \approx 0.05$ . Better than an order of magnitude less residence time is required. The packing required to make  $\alpha \approx 3$  can be easily obtained in a fluidized bed, where the sites have a sedimentation velocity exceeding  $10\text{m/sec}$  which is consistent with a device having a relatively high gas velocity.

It is clear from these comparisons with the conventional electrostatic precipitator that the electrofluidized or electropacked bed configurations are, at least from the basic point of view, very attractive as an approach to the control of submicron particulate. In fact, they can be envisioned in a broad range of applications. These not only include the control of submicron particulate, as highlighted here, but also control of a wide range of particle sizes and types. In the following chapters, the focus of attention is on the electrically augmented scrubber configurations. However, it should be understood that information gained from these investigations

is applicable in many cases to the electrofluidized and electropacked beds considered in this subsection. For further discussion of the EFB as an air pollution control device, see Zahedi and Melcher (1974).

### 3 Survey of Devices and Studies

#### 3.1 Charged Drop Control Systems

Processes that must be incorporated into any system making use of charged drops for the collection of particulate are summarized schematically in Fig. 3.1.

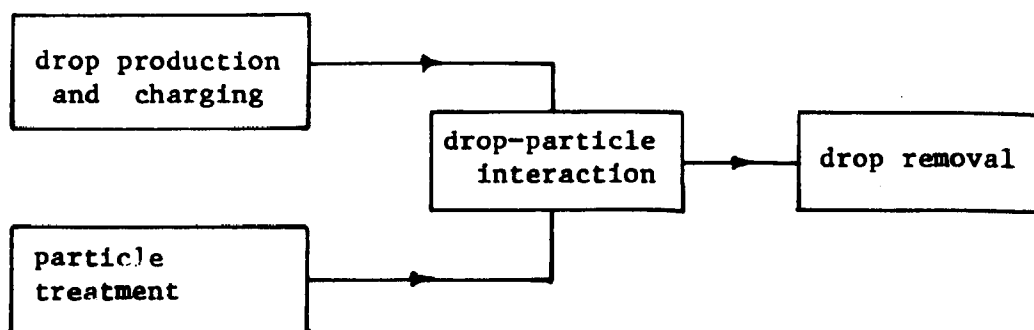


Fig. 3.1 Overall charged drop scrubbing system

The basic collection mechanism, the drop-particle interaction, is emphasized in Chapter 2, and of course is at the heart of any system. But, practical systems differ according to (i) the technique used for generating and charging the drops, (ii) the method of particle treatment prior to collection of particulate by the drops, and once the interaction has taken place, (iii) the means provided for removal of the drops. In fact all of the processes shown in Fig. 3.1 can take place within a single region, but more likely they occur in physically separated regions.

Of the three ancillary processes, only that concerned with drop production and charging requires discussion here. This is because conventional techniques for particle treatment, such as charging by ion impact, are familiar from precipitator technology (White, Chap. 5, 1962). Also, drops can be intentionally made large enough to be removed from the gas with relative ease

so that their removal is again a matter of applying standard technology. Examples of devices that can be used at this stage are the ESP and the centrifugal separator (cyclone). It is convenient to classify methods of making charged drops according to:

- a) the manner in which the drops are formed in a mechanical sense.

Mechanisms are of two types: i) Mechanical atomization, in which a liquid bulk is broken up into drops. This is typically done in stages by first forming liquid sheets or jets or jets that reduce to drops which in turn subdivide to the required size. ii) Condensation; a saturated phase is condensed on nuclei leading to droplets that can be made to grow to the proper size.

- b) the means used to charge the drops. Again, methods fall into one of two categories: i) Bulk charging; the drops are charged after they have been established essentially as mechanical entities. Charging by subjecting drops to the combination of an electric field and an ion flux from a corona discharge is an example (ion-impact charging) ii) Charging at birth. Condensation on ions is a charging mechanism in this category. Another is influence or induction charging, which occurs as drops are in contact with a reservoir of charge and under the influence of a "charging" field.

The formation of charged drops usually amounts to adding one of the electrical charging methods to a conventional mechanical process. Although the electric field can be used to augment the instability of sheets, jets, and drops in an atomization process, the main source of energy for making the drops is usually mechanical or perhaps thermodynamic. In the case of influence charging, no electrical energy is required in principle and with corona charging

the process is typically in a region removed from that where the particles are formed. Hence, the electric field energy does not usually contribute in an essential way to the energy supplied to the mechanical drop formation. The electrohydrodynamic spraying technique for producing charged drops is an exception because it does make use of the electric field to form the drops in a mechanical sense. Fluid pumping, atomization, and charging are to some degree accomplished in a single process.

The main way in which the drop processing will effect the viability of the charged drop scrubber is through the operating costs. As will be apparent from the chapters that follow, the amount of charge that can be induced on a drop is not usually a limitation to the performance. Far more charge can in principle be placed on a drop than is optimal for minimizing gas residence time required for cleaning. As will be seen, this is because too much charge results in too short an effective drop lifetime. For this reason, a more detailed account of techniques for generating charged drops, including specific experimental results and identification of the essential physical processes is relegated to Sec. 5.4.

### 3.2 Patents

In the summary of patents directly relating to the use of electric fields and drops for collecting particulate given in Table 3.2.1, primary emphasis is given to the drop-particle interaction. The nomenclature used conforms to that introduced in Sec. 2.5 and summarized by Table 2.5.1. Also included is a categorization of the method of: (a) charging and producing drops, (b) charging particulate, and (c) removing drops, if any. INS, ESP, and SCP interactions encompass conventional mechanical scrubbing and electrostatic precipitation, and are included in Chap. 2 only for purposes of comparison.

Table 3.2.1 Summary of Patents Relating Directly to Electrically-Induced Collection of Particles on Drops  
(See Table 2.5.1 for Classification by Configuration) \* designates cases where drop-particle interaction is not described and must be inferred

Date	Designation (See Table 2.5.1)	Method of Drop Pro- duction and Charging	Particle Treat- ment	Method of Drop Removal	Inventor	Patent No.	Title
1934	Wet-wall ESP + EIS	induction and/or ion impact	ion impact	electrical precipitation	Wintermute	1,959,752	Liquid Flushing for Discharge Electrodes
1960	EIS	induction	none	settling	Schmid	2,962,115	Apparatus for Separating Solid and Liquid Particles for Gases and Vapours
1970	EIS*	induction	none	space charge precipitation	Marks	3,520,662	Method and Apparatus for Suppressing Fumes with Charged Aerosols
1970	EIS*	induction	none	inertial	Marks	3,503,704	Smokestack Aerosol Gas Purifier
1933	CDS-I or CDS-II*	"frictional"	charged in com- bustion zone	inertial	Wagner	1,940,198	Apparatus for Cleaning Gas
1944	CDS-I	ion impact or induction	ion im- pact	inertial im- pact or pre- cipitation	Penney	2,357,354	Electrified Liquid Spray Dust Precipitators



Table 3.2.1 (cont.)

1944	CDS-I	ion impact or induction	ion im- pact	inertial im- pact or pre- cipitation	Penney	2,357,355	Electrical Dust Pre- cipitator for Utilizing Liquid Sprays
1950	CDS-I	induction	ion impact	"	Gilman	2,523,618	Electrostatic Apparatus (Improvement on Penney's)
1950	CDS-I	"	"	"	"	2,525,347	"
1960	CDS-I	ion impact	ion impact	inertial impact	Peterson	2,949,168	Electrical Precipitator Apparatus of the Liquid Spray Type
1967	CDS-I	"	"	"	"	3,331,192	"
1967	CDS-I	"	"	settling	Romell	3,440,799	Gas Scrubber
1957	EIS & CDS-I	Spinning disk induc- tion	ion impact	inertial impact and precipitation	Ransburg	2,788,081	Electrostatic Gas Treating Apparatus
1958	EIS & CDS-I	induction	ion impact	inertial im- pact & pre- cipitation	DeGraaf, Hass, Van Dorsser and Zaalberg	2,864,458	Liquid Electrostatic Precipitation
1968	CDS-I	induction	"natural"	settling and precipitation	Ziems & Bönicke	3,384,446	Apparatus for Disinfecting Gases
1971	CDS-I	bubbles instead of drops charged by induction	"	-	Owe Berg	3,601,313	Method and Means for the Removal of Liquid or Solid Particles from a Volume of Gas

1961	"EFB"	drops not charged but polarized by ambient field	frictional electrification by gas	precipitation	Vicard	2,983,332	Process and Apparatus for the Purification of Gases
1965	SAG	bubbles surround charged particle which "sees" its image and "agglomerates" with it	ion impact	-	Allemann, Moore & Upson	3,218,781	Electrostatic Apparatus for Removal of Dust Particles From a Gas Stream
1972	CDS-I	induction in a venturi	ion impact	"conventional" devices; e.g. centrifugal separator	Vicard	3,668,835	Electrostatic Dust Separator

Hence, they are not included in Table 3.2.1.

In any patent, there is always the question of whether or not what is claimed is physically possible. Thus, the designations are based on what can be inferred from the claims made and certainly not on proffered evidence from a clear correlation between controlled experiments and theoretical models. By far the most significant in the list for the use of electrically induced collection of particulate on drops are the 1944 patents due to Penney. These recognize the crucial difference between having collecting surfaces consisting of electrodes firmly fixed in position and drops that are free to respond to the electric field with even greater mobility than the particles to be collected.

What is generally evident from the patent literature is an interest in charged drop scrubbers that extends over a period of 40 years. Even so, there is no clear identification and verification of the essential scaling issues underlying the practicality of such devices.

Devices that use charged particles that are not drops as collection sites are the subjects of patents summarized in Table 3.2.2. Here, some of the limitations inherent to a drop system can be obviated. For example, the collection site density can be made sufficiently large that the use of an ambient electric field to polarize the sites is justified (EFB and EPB types of devices). Also, frictional electrification is available as a mechanism for producing collecting fields associated with the sites.

The patents of Table 3.2.2 are included because some of the most practical applications of the concepts developed in the following chapters probably will be to systems making use of collection sites other than drops.

Table 3.2.2 Certain Patents Relating to the Use of Electrically Induced Agglomeration  
in the Control of Particle Pollutants

Date	Designation (See Table 2.5.1)	Description	Inventor	Patent No. (U.S. unless otherwise noted)	Title
1956	SAG	Bi-polar impact charging of solid particles used to induce agglomeration	Prentiss	2,758,666	Carbon Black Separation
1960	CDS-I	Frictional electrification of solid pellets used to induce collection of naturally charged or uncharged particles	Johnstone	2,924,294	Apparatus for Cleaning Gases with Electrostatically Charged Particles
1961	EFB	Particles such as polystyrene spheres, triboelectrified by fluidization are used to collect dust which is "naturally" charged	Silverman et al.	2,992,700	Electrostatic Air Cleaning Device and Method
1961	EPB	Semi-insulating packed bed of spheres in ambient field collect particulate charged by ion impact	Cole	2,990,912	Electrical Precipitator and Charged Particle Collection Structure Therefore

Table 3.2.2 (cont.)

1922	SAG	Bi-polar impact charging of solid used to induce "flocculation"	Möller and The Lodge Fume Co.	British 183,768	Method and Device for Separating Suspended Particles from Electrically Insulating Fluids Especially Gases
1960	SAG	Bi-polar impact charging to induce self-agglomeration	Jucho	British 846,522	Improvements in or Relating to Electrostatic Precipitation
1929	EPB	Packed bed of electrete particles with particulate apparently only charged by "natural" processes	Watson	British 292,479	Improvements in or Relating to the Separation of Impurities from Circulating Air, Gas, or Vapor
1939	EPB/ EFB	Particles used as collection sites in ambient a-c field. Particulate charged by "contact" with bed particles which flow downward in vertical duct with cross-flow of gas	Edholm	Swedish 96717	Satt Att Befria Gaser Fran Dari Suspenderade Stoft-partiklar Jamte Harfor Avsedd Anordning
1973	CDS-I	Bi-polar impact charging used to induce agglomeration	Melcher & Sachar	3,755,122	Method for Inducing Agglomeration of a Particulate in a Fluid Flow

### 3.3 Literature

Once it is recognized that charge and field effects on particle interactions are of interest in such widely separated areas as meteorology, colloid chemistry, and industrial process control, it is not surprising that the literature of the basic area is extensive, in some respects highly developed, and somewhat fragmented. There are a large number of investigations reported on charge effects in the stability and aging of aerosols: (Fuchs, 1964; Devir, 1967; Gillespie, 1953; Gillespie, 1960; Kunkel, 1950; Muller, 1928).

Other reports relate to cloud-drop interactions with ions, particulate, and droplets. An excellent overview of the electrical behavior of aerosols is given by Whitby and Liu (1966). The spectrum of phenomena is, of course, relevant to the use of drop-particle interactions in cleaning industrial gases. The type of phenomena with which these studies are concerned is generally in the category of self-agglomeration (SAG). As discussed in Chap. 2, such processes are not generally useful on an industrial scale.

The large number of parameters and processes that could be brought into play can be reduced by recognizing at the outset certain limitations on the practical systems of interest here. First, the drops are in the range of 10 - 100 $\mu$ m. Penney states that there is little point in introducing the drops unless they themselves are easily removed (Penney, 1944a, Table 3.2.1), which tends to place a lower bound on the size of useful drops. He gives an example of drops in the size range of 0.1 - 0.5mm, with 10 $\mu$ m as a lower bound. Typical devices such as inertial impact scrubbers, cyclone scrubbers and the like, as well as electrostatic precipitators, begin to have limited capabilities as the particle size is reduced much below 10 $\mu$ m. Hence, 10 $\mu$ m is a typical lower limit on the range of drop size of practical interest.

Second, for industrial applications concern is with processes that occur in seconds, rather than aging processes that take minutes or more to produce a significant effective change in particle size. This is a major reason for considering interactions between particles and relatively large drops. A simple collision results in a drastic change in effective size.

Considerable literature exists for studies of interactions between isolated "drops" and various types of charged particles. The manner in which a particle acquires charges from a sea of ions in an ambient electric field is fundamental to the theory of electrostatic corona charging as used in conventional precipitators. With a primary motivation from problems in atmospheric electricity, many authors have studied the interplay between drop charging in an ambient field and the relative motion of the gas in which both drops and ions are entrained (Pauthenier and Moreau-Hanot, 1932; Whipple and Chalmers, 1944; Gott, 1933; Gunn, 1957).

As long as the particle inertia is not an important factor in the particle collection, the charged particles can be viewed as heavy ions, and much of the theory developed in a meteorological context is helpful in understanding the particle collection process. In the next chapters, the rate of particle collection on an isolated drop is incorporated into models. The derivations summarized in Sec. 6.2.1 follow most closely those of Whipple and Chalmers (1944). With the objective of refining the theory for the collection of extremely small particles, Zebel (1968) has extended the Whipple and Chalmers analysis to include a diffusion boundary layer around the drop. His analysis appears to be of value mainly because of the light it sheds on the processes by which the particles are actually collected. The addition of diffusion to the model allows a prediction of the diffusion boundary layer

thickness. For relatively strong electric forces, the charging rate is identical to that predicted by Whipple and Chalmers.

By using ions, Gott (1933) has verified the Whipple and Chalmers model of electrical charging. Kraemer and Johnstone (1955) consider the interactions between a charged aerosol and a single charged or potential-constrained spherical particle. Their work also relates largely to an inertialess representation of the particle collisions with the spherical collector, but it includes some numerical representations of the effects of particle inertia. They make the comment that, in general, the effects of inertial impact and other distinguishable collection mechanisms can be represented by superimposing collection efficiencies computed for the mechanisms considered separately. This is an especially good approach if one of the mechanisms is dominant. In this work, that viewpoint is implicitly taken.

Kraemer and Johnstone also consider effects of particle space charge on the collection process, but do not include an ambient field. One of their interaction mechanisms which involves the mutual attraction of charged drop and particle charges of opposite sign is a model for the CDS mechanism. The " $4K_E$ " collection efficiency is consistent with Whipple and Chalmers in the limit of no ambient electric field. Hence, their experimental observations on the collection efficiency of dioctylphthalate aerosol particles on a spherical collector are in agreement with the predictions of this model, and hence lend support to its use. Complications of self-consistent field and particle charge are addressed in the theoretical work of Smirnov and Deryagin (1967). The effects of finite particle size and inertia are brought into the picture in various numerical studies (Paluch, 1970; Sartor, 1960; Semonin and Plumlee, 1966) aimed at understanding cloud drop-droplet interactions.



From the point of view of scrubber technology, adding electrical forces to a conventional scrubber by charging particulate and drops should improve the performance. Numerical modeling corroborates this expected improvement (Sparks, 1971). But, the charging adds additional parameters to a theoretical model, and numerical studies inherently include so many parameters that it is difficult to achieve the physical insights necessary to understand the basic limitations on the collection process. In the submicron range of interest here, field effects are in fact dominant, and by exploiting this fact, the number of parameters can be greatly reduced. It is in this way that the basic engineering limitations can be perceived.

Not included in any of the theoretical models or controlled in any basic experiments is the effect of gas turbulence. The turbulence referred to here is not just in the wake of an isolated drop, but rather the turbulence associated with the bulk gas flow. The structure of this turbulence is a function not only of the relative motion of gas and drops, but also of the means used to inject the gas and drops into the volume. In much of the work to be described in Chap. 6, drops and gas are injected as a turbulent jet. Practical devices are almost certain to involve turbulent flows. What are the implications of the associated mixing for the rate of collection of particulate by the drops? Moreover, unanswered questions arise because the drops, unlike a mounted sphere, are free to move in response to the turbulent eddies and to the field.

Faith et al. (1967); Hanson and Wilke (1969); Anonymous (1970) and Marks (1971) suggest the use of charged drops for implementing a space-charge type of precipitator. The drops are either charged by induction during their formation at a nozzle, or by ion impact after being injected into the flow

of dirty gas. In either case, their self-fields are responsible for the collection of the drops and/or particles on conducting walls. These devices are in the category of charged drop precipitators (CDP). The use of space charge to replace one of the electrodes in a conventional precipitator is an application of charged drop technology that uses the conventional collection mechanisms of the wet-wall ESP. The objective is a simplification of systems, or perhaps an improvement in capacity to handle low-conductivity particles (Oglesby et al., 1970). Such devices are not generally perceived as related to charged drop scrubbers, because the drops do not significantly collect the particulate. However, there is a close relation in the sense that, according to the arguments given in Chap. 2 and experiments presented in Chap. 6, such devices have collection times related in a basic way to the charged drop scrubber. The true CDP configuration is subject to the same limitations on residence time for cleaning and drop residence time as the CDS configurations.

Marks (1971) describes devices in which the entering particles are not intentionally charged. The mechanism by which they are collected by the drops before the drops are space-charge-precipitated is not specified. One possible mechanism is EIS interactions, with the drops moving under the influence of the space-charge field and collecting particles by inertial impact. Such a mechanism of collection is possible in the devices described by Hanson as well, although there the particles have the same sign of charge as the drops, hence the Coulomb contribution to the particle-drop interaction tends to obstruct collection.

Eyraud et al. (1966) and Joubert et al. (1964) describe the use of charged drops for collecting submicron biological particles. Their interaction

is one in which the drops are introduced and charged in the immediate vicinity of a corona wire. The arrangement is otherwise similar to that of a single-stage tube-type precipitator. Again, the interaction mechanism is not specified. The author cites the ease with which the drops are removed by the precipitator, but alludes only to the mechanism by which the drops pick up the particles (before being themselves removed) with the statement: "Furthermore, each drop plays the role of a high-voltage electrode for a very limited region of the gas to be cleaned". This implies the CDS type of interaction. However, particles and drops seem to have the same charge, so it is difficult to see how such a mechanism can be effective. But certainly the field-induced radial velocity of the drops caused by their charging and the imposed electric field can lead to an EIS type of induced inertial impact scrubbing.

A pioneering endeavor showing the advantages of using charged drops in the CDS-I configuration to improve wet-scrubber performance is recently reported by Pilat, Jaasund and Sparks (1974). Their work illustrates that a conventional scrubber (INS) operating under practical conditions can in fact have a significantly improved performance in the CDS configuration. The experiments reported are for practical rather than controlled conditions, and hence do not lend themselves to the quantitative scrutiny necessary to verify laws for the scaling of such devices. More is said in Chap. 7 about the relation of these results to the models developed in Chap. 6.

One of the main points of Chap. 2, supported by critical experiments in Chap. 6, is that CDS-I, CDS-II and CDP types of devices are characterized by residence times for cleaning of the same order. Moreover, operating with sufficient charge density to equal that provided by drops in these other

devices, the cleaning time for SCP devices is of this same order. Hence, it is possible to obtain improvements in the performance of an inertial scrubber by (i) charging the particulate alone (SCP), by (ii) charging drops and particulate to the same sign (CDP) and by (iii) charging the drops and particles to opposite polarity (CDS-I or CDS-II). Because each of these interactions is akin to that occurring in an electrostatic precipitator, it is important to have the ESP as well as the INS in view in forming conclusions as to the significance of collection efficiencies.

## 4 Electrically Induced Self-Precipitation and Self-Discharge

### 4.1 Objectives

By interrelating models and controlled experiments, an examination is presented in this chapter of self-precipitation (SCP) and self-discharge (SAG if the particles also agglomerate mechanically) in submicron aerosol systems.

There are two broad objectives. First, unipolar and bicharged aerosols are used as the fine particulate system in Chap. 6 where collection by systems of charged drops is developed. Study of the dynamics of the charged aerosol alone establishes the degree of confidence that should be associated with the theoretical models for self-precipitation and self-discharge processes as they occur along with other processes in the more complex systems. Also, much of this chapter is concerned with experimental controls that are used in Chap. 6.

Second, the SCP and SAG processes are important in their own right for understanding charged drop scrubbers. As discussed in Chap. 2, the SCP is in fact useful as a bench-mark in establishing how charged drop collection devices relate to the electrostatic family of collection devices. In previous attempts to examine SCP and SAG processes, often either the size and charge were not well controlled, or the charge was insufficient to cause electrostatic effects to be dominant. (For work on the SCP mechanism, see Dunskaia and Kitaev, 1960; Foster, 1959; Faith, Bustang and Hanson, 1967; Hanson and Wilke, 1969 and for the SAG mechanism see DallaValle, Orr and Hinkle, 1954; Devir, 1967.) This is not the case in the experiments to be described in Sec. 4.8. An evaporation-condensation generator is used to produce an aerosol sufficiently monodisperse that light scattering techniques may be used for

sizing. Two other devices allow the aerosol to be charged to a high level with very little loss of particles and the magnitude of this charge to be determined. These techniques are the subject of Secs. 4.4 - 4.7. Because the residence time of the charged aerosol is also well controlled, all parameters necessary to make an absolute prediction of performance are available.

A significant result of this chapter, again brought out by the calculations and born out by the experiments is that the loss of charged particles either through self-precipitation on the walls or through creation of neutral particles by self-discharge is characterized by the same time scale  $\tau_a = \epsilon_0/nqb$ . To emphasize this point, the evolution of the particle concentration for a variety of systems, both stationary and moving is discussed. The results in one case from Sec. 4.2.3 are used to predict the performance expected of the self-discharge experiment of Sec. 4.8. Another is used to calculate a calibration curve for a device from which both the charge density and mobility may be determined. For those not primarily interested in experimental technique, Secs. 4.2, 4.3 and 4.8 are the essence of this chapter.

## 4.2 Theory of Self-Precipitation Systems

### 4.2.1 General Equations

The flux density  $\bar{\Gamma}$  of charged submicron particulate can be represented for the present purposes as having contributions from self-diffusion, from migration in the face of the electric field, and from convection due to the motion of the surrounding gas.

$$\bar{\Gamma} = -D_B \nabla n + nb\bar{E} + n\bar{v} \quad (1)$$

Here,  $D_B$  is the self-diffusion coefficient which can be evaluated from the expression (Hidy and Brack, 1970, p. 171).

$$D_B = \frac{kT}{6\pi\eta a} \left(1 + \frac{A'\lambda}{a}\right) \quad (2)$$

where  $\lambda$  is the mean free path of the gas molecules ( $\sim 6 \times 10^{-8}$  m at STP) and  $A'$  is a function that can be considered a constant, 1.2, for Knudsen numbers ( $\lambda/a$ ) much less than one. The term in parenthesis accounts for the slippage of gas around the particle and is known as the Stokes-Cunningham correction. As an example, for a particle with a radius of  $0.5 \mu\text{m}$ :  $D_B = 1.3 \times 10^{-10} \text{ m}^2/\text{sec}$ . Conservation of particles is described by the equation

$$\nabla \cdot \bar{\Gamma} + \frac{\partial n}{\partial t} = 0 \quad (3)$$

Given the gas velocity  $\bar{v}$ , Eqs. (1), (3) and Gauss' Law

$$\nabla \cdot \epsilon_0 \bar{E} = nq \quad (4)$$

represent the evolution of the particle density. Flows of interest are likely to be essentially incompressible, so that  $\nabla \cdot \bar{v} = 0$ , and Eqs. (1), (3) and (4) combine to give

$$\frac{dn}{dt} = D_B \nabla^2 n - \frac{bq}{\epsilon_0} n^2 \quad (5)$$

where

$$\frac{dn}{dt} \equiv \frac{\partial n}{\partial t} + (\bar{v} + b\bar{E}) \cdot \nabla n \quad (6)$$

Hence, the left hand side of Eq. (5) is the rate of change with respect to time of the particle density as seen from the frame of reference of one of the particles. (With diffusion included in the model, this particle is defined in an average sense.) The local density decreases for two reasons,

represented by the terms on the right in Eq. (5): diffusion away from regions of elevated density and migration away from regions where the space charge generates a field tending to make the like charges repel.

Effects of Brownian Diffusion The gradient in particle concentration giving rise to diffusion is typically caused by the presence of absorbing surfaces. From Eq. (5) it is evident that in a system characterized by a length scale  $\ell$  between these absorbers, appreciable particle removal occurs in times of the order  $\tau_{dc}$  such that the rate of change on the left is accounted for by the diffusion term on the right;  $n/\tau_{dc} \approx D_B n/\ell^2$ . Hence,

$$\tau_{dc} = \ell^2/D_B \quad (7)$$

As a typical example, particles of  $0.5\mu\text{m}$  radius between absorbers having a spacing  $\ell \approx 1\text{cm}$  will be lost to the walls on a time scale of  $\tau_{dc} = 7.7 \times 10^6 \text{sec}$ . Clearly, particle removal by Brownian diffusion is unimportant in processes that must occur in seconds or less. The actual time scale is determined by the term that dominates on the right in Eq. (5). If the second term dominates, then similar dimensional arguments show that the characteristic time is  $\tau_a = \epsilon_0/nqb$ . If attention is again focused on aerosol particles  $0.5\mu\text{m}$  in radius with a charge and within a field typical for the highly charged aerosol systems to be considered:  $b \approx 10^{-7} \text{m/sec/V/m}$  and  $nq \approx 10^{-4} \text{coul/m}^3$ , then  $\tau_a \approx 1 \text{sec}$ . In laminar or turbulent flow, the length scale  $\ell$  determining the diffusion is the thickness of a boundary layer and so can be small enough to greatly reduce  $\tau_{dc}$ . But even with layers having typical thicknesses of  $10^{-4} \text{m}$ , the time scale for diffusional deposition is too long to be of interest.



## 4.2.2 Laminar Flow Systems

In the absence of the diffusion term, Eq. (5) can be integrated to give

$$\frac{n}{n_0} = \frac{1}{1 + \frac{t}{\tau_a}} ; \quad \tau_a \equiv \frac{\epsilon_0}{n_0 q b} \quad (8)$$

Remember that this expression pertains to a particle of fixed identity which when  $t = 0$  is surrounded by particles having density  $n_0$ , and which moves along the particle line

$$\frac{d\bar{r}}{dt} = b\bar{E} + \bar{v} \quad (9)$$

Hence, to evaluate the detailed distribution of  $n$ , specification must be made of the geometry and boundary conditions which (together with Poisson's equation) determine  $\bar{E}$ . Some examples show how the Eqs. (8) and (9) can be used to establish a qualitative and even a quantitative description in specific cases.

Closed Volume of Still Gas A closed container having walls that are not sources of  $n$  initially filled uniformly with particle density  $n_0$  will self-precipitate particles on the wall in such a way that the density everywhere is either given by Eq. (8) or is zero. Thus, at any instant, the volume is filled by regions of zero density and uniform density given by Eq. (8). To see this, consider that an arbitrary particle moves from some location (a) when  $t = 0$  to a second location (b) also within the volume in time  $t$ . The density at location (b) is given by Eq. (8). During the same interval of time a particle at some other location (c) has moved to the position (a). Because Eq. (8) also applies to this particle (if the position (c) is within the volume) then the density at (a) after the time  $t$  has elapsed is the same as at (b). The points are arbitrary, so it follows that the density decays

throughout the region connected by particle lines (Eq. (9)) to points within the volume in a uniform fashion. The exception comes from the cases where a particle line originates at a boundary. In that case, the density along the line is zero because there is no source of particles at the wall.

Flow Through Duct of Uniform Cross-Section Even though a steady-state process when pictured from the laboratory frame of reference, the evolution of the particle density in a duct (for example a space-charge precipitator) is nevertheless represented by Eq. (8). Let the flow be fully developed and in the  $z$  direction:  $\bar{v} = U(x,y)\bar{i}_z$ . If the duct cross-section has a smallest dimension that is short compared to distances over which the charge density associated with the particles decays appreciably, then the electric field is essentially transverse  $\bar{E} \approx \bar{E}_T$ , and Eq. (9) for the particle trajectories becomes approximately

$$\frac{d\bar{r}}{dt} = b\bar{E}_T + U(x,y)\bar{i}_z \quad (10)$$

For slug flow with particles introduced at  $z = 0$  with a uniform density profile  $n = n_0$  at  $z = 0$ , the decay of density follows by first recognizing that the  $z$  component of the particle trajectories, Eq. (10), is

$$\frac{dz}{dt} = U \quad (11)$$

and since this expression can be integrated and substituted into Eq. (8),

$$\frac{n}{n_0} = \frac{1}{1 + \frac{z}{U \tau_a}} \quad (12)$$

The effective time is simply the transport time, in this case the same for

each particle at a given location  $z$ .

If the profile of either the velocity or the density is not uniform, the relation between the particle time (in terms of which Eq. (8) is represented) and the position in the duct is determined in part by Gauss' Law. In Sec. 4.8 experimental study is made of the self-precipitation in a cylindrical duct. Although Eq. (12), evaluated with  $U$  the mean flow velocity, gives a reasonable picture of the density decay, a more detailed theory recognizes the parabolic velocity profile. A straightforward numerical analysis, in which the particle density is taken as uniform at  $z = 0$ , first recognizes that the particle density is given by Eq. (8) along the lines of Eq. (9), which become

$$\begin{aligned} dz &= 2U[1 - (\frac{r}{R})^2]dt \\ dr &= bE_r(r)dt \end{aligned} \tag{13}$$

where  $U$  is the mean velocity and  $R$  is the duct radius. From the first of these expressions, the particle originating at some radial position  $r$  in the  $z = 0$  plane reaches the plane  $\Delta z$  in the time  $\Delta t = dz/2U[1 - (\frac{r}{R})^2]$ . Its density there follows from Eq. (8) while the change in radial position is given by Eq. (13b), which can be approximated using the electric field evaluated in the  $z = 0$  plane. Because  $\bar{E}$  is purely transverse, it follows from Gauss' Law that this field is

$$E_r = \frac{1}{r} \int_0^r \frac{nqr}{\epsilon_0} dr \tag{14}$$

so that given  $n(r)$ ,  $E_r(r)$  follows by integration. The density profile is thus found at the plane  $z = \Delta z$ , in turn the electric field in this plane

is determined from Eq. (14) and then the process repeated to find the profile in the plane  $z = 2\Delta z$ .

Figure 4.2.1 shows the evolution of particle density found by including the detailed effect of the parabolic velocity profile. The spatial decay of the particle flux is compared to the decay of the slug flow and to an experiment in Fig. 4.8.2.

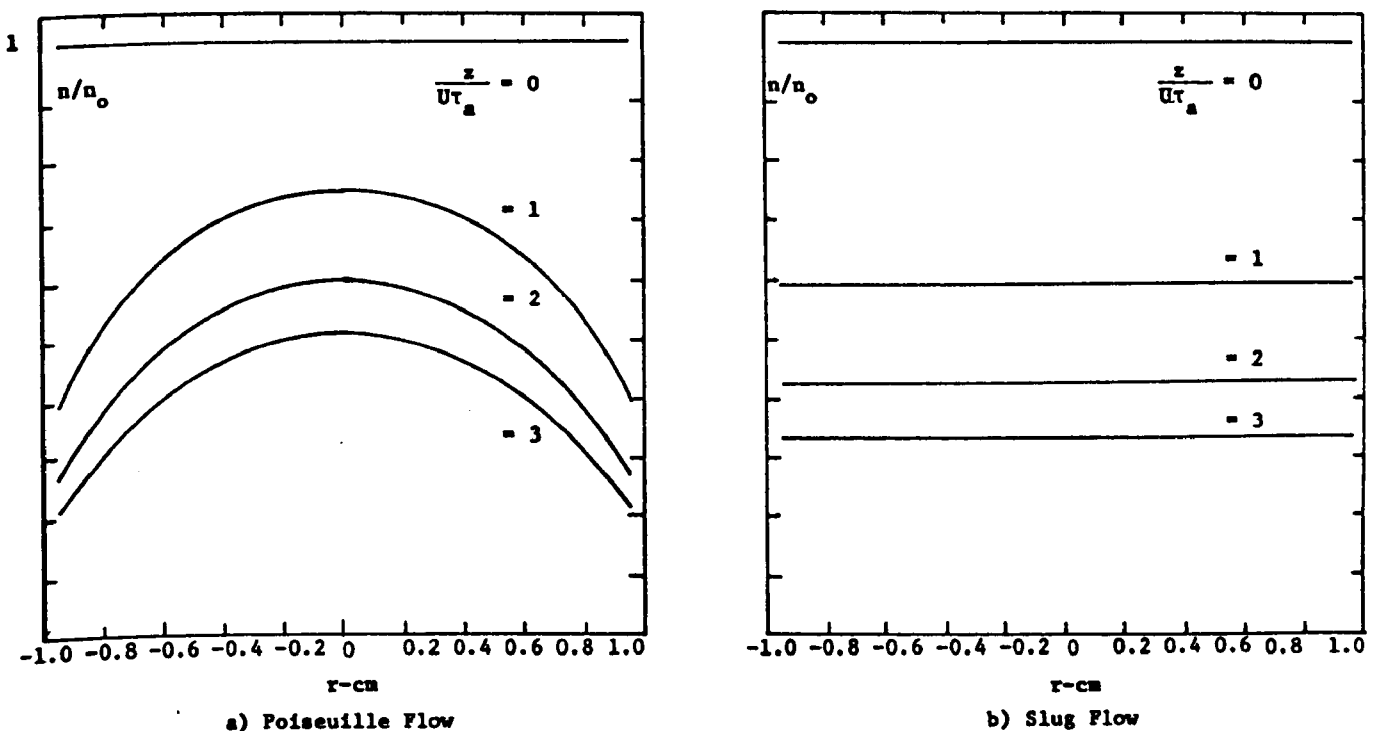


Fig. 4.2.1 Self-precipitation in a cylindrical channel with radius 0.95cm carrying a flow with  $F = 1.08 \times 10^{-4} \text{ m}^3/\text{sec}$

Because the precipitation field is due to the charge itself, it is to be expected that the rate of decay, whether it be temporal or spatial, is typically slower than that associated with "imposed" field systems such as the conventional precipitator. Fig. 4.2.2 makes a comparison of the typical decay laws to emphasize this point.

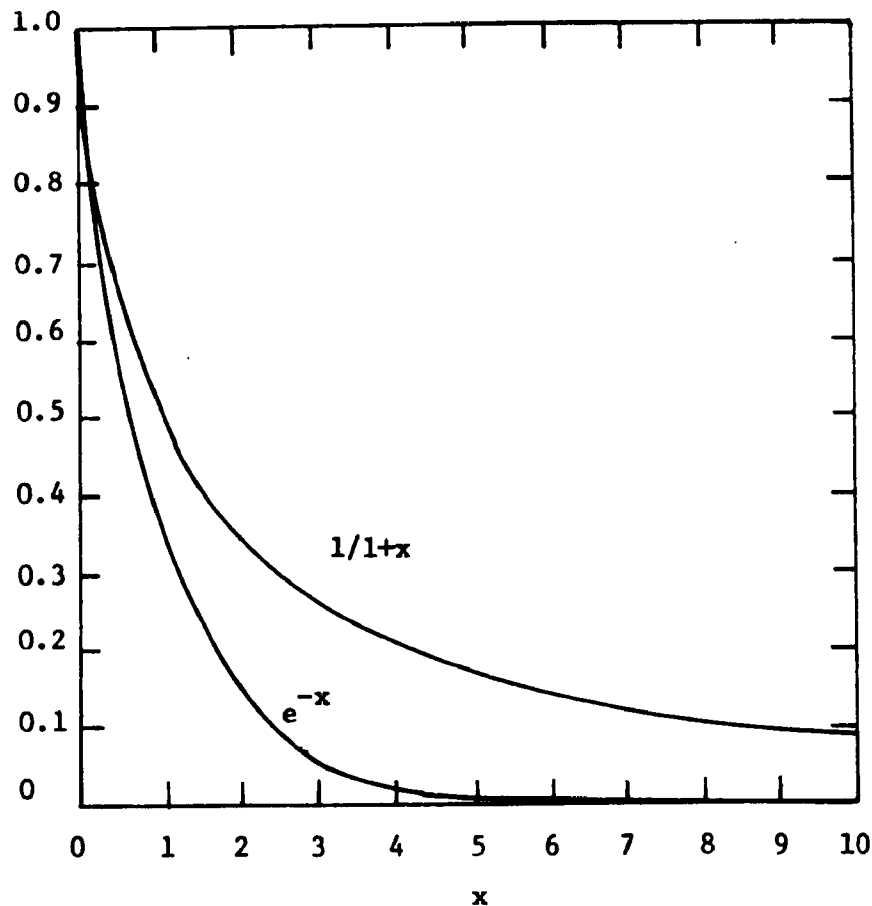


Fig. 4.2.2 Comparison of typical decay laws for self-precipitation and "imposed" field types of devices.

#### 4.2.3 Turbulent Flow Systems

If the gas is in a state of turbulence, then the density distribution of a submicron system of particles is strongly influenced, even when the mean flow is zero. Nevertheless, the ubiquitous time constant  $\tau_a$  retains its significance. To see this, consider limiting cases in which the turbulence completely dominates and renders the distribution of particles uniform throughout the volume of interest.

Closed Volume of Gas With no Mean Flow If a container having volume  $V$  enclosed by a surface  $S$  is filled with charged particles and kept thoroughly mixed, perhaps by means of a mixing vane or a fan, the integral form of the particle conservation equation gives the rate of loss of particles to the

walls directly. Because there is no normal velocity at the walls,

$$\frac{d}{dt} \int_V n dV = - \oint_S n b \bar{E} \cdot \bar{n} da \quad (15)$$

This expression applies in general. But because the mixing guarantees that the distribution of  $n$  is uniform, and because Gauss' Law relates the total flux of  $\bar{E}$  normal to the container to the total charge enclosed, Eq. (15) becomes

$$\frac{d}{dt} (nV) = -nb \oint_S \bar{E} \cdot \bar{n} da = -nb \left( \frac{nqV}{\epsilon_0} \right) \quad (16)$$

Hence, the volume  $V$  of the container cancels out and the decay in density is predicted by the familiar expression

$$\frac{dn}{dt} = -n^2 \left( \frac{bq}{\epsilon_0} \right) \quad (17)$$

The solution is again given by Eq. (8)

Steady Flow Through Region With Complete Mixing The remarkable fact is that because of Gauss' Law, self-precipitation is at most influenced very little by the specific nature of the geometry. In the cases of complete mixing, the geometry has no effect. This is further illustrated by considering an important type of situation in which particles enter and leave a volume  $V$  (of arbitrary geometry) entrained in a gas having the volume rate of flow  $F$ . Under steady state conditions, conservation of particles requires that

$$F(n_{in} - n_{out}) = \oint_S n b \bar{E} \cdot \bar{n} da \quad (18)$$

With complete mixing within the volume,  $n$  is constant over the enclosing

surface and equal to the density  $n_{out}$  at the exit. Under the assumption that the electrical contribution to the flux of particles at the inlet and outlet of the container can be ignored, Eq. (18) becomes

$$F(n_{in} - n_{out}) = n_{out}^2 \left( \frac{bqV}{\epsilon_0} \right) \quad (19)$$

This expression can be solved for the exit particle density  $n_{out}$ . Definition of the residence time as  $\tau_{res} \equiv V/F$  (see Sec. 2.1) and  $\tau_a \equiv \epsilon_0/n_{in}qb$  makes it possible to write this expression in the form

$$\frac{n_{out}}{n_{in}} = [-1 + \sqrt{1 + 4(\tau_{res}/\tau_a)}] / 2(\tau_{res}/\tau_a) \quad (20)$$

to again emphasize the crucial role of  $\tau_a$  relative to the residence time.

The dependence of  $n_{out}/n_{in}$  on  $\tau_{res}/\tau_a$  is shown in Fig. 4.8.4 which compares this prediction to experimental results.

### 4.3 Analysis of Self-Discharge Systems (SAG)

#### 4.3.1 Mechanisms for Self-Discharge

Langevin and Harper Models In the previous sections, it is clear how the space charge of the unipolar aerosol particles generated an electric field which resulted in the drift of these charged particles toward the boundaries. However, in the case where the system contains equal amounts of positive and negative particles, so that no macroscopic electric field is created, the model which represents the drift of oppositely charged particles under the influence of their mutual fields is not as straightforward. Whereas before the Brownian motion of the particles could be ignored because the electric field generated by reasonable particle densities resulted in a

relatively large drift velocity, here it cannot be so easily dismissed. In its most primitive idealization the pertinent electric field is that of a charged sphere, which decays inversely with the square of the distance. At reasonable separation this results in such a small drift that often it cannot compete with diffusion processes.

To arrive at some criterion for deciding whether diffusion or migration is dominant, it is helpful to reduce the problem to one of two oppositely charged spheres, as shown in Fig. 4.3.1. The equation governing the separation between the spheres can be reduced to (Harper, 1932)

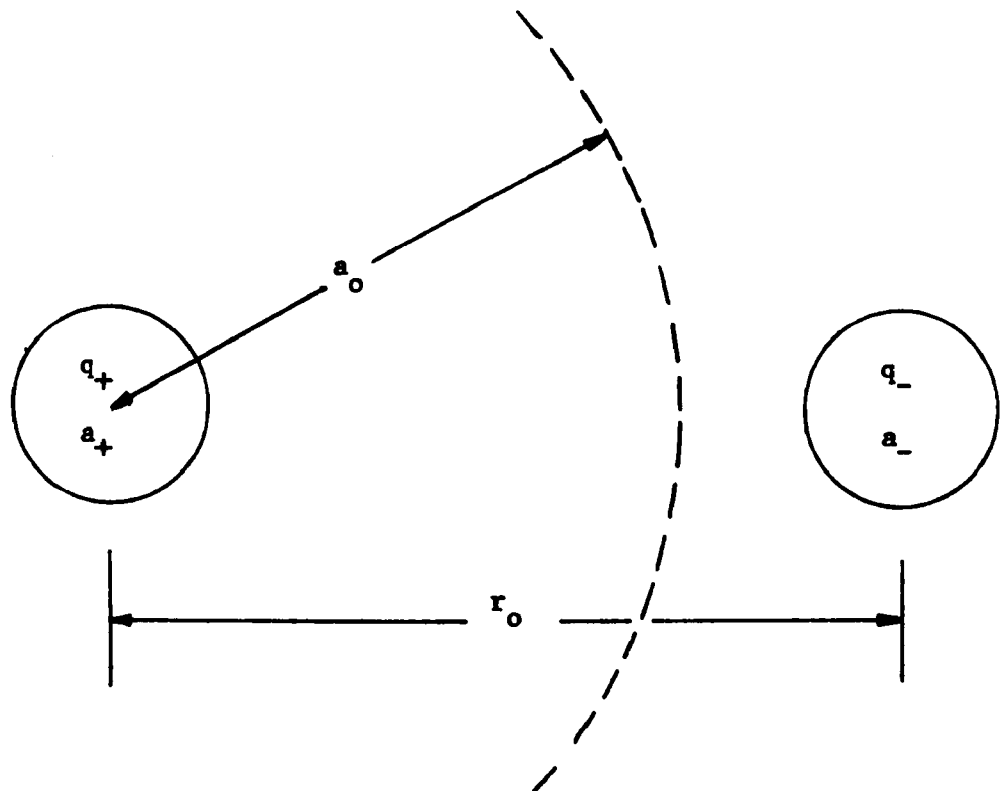


Fig. 4.3.1 Self-discharge model consisting of a pair of oppositely charged particles



$$\frac{dr}{dt} = \frac{(D_+ + D_-)}{r} - \frac{(q_+ b_- + q_- b_+)}{4\pi\epsilon_0 r^2} \quad (1)$$

where the first term on the right side of the equation includes the effects of diffusion and the second the effects of electrostatic attraction. Here, both  $q$  and  $b$  are defined positive. The diffusion coefficients are determined by the Brownian motion of the particles (Eq. 4.2.2) and are constants, independent of the particle separations. This will not be true in the case of turbulent diffusion to be examined in the next chapter. From this equation it is clear that there exists a finite sphere of influence for the forces of electrostatic attraction. If the particles are initially separated by a distance greater than  $a_0$ , where

$$a_0 = \frac{(q_+ b_- + q_- b_+)}{4\pi\epsilon_0 (D_+ + D_-)}, \quad (2)$$

then a collision will not occur. However, if the initial separation is less than  $a_0$ , coalescence between the two spheres will take place. Within a constant factor, the above critical distance corresponds to the separation at which the thermal energy of the spheres equals that required to separate them by an infinite distance. For initial separations less than  $a_0$  the gas is incapable of giving the spheres sufficient energy to achieve complete escape, while for greater initial separations it can.

Next, consider the situation where instead of just two isolated spheres, there are an infinite number of oppositely charged ones distributed in such a way that over dimensions large compared with the initial particle separation  $r_0$ , there is no macroscopic (ambient) electric field. The objective is to find the rate at which charged particles are lost from the

system. (It is assumed from this point on that the oppositely charged spheres have the same magnitude of charge. If this condition were not made, then the system could not be specified by just three species of particles: positive, negative, and neutral. Depending on the differences between the initial charges, additional species would be generated. This considerably increases the complexity of the system. An example of how such a process can be dealt with is found in the classical literature on Brownian coagulation of aerosols (Overbeek, 1952).) To begin, assume that  $r_0$  is small compared with  $a_0$ . Then the interparticle electric fields will be dominant in determining the motions of the particles. The rate at which negative particles drift across a sphere of some arbitrary radius smaller than  $r_0$  surrounding a positively charged particle is on the average

$$G_- = \oint n_- \bar{v}_- \cdot d\bar{a} = n_- q(b_+ + b_-)/\epsilon_0 \quad (3)$$

This is the rate at which a single positive sphere removes negative ones from the system. Remember that the mobility  $b$  of a particle is defined as a positive quantity. In a unit volume, the total rate at which negative particles disappear through this process would be

$$\phi_- = n_+ G_- = \frac{n_+ n_- q(b_+ + b_-)}{\epsilon_0} \quad (4)$$

A similar equation can be written for the rate at which positive particles are absorbed:

$$\phi_+ = n_- G_+ = \frac{n_- n_+ q(b_+ + b_-)}{\epsilon_0} \quad (5)$$

Such a model has been studied extensively in the context of ion recombination,

where it is termed the Langevin or very high pressure limit (Cobine, 1958; Thomson and Thomson, 1969).

To see the significance of this result, consider the opposite extreme where the initial separations are large compared with the radius of the electrostatic sphere of influence. A different view of the recombination process must be taken. The motion of the particles is dominated by diffusion until they approach the central particle to within a distance  $a_0$ . Once that point is reached, they are guaranteed to be captured. Thus, the calculation becomes one of strictly diffusion with the conditions that the charged particle density be some constant far away from the central oppositely charged sphere and be zero at the distance  $a_0$ . The rate at which these particles diffuse into the sphere of electrostatic influence is then (Hidy and Brack, 1970, p. 177):

$$G_{\pm} = 4\pi(D_{+} + D_{-})a_0 n_{\pm} \quad (6)$$

In ion recombination this limiting situation is termed the Harper or high pressure model.

If the expression for the radius of the sphere of influence, Eq. (2), is substituted into Eq. (6), it is consistent with the Langevin model, Eq. (3). The same expression for aerosol recombination is applicable independent of the initial concentration, even in the extreme case where actually diffusional effects are chiefly responsible for bringing oppositely charged particles together.

Effects of Debye-Hückel Shielding One final observation should be made. In both of the previous developments the field responsible for the drift of the charged particles toward an oppositely charged central sphere is assumed

to be determined just by the charge on the central one. The collective effects of the other charged particles are ignored. An estimate for this effect can be made in the limit where Brownian motions dominate the electrical ones in these outer regions. This theory, first developed by Debye and Hückel for strong electrolytes (McDaniel, 1964), confirms that the other charges produce a shielding effect that causes the electric field to decay much more rapidly than  $1/r^2$ . The result indicates that for distances greater than a Debye length, defined as

$$a_{db} = \sqrt{\frac{\epsilon kT}{\sum_i n_i q_i^2}}, \quad (7)$$

the charged particles are fairly well screened from the influence of the central one.

In the case where there are just two species of equal size carrying equal, but opposite charges, and the density of each species is related to its mean spacing by

$$n_+ = n_- = \frac{1}{r_o^3}, \quad (8)$$

with the use of Eq. (4.2.2), the expression relating the three critical lengths of the system becomes

$$\left(\frac{a_o}{r_o}\right) = \frac{1}{4\pi} \left(\frac{r_o}{a_{db}}\right)^2. \quad (9)$$

If  $1/4\pi$  is approximated by one it follows that the three lengths can follow one of two possible ordering schemes:

$$a_o < r_o < a_{db} \quad (10a)$$

$$a_{db} < r_o < a_o \quad (10b)$$

If case (a) is the correct relation for a given physical situation, then use of the Debye-Huckel potential is justified. However, this leads to a very small modification of the coagulation rate (Hidy and Brack, 1970, p. 300). If the particles are so highly charged that case (b) applies, the Debye-Huckel picture no longer applies. It does not make sense to speak of a Debye-Huckel length that is small compared with the mean particle spacings. Since  $a_o > r_o$ , the coagulation process will be determined by the drift of the particles in their mutual electric fields. This rate (Langevin) has been previously shown to equal that of case (b) (Harper, 1932). Thus, the shielding can be argued to have little influence on the agglomeration rate of the system.

As an experimentally typical case, let  $n_o = 10^{12}/m^3$ ,  $b = 10^{-7} m/sec/V/m$ ,  $D_B = 10^{-10} m^2/sec$ , and  $q = 10^{-17} coul$ . These values imply that both  $r_o$  and  $a_o$  are on the order of  $100\mu m$ , and  $a_{db}$  is approximately  $10\mu m$ . Thus, neither diffusion processes nor electrostatic ones can be considered dominant. However, since both limiting models yield the same discharge rate, it seems reasonable that the same expression will also apply in the region in which both are of equal importance.

#### 4.3.2 Self-Discharge Dynamics

Conservation of either the positive or the negative species of particles within a fixed volume  $V$  enclosed by the surface  $S$  can in general be represented by

$$\frac{d}{dt} \int_V n_{\pm} dV = - \int_V \phi_{\pm} dV - \oint_S \bar{\Gamma}_{\pm} \cdot \bar{n} da \quad (11)$$

where  $\bar{\Gamma}_{\pm}$  is given by Eq. (4.2.1) without the diffusion term and  $\phi_{\pm}$ , given by Eqs. (4) and (5), represents the particles lost due to discharge with particles of the opposite polarity. With Eqs. (4) and (5) representing the latter, for incompressible flow ( $\nabla \cdot \bar{v} = 0$ ) and with recognition taken of Gauss' Law, ( $\nabla \cdot \epsilon_0 \bar{E} = n_+ q_+ - n_- q_-$ ) Eq. (11) becomes

$$\frac{\partial n_{\pm}}{\partial t} + (\bar{v} \pm b_{\pm} \bar{E}) \cdot \nabla n_{\pm} = \frac{-n_- n_+ q (b_+ + b_-)}{\epsilon_0} \pm \frac{n_{\pm} b_{\pm}}{\epsilon_0} (n_+ q_+ - n_- q_-) \quad (12)$$

This expression includes both effects of self-discharge and self-precipitation. However, if the particles are injected into the system in pairs, or initial conditions preserve charge neutrality at each point within the volume and electrodes are not used to impose an ambient electric field, then space charge neutrality is maintained. This is seen by assuming at the outset that  $n_+ = n_- \equiv n$ ,  $b_+ = b_- \equiv b$  so that Eq. (12) reduces to

$$\frac{\partial n}{\partial t} + \bar{v} \cdot \nabla n = \frac{-2n^2 qb}{\epsilon_0} \quad (13)$$

and observing that Gauss' Law is then identically satisfied by  $\bar{E} = 0$  because  $n_+ q_+ - n_- q_- = 0$ .

Stationary System If the gas is at rest Eq. (13) becomes

$$\frac{\partial n}{\partial t} = - \frac{2n^2 qb}{\epsilon_o} \quad (14)$$

with a solution

$$\frac{n}{n_o(x)} = (1 + \frac{t}{\tau_a})^{-1}; \quad \tau_a = \frac{\epsilon_o}{2n_o(x)qb} \quad (15)$$

As anticipated by the discussion in Sec. 2.4, Eq. (15) states that if the particles are initially uniformly distributed, then the decay is of the same form as discussed for self-precipitation. In fact the time constant  $\tau_a$  is the same if it is defined in terms of the total charged particle concentration  $2n_o$ . If the initial concentrations have some spatial distribution, then the subsequent decay at a given point can be described by the above relation with a time constant based on the initial conditions at that point.

Convective Systems For fully developed flow in the z-direction so that  $\bar{v} = U(x,y)\bar{i}_z$  and steady-state conditions Eq. (13) becomes

$$U(x,y) \frac{dn}{dz} = - \frac{2n^2 qb}{\epsilon_o} \quad (16)$$

Unlike the situation for self-precipitation, no conditions on the particle concentration at  $z = 0$  are necessary to be able to find a solution to Eq. (16)

$$\frac{n(x,y,z)}{n_o(x,y)} = (1 + \frac{z}{\ell_a(x,y)})^{-1}; \quad \ell_a(x,y) = \frac{U(x,y)\epsilon_o}{2n_o(x,y)qb} \quad (17)$$

The implication is that the concentration along every particle line (x,y) will decay at rate determined by its concentration and the velocity at  $z = 0$ .

If the time constant  $\tau_a$  is based on the total charge concentration, slug flow

with a concentration that is uniform across the inlet gives rise to a self-discharge process that is described by an expression identical to the one for self-precipitation.

$$\frac{n(z)}{n_o} = \left(1 + \frac{z}{\ell_a}\right)^{-1} ; \ell_a = \frac{\epsilon_o U}{2n_o q b} \quad (18)$$

In experiments to be described in Sec. 4.9, the quantity measured is the fraction of the original flux of charged particles that remains at some position downstream. The flow for that experiment is modelled as plane Poiseuille (boundaries at  $x = \pm s/2$  and  $y = 0$ , where  $w \gg s$ )

$$U(x) = U_c \left[1 - \left(\frac{x}{s/2}\right)^2\right]; \quad U_c = \frac{3F}{2ws} \quad (19)$$

and the concentration is essentially uniform at the inlet. The volume rate of gas flow is  $F$ , while the total entering particle flux is given

$$\gamma_o = \int_{-s/2}^{s/2} w n_o U(x) dx = n_o F \quad (20)$$

Downstream the total particle flux becomes

$$\gamma = \int_{-s/2}^{s/2} w n(x, z) U(x) dx \quad (21)$$

After integration and normalization to the input flux, the fraction of the aerosol that has not been discharged at a location  $z$  downstream is found to be (Dwight, 1961)

$$\frac{\gamma(z)}{\gamma_o} = \frac{3}{2} \left( \ell_a \left| \frac{\sqrt{D} + 1}{\sqrt{D} - 1} \right| \frac{(1 - D)^2}{2\sqrt{D}} + \left(\frac{5}{3} - D\right) \right) ; \quad (22)$$



where 
$$D \equiv 1 + \frac{2n_o qbz}{\epsilon_o U_c}$$

This expression is compared to experimental results in Sec. 4.9.

#### 4.4 Generation of Monodisperse Submicron Aerosols

##### 4.4.1 Classification of Techniques

Several of the methods for producing monodisperse particles in the range of  $100\mu\text{m}$  in diameter can be modified to manufacture submicron aerosols (Browning, 1958). Perhaps the easiest is the dispersion of a powder. Besides being commercially available, there are several types of aerosols that occur naturally, such as lycopodium spores. The problem is to find a means of easy dispersal, because the presence of moisture and triboelectric charges causes the materials to cake. The dispersion difficulty can be overcome if the particles are mixed with a liquid to form a suspension, and the latter is atomized, and then heated until all the liquid has been evaporated. The difficulty here lies in guaranteeing that each droplet formed contains only one particle. If this is not true, the aerosol will be quite polydisperse. In addition, droplets that contain no particles will form residues after evaporation and contribute to the non-uniformity of the particle size distribution. There are also ways of controlling the atomization process of a pure liquid to produce uniform droplets, as through vibration of an orifice plate. Unfortunately, these methods become very difficult in the small size ranges desired.

There is a broad category of techniques, involving condensation, which work particularly well in this regime (Fuchs, 1966). Basically, they consist of vaporizing a material and then allowing it to recondense in a controlled manner. This is usually accomplished by allowing it to cool slowly in the

presence of condensation sites. If the latter were not included, the vapor would either condense on the walls of the container or, if the vapor became very supersaturated, would spontaneously recondense, forming a polydisperse aerosol. A device of this variety is used in the experiments and will be described in greater detail in the next section.

#### 4.4.2 Liu-Whitby Generator

This particular approach was first developed by Sinclair and LaMer (LaMer, Inn, and Wilson, 1950). Their method was considerably simplified by Rapaport and Weinstock (1955) and still further refined by Liu and Whitby (Liu, Whitby and Yu, 1966; Tomaides, Liu and Whitby, 1971). In its present version (Figs. 4.4.1 and 4.4.2), the process begins with the atomization of a solution of a very volatile material and a relatively involatile one. In these experiments the former was selected to be ethyl alcohol and the latter dioctylphthalate. This dispersion is accomplished with a collision atomizer (Green and Lane, 1965), which produces an aerosol in the range of about a micron in diameter. The particle laden gas then passes through a heated zone with the temperature adjusted so that all the material is vaporized. The vapor laden gas then passes through a drift zone where it slowly recondenses onto sites corresponding to the impurities in the original solution that remained after the evaporation of each drop. This process is not uniform across the channel, as can be seen from the conical condensation zone. This tends to cause the particles near the wall to be slightly different in size from those in the middle (Nicolaon, Cooke, Dans, Kerker and Matijevic, 1971). If an especially monodisperse aerosol is desired, just the central region should be sampled and the remainder discarded. The size of the particles produced can be varied by altering the

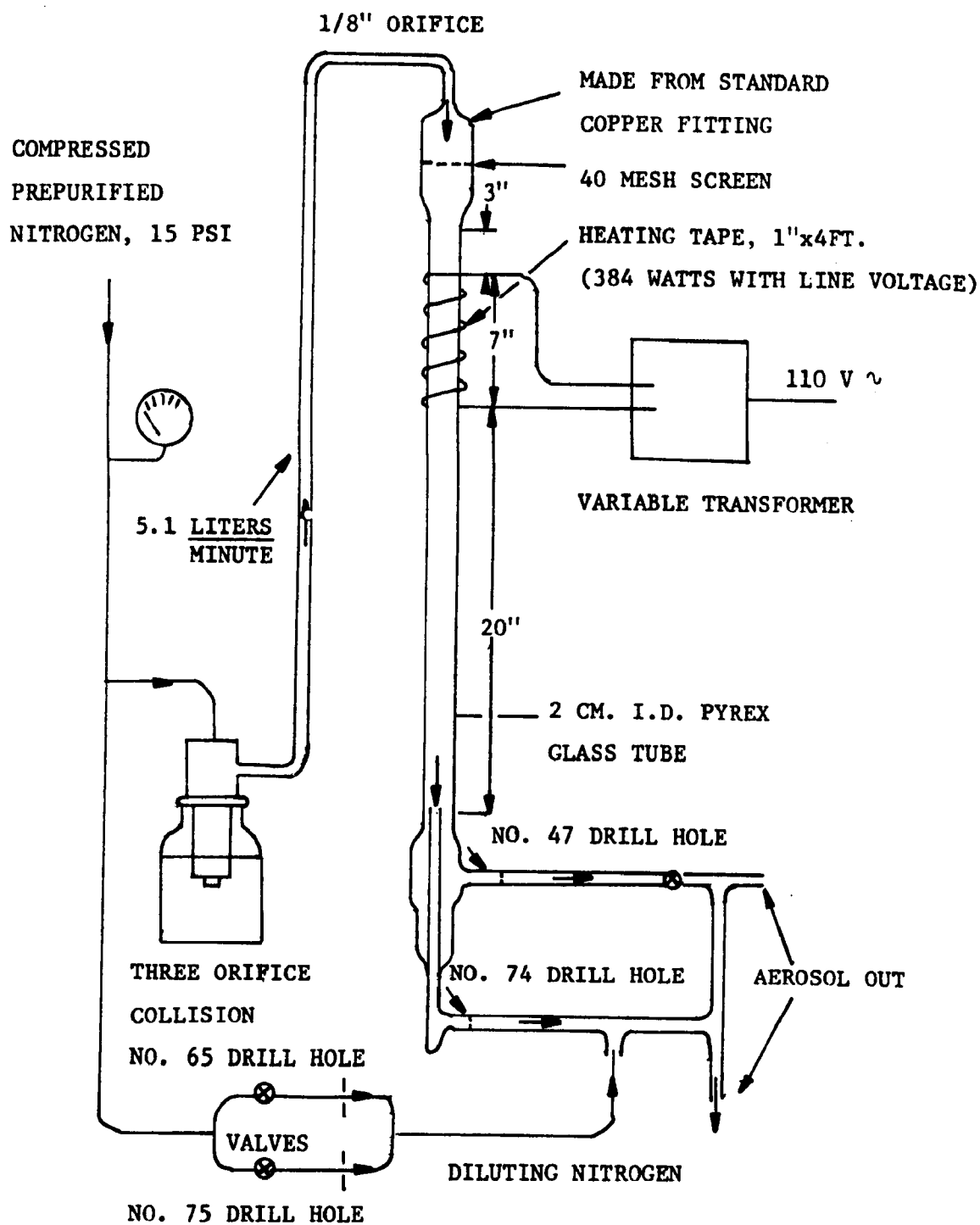


Fig. 4.4.1 Monodispersed aerosol generating system (Liu, Whitby and Yu, 1966)

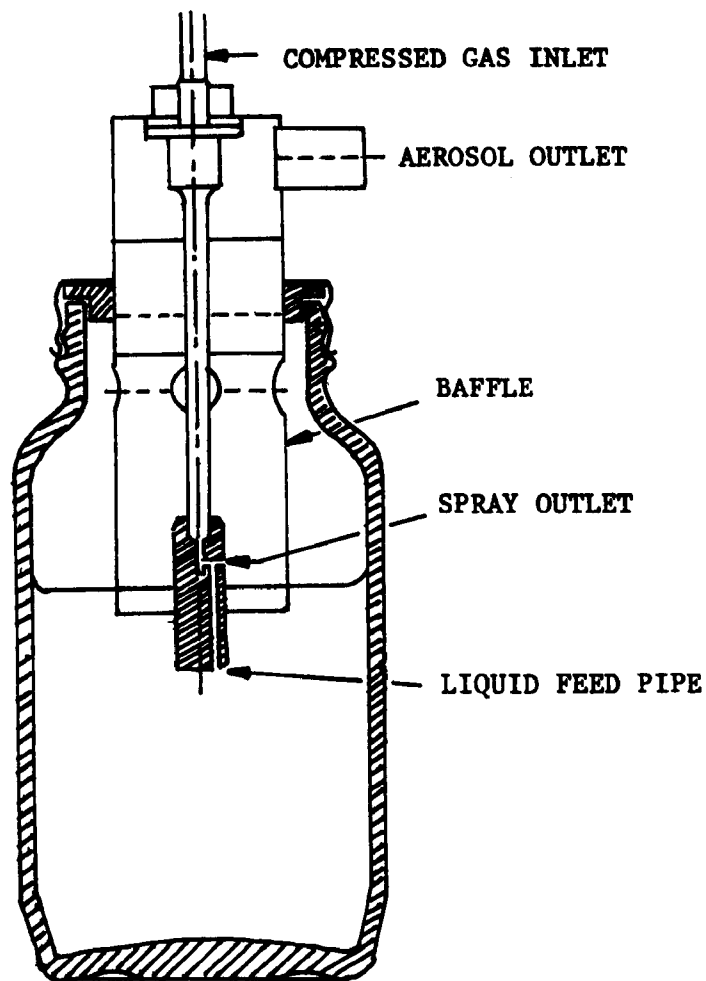


Fig. 4.4.2 Collision atomizer (Liu, Whitby and Yu, 1966)

percentage of DOP in solution from a maximum of about  $1\mu\text{m}$  in diameter when pure DOP is used. This variation of size with concentration and the recommended heater voltages are given in Fig. 4.4.3 for the device described by Liu and Whitby. These should serve as an estimate only. Methods for checking the actual size of the particles produced in a given situation will be discussed in Sec. 4.5.

The device requires approximately 15 minutes to warm up and operates quite stably and reproducibly over extended periods of time if certain

precautions are taken. First, the solution will tend to degrade over a period of time, resulting in a polydisperse aerosol. The presence of water hastens this process. For this reason the solution cannot be stored for prolonged periods, and pure ethyl alcohol, rather than denatured alcohol, should be used. It is important that the aerosol should not be overheated. The proper value of the heating tape voltage can be determined by setting the pressure at the desired level and examining the Tyndall spectra of the output as the voltage is raised. The aerosol will appear polydisperse for voltages too low and too high. As indicated, the size is determined principally by the percentage of DOP in solution. However, the velocity at which the aerosol flows through the heating and condensation zones, hence the pressure applied to the atomizer, is also an important factor. Any time that the pressure is altered to change the aerosol flow rate, the heater voltage will have to be reset, and the size of the particles should be rechecked. The curve of Fig. 4.4.3 should be regarded as approximate, and the size checked from the Tyndall spectra prior to each experiment.

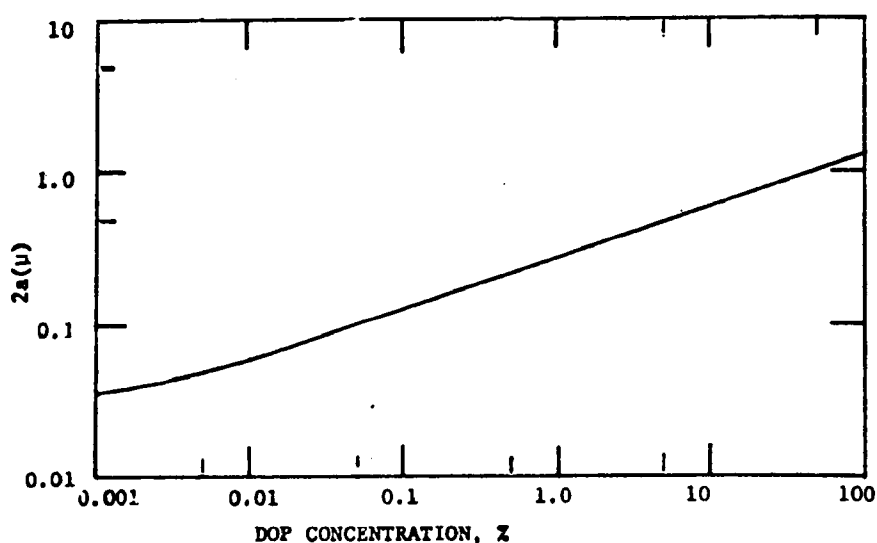


Fig. 4.4.3 Calibration curve showing the variation of the number median diameter of the aerosol with the volumetric concentration of DOP in the atomizer

#### 4.5.1 Light Scattering by Small Particles

Since the particles produced by the generator are so uniform in size, relatively simple optical methods can be employed for sizing. The procedures to be described are relatively uncomplicated and can be included in the start-up operation of the system. Before these methods are described in detail, it would be helpful to review several general aspects of the phenomena. The problem is usually posed in the following way (Fig. 4.5.1) (Van De Hulst, 1962). Monochromatic light of wavelength  $\lambda_\ell$  is incident on a sphere of radius  $a$  and refractive index  $n_\ell$ . A plane of polarization is then defined by the incident and scattering directions. The incident radiation is resolved into two perpendicular components, one in the plane,  $E_{o1}$ , and the other perpendicular to it,  $E_{or}$ . The light scattered can then also be resolved into a parallel and a perpendicular component. The first is a function of only  $E_{o1}$ , and the second just of  $E_{or}$ . In terms of the amplitude of the incident radiation and its orientation to the scattering plane, the scattered far-field can be expressed as

$$\frac{E_{sr}}{E_o} = \frac{S_1(\theta)}{jkr} \cos\phi e^{j(kr-\omega t)}; \quad \frac{E_{sl}}{E_o} = \frac{S_2(\theta)}{jkr} \sin\phi e^{j(kr-\omega t)} \quad (1)$$

Many radii away from the particle, these fields decay inversely with the distance from the sphere, independent of the particle size. The angular dependence is, however, a strong function of the size and the physical nature of the particle.

If the particle is very small compared with the wavelength of the incident radiation, the scattering is termed Rayleigh. In that case the

perpendicular component leads to uniform scattering and the parallel component to a variation that equals the perpendicular in the forward and backward directions, but decays to zero in directions perpendicular to the direction of the incident beam. For reference, the scattering functions are:

$$S_1(\theta) = j\alpha_l^3; S_2(\theta) = j\alpha_l^3 \cos\theta; \alpha_l \equiv \frac{2\pi a}{\lambda} \quad (2)$$

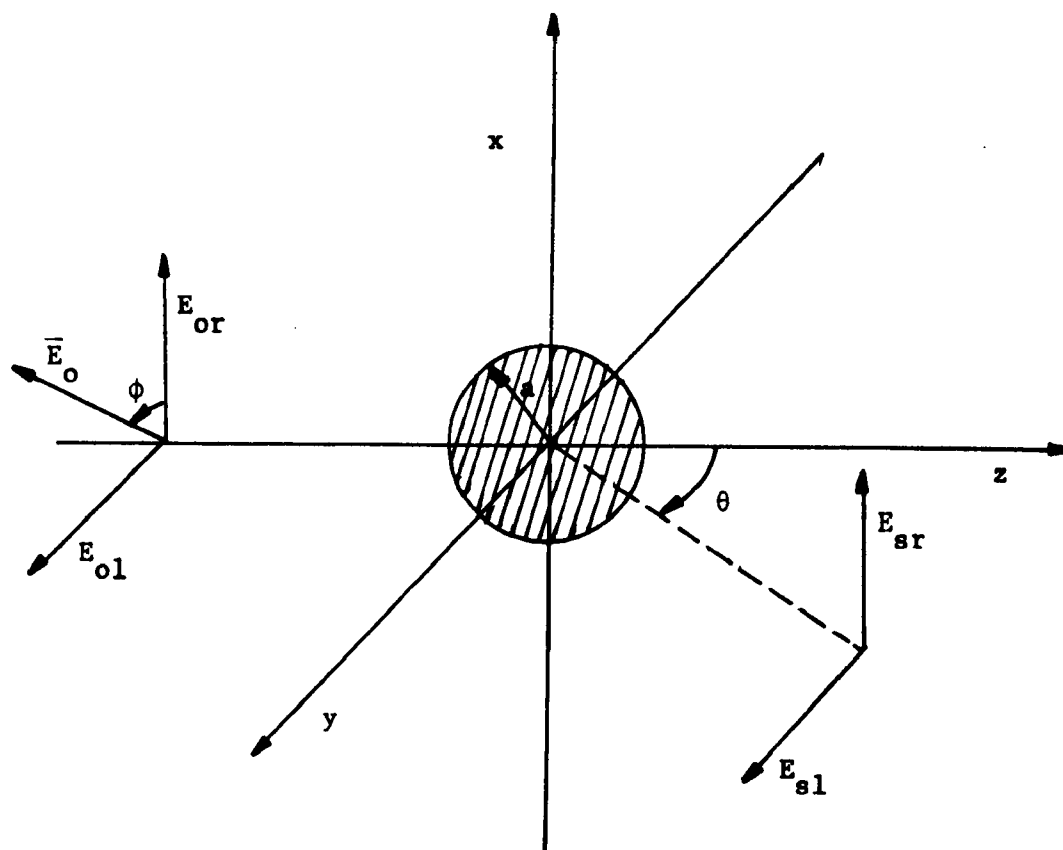


Fig. 4.5.1 Light scattering from a single sphere

As the particle size increases and becomes comparable with the wavelength of the radiation, the scattering is classified as Mie. The patterns begin to acquire structure, as evidenced by the development of lobes in several directions, with the major peaks occurring in the forward and backward directions. The number and position of these peaks is strongly dependent

on the ratio of the circumference of the particle to the wavelength of the light,  $\alpha_p$ , and the refractive index of the droplet material,  $n_p$ . As the radius increases further, much of the scattering is concentrated within a steadily decreasing angle about the forward direction. This is termed the diffraction limit, because the pattern in the forward direction begins to resemble the Fraunhofer pattern for light incident on a disk or a circular aperture:

$$S_1(\theta) = S_2(\theta) = \frac{\alpha^2 J_1^2(\alpha \sin \theta)}{\alpha \sin \theta} \quad (3)$$

Since the size of the submicron particles of interest is commensurate with the wavelength of visible light, optical techniques can be used to take advantage of the complex Mie patterns produced. In fact, it is possible to accurately size an aerosol from about 0.1 to about 1.0  $\mu\text{m}$  in diameter.

#### 4.5.2 Higher Order Tyndall Spectra

If instead of monochromatic light, a distribution of wavelengths, as emitted from an incandescent source, is incident upon these submicron particles, it follows that the scattering will be the superposition of many patterns, each attributable to a different wavelength. As noted previously, the patterns will in general have peaks in different locations, except in the forward and the backward directions. Physically, this implies that if white light is directed at the particle, the scattered light will appear colored. The larger the particles, the greater the number of peaks in the patterns and consequently, the more times the spectra orders are repeated. By noting the position and the number of peaks of a selected color, an estimate can be made of the size (Sinclair and LaMer, 1949; Kitani, 1960). To quantify this, the scattering patterns for all the wavelengths in this range



can be evaluated. The approach that is usually taken is the following. Red ( $\lambda_r = 0.629\mu\text{m}$ ) is selected as the color, and its pattern calculated numerically (Gumprecht and Sliepcevich, 1951; Zahedi, 1974), as well as that for green ( $\lambda_g = 0.524\mu\text{m}$ ). The latter is chosen because the eye is most sensitive to this wavelength, and, since both colors are contained in the incident radiation, the scattered red radiation must be at least as large as the scattered green to be seen as red. The peaks in this ratio are the angles at which red will be seen. The variation of these angles for DOP ( $n_l = 1.486$ ) is shown in Fig. 4.5.2. The circled points indicate situations in which a peak exists but has a magnitude less than one. Thus, the scattered radiation appears green.

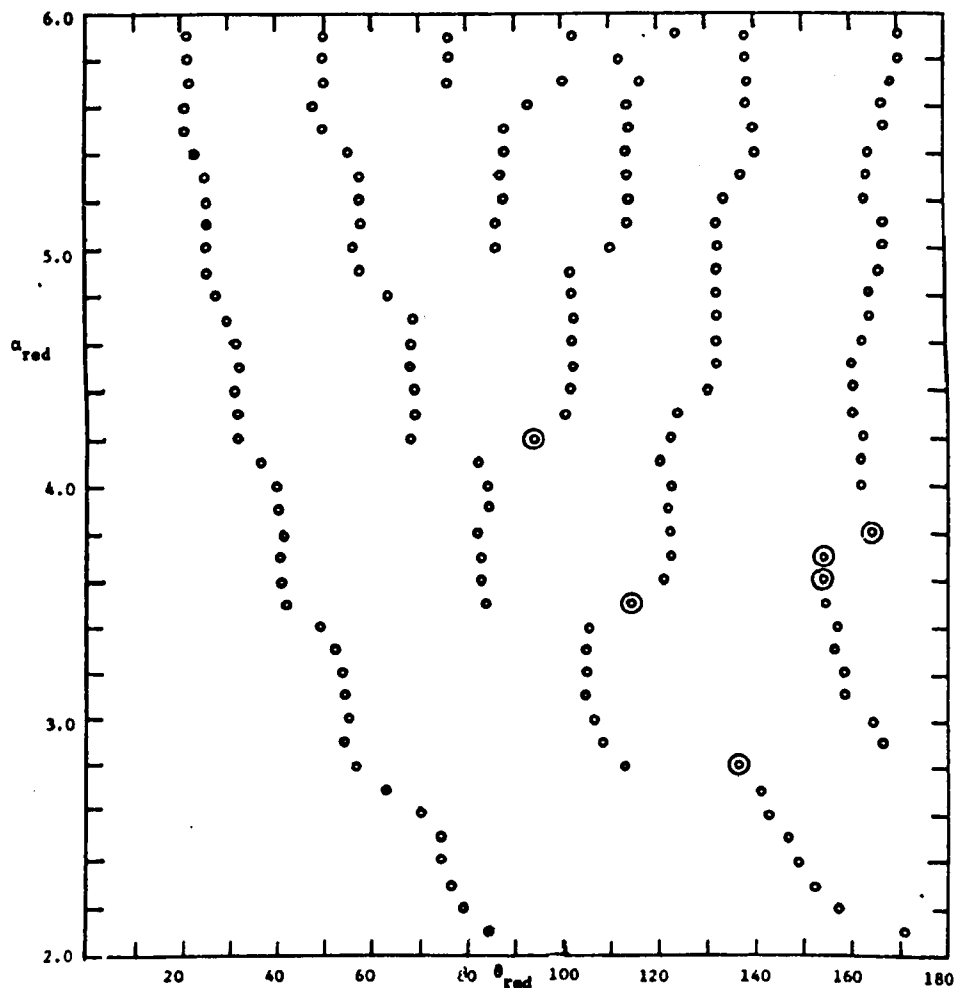


Fig. 4.5.2 Tyndall red angular positions for DOP. Each point is numerically calculated. Circled points indicate a peak, but for which the ratio of red to green is less than unity.

The apparatus used is deceptively simple (Fig. 4.5.3) (LaMer and Sinclair, 1943). It consists of a sealed chamber with inlet and exit ports and an observation window. Light from a high intensity incandescent bulb is made parallel by a lens and focused across the chamber into a light trap on the other side. The entire structure is then rotated past the observation point. Because the incident light is unpolarized, the patterns of the parallel and the perpendicular components are superimposed.

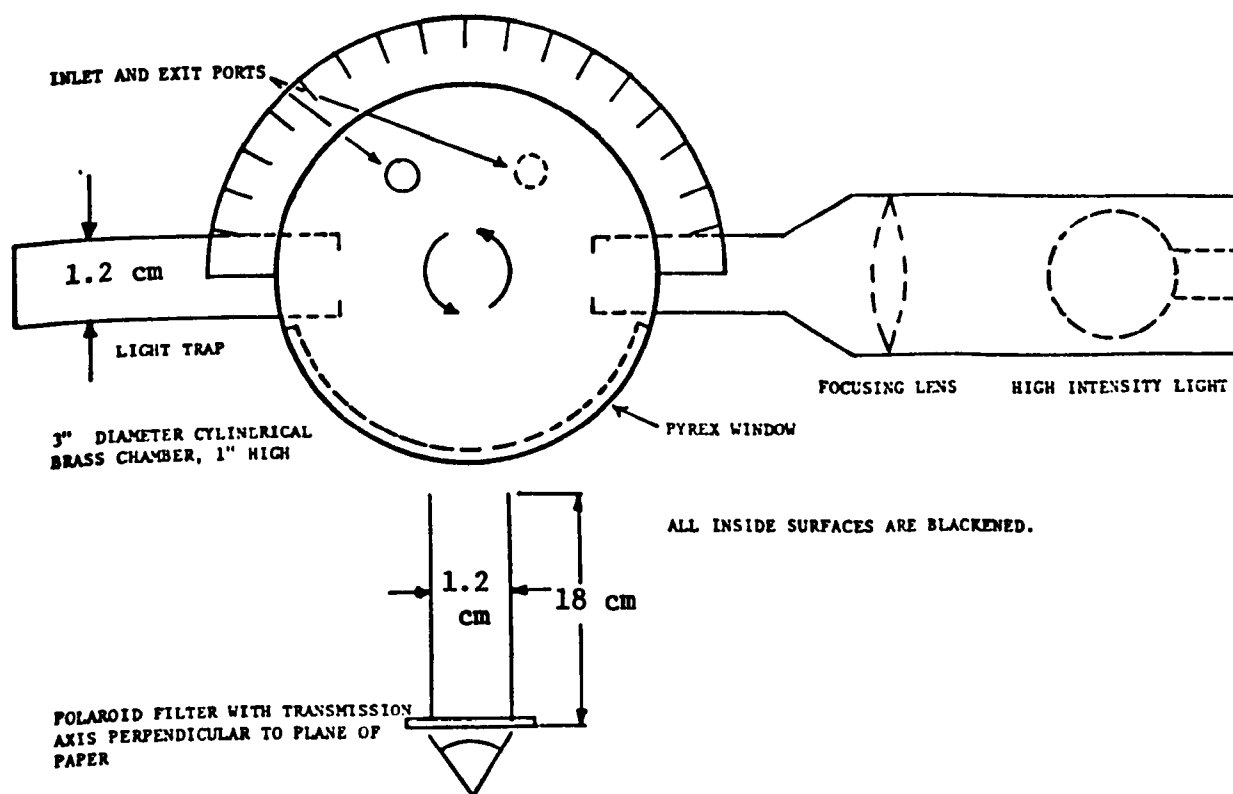


Fig. 4.5.3. Tyndall spectra observation device ("Owl")

A polaroid filter is used to select just the perpendicular component since this usually leads to a sharper pattern. In a typical experiment the angles corresponding to the reds are noted and then sought in the calibration curve of Fig. 4.5.2. As can be seen from the figure, the curve does not vary

smoothly but advances in jumps. This sets a limit of the order of a few hundredths of a micron on the resolution attainable with this method. Due to the overlapping of the patterns for an aerosol that is not precisely homogeneous, there is an upper limit on the size. If  $\alpha$  becomes less than about 2, the pattern starts to resemble the Rayleigh case. The peaks broaden to such an extent that it becomes almost impossible to localize them. In this region it is usually necessary to employ the method relying upon the polarization ratio, to be described in Section 4.5.3. If no colors are visible in the scattered radiation, only a diffuse white light, the aerosol is polydisperse. The two most frequent causes are incorrect heating in the generator and a decomposed solution. If properly adjusted, the generator will always produce an aerosol which exhibits Tyndall spectra. The colors will not be deep reds, blues, and greens, but will be somewhat dampened. The reds, for example, will appear a bright pink. For this reason the method requires some practice and patience, and must usually be performed in a darkened room.

#### 4.5.3 90° Scattering Ratio

In the event that the particle size is so small that the location of the single red occurring near 90° becomes unresolvable, the polarization ratio can be used in some cases to give an estimate of the particle radius (Heller and Tabibian, 1962; Maron, Elder and Pierce, 1963; LaMer and Sinclair, 1943). If unpolarized light is incident upon the sphere, then the ratio of the intensity of the parallel scattered radiation to the perpendicular portion leads to a curve as given in Fig. 4.5.4 for DOP. For very small radii the ratio approaches zero, as is expected from the previous discussions of Rayleigh scattering. For a given wavelength, the ratio at first increases

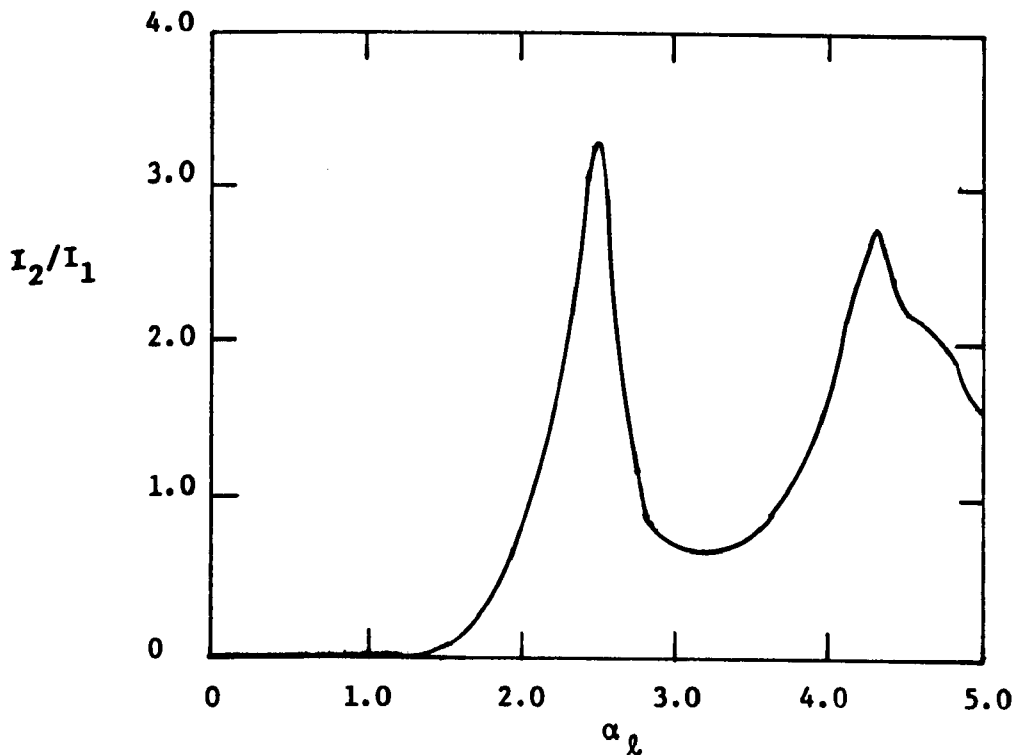


Fig. 4.5.4 90° scattering ratio for DOP

with radius, until it reaches some maximum value and then begins to oscillate. Since a value of the ratio does not necessarily correspond to a unique value of the radius, additional information giving a rough estimate of the size is usually required. For this generator the calibration curve of the radius versus DOP concentration is usually sufficient. Even with this information it is difficult to deduce the correct average radius from some measurements. Any real aerosol will be distributed over a range of sizes. In the case of the Tyndall spectra this does not cause irreparable harm, because the calibration curve varies relatively slowly. Here, however, even a relatively small standard deviation of the particle size distribution can cause significant errors, first because the ratio varies very rapidly with  $\alpha$  in some regimes, and secondly because it oscillates as  $\alpha$  ranges over a fairly

small spectrum.

In spite of its shortcomings the method does give valuable information relatively easily. Experimentally, the technique is straightforward. Unlike the Tyndall approach, the wavelength here is fixed. This means that a laser is used as the light source. If the laser is polarized, then it is usually most convenient to orient the polarization vector at  $45^\circ$  with respect to the scattering plane. (It should be noted that some lasers that claim to be unpolarized actually are polarized. Even worse, this polarization oscillates at a relatively slow frequency (1 Hz) between two perpendicular directions and is especially inconvenient experimentally.) The aerosol is injected into a blackened chamber (Fig. 4.5.5) together with a second source of clean air. This accelerates the aerosol into the single outlet and produces a stable filament. The intersection of the laser beam and the filament defines a relatively small scattering volume. The detector is usually a photomultiplier tube with a polaroid filter covering its input. The tube is placed far enough away from the scattering volume that the solid angle intercepted by the detector is relatively small ( $1.5 \times 10^{-3}$  steradian). In performing a measurement the polaroid is oriented first in the plane and then perpendicular to it, and the ratio between the two measurements formed. One other precaution should be taken. In some cases the photomultiplier tube will have different responses to the different polarizations. This point should be checked before any data is taken.

#### 4.5.4 Extinction

If a parallel beam of light passes through a region containing aerosol particles, then the amount of power remaining in that portion of the beam propagating in the forward direction will diminish according to

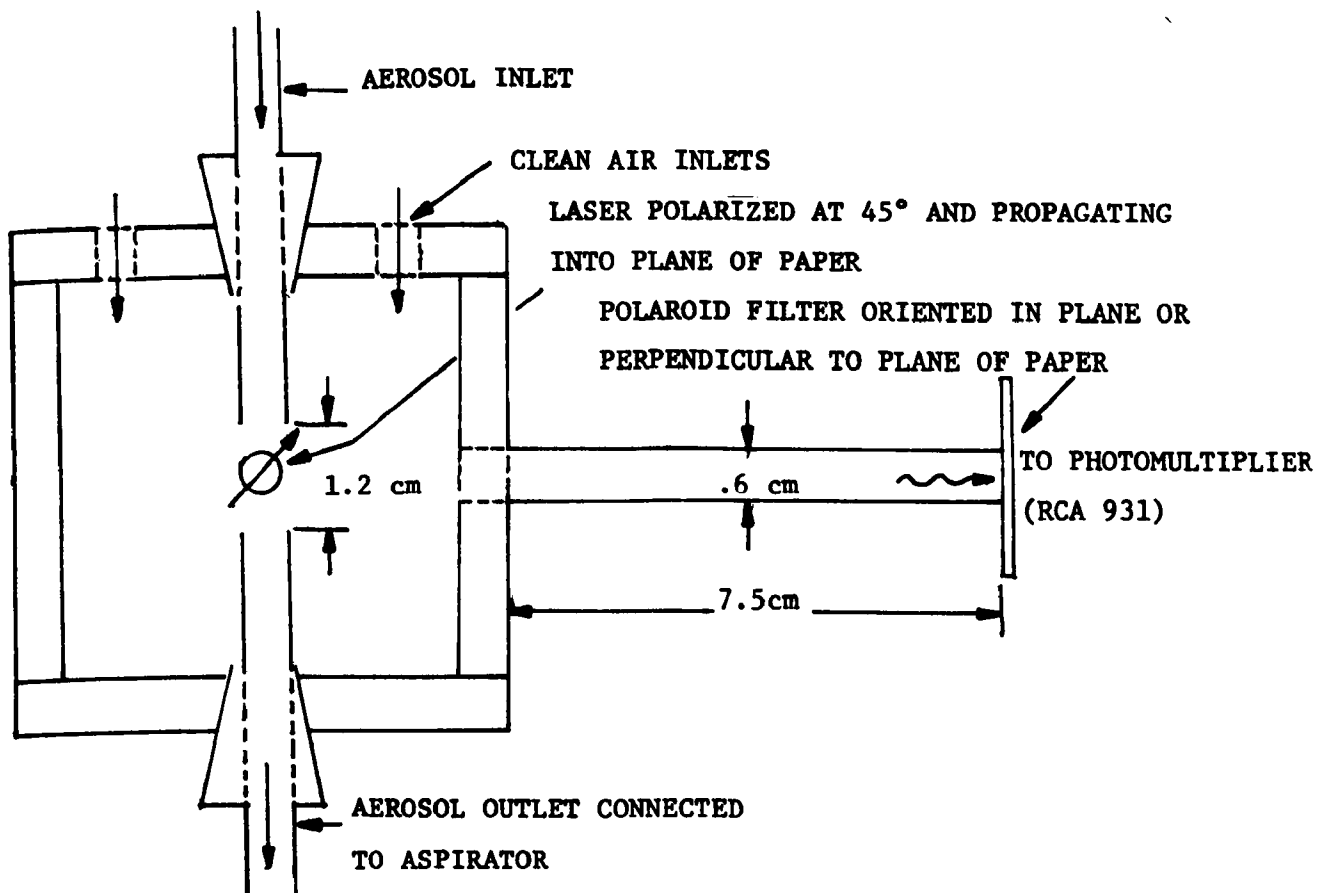


Fig. 4.5.5 90° scattering apparatus

(Lothian and Chappel, 1951):

$$\frac{I(L)A_b}{I(0)A_b} = \exp(-nK_s \pi a^2 L) \quad (4)$$

where  $A$  is the cross-sectional area of the beam and  $I(z)$  its intensity. In the limit of small concentrations and short path lengths, this can be approximated by

$$\frac{I(0) - I(L)}{I(0)} = nK_{sl} \quad (5)$$

A condition for the application of these relations is that the particle concentration be dilute enough for secondary scattering to be ignorable. One criterion for this is that the particles be separated by at least 100 radii (LaMer and Sinclair, 1943). For aerosols produced by the Liu generator, this will always be true. If the size of the particles is known, then such

a measurement will yield the particle concentration upon evaluation of the extinction coefficient  $K_{sl}$ . As with the previous scattering parameters,  $K_{sl}$  is a function of  $\alpha_l$  and  $n_l$ . Such a variation is given in Fig. 4.5.6 for the case of DOP.  $K_{sl}$  increases from zero to a rather broad maximum in the range of  $\alpha$  from 3 to 5, and then begins to oscillate. If the curve were extended to very large  $\alpha_l$ , the extinction coefficient would be seen to approach a limiting value of 2. Thus particles very large compared to the wavelength scatter twice as much light as is incident upon an area corresponding to their geometrical cross section.

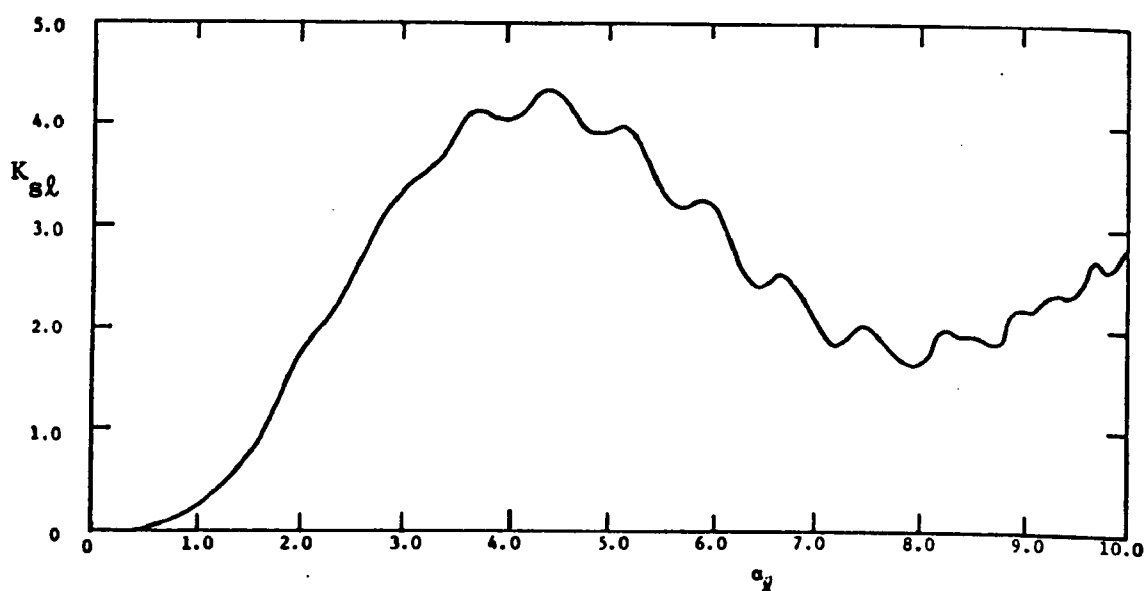


Fig. 4.5.6 Extinction coefficient for DOP spheres as a function of  $\alpha_l$

If the particles are not monodisperse or the radiation not monochromatic, then an appropriate averaging procedure must be used. Fortunately, there is a range of  $\alpha_l$  for which  $K_{sl}$  is relatively constant. By using a laser as a light source and using particles monodisperse enough to exhibit Tyndall spectra, the variation of  $\alpha$  can be made to lie within this band.

The above relation also contains the conditions that the incident beam be parallel, i.e., have no divergence, and the detector be sensitive to only the forward traveling radiation. One method of accomplishing this with a point source is shown in Fig. 4.5.7. If a laser is used, the condition on the incident beam is well satisfied even without the use of a pinhole and lens arrangement. However, such is not the case with the detector. Depending on the acceptance angle of the detector,  $\theta_d$ , the value of the coefficient  $K_{sl}$  to be used in interpreting experimental results may have to be modified (Brillouin, 1949). For a finite angle, radiation will be detected which the above calculation assumes to be scattered. For visible wavelengths and submicron particles this effect can usually be ignored if the detector angle is less than about 5 degrees. If the  $\alpha_l$  is large ( $\alpha_l > 50$ ), then to exclude all the scattered light the detection angle must be extremely small ( $\theta_d < \frac{1}{\alpha_l}$ ).

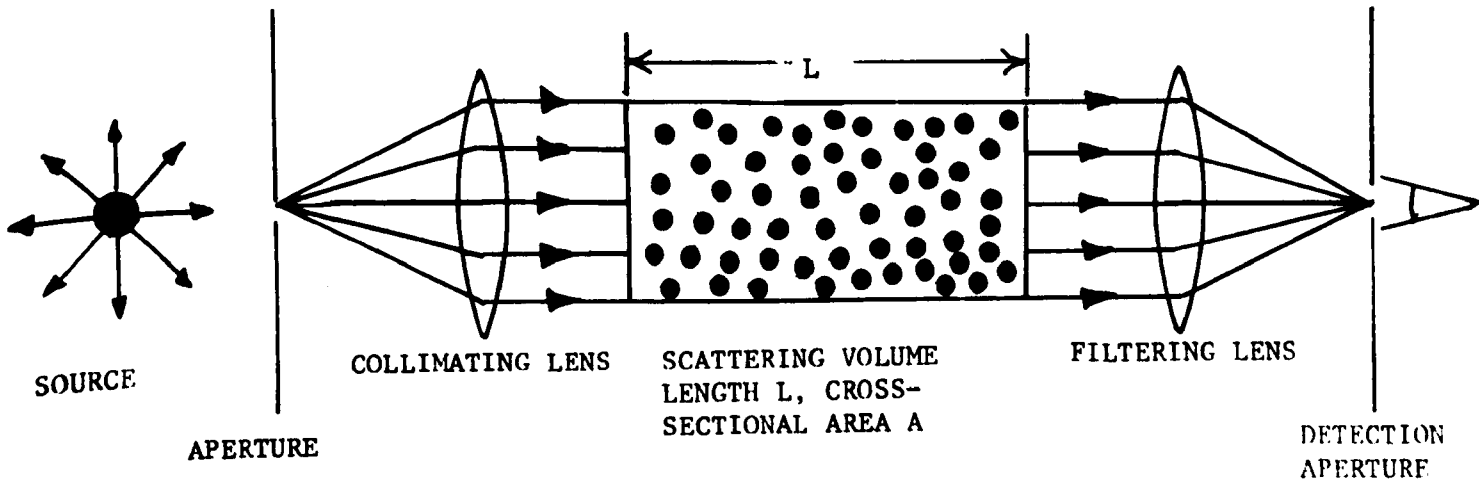


Fig. 4.5.7 Light extinction system for a divergent light source

There also exists the alternative of using a large enough angle to include the diffracted portion of the scattered light corresponding to the central lobe ( $\theta_d \sim \frac{10}{\alpha_l}$ ). In this case the correct value of the coefficient would



be approximately one. Finally, if the width of the cell is made sufficiently small compared with its length, then the detection angle over most of the cell will be smaller than the limiting value without the use of a lens and a pinhole.

The experimental system appears in Fig. 4.5.8. Light from a polarized Helium-Neon laser passes first through a beam expander and then through a polaroid filter. The first allows easier alignment of the beam and the axis of the extinction cell, and the second serves as an attenuator. The light is then split and passed through the two cells, blackened on the inside to prevent reflection of the scattered light. The detection angle is therefore small. During operation one cell contains the aerosol and the other serves as the reference. With no aerosols the outputs of the two phototubes are equalized. The difference between them corresponds to the amount of the light scattered by the aerosol from the beam. The use of a differential signal also serves to significantly reduce the noise associated with a slow variation ( $\sim 1$  Hz) in the laser output. Prior to any experiment the reference signal is measured, since a coating of oil will form over the light entrance and exit ports, reducing the incident radiation from its initial value. For this reason the measurements should be performed relatively rapidly, and each should be followed by a flushing of the system with clean air. The length of the cells should be selected so as to allow enough attenuation for the absorption or transmission to be accurately determined. In this apparatus the option of either a 7.5 cm or a 30 cm-inch cell provides sufficient flexibility.

#### 4.6 Ionic Charging of Submicron Aerosols

##### 4.6.1 Diffusion and Impact Charging

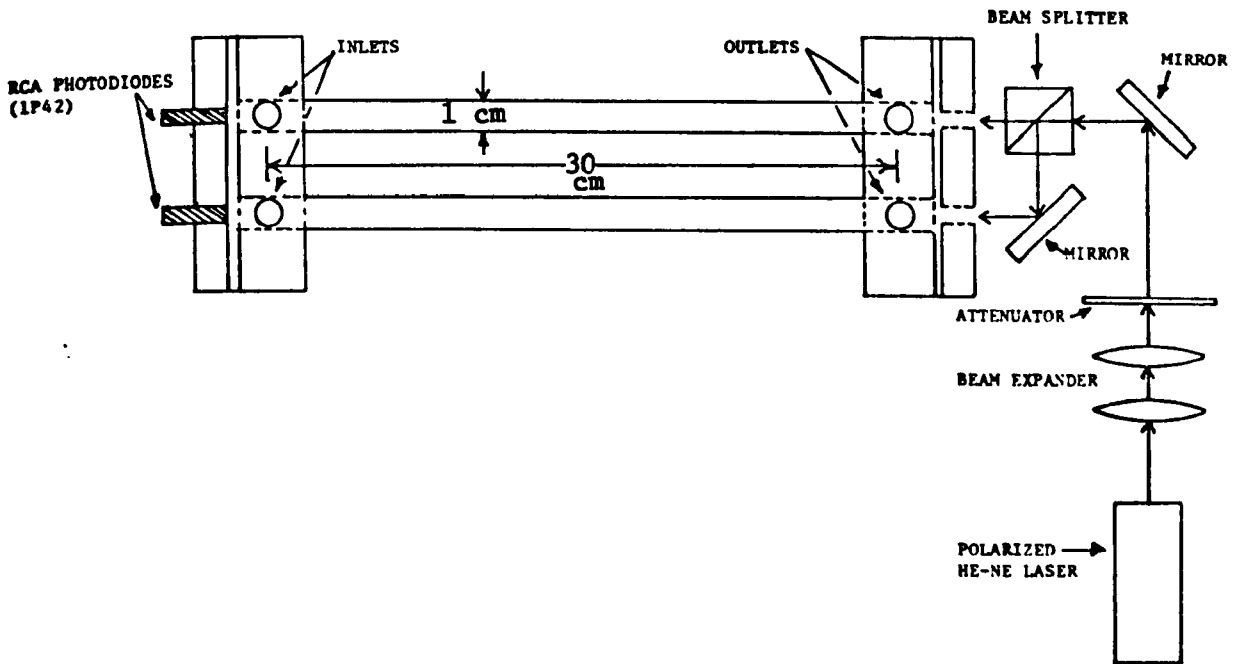


Fig. 4.5.8 Light extinction system for a laser light source and a detector aperture determined by cell dimensions

Two models have been developed which fairly accurately describe the limiting processes by which particles are charged if exposed to an ionic atmosphere (White, 1963, p. 126). In the absence of an ambient electric field, diffusion of the ions onto the surface will lead to an accumulation of charge according to

$$q = \frac{4\pi\epsilon_0 a kT}{e} \ln \left( 1 + \frac{C'' a e^2 n_1 t}{4\pi\epsilon_0 kT} \right); \quad C'' = \sqrt{\frac{kT}{m}} \quad (1)$$

where  $n_1$  is the ion density far away from the sphere,  $T$  is the temperature,  $e$  is the unit electron charge ( $1.6 \times 10^{-19}$  coul),  $k$  is Boltzmann constant ( $1.381 \times 10^{-23} \frac{\text{m-nt}}{\text{deg C}}$ ), and  $a$  is the radius and  $m$  the mass of the sphere. The ions are assumed to carry one unit of charge. As charge is collected, the charging rate will continuously decrease, never, however, becoming zero.

If there is an ambient electric field,  $E_c$ , present, the mechanism is

termed impact charging. Depending upon their polarity, ions will flow onto the sphere at points where the field points either in or out. If the particles are considered to be perfect conductors, the charging of the sphere proceeds as

$$\frac{q}{q_c} = \frac{4t/\tau_i}{(1+4t/\tau_i)} \quad ; \quad \tau_i \equiv \frac{\epsilon_o}{n_i e b_i} \quad ; \quad q_c \equiv 12\pi\epsilon_o a^2 E_c \quad (2)$$

It is evident that after several time constants have elapsed, the charge on the sphere becomes relatively constant. The calculations above have assumed that the sphere is at rest. If this is not true, the velocity of the sphere must be compared to that of the ions in the ambient electric field to determine precisely which charging equation should be used or, indeed, whether there will be any charging at all. (See Sec. 6.2.1 for a detailed discussion.)

In an actual device both mechanisms are present. However, for very small particles diffusion is the primary mechanism, and for large ones it is impact. The particle size at which these effects are commensurate depends on the strength of the ambient field. For the relatively large charging fields used here, the crossover point occurs at radii on the order of about 0.1  $\mu\text{m}$ . Upon specification of the particle size and charge, the particle mobility can be calculated. Experimental corroboration of these models has been given by Hewitt for submicron DOP aerosols (Hewitt, 1957).

#### 4.6.2 High Efficiency Charger for Submicron Aerosols

The device used is a modified version of the design cited by Langer et al. (1964) (Fig. 4.6.1). It consists of a small plexiglass box with two inlets and one outlet. The aerosol enters the charging region through the lower glass tube. To minimize the effects of the ionic wind, the diameter

is selected so as to produce an aerosol velocity of at least 10m/sec in the charging zone. Upon the outlet is soldered a metal washer at a 45-degree angle. The source of the ion flux is a small loop of platinum wire bent slightly and positioned so as to be equidistant from the outer edge of the washer. This guarantees that ions will be drawn just from the tip of the loop and will flow so as to intersect the aerosol stream. The resistors are added to stabilize the corona. If air is used for both the generator and the accelerating gas, the voltage-current relations for the positive and negative corona will be similar. In this experiment prepurified nitrogen is used. This leads to a positive corona very similar to that using air, but a negative one which exhibits a current which increases much more rapidly with voltage. This is attributed to the increased mobility of the negative ions in such a gas, on the order of  $1.45 \times 10^{-2}$  as compared with  $1.28 \times 10^{-4}$  for the positive ones (Cobine, 1958, p. 38). Use of a much larger resistor, however, allows control over this current.

To start up, the aerosol is turned on and sufficient clean gas introduced to produce a stable filament. The voltage is then set at a value slightly greater than that necessary to initiate the corona. This is usually in the range of 6 to 10 kV with currents of a few microamperes. The amount of accelerating gas may then have to be increased to regain a stable filament. If much higher currents are used, the amount of accelerating gas needed will result in considerable dilution of the aerosol. The position of the corona loop is then adjusted so that the ionic flux causes the aerosol stream to be depressed slightly. This assures that all of the aerosol is exposed to the ions. If adjusted as suggested, the charger will operate stably and reproducibly for extended periods. When shutting down, the aerosol should be

first turned off, then the accelerating gas and corona. When starting up again, the reverse order should be used. This will minimize the contamination of the wire. To be certain that the corona is always operating properly, a high intensity beam of light is focused on the charging zone. If the stream appears to fluctuate or back corona is seen on the washer, the charger should be shut down and cleaned. This involves washing the outlet tubing with alcohol and briefly placing the corona loop in a small flame to heat it to incandescence. This burns off any oil that may have been deposited. The device should then be reassembled and recalibrated.

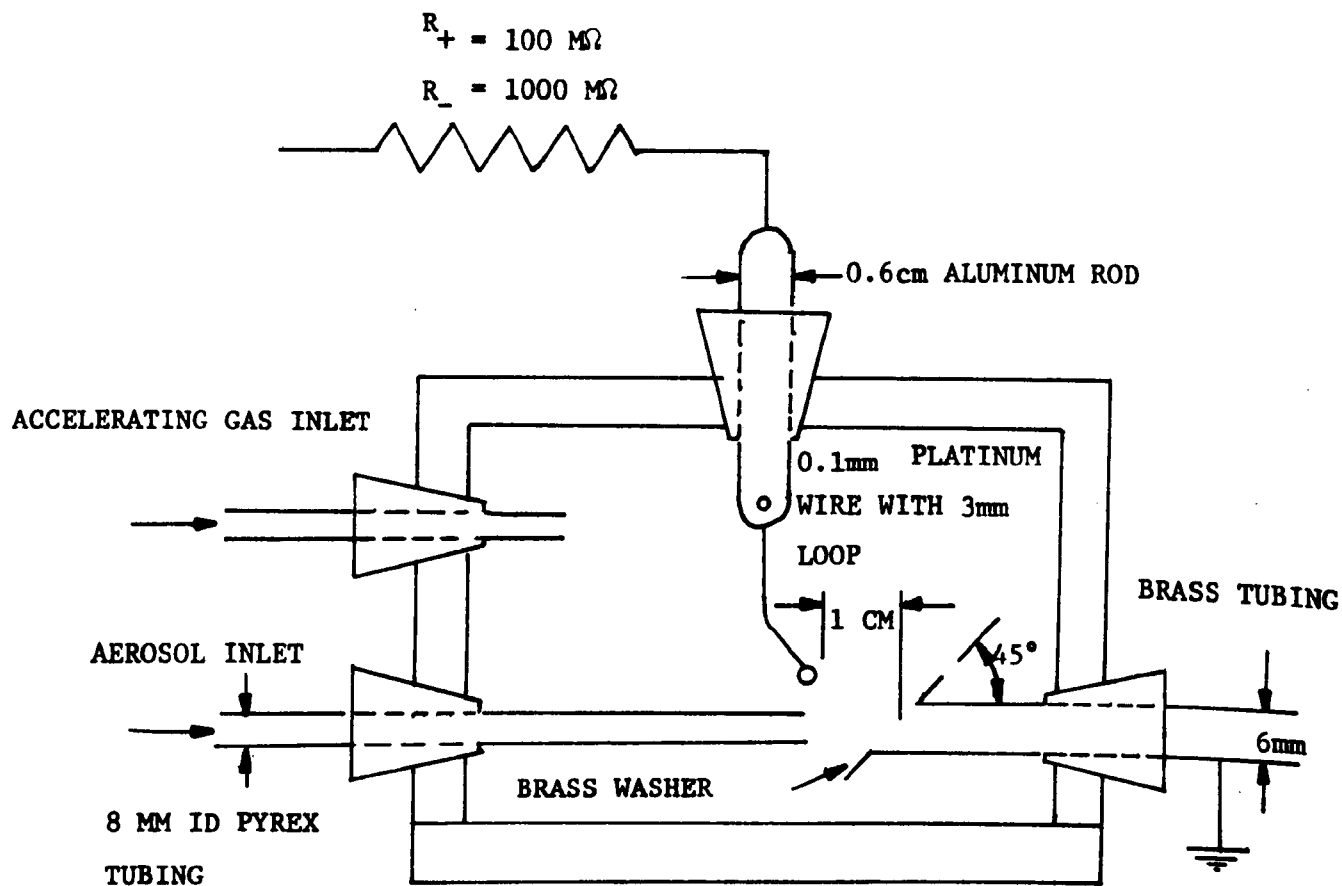


Fig. 4.6.1 Aerosol charger showing alternative resistors for positive and negative charging

## 4.7 Analysis of Submicron Aerosols for Charge Density and Mobility

### 4.7.1 Imposed Field Analyzers

To ascertain the electrical properties of the aerosol, the charged stream is passed through an analyzer. Two types used in the experiments of this and the next two chapters are shown in Fig. 4.7.1 (Tammet, 1970). The radial flow configuration (Hurd and Mullins, 1962) with the additional feature of air injection to prevent contamination, is particularly useful in dealing with the DOP, because precipitation on the walls results in an appreciable leakage current unless the conduction path is broken by a surface that remains free of contamination.

By an imposed field analyzer it is meant that the electric field associated with the applied voltage  $V$  between the electrodes (in either system) is much larger than that due to the space charge of the aerosol. In that case, Eqs. (4.2.5) and (4.2.6) are approximated by ignoring the space charge term (proportional to  $n^2$ ) and taking the electric field as being  $-V/s$  in the  $x$  direction. (Of course, diffusion is also ignored.)

$$\frac{dn}{dt} = 0 \quad (1)$$

$$\frac{d\bar{r}}{dt} = b\bar{E} + \bar{v} = -b \frac{V}{s} \bar{i}_x + \bar{v} \quad (2)$$

Thus, the particle density  $n$  is constant along particle trajectories, and these trajectories are found from a known  $\bar{E}$  and  $\bar{v}$ . The volt-ampere characteristic of the analyzer can be found without recourse to the specifics of the velocity profile provided that the particles can be taken as uniformly distributed with density  $n$  over the cross-section in the entrance region of the analyzer. The trajectory of a particle starting at the entrance surface

position (a) in Figs. 4.7.1a and 4.7.1b will either be intercepted by the current collecting bottom electrode or it will pass out of the system. As a function of voltage, the volt-ampere characteristic divides into two regions. At low voltages, only a fraction of the particles are collected. Those entering above a critical value of  $x$ ,  $x_0$ , are not collected while those below are. To compute the total current collected in this region of  $V$  observe from Eqs. (1) and (2) that the particle density is constant along all of the trajectories which terminate on the collecting electrode because these emanate from the entrance region  $x < x_0$  where  $n = n_0$ . Hence, in this part of the characteristic,

$$I = - \int_A nqbE_x da = \int_A \frac{nqbV}{s} da \quad (3)$$

where the integration is over the area of the collecting electrode. With the multi-electrode system of Fig. 4.7.1a,  $A$  is the total area of the collecting surface. The velocity makes no contribution to the integration because it is zero at the electrode. Because  $n = n_0$  at all positions on the electrode, Eq. (3) becomes

$$I = \left[ \frac{n_0 qbA}{s} \right] V \quad (4)$$

With the voltage raised above the point where all entering particles are collected, the total current is simply that entering the analyzer because of the aerosol convection

$$I \equiv I_{sat} = n_0 qF \quad (5)$$

where  $F$  is the volume rate of gas flow.

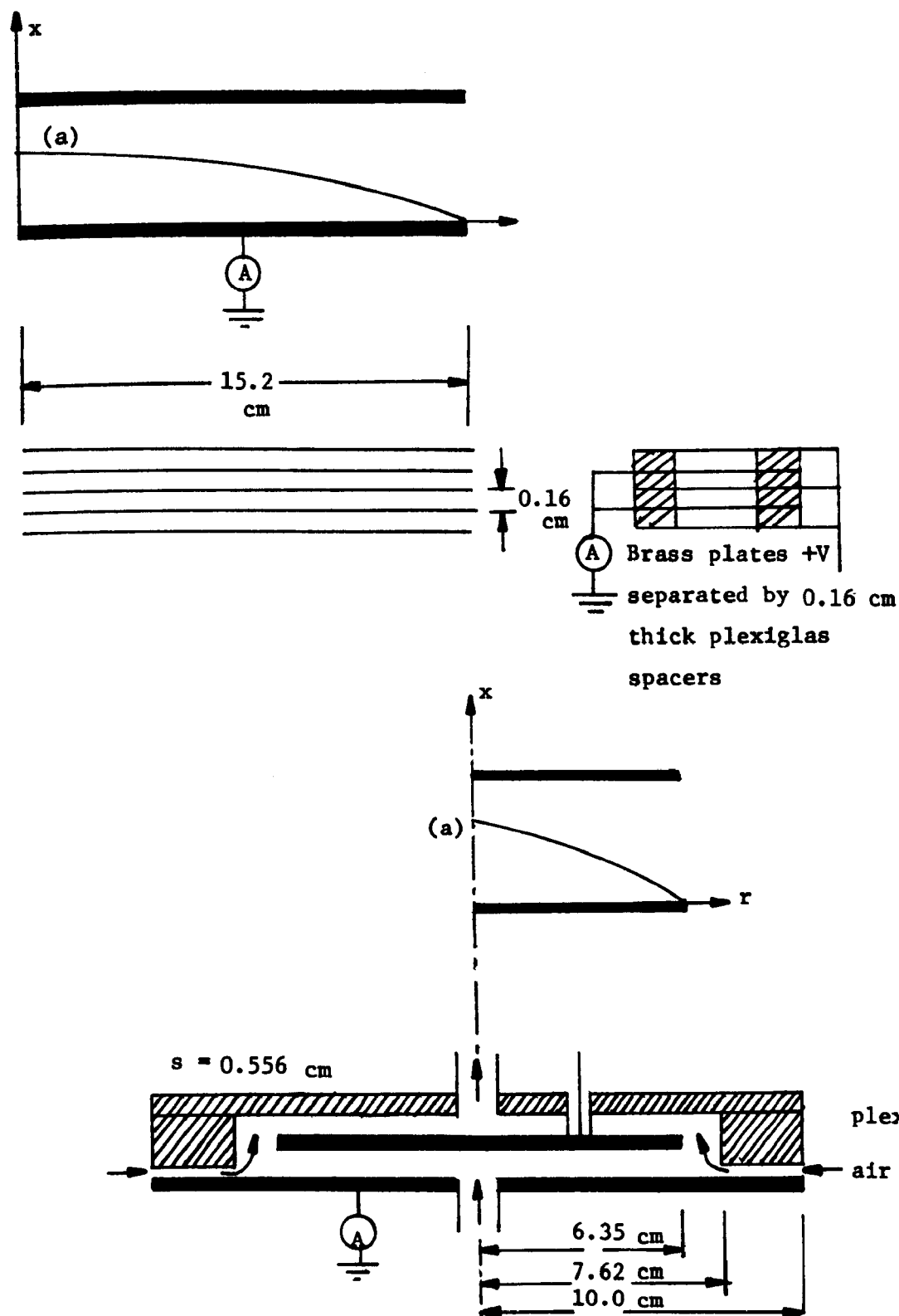


Fig. 4.7.1 Analyzer configurations (a) plane flow with multiple parallel electrodes (b) radial flow with air injection to prevent leakage current.



It follows that the ideal imposed field analyzer characteristic is as shown in Fig. 4.7.2. Combining Eqs. (4) and (5) shows that the saturation voltage is

$$V_{\text{sat}} = \frac{sF}{bA} \quad (6)$$

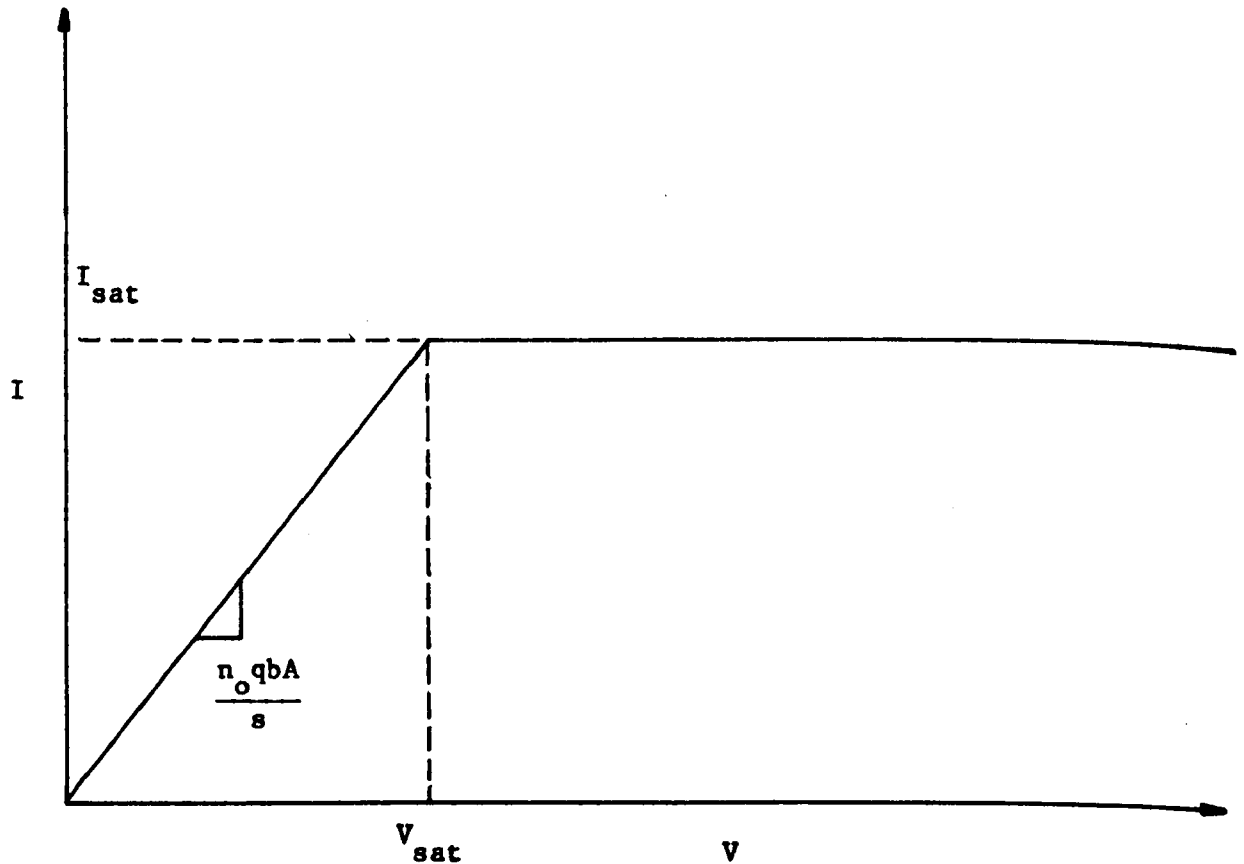


Fig. 4.7.2 Ideal imposed-field analyzer volt-ampere characteristic for either of configurations in Fig. 4.7.1

Typical data taken using the radial flow configuration is shown in Fig. 4.7.3. In addition to the low voltage linear dependence and high

voltage saturation of the current, there is an evident current  $I(0)$  even with  $V = 0$ . This is the result of self-precipitation, and in dealing with aerosols of high charge density, as is the case here, can itself be the basis for inferring the aerosol parameters. Before pursuing this point in the next subsection note that the space charge density  $n_0 q$  can be determined using the data of Fig. 4.7.3 and Eq. (5) regardless of whether or not space charge effects are important.

#### 4.7.2 Space-Charge Effects

It is to determine the mobility that the slope of the linear region of the curve is used and that is ambiguous to a degree that becomes less tolerable as the space charge current  $I(0)$  becomes on the order of  $I_{sat}$ . Both the mobility and the charge density contribute to  $I(0)$ , but because the latter is known from measurement of  $I_{sat}$ , it is possible to use  $I(0)$  as a measure of  $b$ . In the radial flow configuration this is done by exploiting the results of the following analysis.

An analytical model for the space charge current follows directly from Eqs. (4.2.5) and (4.2.6) if the flow is represented as having no  $x$  dependence. (This is the equivalent of slug flow in the radial geometry.)

$$\bar{v} = \frac{F}{2\pi r s} \bar{i}_r \quad (7)$$

Hence, the radial component of Eq. (4.2.9) is simply

$$\frac{dr}{dt} = \frac{F}{2\pi r s} \quad (8)$$

which, with the assumption that the aerosol is injected at the radius  $r_0$  with a uniform concentration  $n_0$ , can be integrated to give

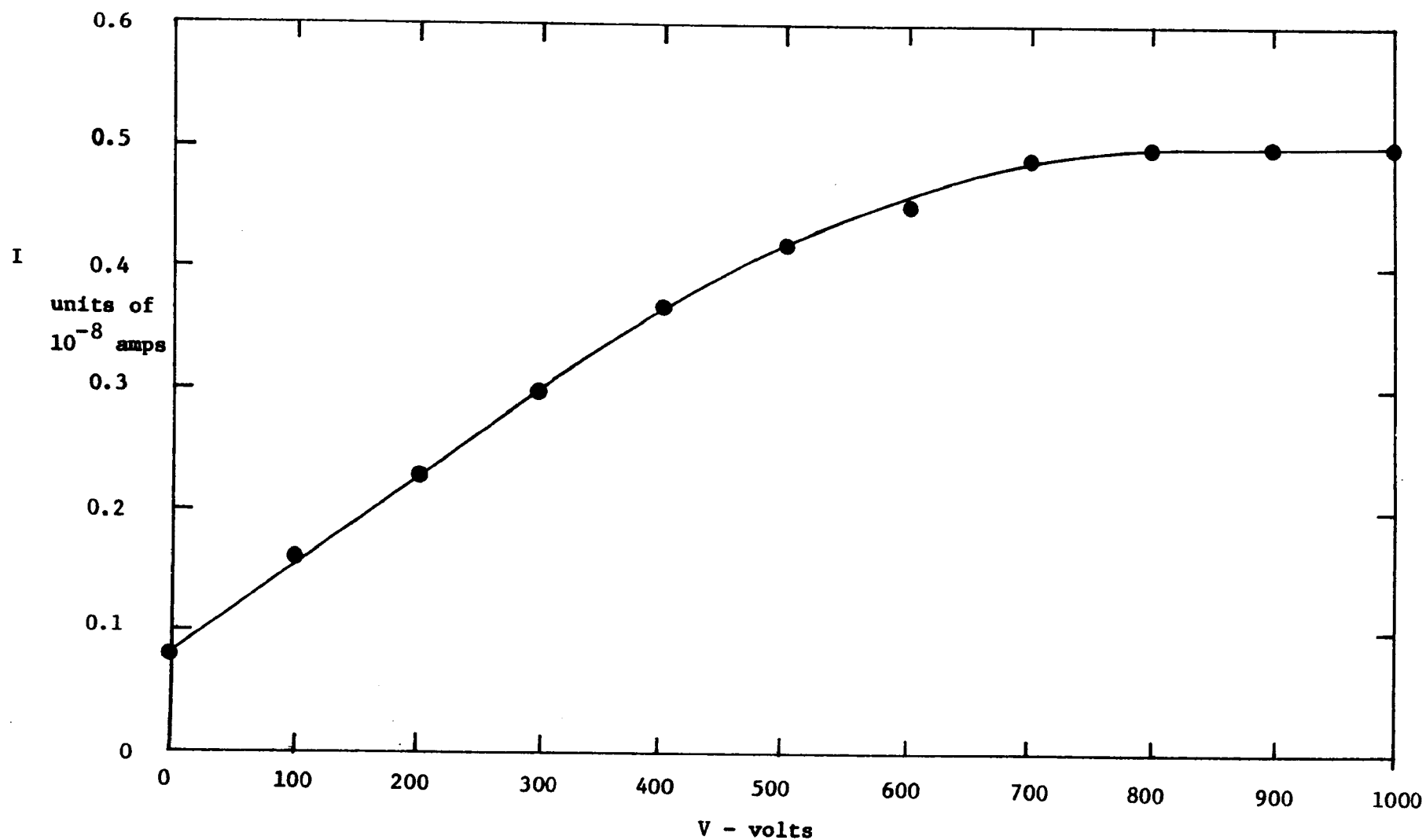


Fig. 4.7.3 Typical analyzer V-I characteristic determined using the radial flow air injection configuration of Fig. 4.7.1b.  $F = 1.08 \times 10^{-4} \text{ m}^3/\text{sec}$ ,  
Hence from data  $b = 1.45 \times 10^{-7} \text{ m/sec/V/m}$ ,  $nq = 4.63 \times 10^{-5} \text{ coul/m}^3$

$$t = \frac{\pi s}{F}(r^2 - r_o^2) \quad (9)$$

The particle density, in terms of the time measured in the frame of reference of the particle, is given by Eq.(4.2.8). The radial distribution is deduced by combining this expression and Eq. (9).

$$\frac{n}{n_o} = \frac{1}{1 + [\frac{\pi s}{F}(r^2 - r_o^2)] \frac{1}{\tau_a}} ; \tau_a \equiv \frac{\epsilon_o}{n_o q b} \quad (10)$$

Thus, the particle concentration at all radial positions is also uniform.

The difference between the radial particle current at the outer radius of the analyzer where  $r = r_1$  and at the inlet, where  $r = r_o$  is the total self-precipitation current, which is twice the self-precipitation current  $I(0)$  measured at one of the electrodes. Hence,

$$2I(0) = F[n(r_o) - n(r_1)]q \quad (11)$$

Substituting the appropriate values of  $n(r)$  from Eq. (10) leads to the expression

$$\frac{I(0)}{I_{sat}} = \frac{1}{2} \left[ \frac{(\tau/\tau_a)}{1 + (\tau/\tau_a)} \right] ; \tau \equiv \frac{\pi s(r_1^2 - r_o^2)}{F} \quad (12)$$

Note that  $\tau$  is the residence time of the gas in the analyzer.

To assess the faithfulness of the slug flow model the flow is pictured as Poiseuille,

$$v_r(x,r) = \frac{3F}{\pi s^3 r} [(s/2)^2 - x^2] \quad (13)$$

Using a numerical approach taking advantage of the solution from Eq.(4.2.8),

it is possible to calculate a curve for the fraction of the current entering the system that is precipitated on the plates between radii  $r_0$  and  $r_1$ . These results are displayed in Fig. 4.7.4. The upper curve corresponds to the results for a slug flow with the same flow rate. Since the simplified model agrees reasonably well with the exact one, the analytic expression developed there will be used to calculate the mobility of the charged particles.

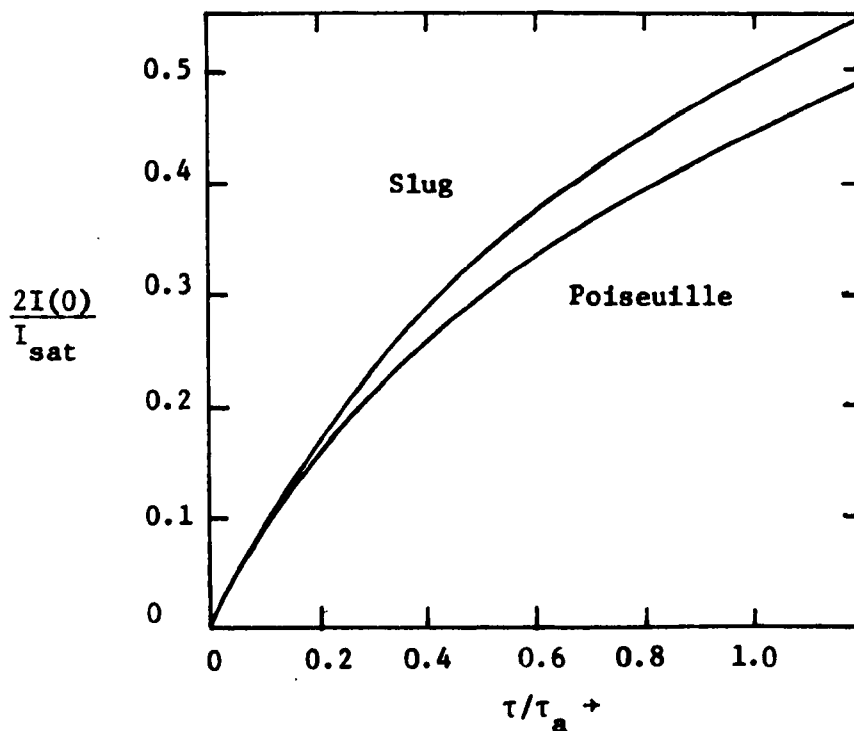


Fig. 4.7.4 Self-precipitation for a radial flow: comparison of exact solution for Poiseuille flow with one from slug model

Once the saturation current and the self-precipitation current are measured, it is possible to calculate both the inlet charge density and mobility. The former follows from Eq. (5)

$$n_0 q = I_{sat} / F \quad (14)$$

In turn, Eq. (12) allows calculation of the ratio of the residence time to the self-precipitation time

$$\tau/\tau_a = \frac{2I(0)/I_{sat}}{1 - 2I(0)/I_{sat}} \equiv C' \quad (15)$$

Since the charge density and volume flow rate are known, the particle mobility can then be calculated

$$b = \frac{C' \epsilon_0}{n_0 q \tau} \quad (16)$$

If the space-charge current is not appreciable, then the imposed-field analysis is appropriate and  $b$  is determined from a measurement of the slope in the region  $V < V_{sat}$ .

#### 4.8 Self-Precipitation Experiments (SCP)

With the objective of underscoring the role played by  $\tau_a$  with respect to the dynamics of the charged submicron particles, two types of experiments are now described that are in the category of SCP devices. The first of these illustrates self-precipitation in a laminar flow system, while in the second, complete mixing is used to illustrate self-precipitation when the flow is dominated by turbulence.

##### 4.8.1 Laminar Flow Experiment

In the apparatus of Fig. 4.8.1, self-precipitation from a laminar flow takes place in a metallic duct of circular cross-section. The aerosol is generated and charged by means of the apparatus described in Secs. 4.4 and 4.6. Then, it is injected into the duct at a position that can be varied by sliding the rigid injection tube in or out of the coaxial duct. By making the injection tube rigid, the geometry of the flow into the system is maintained

essentially invariant, thus assuring constant inlet conditions as the duct length  $z$  is changed. At the exit the analyzer is used to measure the particle density and mobility. The radial flow apparatus and measuring techniques are described in Sec. 4.7.

To make the self-precipitation measurements meaningful, the residence time  $\tau_{\text{tub}}$  in the tubing connecting the outlet to the analyzer must be short compared to that in the duct. In the experiments, this residence time in the connecting tubing is about 0.05 secs. The volume rate of flow  $F = 1.08 \times 10^{-4} \text{ m}^3/\text{sec}$ , and hence residence time in the duct is on this order for  $z < [4F/\pi D_o^2] \tau_{\text{tub}} \approx 2 \text{ cm}$ . Also, the Reynolds number for the duct flow is  $R_y = 4\rho F/\pi\eta D_o \approx 400$ , which assures a laminar flow.

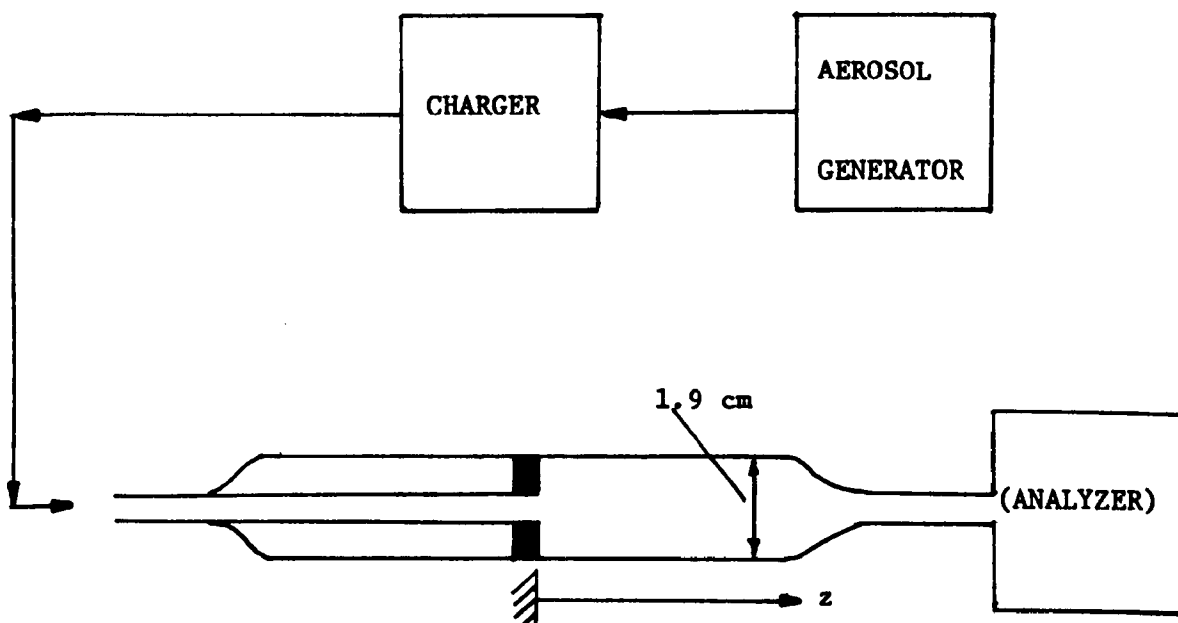


Fig. 4.8.1 Laminar flow self-precipitation experiment

Aerosol generator, charger and analyzer respectively described in Secs. 4.4, 4.6 and 4.7

The experimental results are the data points of Fig. 4.8.2, which show the outlet concentration as the duct length is varied. In essence, this is the decay in particle concentration over the length of a duct of fixed length. The broken curve is based on the slug flow model of Sec. 4.2.2, Eq. (4.2.12). Also described in Sec. 4.2.2 is a more detailed analysis which includes the parabolic profile of a fully developed laminar flow. This theory results in the solid curve of Fig. 4.8.2.

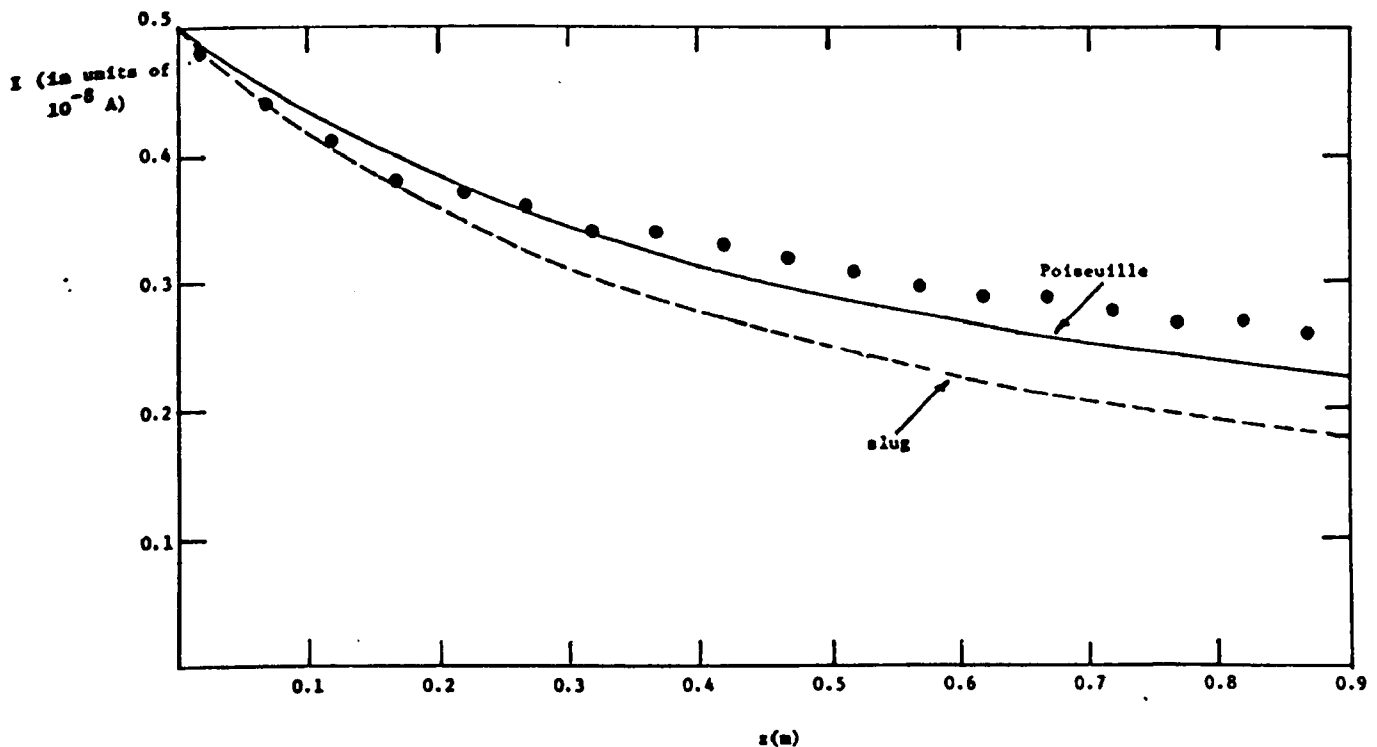


Fig. 4.8.2 Self-precipitation of aerosol from experiment of Fig. 4.8.1  
Broken curve is based on slug flow model, Eq. (4.2.12), while solid curve is result of theory including effect of parabolic velocity profile (Sec. 4.2)



As is evident by the correlation of the simple slug flow model with either the experiment or the more detailed parabolic profile model, the essence of the SCP device in laminar flow is not extremely sensitive to the details of the flow. Chief among the ways in which the experiment does not correspond to the assumptions of the theory are (i) the inlet particle profile is not exactly uniform but is in fact established by a complex mixing zone where the particles are injected through a "T", and (ii) the flow is not fully developed until the boundary layer extends well into the duct.  $z > 0.04\rho F/\eta \approx 20\text{cm}$  (Schlichting, 1968, p 231). Hence, the parabolic profile does not fully develop until the channel has a length on the order of 20cm. In support of this latter point is the fact that for short duct lengths the data tends to follow the slug flow theory more closely than the fully developed flow theory.

#### 4.8.2 Turbulent Flow Experiment (SAG)

A very simple experiment that emphasizes the universality of the self-precipitation model with complete mixing is shown in Fig. 4.8.3.

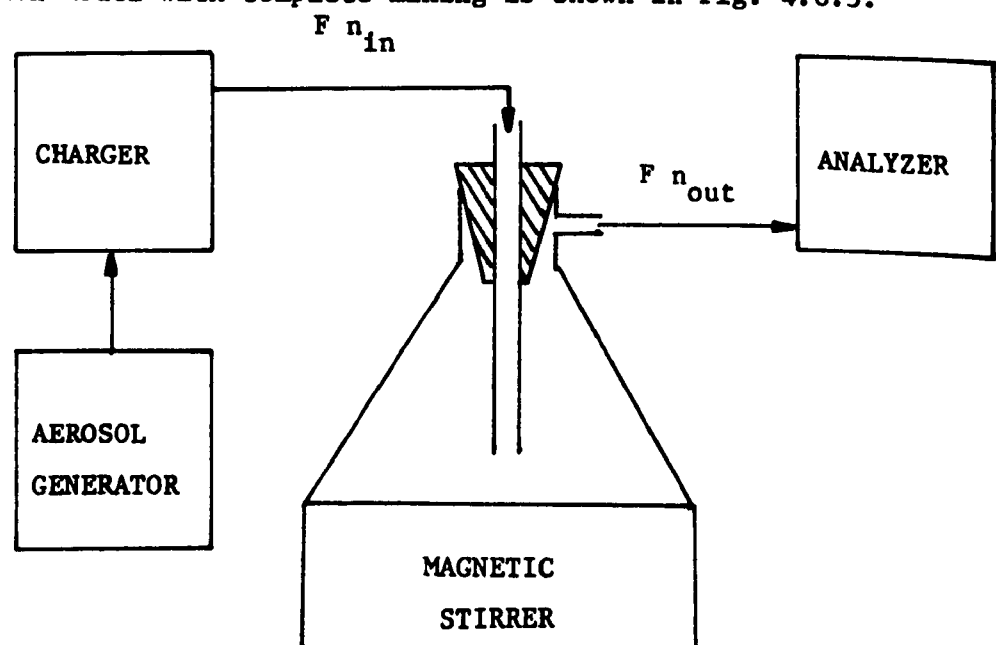


Fig. 4.8.3 Self-precipitation experiment with mixing. Aerosol generator, charger and analyzer respectively described in Secs. 4.4, 4.6 and 4.7

The theoretical basis for this class of SCP phenomena is described in Sec.

4.2.3. The ancillary apparatus is similar to that of Fig. 4.8.1, except that the self-precipitation volume is now arbitrary, both in geometry and electrical properties of the wall materials. The residence time is in fact varied by changing the container, which in the experiment consists of various glass flasks. Mixing within the volume is obtained by means of a magnetic stirrer at the bottom of the flask.

The solid curve of Fig. 4.8.4 is the decay in outlet concentration caused by self-precipitation as a function of normalized residence time, predicted by Eq. (4.2.20). The three data points are the result of experiments performed using three different flasks. There seems to be little doubt but that if complete mixing is assured (without in the process incurring inertial impaction on the walls or on a fan used to induce the turbulence) the simple model for the SCP interaction is an excellent one. In the experiments summarized by Fig. 4.8.4, the discrepancy at the largest residence time is probably due to incomplete mixing in the relatively large volume used.

The SCP model with complete mixing is important in the context of charged drop scrubbers, because the drops are almost certainly injected into the active volume as a turbulent jet, tending to have the same effect on the distribution of particulate as does the magnetic stirrer in the experiment of Fig. 4.8.3. Thus, the electrically induced contribution to performance in the absence of drop charging is represented with considerable generality by Eq. (4.2.20) and the solid curve of Fig. 4.8.4.

#### 4.9 Self-Discharge Experiments (SAG)

The major difficulty in studying the dynamics of bicharged systems

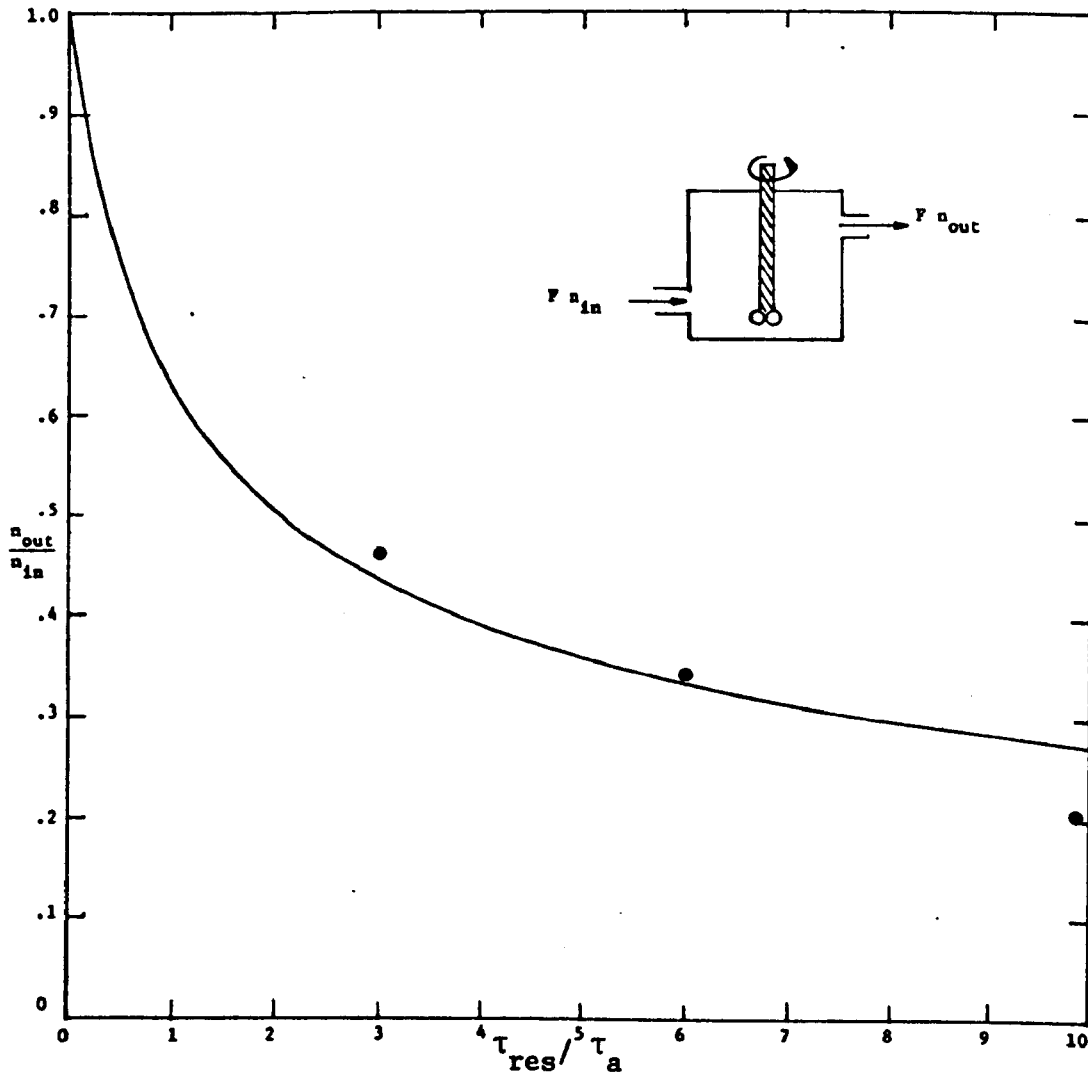


Fig. 4.8.4 Self-precipitation with mixing. Solid curve is predicted by Eq. (4.2.20). Data points are experiments performed using three different flasks having different volumes  $V$  so that residence time  $\tau_{res}$  is varied while holding  $\tau_a$  fixed.

of particulate with space charge neutrality comes from simultaneously obtaining two families having opposite polarity, equal mobilities and densities. In the experiments described here, aerosol particles of the same size are used for both families, and hence the requirement is for equal charging of both families. This is difficult because the charging characteristics of positive and negative corona chargers tend to be very different.

To obtain as high a degree of control as possible over variables while changing the effective length of the interaction duct, the output of the aerosol generator is split into two equal portions, which are then inserted

into separate chargers as shown in Fig. 4.9.1. These are mounted on a movable platform, and their outlets connected to straight sections of grounded copper tubing. The diameter of these (3.17mm I.D.) is selected so as to represent a negligible delay to the flow. The outputs of these tubes are combined in a nozzle which injects the flow into a rectangular channel ( $d = 9.55\text{mm} \times w = 3.18\text{cm} \times 61\text{cm}$ ). The outlet is then led directly into a multi-electrode parallel flow analyzer (Sec. 4.7.1) consisting of five sections stacked one upon another, and then to an exhaust. The volume flow rate of the aerosol is measured along with the analyzer V-I characteristics.

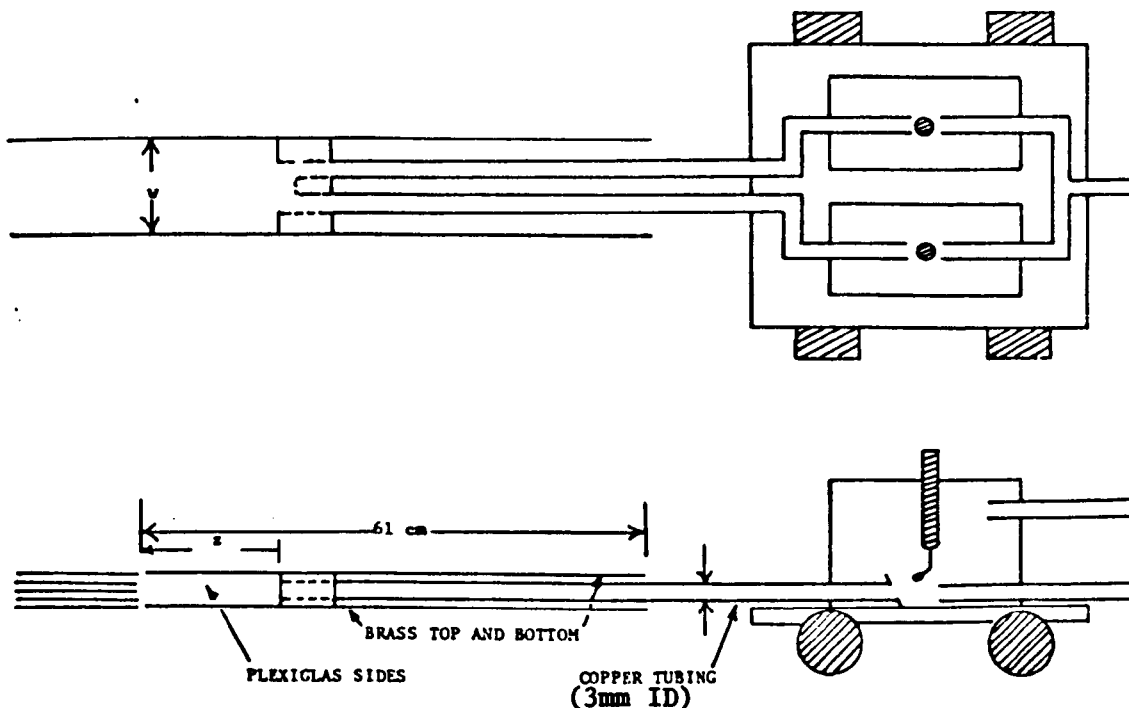


Fig. 4.9.1 Charged aerosol experimental system

One charger is adjusted for positive corona, and the other for negative. Since the charge acquired by a particle through the impact process is proportional to the charging electric field, the magnitudes of the voltages applied to the platinum loops are set about the same. The gas flow rate selected produced an average velocity within the channel of  $0.37\text{m/sec}$ ,

implying a Reynolds number of  $R_y = 75$ , based on an effective diameter  $dw/(2w + 2d) = 3.66 \times 10^{-3}$  m and a laminar flow. To begin, the nozzle is placed as close as possible to the analyzer. The analyzer V-I characteristic is measured, with and without aerosol. This is necessary because with the multi-electrode type of analyzer used, the accumulation of a film of DOP on the inner insulating surfaces results in a leakage resistance. The current from this resistance associated with each analyzer voltage is then subtracted from the measured currents. The results are given in Fig. 4.9.2. As discussed in Sec. 4.7.1, the initial slope and the saturation value of the current together with the gas flow rate provide the information necessary to calculate the mobility of the particles and their

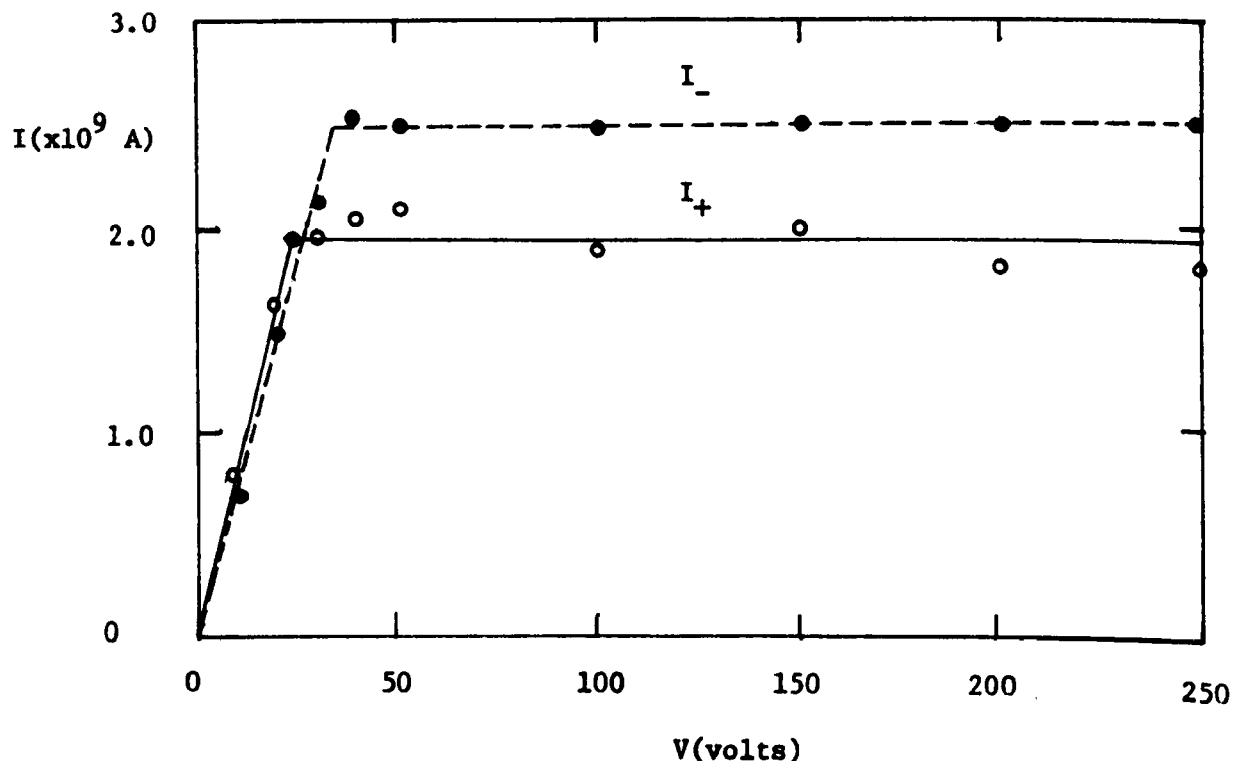


Fig. 4.9.2 Analyzer curves for self-discharge experiments with bicharged aerosols  $F = 1.1 \times 10^{-4}$  m<sup>3</sup>/sec  
 $n_+q = 1.8 \times 10^{-5}$  coul/m<sup>3</sup>  $b_+ = 2.9 \times 10^{-7}$  m/sec/V/m  
 $n_-q = 2.3 \times 10^{-5}$  coul/m<sup>3</sup>  $b_- = 2.4 \times 10^{-7}$  m/sec/V/m

charge density. Note that because the aerosol enters the analyzer with space charge neutrality, the imposed-field analyzer characteristic tends to be sufficiently accurate for the deduction of charge density and mobility. By measuring the currents  $I_+$  and  $I_-$  on each of the sets of electrodes (see inset of Fig. 4.9.3) the decay of each species is ascertained. It is evident from the data of Fig. 4.9.2 that the magnitudes of the positive and negative charges are about the same, and the entering aerosol practically charge-neutral.

Next, with the analyzer voltage set high enough so as to capture all charged particles ( $V > V_{\text{sat}}$ ), the nozzle is pulled back in discrete steps, and the currents from both sets of plates noted. These values, corresponding to the amount of current, both positive and negative, associated with particles which have not yet self-discharged, are plotted in Fig. 4.9.3.

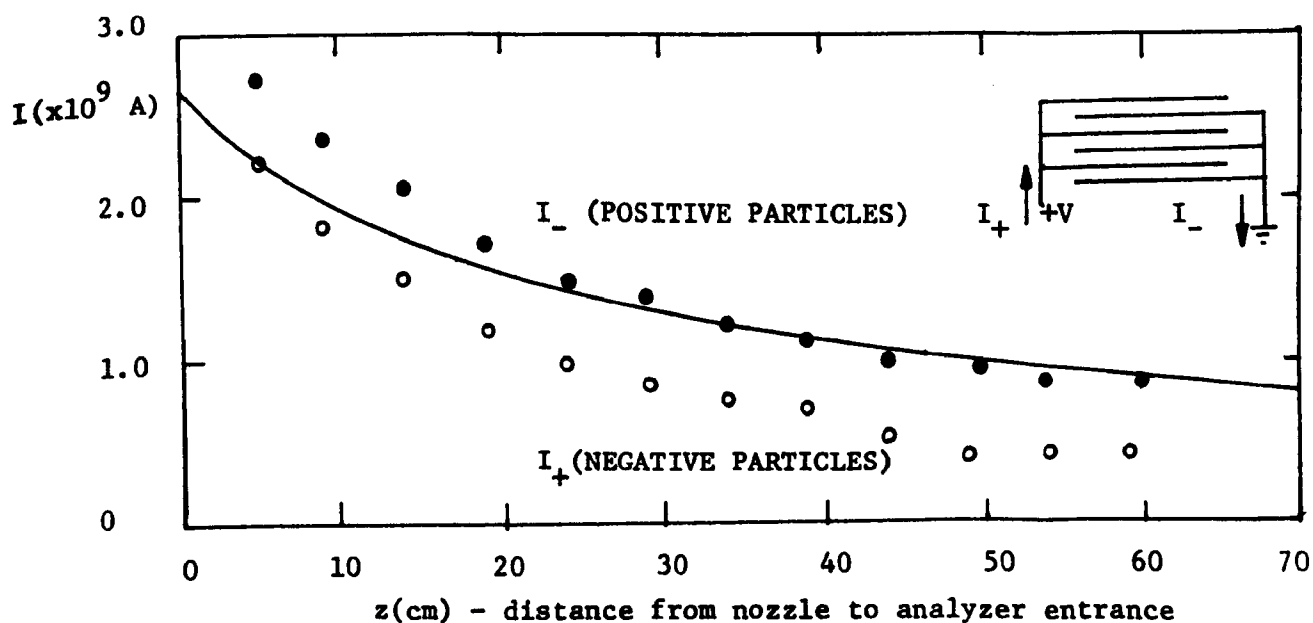


Fig. 4.9.3 Experimental self-discharge of bicharged aerosol in laminar flow as a function of distance down the duct. Solid curve is theory based on Eq. (4.3.22) with the initial condition found by extrapolation back from the first data point. Inset defines analyzer currents

This variation can be compared to the theoretical predictions from Eq. (4.3.22). Since the first point was taken 5cm downstream of the nozzle, the theory is used to infer the entrance current. The solid curve in Fig. 4.9.3 is predicted using the charge-density and mobility measured for the negative particles.

From the mobility measurements, it appears that both positive and negative particles carry essentially equal magnitudes of charge. Thus, the product or products of a discharge event can be considered effectively neutral. The relatively sharp transition in the measured I-V characteristics from the linear to saturated regimes also indicates that there is relatively little variation of the mobility among the particles. Although the magnitudes of the charge densities are slightly different, the amount of net charge introduced is not sufficient to cause self-precipitation to be comparable with self-discharge.

As in the laminar experiments of Sec. 4.8.1, the flow exhibits a transition from a jet leaving the nozzle to a fully developed essentially plane Poiseuille flow within the range of channel lengths observed. The calculations assume, however, that the flow can be modelled as plane Poiseuille from the entrance onward. Thus, the degree of correlation between theory and experiment represented by Fig. 4.9.3 is consistent with experimental controls over the flow.

From the results of these experiments there can be no mistaking the role of  $\tau_a$  in determining the rate of self-discharge among the submicron bipolar particles. Whether this discharge results in mechanical agglomeration and hence is in the category SAG must depend on the details of the particles. For the DOP used in these experiments, self-discharge almost certainly is

equivalent to self-agglomeration. What is important to the performance of the charged drop scrubber is not whether or not the discharge is also an agglomeration event, since there is little change in the size of the particle in any case, but that the bicharged particles lose their charge in the same typical time  $\tau_a$  that the unipolar particles tend to self-precipitate. Insofar as charged-drop scrubbing is concerned, the particles are no longer accessible for collection once they have discharged.



## 5 Electrically Induced Self-Discharge and Self-Precipitation of Supermicron Drops

### 5.1 Objectives

If emphasis is to be given to any of the differences between devices making use of charged drops for collection of particulate and the conventional electrostatic precipitator, then it should be to the fact that the drops, unlike electrodes, are themselves free to move in response to not only imposed electric fields, but self fields and aerodynamic forces as well. Because any charged drop collection device is strongly influenced by the dynamics of the drops, it is appropriate in this chapter to isolate for investigation this aspect of charged drop devices.

With the subject shifted from submicron particulate to supermicron drops, the two objectives in this chapter parallel those of Chap. 4. First, theoretical models and controlled experiments are used to develop a picture of the dynamics of systems of unipolar and of bicharged drops. Interest is confined to the self-precipitation of unipolar drops and self-discharge of bicharged drops in turbulent flows, since these are of greatest interest in practical applications. The comparison of theories and experiments is essential to interpreting in a self-consistent fashion the more complex experiments of the next chapter where systems of charged submicron particles and supermicron drops interact.

Second, techniques for generating monodisperse uniformly charged drops in the unipolar and bipolar systems are developed. Included is a discussion of generating methods that are of interest for large scale practical systems, but are not exploited in Chap. 6. Thus, Sec. 5.4 is in essence an overview of the most likely methods for making charged drops in practical systems.

## 5.2 Self-Precipitation in Systems of Unipolar Drops

### 5.2.1 Mechanisms for Deposition

To a considerable extent, the results of Sec. 4.2 for the self-precipitation of unipolar submicron particles anticipate those of this section. Certainly after Chaps. 2 and 4 it should come as no surprise that if electrical forces dominate, drops tend to be deposited on the walls at a rate determined by  $\tau_R \equiv \epsilon_0 / NQB$  (where  $N$ ,  $Q$  and  $B$  are respectively the drop number density, charge, and mobility) rather than  $\tau_a = \epsilon_0 / nqb$ . But, typically, drops of interest in this and the next chapter are  $50\mu\text{m}$  in diameter, a size sufficient to make inertial effects of possible importance. (Inertial effects are not represented by  $\tau_R$ .) Related to this fact is the influence of turbulent mixing, which, because of the finite drop inertia, is a contributor to the rate of loss of drops at the walls, and also plays an important role in determining the space-time evolution of a system. The following discussion shows that for the drops, several time constants, representing turbulent diffusion, inertial effects of the drops, and electrically induced self-precipitation can be on the same order. The discussion is intended to place in perspective the use of simple models for electrically dominated self-precipitation which will be compared to experiments in Sec. 5.5.

Turbulent Diffusion If the system is sufficiently agitated that it may be classified as turbulent, then the inherent eddies provide a mechanism far more effective than Brownian motion for diffusing flow constituents. In the bulk of the flow, this process is dominated by the large scale motions and characterized by a diffusion coefficient of the order (Levich, 1962, p. 141)

$$D_T \approx (\Delta U) l_T \quad (1)$$

where  $l_T$  is the length scale of these eddies, and  $\Delta U$  the magnitude of the associated fluctuation velocity. In channel flow, the large eddies are limited by the channel width,  $s$ . It is of course, this turbulent mixing that is assumed to dominate in determining the distribution of submicron particles in the "turbulent mixing" models of Chap. 4. Because of the appreciable inertia of the drops, the effect of turbulent mixing on their distribution needs closer scrutiny than is necessary for the submicron particles. For a system with dimensions on the order of 1cm and fluctuation velocities of about 10cm/sec,  $D_T = 10^{-3} \text{ m}^2/\text{sec}$ , and for drops 50 $\mu\text{m}$  in diameter,  $D_T$  is much larger than its Brownian counterpart, where

$$D_B = \frac{kT}{6\pi\mu R} = 4.72 \times 10^{-13} \text{ m}^2/\text{sec};$$

$$\tau_B = \frac{s^2}{D_B} = 2.12 \times 10^8 \text{ sec} \quad (2)$$

This large value for  $D_T$  does not apply throughout the system. In the vicinity of the walls the fluid velocity vanishes, and along with it, the coefficient of turbulent diffusion. In fact, the rate at which massless particles are deposited on the boundaries is determined by their Brownian diffusion through an outer thin laminar layer, (Levich, 1962, p. 150) whose thickness is a function of the level of turbulence in the outer flow. Since  $D_B$  is so small, the fluid must become extremely agitated before this rate becomes significant. At this point, the particle mass becomes important, since it offers a way to short-circuit this last obstacle. For high enough levels of turbulence, the drop can acquire sufficient velocity outside of the Brownian diffusion layer to project itself across the layer to the boundary. This requires that the stopping distance for the drop

with an initial velocity on the order of the velocity of the large scale eddy velocity,  $\Delta U$ , be on the order of the thickness of this layer:

$$l_s = \tau_{sR} \Delta U; \quad \tau_{sR} = \frac{2\rho_R R^2}{9\eta} \quad (3)$$

where  $\rho_R$  is the mass density of the droplet material and  $\eta$  the viscosity of air. (The scrubbing lifetime  $\tau_{sR}$  is introduced in Sec. 2.2). In that event, the flux density of the particles precipitating themselves on the boundaries is given by Davies (1966, pp. 235-246)

$$\Gamma = N\Delta U \quad (4)$$

where  $N$  is the droplet concentration some distance away from the wall.

The degree to which the turbulent mixing influences the drop distribution in the bulk of the interaction region also depends on the scrubbing lifetime  $\tau_{sR}$  relative to times characterizing the eddies. A drop entrained in a flow characterized by eddy time constants

$$\tau_T = \frac{(l_T)^2}{D_T} = \frac{l_T}{\Delta U} \quad (5)$$

will assume the velocity of the eddy if  $\tau_T$  is long compared to  $\tau_{sR}$  but will "iron out" the fluctuations if  $\tau_T$  is short compared to  $\tau_{sR}$ . For drops of  $25\mu\text{m}$  radius,  $\tau_{sR} \approx 7 \times 10^{-3}$  sec while the eddy time constant for a system having  $\Delta U \approx 10\text{cm/sec}$  and  $l_T = 1\text{cm}$  is  $\tau_T = 10^{-1}$  sec. Hence, the large scale eddies have a strong influence on the distribution of drops ( $\tau_T > \tau_{sR}$ ), but the smaller eddies are likely to be penetrated by the drops ( $\tau_T < \tau_{sR}$ ). For the developments of this chapter, it is the former point that is important. Because the small scale eddies do entrain submicron particles, the latter point, the fact that mixing can occur relative to the drop, is important

to the drop-particle interactions to be taken up in the next chapter.

Electric Self-Precipitation With the drops given a unipolar charge, they acquire a migration velocity superimposed upon the random velocities associated with the turbulence. The relative importance of turbulence and self-precipitation in determining the distribution of drops is reflected in the ratio of turbulent particle flux  $\Gamma_T$  to the electrically induced migration flux  $\Gamma_E$  associated with the self-field. In a channel of width  $s$ ,  $l_T \sim s$  and  $E \approx NQs/\epsilon_0$ , so that

$$\frac{\Gamma_T}{\Gamma_E} = \frac{D_T N/s}{BEN} = \frac{D_T/s^2}{NQB/\epsilon_0} = \frac{\tau_R}{\tau_T} \quad (6)$$

Thus, if the drop self-precipitation time  $\tau_R$  is short compared to the large scale eddy diffusion time  $\tau_T$ , the electric field is dominant.

For charging conditions typical of the drop experiments to be described ( $N = 2 \times 10^9/\text{m}^3$ ,  $Q = 4 \times 10^{-14}$  coul,  $B = 5 \times 10^{-6}$  m/sec/V/m,  $R = 25\mu\text{m}$ ), and the time necessary for significant self-precipitation of the drops is  $\tau_R = \epsilon_0/NQB = 0.025$  sec. If the system is turbulent to the extent that  $\Delta U = 10\text{cm/sec}$  and  $s = 1\text{cm}$ , then the large scale diffusional time is of the order  $\tau_T = s^2/D_T \approx s/\Delta U \approx 0.1$  sec. Hence, the self-precipitation is dominant. But, for lesser drop charges, the turbulent diffusion and electrical self-precipitation are of comparable importance in determining the drop motions and deposition on the walls.

Note that if drop charge or density increases, then effects of the finite drop inertia must eventually come into play. The effects of inertia must be considered if

$$\tau_R \gtrsim \tau_{sR} \quad (7)$$

For typical conditions in the experiments of this chapter,  $\tau_{sR} \approx 7 \times 10^{-3}$  sec, which is somewhat shorter than  $\tau_R$ . Thus, inertial effects are at most of marginal importance.

### 5.2.2 Self-Precipitation Model for a Channel Flow

The point of this section is that there is a regime in which electrical effects are dominant in determining the space-time evolution. In this regime, the appropriate model is similar to what would be used to describe the self-precipitation of submicron particles in a turbulent flow. The drops are considered to be entrained in a turbulent flow through a duct having cross-sectional geometry that is uniform but arbitrary, with area  $A$  and perimeter  $S$ . Conservation of particles for a cylindrical volume of incremental length  $\Delta z$  in the flow direction and cross-section coinciding with that of the duct, requires that

$$UA[N(z + \Delta z) - N(z)] = -NB \oint_S \bar{\mathbf{E}} \cdot \bar{\mathbf{n}} d\ell \Delta z \quad (8)$$

where the integration is over the perimeter of the incremental section of duct. It is assumed in writing Eq. (8) that the large scale eddies give rise to sufficient mixing that the drop profile and mean gas velocity across the channel are essentially uniform. Also, the spatial evolution is sufficiently slow to justify the assumption that the space-charge generated electric field is transverse to the flow. By Gauss' Law, this latter approximation requires that

$$\oint_S \bar{\mathbf{E}} \cdot \bar{\mathbf{n}} d\ell = \frac{ANQ}{\epsilon_0} \quad (9)$$

so that in the limit  $\Delta z \rightarrow 0$ , Eq. (8) becomes a differential equation for the

evolution of  $N(z)$ .

$$\frac{dN}{dz} = - \frac{N^2 BQ}{U\epsilon_o} \quad (10)$$

If the drops enter the duct with density  $N_o$ , then it follows from Eq. (10) that

$$\frac{N}{N_o} = \frac{1}{1 + \frac{z}{\ell_R}} ; \quad \ell_R \equiv \frac{U\epsilon_o}{N_o QB} = U\tau_R \quad (11)$$

This model could have just as well been introduced in Sec. 4.2.3 where models are developed for self-precipitation of submicron particles from turbulent flows. Of course, for the submicron particles,  $\tau_R \rightarrow \tau_a$  and  $\ell_R \rightarrow \ell_a$ .

The restrictions on the use of Eq. (8) to describe drops, as compared to submicron particles, are more severe. They come from two sides. If the charge density  $NQ$  is so low that  $\tau_R > \tau_T$ , where  $\tau_T$  is based on the large scale eddies, then turbulent diffusion will dominate in determining the rate of deposition on the walls. Thus, with only a little charge on the drops the rate of spatial decay predicted by Eq. (11) is too low.

As  $NQ$  is raised so high that  $\tau_R < \tau_{sR}$ , restrictions on the model from the other side come into play because of inertial effects. In this range, the rate of decay from Eq. (11) is too high. Hence, to be valid the model must be used where  $\tau_R$  is in the range

$$\tau_{sR} < \tau_R < \tau_T \quad (12)$$

For the drops of interest in this and the next chapter,  $R = 25\mu\text{m}$  and inertial effects are of only marginal importance. It is in fact possible to make  $NQ$  large enough to bring inertial effects into play, but this is likely to correspond to a charge density greater than optimal when the drops are used to perform a scrubbing function.

### 5.3 Analysis of Self-Discharge Systems

#### 5.3.1 Mechanisms for Discharge

The evolution of a system of bicharged drops is a function of processes occurring on at least two length scales. There is the system scale, in which the drops are distributed through mechanisms such as turbulent diffusion and convection as well as self-field induced electrical migration. Because the systems of interest in this section are initially composed of pairs of charged drops having the same size and mobility but opposite sign of charges, it is to be expected from the dynamics of bicharged submicron particles discussed in Sec. 4.2.3, that the drop distribution on this systems scale is determined by turbulent diffusion and convection alone.

The second scale is of the order of the distance between drops. With  $N$  the density of one species of drop, this distance is of the order

$$\alpha R \approx \frac{1}{(2N)^{1/3}} \quad (1)$$

On this scale, oppositely charged drops are encouraged by the electrical forces to mutually discharge. This tendency is possibly influenced by molecular diffusion, but is almost certainly in the face of the fine scale turbulent mixing. The following discussion of the self-discharge process is intended to bring out the physical mechanisms involved on the interdrop scale.

Turbulent Diffusion First, assume that the inertia of the drops is negligible, in the sense that  $\tau_{sR}$  is short compared to time scales of interest. Levich (1962, p. 215) argues that for drops small compared with the microscale of the turbulence  $l_0$  (at which viscous effects become significant) the coefficient of turbulent diffusion can be expressed as



$$D_t \approx \beta \sqrt{\frac{\gamma_T}{\eta}} \ell^2 \quad (2)$$

where  $\ell$  is the scale of the turbulence. The volume rate of energy dissipation (watts/m<sup>3</sup>) can in turn be expressed in terms of the properties of the large scale eddies

$$\gamma_T = \rho (\Delta U)^3 / \ell_T \quad (3)$$

and  $\beta$  is a constant of the order unity while  $\rho$  and  $\eta$  are the mass density and viscosity of the gas respectively.

To establish that on the scale  $R - \alpha R$  Brownian diffusion is overshadowed by turbulent diffusion, observe from Eqs. (2) and (4.2.2) [ $\lambda A/a \ll 1$ ] that the diffusion coefficients are equal for diffusion having the length scale

$$\ell_1 \approx \left( \frac{D_B^2 \eta}{\beta^2 \gamma_T} \right)^{1/4} ; \quad D_B = \frac{kT}{6\pi\eta R} \quad (4)$$

If this scale is even smaller than the drops, let alone distance between the drops, Brownian effects can be ignored. Values typical of the experimental system to be considered in this and the next chapter are  $R = 2.5 \times 10^{-5}$  m,  $\Delta U = 10^{-1}$  m/sec and  $\ell_T \approx s \approx 10^{-2}$  m. Thus, Eq. (4) gives  $\ell_1 < 10^{-7}$  m and it is clear that turbulent diffusion dominates molecular diffusion.

Again, for the moment ignoring effects of drop inertia, the picture that evolves is one in which self-discharge is the result of turbulent diffusion and migration induced by interdrop electric fields. The developments of self-discharge processes for submicron particles, Sec. 4.3, illustrates that the electrically induced discharge occurs on a time scale typically of the order  $\tau_R = \epsilon_0 / 2NQB$ . For a drop system having  $N = 10^9/\text{m}^3$ ,

$Q = 4 \times 10^{-14}$  coul and  $B = 5 \times 10^{-6}$  m/sec, this time is  $\tau_R \approx 2 \times 10^{-2}$  sec.

The fine scale turbulent diffusion is typified by a time scale  $\tau_t = \ell^2/D_t$  which in view of Eqs. (2) and (3) is

$$\tau_t \approx \frac{1}{\beta} \sqrt{\frac{\eta \ell_T}{\rho(\Delta U)^3}} \quad (5)$$

For  $\Delta U \approx 10^{-1}$  m/sec and  $\ell_T \approx 10^{-2}$  m,  $\tau_t \approx 1.5 \times 10^{-2}$  sec. That these times,  $\tau_R$  and  $\tau_t$ , are on the same order illustrates the point that the flights that bring two drops together through mutual attraction are protracted by stochastic aerodynamic forces tending to play the role taken by molecular diffusion for the submicron self-discharge process (Sec. 4.3).

In analogy with the calculation of self-discharge within aerosol systems, the next calculation should be the radius of the electrostatic sphere of influence. If attention is again focused upon the mutual diffusion of two oppositely charged drops, the analogue of Eq. (4.3.2) for the radius at which collision is guaranteed is

$$A_0 = \left( \frac{BQ}{\beta 4\pi\epsilon_0 \sqrt{\gamma_T/\eta}} \right)^{1/3} \quad (6)$$

Here, the length scale for evaluating the diffusion coefficient, Eq. (13), is taken as  $A_0$  itself. Using the same typical numbers as before in this section, evaluation of Eq. (6) gives  $A_0 \approx 3 \times 10^{-4}$  m. This length is about an order of magnitude smaller than the typical interdrop spacing given by Eq. (1). Hence, further credance is given to the physical mechanisms involved.

Because initial separations are likely to be larger than  $A_0$ , the analogy is continued with a model similar to the Harper one for ions. The rate at

which drops diffuse onto a sphere of radius  $A_0$  with a diffusion coefficient that varies with separation,  $r$ , is according to Levich (1962, p. 216)

$$G = 12\pi A_0^3 N B \sqrt{\frac{\gamma_T}{\eta}} \quad (7)$$

Within a constant, this result is obtained by substituting Eq. (2) into Eq. (4.3.6) for  $D_t = D_+ = D_-$ . Upon substitution for  $A_0$ , the flux of drops to a single drop can be expressed as

$$G = 3NQB/\epsilon_0 \quad (8)$$

This will be seen to be almost identical to the result obtained if diffusive and inertial effects are ignorable.

Effects of Drop Inertia That the time constant  $\tau_{SR}$ , reflecting the time scale on which inertial and viscous drag effects are comparable, is on the order of  $7 \times 10^{-3}$  sec (Sec. 5.2) and that this is only somewhat shorter than either  $\tau_R$  or  $\tau_t$  makes it clear that if the charge density is increased much above levels typical of optimal scrubbing conditions the effects of inertia will come into play. To refine the degree to which inertial effects are important consider an opposite extreme in which the drops are sufficiently charged for their initial separations to be less than  $A_0$ . Their motions are dominated by the electric fields. However, because of the drop inertia and the fact that these fields show such a rapid spatial variation, the particle velocities are less than those predicted for massless particles of the same size and charge. This may lead to significant increases in the discharge times. To ascertain this effect, an idealized Langevin model is employed. Instead of examining the flux of charged particles to an oppositely charged central one, the bipolar system is separated into isolated oppositely charged

pairs, and the time required for each pair to discharge is evaluated. In the limit where inertia is ignorable such a model predicts that discharge occurs at precisely time  $\tau_R$ , whereas the Langevin model predicts that half of the charged pairs will have discharged within that time. The difference is due to the averaging inherent in the latter model.

The equations governing the motion of two drops of equal radius  $R$ , but of opposite charge  $Q$ , starting from initial rest at some prescribed separation (Fig. 5.3.1) are

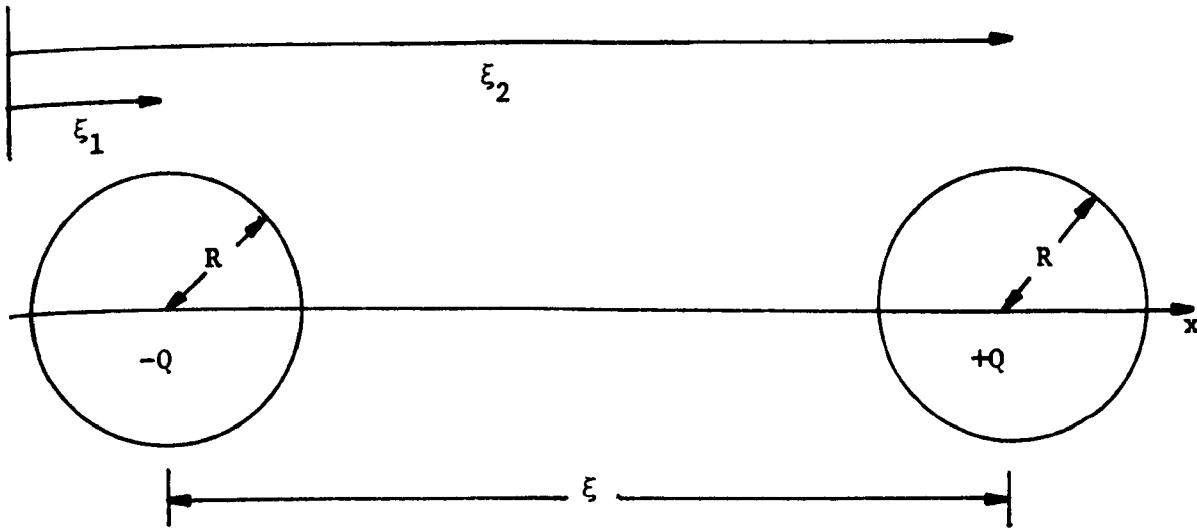


Fig. 5.3.1 Geometry for two-particle model of discharge process between two drops

$$M \frac{dv_1}{dt} + 6\pi\eta R v_1 = + \frac{Q^2}{4\pi\epsilon_0 \xi^2}, \quad (9)$$

$$M \frac{dv_2}{dt} + 6\pi\eta R v_2 = - \frac{Q^2}{4\pi\epsilon_0 \xi^2} \quad (10)$$

where  $v_1 = d\xi_1/dt$ ,  $v_2 = d\xi_2/dt$ ;  $\xi = \xi_2 - \xi_1$ . These equations may be combined into a single normalized equation

$$\xi^2 \left( \frac{d^2 \xi}{d\underline{t}^2} + \frac{d\xi}{d\underline{t}} \right) = -\underline{C} \quad (11)$$

where  $\underline{\xi} \equiv \xi/R$ ;  $\underline{t} \equiv t/\tau_{sR}$ ;  $\underline{C} = \frac{2}{3} \frac{\rho_R}{\epsilon_0} B^2$ ;  $B = Q/6\pi\eta R$ ; the low Reynolds number mobility of the drop in an electric field:  $\tau_{sR} = M/6\pi\eta R$ , the time needed for velocity of a drop injected at  $v_0$  to fall to  $v_0/e$  in the absence of other forces;  $\rho_R$ , mass density of drop material.

Before proceeding, two approximations implicit in writing the equations in the above form should be discussed. The first concerns the modelling of the fluid drag by the Stoke's relation. For larger-sized drops carrying sizeable charges, the velocities during the latter stages of discharge may be large enough so that  $R_y > 1$ . To check this, in Fig. 5.3.2 the maximum velocity (occurring just before impact) is plotted versus  $C$  with the initial spacing in units of drop radii used as a parameter. The normalized velocity can also be expressed in terms of the drop Reynolds number  $R_y$ :

$$\underline{v} = \frac{d\underline{\xi}}{d\underline{t}} = \frac{d(\xi/R)}{d(t/\tau_{sR})} = \frac{\tau_{sR}}{R} v = \frac{\tau_{sR}}{R} \left( \frac{R_y \eta}{2R\rho} \right) = \frac{1}{9} \left( \frac{\rho_R}{\rho} \right) R_y \quad (12)$$

where  $\rho$  is the density of the surrounding gas. When the gas is air and the drop is water, the above relation becomes

$$\underline{v} = 1.11 \times 10^2 R_y \quad (13)$$

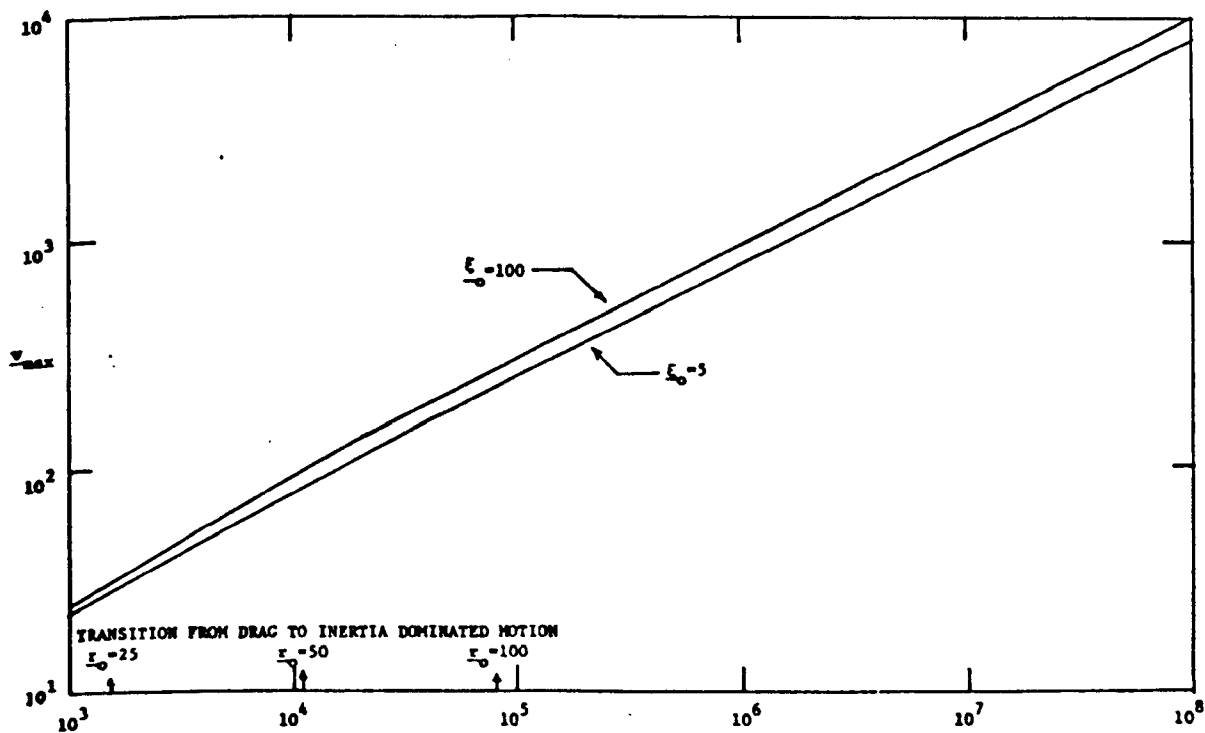


Fig. 5.3.2 Maximum discharge velocity occurring at instant of impact

From the results of later calculations, the points of transition from drag-dominated to inertia-dominated motion are shown. Notice that for all the initial spacings, these occur for  $R_y < 3$ . Thus, for the regimes where drag is an important factor in determining the collapse times it can be modelled by the Stoke's relation. In regimes where the Stoke's model is no longer applicable, the motion is dominated by inertial effects. Criticism of the Stoke's model is academic. There is a further related uncertainty as to whether the drag curve found from measurements on a static drop can be applied to one that is being accelerated. However, for situations where the gas density is much less than that of the drop, these effects are usually small.

The second approximation involves the use of a simple Coulomb's law in describing the attraction between the two charged drops. This is equivalent

to treating them as simple point charges and is applicable only when the drops are separated by many radii. When the drops are within a few radii of each other, the fields of one drop will induce a dipole moment on the other. These will serve to further increase the attractive force. These effects have been calculated (Davis, 1964) and found to be quite unimportant unless the drop centers are separated by less than three radii. Thus their effect has very little to do with the prediction of discharge times.

It is convenient for later calculations to reduce the normalized equation to one of the first order. Upon substituting  $\underline{v} = d\underline{\xi}/dt$ , the equation becomes

$$\frac{d(\underline{v}^2)}{d\underline{\xi}} = -2(\underline{v} + \frac{C}{\underline{\xi}^2}) \quad (14)$$

In the case of drag-dominated motion, the first term is small in comparison with the second. The equation is then easily solved for first  $\underline{v}(\underline{\xi})$  and next  $\underline{\xi}(t)$

$$\underline{\xi} = (\underline{\xi}_0^3 - 3Ct)^{1/3} \quad (15)$$

Thus the time required for the drop centers to move within two radii of each other is

$$\underline{t}_R = \frac{(\underline{\xi}_0^3 - 8)}{3C} \quad (16)$$

In the limit where inertia is the dominating feature, the second term can be neglected, and the remaining equation solved analytically

$$\underline{t} = \left( \frac{\underline{\xi}_0}{2C} \right)^{1/2} \left( [\underline{\xi}(\underline{\xi}_0 - \underline{\xi})]^{1/2} - \underline{\xi}_0 [\sin^{-1}(\frac{\underline{\xi}}{\underline{\xi}_0})^{1/2} - \frac{\pi}{2}] \right) \quad (17)$$

In this case, the discharge time becomes

$$\tau_R = \left( \frac{\xi_0}{2C} \right)^{1/2} \left( [2(\xi_0 - 2)]^{1/2} - \xi_0 [\sin^{-1} \left( \frac{2}{\xi_0} \right)^{1/2} - \frac{\pi}{2}] \right) \quad (18)$$

To find  $\tau_R$  for the entire range of parameters  $C$  and  $\xi_0$ , the differential equation is numerically integrated. These results are plotted in Fig. 5.3.3, as a set of points with the corresponding value of  $\xi_0$  written nearby. Also shown are the lines corresponding to the analytic solutions for  $\tau_R$  with the value for  $\xi_0$ . The smooth transition between the two limiting cases is apparent. In the limit where the inertia of the drops can be neglected and their separation is many times their radii, the expression for the discharge time can be recast into a familiar form. Thus,

$$\tau_R = \frac{\tau_{SR} \xi_0^3}{3C} = \frac{\pi}{3} \frac{\epsilon_0}{N_0 Q B} \quad (19)$$

where  $N_0 = 1/2\xi_0^3$  is the initial concentration of one species of drop.

As will now be seen, this is essentially the familiar result of the Harper model.

### 5.3.2 Self-Discharge Model for a Turbulent (Slug-Flow) Channel Flow

Consider now the spatial evolution of a system of bicharged drops in a duct having cross-sectional area  $A$ . If the flow is turbulent, the velocity profile is essentially uniform. Hence, conservation of one of the drop species with a volume of length  $\Delta z$  in the flow direction is represented by

$$UA[N(z + \Delta z) - N(z)] = -NGA\Delta z \quad (20)$$



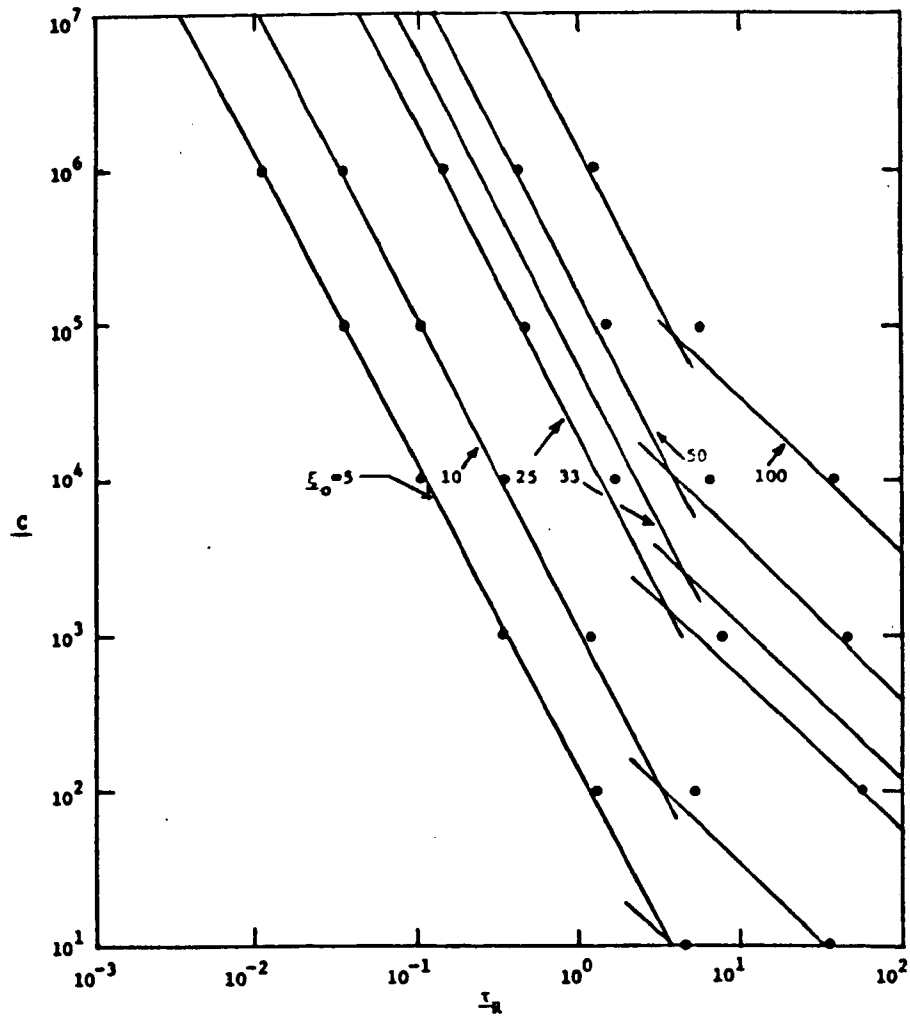


Fig. 5.3.3 Normalized discharge time  $\tau_R$

where  $NG$  is the number of drops per second discharged by  $N$  drops per unit volume. With  $G$  given by Eq. (7) (the Harper model), in the limit  $\Delta z \rightarrow 0$ , Eq. (20) becomes

$$\frac{dN}{dz} = - \frac{N^2}{U} \left( \frac{3QB}{\epsilon_0} \right) \quad (21)$$

Hence, the spatial decay of the drops having a given sign of charge and entering the duct with the density  $N_0$  is

$$\frac{N}{N_o} = \frac{1}{1 + \frac{z}{\ell_R}} ; \quad \ell_R \equiv \left( \frac{\epsilon_o U}{K' N_o Q B} \right) \quad (22)$$

where according to the extension of Harper's model,  $K' = 3$ . With the total initial drop density  $2N_o$  rather than  $3N_o$ , this is the same expression that would be found carrying the submicron particulate model of Sec. 4.3.2 over to the drop system. The time constant of Eq. (18) is for discharge of drops having the largest possible spacing, and hence would be expected to be larger than implied from Eq. (22). In any case, the models strongly support the crucial role of  $\tau_R$  in the self-precipitation process but do not pin down the precise value of  $K'$ .

#### 5.4 Techniques for Generation of Charged Drops

This section serves two purposes. First, it is intended to give an overview of the main techniques for generating charged drops of the type of interest in scrubbing devices. Second, the specific techniques used for generating monodisperse systems of unipolar and bicharged drops for the experiments of this and the next chapter are described.

From the point of view of forming the drops, most devices fall in one of two categories. In the pressure nozzle or orifice plate, a fine stream is ejected under considerable pressure through an orifice. Through capillary action, this stream breaks up into drops. In the pneumatic atomizer type of device, an air stream impinges on the water, greatly increasing the effective atomization. In either of these approaches, drop charging can be implemented by either charge induction through electrodes with elevated potential placed in the vicinity of where the drops break off, or by means of a corona discharge and ion impact charging. Sections 5.4.1

and 5.4.2 illustrate the two types of mechanical drop formation with the charging accomplished by means of induction. Brief attention is given to the alternative ion-impact charger in Sec. 5.4.4.

#### 5.4.1 Fundamental Limits on Charging and Polarization of Isolated Drops

Both the induction and ion impact charging mechanisms are limited by how much charge can be placed on a drop without inducing electromechanical instability or fissioning of the drop. The maximum charge that can be placed on a drop without an ambient electric field is called "Rayleigh's limit" (Rayleigh, 1882), and is given in MKS units by

$$Q_{\text{Ray}} = 8\pi \sqrt{\epsilon_0 \gamma R^3} \quad (1)$$

where  $\gamma$  is the surface tension. This is one upper bound on the drop charge. For water,  $\gamma = 7.2 \times 10^{-2}$  newt/m and Eq. (1) is conveniently written as

$$Q_{\text{Ray}}(\text{coulombs}) = (2 \times 10^{-5}) R^{3/2} \quad (2)$$

where  $R$  is in meters.

Similar electromechanical considerations place an upper limit on the electric stress that can be applied to an uncharged drop in an initially uniform electric field without producing rupture. This is a limit on the maximum polarizing field. In this case, instability results in two or more drops which, because of the initial drop polarization, are likely to be charged. The critical electric field is (Taylor, 1964)

$$E_{\text{Tay}} = 0.458 \sqrt{\frac{\gamma}{\epsilon_0}} R^{-1/2} \quad (3)$$

For water drops in air, Eq. (3) becomes

$$E_{\text{Tay}} = \frac{4.12 \times 10^4}{\sqrt{R}} \quad (4)$$

Table 5.4.1 Rayleigh's Limiting Charge  $Q_{\text{Ray}}$ , Taylor's Limiting Electric Field Intensity  $E_{\text{Tay}}$  and the Saturation Charge as a Function of Drop Radius  $R$

$R - m$	$Q_{\text{Ray}} - \text{coulombs}$	$E_{\text{Tay}}$	$Q_c \text{ at } E_c = 10^6 \text{ V/m}$
$10^{-6}$	$2 \times 10^{-14}$	$4.12 \times 10^7$	$3.34 \times 10^{-16}$
$10^{-5}$	$6.32 \times 10^{-13}$	$1.3 \times 10^7$	$3.34 \times 10^{-14}$
$10^{-4}$	$2 \times 10^{-11}$	$4.12 \times 10^6$	$3.34 \times 10^{-12}$
$10^{-3}$	$6.32 \times 10^{-10}$	$1.3 \times 10^6$	$3.34 \times 10^{-10}$

In estimating drop charges, use is made of the saturation charge on a drop charged by ion impact in a field  $E_c$  (Eq. 5.4.20)

$$\begin{aligned} Q_c &= 12\pi\epsilon_0 R^2 E_c \\ &= 3.34 \times 10^{-10} R^2 E_c \end{aligned} \quad (5)$$

Table 5.4.1 shows the dependence on drop radius of Rayleigh's limiting charge, of Taylor's limiting electric field intensity, and the ion-impact saturation charge given by Eq. (5). Note first that, under the assumption of a charging field  $E_c$  approaching the breakdown strength of air, the saturation charge is less than Rayleigh's limit. Hence, there is some leeway on the drop charge

that can be used insofar as Rayleigh's limit is concerned. Second, only for the extremely large drops are electric field intensities required to produce rupture of an uncharged drop within a range where they might be encountered in a practical device. (The breakdown strength of dry air between uniform electrodes is about  $3 \times 10^6 \text{ V/m.}$ ) Thus, under practical conditions, there does not appear to be any limit on the drop charging or polarization brought about by instability.

#### 5.4.2 Pressure Nozzles and Orifice Plate Generators with Charge Induction

For the purpose of generating monodisperse charged drops, the multiple orifice pressure nozzle of Fig. 5.4.1 can be used. The charging bars can be at different potentials  $v_a$  and  $v_b$  relative to the orifice plate so that charge induction can be used to produce a mixture of drops with charges in two families. By making the voltages equal, unipolar drops are generated. With the voltages equal and opposite, bicharged drops result.

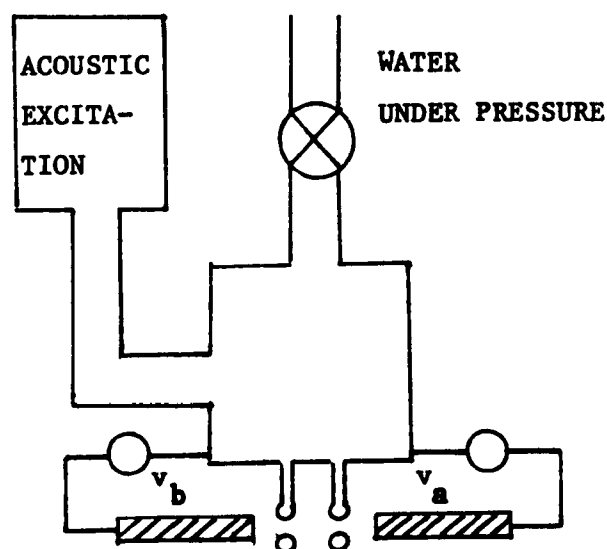


Fig. 5.4.1 Cross-sectional view of acoustically excited pressure nozzle with induction type charging electrodes

This type of generator has the virtue of behaving in a predictable fashion, in part the result of acoustically exciting the orifice plate so as to control the break-up of the streams into drops.

Used in "reverse" to specify the orifice, flow conditions and acoustic excitation frequency, the following analysis is the basis for design of an apparatus to generate charged drops of given size and charge.

Mechanical Atomization The actual generator consists of 512 orifices arranged in two parallel rows approximately 5 inches in length. From each orifice comes a cylindrical stream of water. This jet is unstable, in the sense that infinitesimal disturbances upstream with a certain frequency can result in a disturbance that grows without limit the further downstream one proceeds (Melcher, 1963). The variation of this spatial growth rate with frequency is shown in Fig. 5.4.2

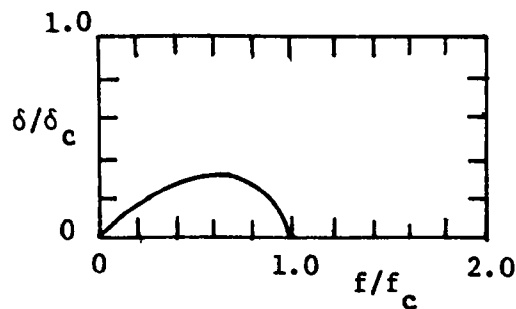


Fig. 5.4.2 Growth rates of instabilities on convecting liquid streams

$$\delta_c = \sqrt{\frac{\gamma}{c^3 \rho_s U_s^2}} \quad (6)$$

where  $\rho_s$  is the density of water,  $\gamma$  its surface tension,  $c$  the jet radius, and  $U_s$  its velocity. All frequencies lower than

$$f = f_c = \frac{U_s}{2\pi c} \quad (7)$$

are convectively unstable in this sense, with a maximum growth rate occurring at

$$f = f_m = 0.11 \frac{U_s}{c} \quad (8)$$

If the source of this stream is vibrated at a frequency  $f_s$  in this range, disturbances corresponding to a wavelength of approximately

$$\lambda_s \approx \frac{U_s}{f_s} \quad (9)$$

result. Downstream, the amplitude of the disturbance becomes sufficient to cause the stream to break into drops. This size of the drops can be determined from mass conservation

$$R = \left( \frac{3}{4} c^2 \lambda_s \right)^{1/3} \quad (10)$$

In general, the stream contracts upon exiting from the pressurized region behind the plate, and thus its size does not correspond to that of the aperture. The coefficient of contraction,  $C_c$ , the ratio of the actual stream area to that of the orifice, can be determined once the physical characteristics are specified. The untapered orifices of the experimental device have a diameter of  $30.5\mu\text{m}$  and are fed from an effectively infinite reservoir. The initial velocity of the drop is found to be approximately  $10\text{m/sec}$ . This implies a Reynolds number based on the orifice diameter,  $d_o$ , of (Rouse, 1957)

$$R_y = \frac{\rho_s U_s d_o}{\eta_s} \approx 300 \quad (11)$$

where  $\eta_s$  is the viscosity of the water. From Fig. 5.4.3, the coefficient of discharge,  $C_d$ , related to the flow rate,  $F$ , and the coefficient of con-

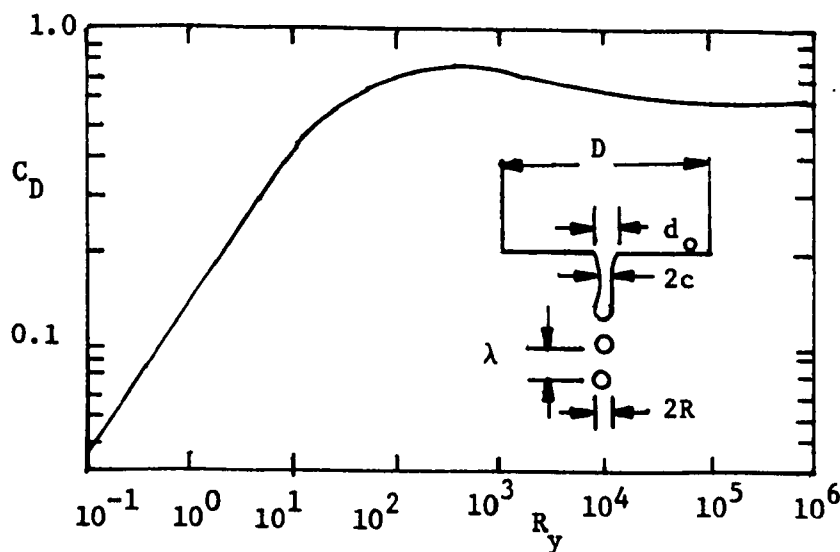


Fig. 5.4.3 Coefficient of discharge for a circular orifice as a function of Reynolds number

traction,  $C_c$ , by (Rouse, 1957, p.55)

$$F = C_D \frac{\pi d_o^2}{4} \sqrt{\frac{2\Delta p}{\rho_s}} \quad (12)$$

$$C_D = C_c / \sqrt{1 - C_c^2 \left(\frac{d_o}{D}\right)^4} \quad (13)$$

can be determined to be 0.7, where  $D$  is the diameter of the reservoir and  $\Delta p$  is the pressure difference across the orifice. Since  $d_o/D \rightarrow 0$ , the coefficients of discharge and contraction are practically equal. This implies for the initial drop stream radius

$$c = \frac{C_c d_o}{2} = 10.7 \mu\text{m} \quad (14)$$

The cutoff frequency for a stream of this size and velocity would be

$$f_c = 150 \text{ kHz} \quad (15)$$

A frequency of 54 kHz is selected to both coincide with one of the vibrational



modes of the orifice plate and be near  $f_m$ . The corresponding wavelength is  $1.85 \times 10^{-4}$  m. The resulting drops have a radius of  $25\mu\text{m}$ , determined from Eq. (10).

**Charging** With the acoustic frequency adjusted to a resonance of the orifice plate, the vibration amplitude is varied until the break-up point of the streams occurs just between the inducer bars of Fig. 5.4.1. At the instant that drops break away, they act as one electrode of a capacitor, with the other electrode the inducer bar. Hence, drop charge is of polarity opposite to that of the inducer bar voltage. The time required for the charges to migrate from the base of the stream to the tip, the relaxation time, is approximately (Woodson and Melcher, 1968, p. 370)

$$\tau_{\text{Re}} \approx \frac{\epsilon}{\sigma} \quad (16)$$

where  $\epsilon$  is the dielectric constant for the material and  $\sigma$  the electrical conductivity. As long as this period is short compared with the time necessary to form a drop, the charging mechanism will be effective. For water,  $\sigma$  varies considerably, but is typically  $4\text{mho/m}$ ,  $\epsilon = 80\epsilon_0$  and hence the relaxation time is  $\tau_{\text{Re}} \approx 10^{-10}$  sec. The time necessary to create a drop is the inverse of the applied acoustic frequency. Thus, it is evident from the extremely short time  $\tau_{\text{Re}}$  that on the time scale of the drop creation, the water can be treated as a perfect conductor.

Because the inducer bar-drop system comprises essentially an ideal two-terminal pair capacitance system, it is expected that the charge induced is related to the inducer bar voltages by relations of the form

$$\begin{bmatrix} Q_a \\ Q_b \end{bmatrix} = \begin{bmatrix} C_a & C_m \\ C_m & C_b \end{bmatrix} \begin{bmatrix} V_a \\ V_b \end{bmatrix} \quad (17)$$

where the capacitance coefficients are functions only of  $\epsilon_0$  and geometry. Symmetry requires that  $C_a = C_b$ . The mutual capacitance  $C_m$  reflects the charge induced on a given stream by the opposite inducer bar. This cross-coupling is small, as can be seen by the fact that a complete screening model gives a fairly accurate estimate for  $C_a$  and  $C_b$ . That is, if it is assumed that one of the drop sheets acts as a planar capacitor plate relative to the nearer inducer bar, then all of the electric field lines from that bar terminate on the nearest sheet of drops. For the left electrode of Fig. 5.4.1 with sheet spacing  $d$ , this field is essentially  $v_b/d$ .

A more detailed view of the geometry is shown in Fig. 5.4.4, where the spacing between streams in a given sheet is  $h$  and the spacing between drops is essentially  $\lambda_s$  as given by Eq. (9). According to this complete screening model, all of the flux that would terminate on the area  $\lambda_s$  associated with each drop in fact terminates on the drop just as it is breaking free. Hence,

$$C_a = C_b \approx \frac{\epsilon_0 \lambda_s h}{d} = \epsilon_0 \frac{h}{d} \frac{U_s}{f_s} \quad (18)$$

This expression is useful for design purposes. For the experimental system,  $d = 1.62 \times 10^{-3}$  m,  $h = 4.96 \times 10^{-4}$  m and  $\lambda_s = 1.84 \times 10^{-4}$ , and Eq. (8) gives  $5 \times 10^{-16}$  F. The measured charging characteristics are given in Fig. 5.4.5. They are essentially linear, deviating slightly toward the higher voltages. It is thought that the intense field causes the streams to be attracted to the bars, decreasing their separations and enhancing the charging for a given applied voltage. Note that the measured inducing capacitance is  $4 \times 10^{-16}$  F, as compared to  $5 \times 10^{-16}$  F estimated using Eq. (18).

#### 5.4.3 Pneumatic Atomization With Induction Charging

By using an inducer electrode in the vicinity of the region where the

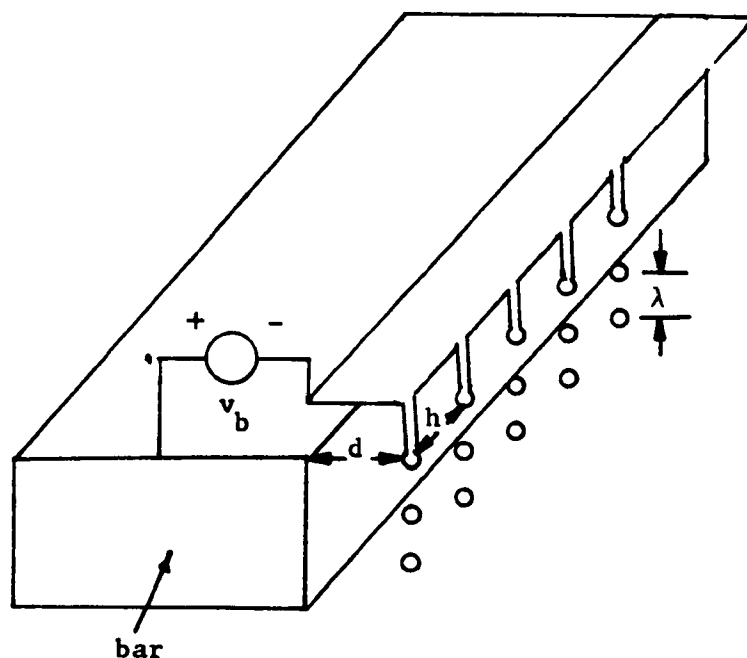


Fig. 5.4.4 Geometry of inducer bar relative to one of the two sheets of drops

drops break away, pneumatic nozzles, of the type used to make fog, can be adapted to produce charged drops. Such drop generators are shown in Fig. 5.4.6. Two devices, one an adaptation of a commercial unit and one with 10 nozzles (Herold, 1967; Reeve, 1967) are illustrative of the general class of pneumatic-induction generators. Although they are found to give charge densities  $NQ$  of the same order as obtainable with the orifice type generators of Sec. 5.4.2, they also produce polydisperse nonuniformly charged drops. Hence, they are not used in the studies described in Chap. 6. However, the generators are applicable to practical devices. In each unit, the atomization air tends to maintain the electrical clearance between the electrode and the metallic structure used to inject the water. The extent to which the air is successful in this is reflected by the impedance seen by the inducer source, which is equivalent to a resistance of about  $50 \text{ M}\Omega$

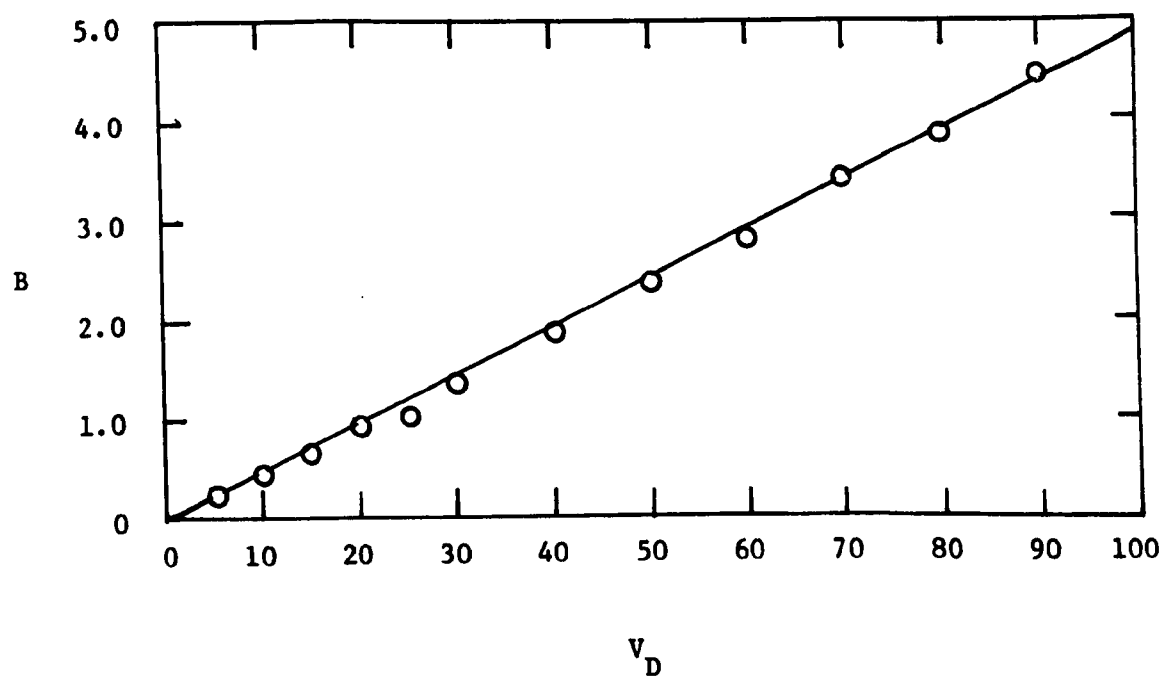
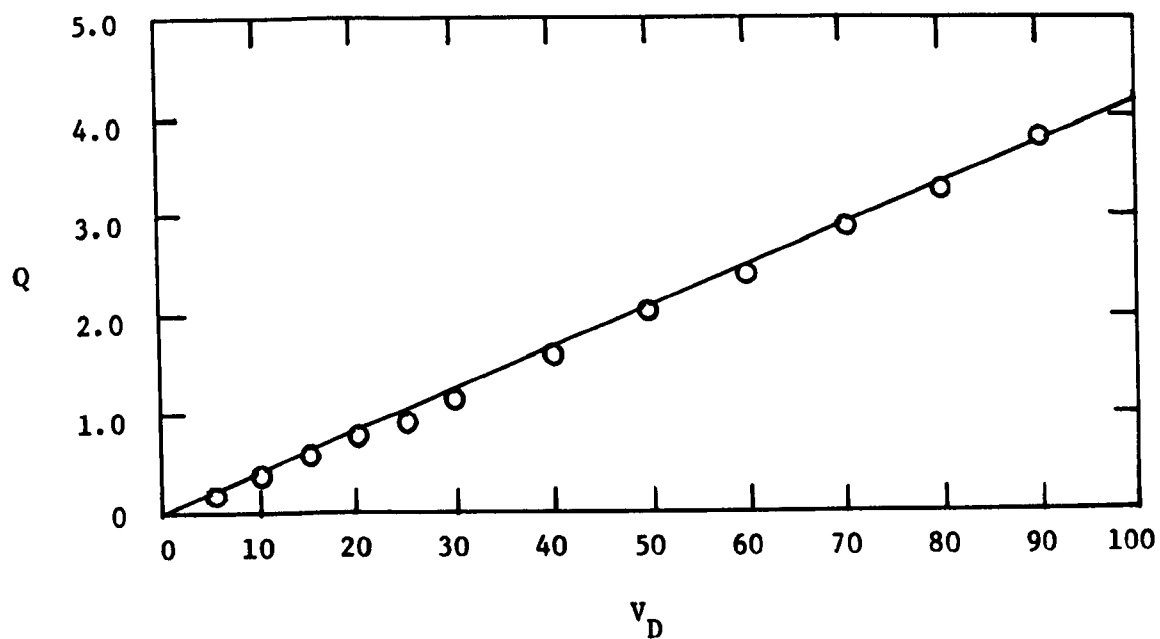
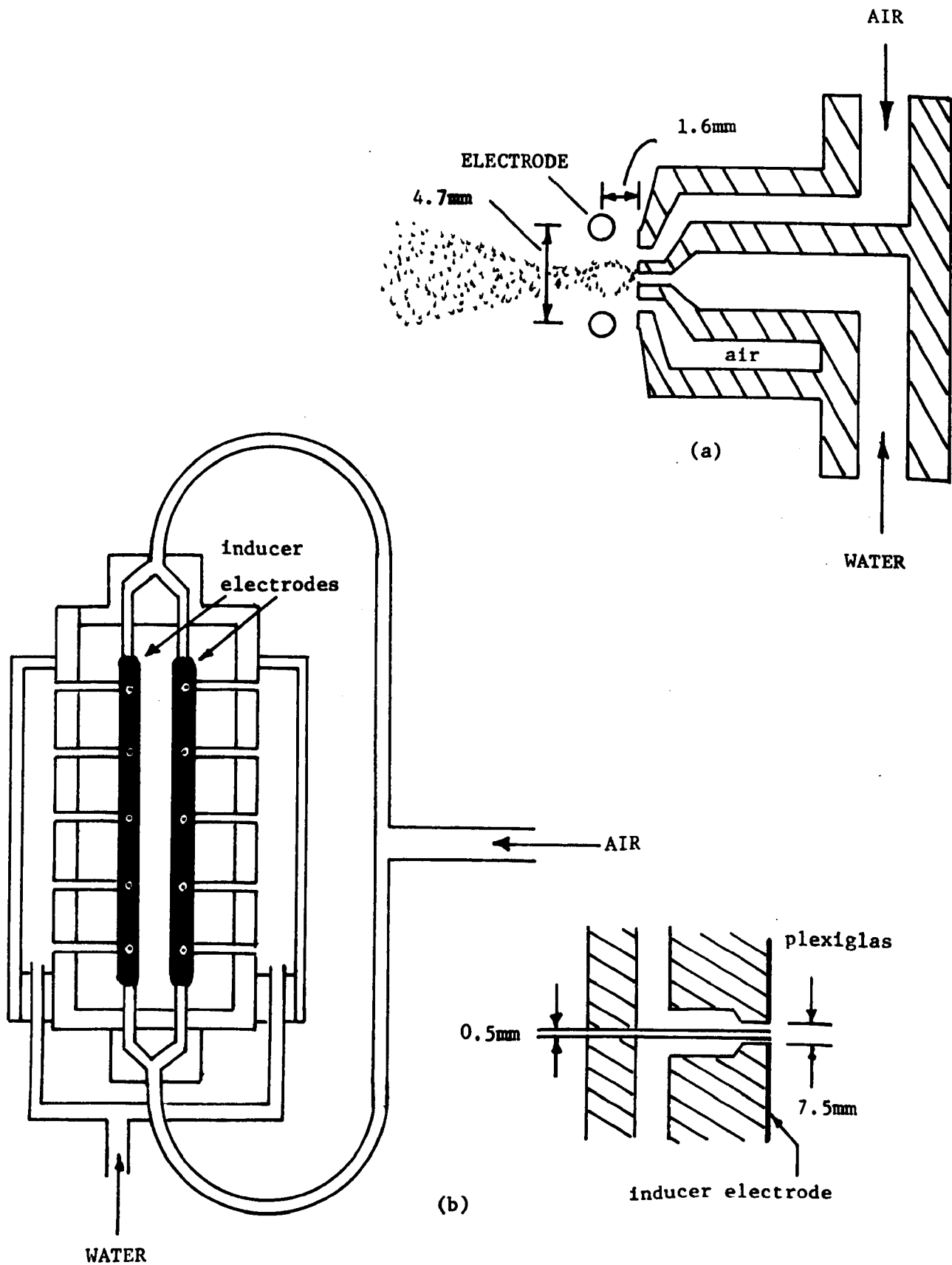


Fig. 5.4.5 Drop charge and mobility as a function of inducer bar voltage.  
 $V_D = v_a = v_b$ ,  $Q$  in units of  $10^{-14}$  coul,  $B$  in units of  $10^{-6}$  m/sec/V/m.



**Fig. 5.4.6 Pneumatic nozzles with induction chargers (a) commercial nozzle with inducer electrode added (b) multi-nozzle unit with built in chargers**

and a capacitance of  $7 \times 10^{-12} \text{F}$  for the 10 nozzle unit.

As in the orifice type generator with induction charging, the drop charge is a linear function of inducer voltage. Figure 5.4.7 shows the total current carried by the drops as a function of inducer electrode voltage. These tests are for a 60Hz inducer voltage, so that the drop current issuing from the generator is a traveling charge wave. This illustrates the convenient control that can be obtained by the induction method over the drop charge, and allows simple induction measurement of the drop-beam charge-density by means of an induction electrode downstream. Such measurements show that for the multi-nozzle unit injecting into a channel flow having velocity 18m/sec and cross-sectional area of  $80\text{cm}^2$ , and with an inducer voltage of 200 volts,  $NQ$  is in excess of  $2 \times 10^{-4} \text{C/m}^3$ . Drop size ranges from  $25\mu\text{m}$  to a few  $\mu\text{m}$ . With this range divided into three families by number, 10% are of average diameter  $22\mu\text{m}$ , 25% are  $11\mu\text{m}$  and 65% are  $5\mu\text{m}$ .

#### 5.4.4 Ion-Impact Charging

An alternative to the induction charging which is applicable to either of the mechanical techniques for forming drops discussed in the previous section, employs a corona discharge and an ambient electric field. In the supermicron range of interest for the drops, the charging process is classically modelled by what amounts to a zero flow limit of the laminar flow drop collection model described in detail in Sec. 6.2.2. The role of the submicron particles in that section is played here by ions originating in a corona discharge. In a flux of ions created by an ambient charging field  $E_c$ , the drop acquires a charge

$$Q = Q_c \left[ \frac{t/\tau_1}{1 + t/\tau_1} \right] \quad (19)$$

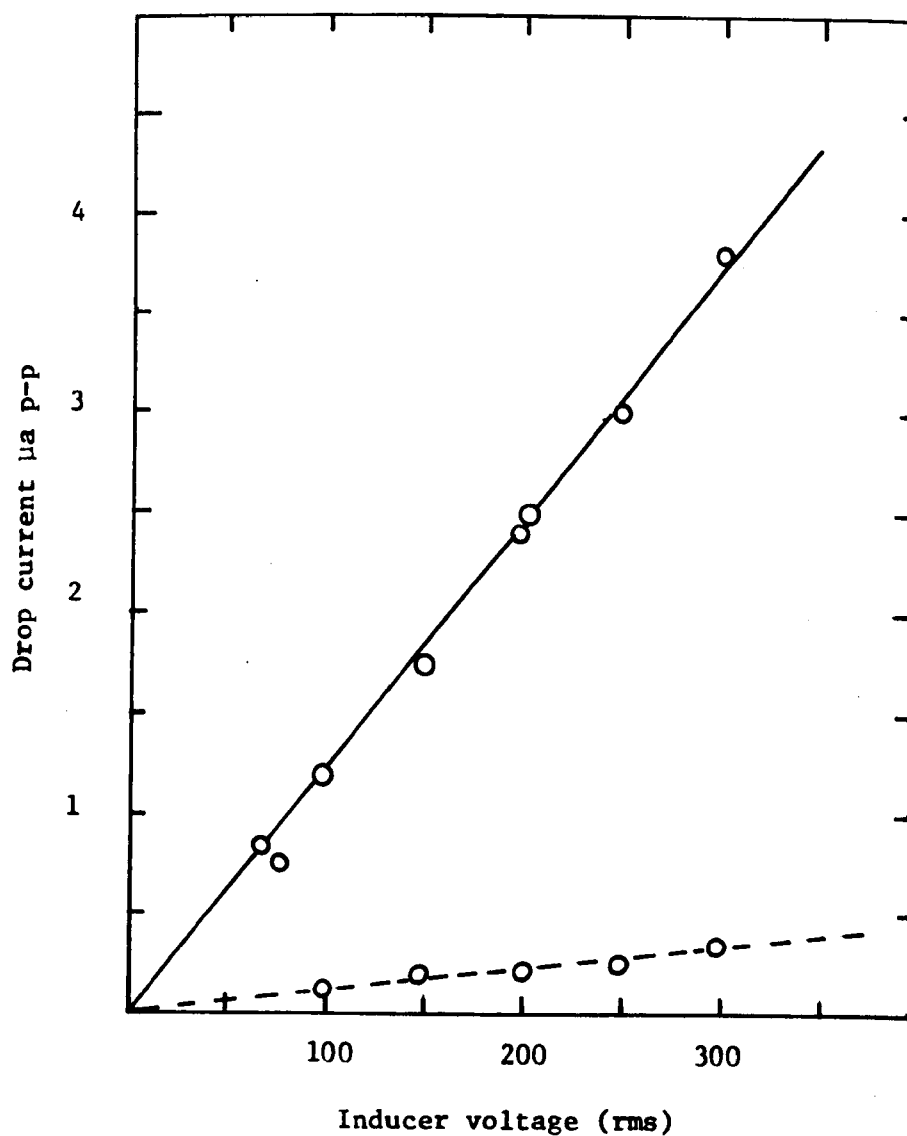


Fig. 5.4.7 Current carried by drops generated using 60 Hz inducer voltage. Solid curve is multi-nozzle unit with 40 psi air pressure while broken line is single commercial nozzle.

where the maximum possible charge,  $Q_c$ , is

$$Q_c = 12\pi\epsilon_0 E_c R^2 \quad (20)$$

and the characteristic time for charging

$$\tau_i = \frac{4\epsilon_0}{n_i q_i b_i} \quad (21)$$

Here,  $n_i$ ,  $q_i$ , and  $b_i$  are respectively the number density, charge, and mobility of the ions. Note that, except for the factor of 4,  $\tau_i$  takes the same form with respect to ions as does  $\tau_a$  for submicron particles.

The theory of ion-impact charging is well described by White (1963, pp. 126-136). However, there is one important difference between the ESP charging and what is required for the scrubber drops. In the latter context, it is undesirable to remove drops in the charging process and hence before they can serve their scrubbing function. Thus, there is an additional characteristic time, the precipitation time  $\tau_{pc} \equiv s/BE_c$  (see Sec. 2.3) involved in properly designing the charging system. The distance  $s$  between structures used to impose  $E_c$  must be large enough that drops are not precipitated before they are charged

$$\tau_{pc} \gg \tau_i \quad (22)$$

The maximum charge  $Q_c$  is 12 times the charge that would be required to terminate a uniform electric field on the drop cross-sectional area  $\pi R^2$ . Given fields of comparable magnitude for induction charging and impact charging, roughly similar charges per drop are often produced. The induction charger of Sec. 5.4.2 illustrates this point. There, the charge is required to terminate the inducing field on an area also somewhat larger

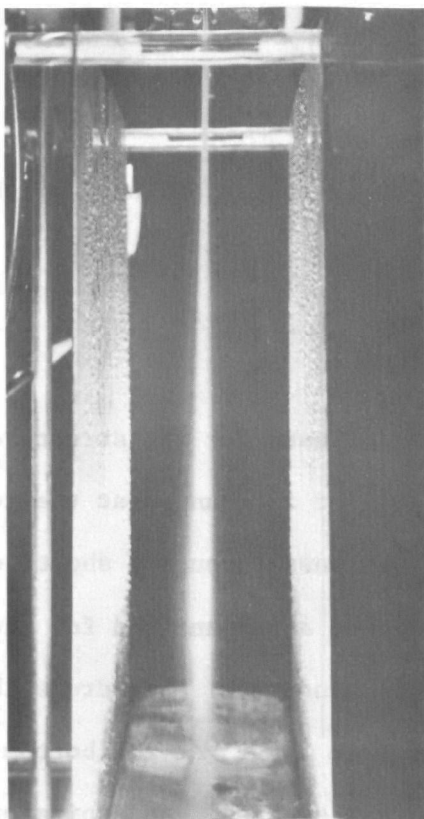


than that of the drop cross-section. Thus, it is not surprising that simple point arrays of corona sources placed in the vicinity of the pneumatic nozzles described in the previous section give drop currents similar to those obtained with the induction chargers. Of course, because the corona requires a threshold voltage for onset and differs considerably in its properties between positive and negative polarity, there is not nearly the flexibility in varying the charge as there is with the induction charger.

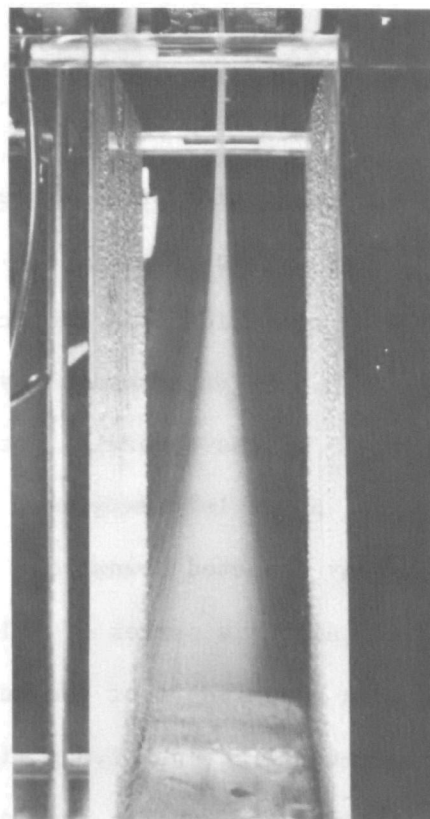
### 5.5 Charged Drop Self-Precipitation Experiments

The tendency of unipolar drops to self-precipitate is made dramatically evident by simply observing the trajectories of drops with various levels of charging. The drop generator described in Sec. 5.4.2 is used to produce the beam of 50 $\mu$ m drops shown in Fig. 5.5.1. If injected into free space with no charge, the drops decelerate within about 20cm from an initial velocity of 10m/sec to about 8m/sec. They then traverse the remaining 20cm of vertical height shown in the figure at an essentially constant velocity. The spreading is typical of a turbulent jet of drops and entrained air. Without charging, the spreading is caused by turbulent diffusion. With a charging voltage of  $V_D = 30$  volts, this diffusion is overtaken by the self-field spreading of the jet. Further increases in  $V_D$  shown in sequence make the highly mobile nature of the drops in their own fields evident. Based on the drop density about 10cm from the orifice plate,  $\tau_R$  assumes the values  $\infty$ ,  $5 \times 10^{-3}$  and  $2 \times 10^{-3}$  sec in the sequence of pictures. These times, which according to Sec. 5.2 characterize the drop self-precipitation process, are to be compared to the residence time; the time taken by drops to traverse the length of the system.

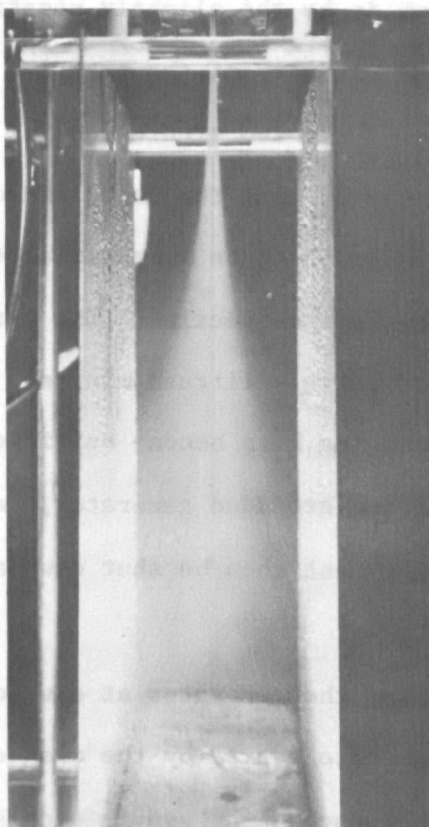
It is the objective of this section to experimentally explore the drop dynamics resulting from drop injection into a system designed to control



(a)



(b)



(c)

Fig. 5.5.1 Jet of 50 $\mu$ m diameter drops ejected into open volume between plane parallel electrodes with 10 cm spacing. Residence time for a drop in 40 cm length of system is about  $5 \times 10^{-2}$  sec.

(a)  $V_D = 0$ , (b)  $V_D = 200$  volts,  $\tau_R \approx 5 \times 10^{-3}$  sec. (c)  $V_D = 300$ ,  $\tau_R \approx 2 \times 10^{-3}$  sec.

the recirculation of air entrained by the drops. This system, shown in cross-section by Fig. 5.5.2, is used in Chap. 6 for the study of charged drop scrubbing of a recirculated aerosol.

#### 5.5.1 Experimental System

Unless otherwise noted, the material used for the structure shown in Fig. 5.5.2 is plexiglas. The drop generator is mounted at the top and the spray directed downward. The drops first pass through a short section containing a series of inlets. These serve as a manifold for the aerosol when experiments of the next chapter are conducted. The drops then enter a central channel 2.5cm wide and about 60cm long. At the bottom water is allowed to drain in such a way that no gas escapes. An aspirator withdraws from the bottom a small flow, slightly greater than that injected through the inlet manifold. The remainder is drawn in by the slightly negative pressure within the channel through leaks in the vicinity of the charging bars. The gas is allowed to recirculate by means of the two side channels, each 2.5cm wide. The recirculating flow is much larger than the inlet and outlet contributions. Provision is made for a probe to be inserted at the bottom capable of moving vertically within the central section. The system can normally operate continuously for approximately fifteen minutes. At this point accumulations of water on the charging bars become sufficiently large to bridge the gap between the bars and the grounded generator, causing the system to become shorted. The apparatus must then be shut down and cleaned.

#### 5.5.2 Drop Velocity Measurements

Although the drops are ejected from the generator at a velocity of approximately 10m/sec, they are rapidly decelerated by the drag exerted on them by the surrounding air. In the process the gas is accelerated.

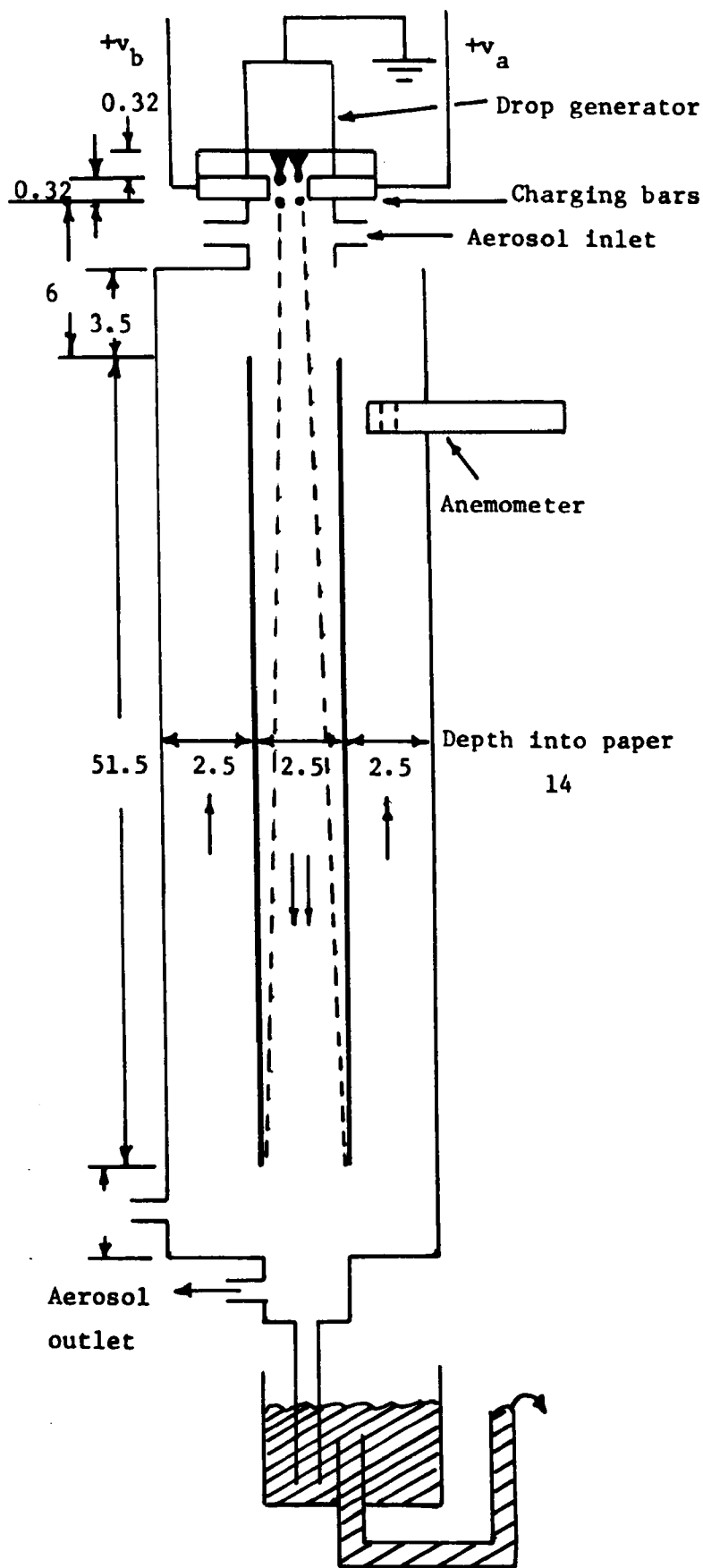


**Fig. 5.5.2** Schematic of experimental system used to study dynamics of unipolar drops and CDS-I, CDS-II and CDP collection of aerosol. All dimensions in cm.

In the experimental system the gas is allowed to recirculate, thereby enabling its velocity to increase to some relatively stable value. During injection into the central section, the two parallel sheets of drops evolve into a jet which eventually spreads by turbulent diffusion to fill the cross section of the channel. When the drops are uncharged, this position is about 10cm downstream of the entrance of the middle section, and when the charging bars are set at 200 volts, it moves upstream to a point about 5cm downstream of the entrance.

Knowledge of the variation of the drop velocity with downstream position is of central importance in any attempts to correlate experiments with the models previously introduced. In addition, the relation of the drop velocity to the surrounding gas velocity is of critical importance in the next chapter in determining the correct model to use in calculating the rate at which charged drops collect charged submicron particles. Two different experimental techniques are used. Both utilize a probe consisting of a 3/8-inch by 4-inch coarse chromel screen suspended from a mounting designed to preserve the insulation of the probe (Fig. 5.5.3). In the first, a very slow square wave (1 Hz) varying from zero down to some negative value is applied to the bars. This is used to trigger an oscilloscope connected to the probe. Fig. 5.5.4 shows the variation of the time at which the probe current achieves half of its final value as a function of the position of the probe (measured with respect to the charging bars). Over most of the channel, the variation is linear, indicating that the drops are moving at a constant velocity. This speed can be calculated from the slope of the curve as 4.9m/sec.

One criticism of this experiment is that it only tests slightly

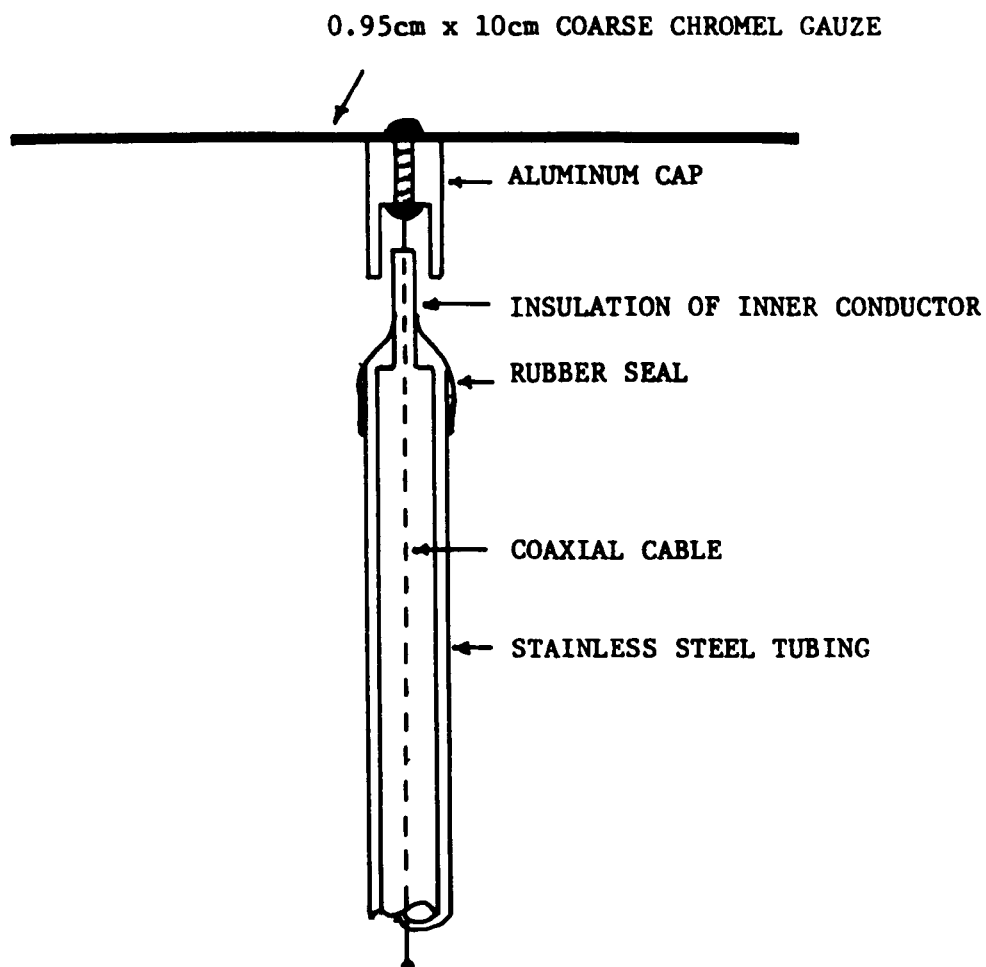


Fig. 5.5.3 Current probe used to measure unipolar drop current impinging from above

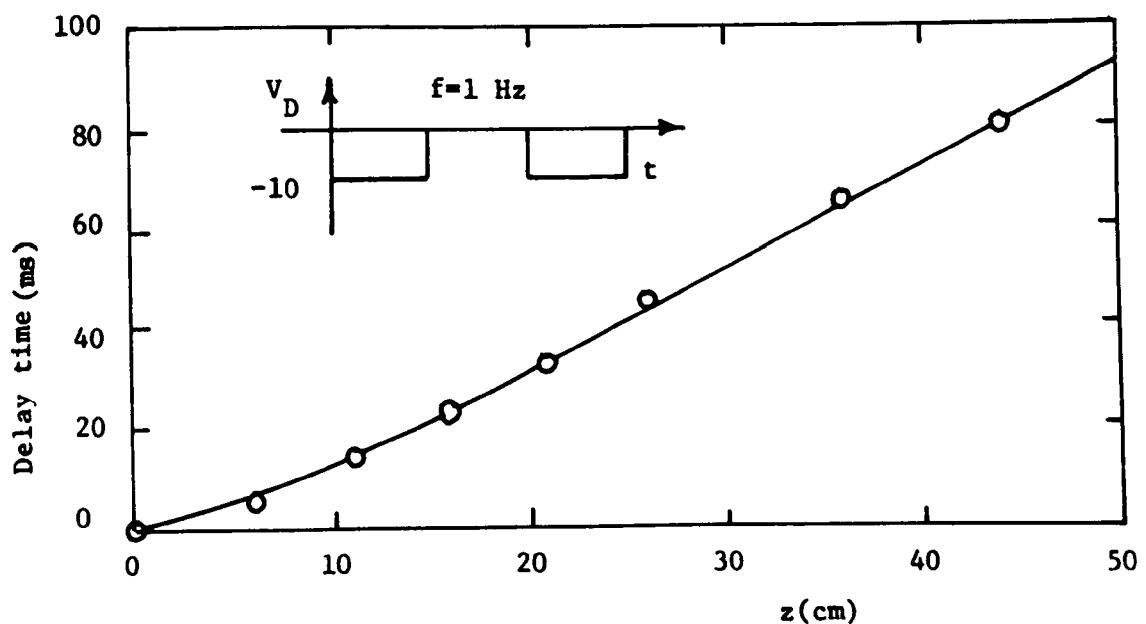


Fig. 5.5.4 Delay time as a function of distance downstream of charging bars

charged drops. Another is that it is unsymmetric in the sense that the measured point is a transition between two physically different systems: one in which the drops are uncharged and the other in which they are charged. The latter exhibits self-precipitation of the drops, hence, possibly a different amount of coupling to the gas, resulting in a different droplet velocity. To rectify this, in the second experiment a balanced square-wave of voltage is applied to the bars, thereby inducing positive and negative drop regions. The frequency is set at 20 Hz. The signal from the probe is fed into a lock-in amplifier, sensitive to signal frequency and phase with respect to the signal applied to the bars. Measurements are then taken of positions at which the output of the amplifier vanishes. These are given in Fig. 5.5.5. Except for effects reflecting the turbulence, it can be argued from several points of view that the frequency measured by any stationary observer downstream is the same as the excitation frequency.

$z_0$ (cm) \ $V_D$	$\pm 5$ V	$\pm 10$ V	$\pm 20$ V	$\pm 100$ V
$v$ (m/sec)	43 )	43 )	43 )	43 )
	4.0	3.8	4.0	4.4
	33 )	33.5 )	33 )	32 )
	4.4	4.4	4.0	4.4
	22 )	22.5 )	23 )	21 )
	6.2	6.2	6.4	
	6.5 )	7.0 )	7 )	

Fig. 5.5.5 Positions  $90^\circ$  out of phase with voltage applied to charging bars for  $f = 20$  Hz and the implied velocities

Thus, since the distance between the measured nulls is half of the spatial

wavelength, the velocity of the drops can be calculated from

$$v = f\lambda_d \quad (1)$$

where  $\lambda_d$  is the wavelength of the signal measured by the probe and  $f$  the frequency of the signal applied to the charging bars. From the data it is evident that over most of the channel length the drops are moving at a relatively constant velocity

$$v = (20 \text{ Hz}) (0.2\text{m}) = 4\text{m/sec} \quad (2)$$

It is also noteworthy that this velocity does not change even when the charging voltage is increased sufficiently to result in the self-precipitation of the majority of drops.

Since the drops eventually move at a constant speed, their speed should correspond to that of the gas,  $U$ . As a check on whether the measured evolution is reasonable, the equation of motion for a single drop is solved

$$\frac{dv}{dt} = - \frac{(v - U)}{\tau_{sR}} ; \tau_{sR} = \frac{2\rho_R R^2}{9\eta} \quad (3)$$

where  $v$  is the drop velocity and  $U$  the gas velocity. Since the gas velocity is much larger than the settling velocity of the drop, gravitational effects are ignored. The solutions for the drop velocity and position are

$$v = (v_0 - U) e^{-t/\tau_{sR}} + U \quad (4)$$

$$z = \tau_{sR}(v_0 - U)(1 - e^{-t/\tau_{sR}}) + Ut \quad (5)$$

After a time corresponding to  $2\tau_{sR}$ , the calculated drop velocity decreases from 10m/sec to 4.8m/sec, just about its terminal value. This position can



be calculated to be about 10cm downstream of the generator, and corresponds quite well with positions beyond which the probe indicates a constant drop velocity.

This agreement between observation and the extremely simple model represented by Eq. (3) is somewhat misleading. In fact, the drops interact aerodynamically with each other, and the drag on a drop is only approximately equivalent to that on an isolated sphere, as pictured by the time constant  $\tau_{SR}$ . Because of these interactions, drops assume a spectrum of velocities as the stream develops into a turbulent jet. Those that move most slowly are expected to be selectively precipitated to the walls, either through turbulent diffusion or self-precipitation.

Because of the complexity of the turbulent jet fluid mechanics, independent measurements are made of the velocity of the gas in the return channels, and hence the average gas velocity in this interaction channel. Two techniques are used. First a hot-wire anemometer, inserted in the upper section of the return channel, indicates a velocity of 0.7m/sec, independent of the voltage applied to the charging bars. In another experiment the time required for an aerosol front injected into the bottom of the side channel to flow to the top is measured. This interval indicates a speed of approximately 1.3m/sec. A gas velocity of 1m/sec in the return channels would imply an average gas velocity of 2m/sec in the central section. This is in contrast with the 4m/sec drop "terminal" velocity measured.

There are at least two possible inferences to be made from this disparity. First, if the drops and gas move in essential synchronism through the lower part of the interaction channel, then it is clear that there must be a profile across the channel that peaks at the center (where the drops are

initially more concentrated and the velocity is of the order of 4-5m/sec) and is depressed at the channel edges. Second, there is the possibility that there is a slip between drops and gas. But this latter conjecture is negated by the observed essentially constant velocity established for the drops by the time they near the lower extremity of the interaction channel. Hence, the evidence is that the drops and gas tend to move together with a profile which is dominated by the center half of the channel cross-section. It is remarkable that even as the drops are charged, and hence their trajectories radically influenced over much of the interaction channel, the mean gas velocity remains essentially invariant.

Visual examination of the flow in the return channel, using puffs of aerosol for visualization, reveals a uniform profile. Hence, the velocities measured in those regions correspond to the average velocities. As a check, the distance over which the profile of the flow in those regions is transformed from a uniform one at the inlet to a fully developed Poiseuille one corresponds to the distance  $z_d$  required for laminar boundary layers to grow from each wall to the center of the channel (Schlichting, 1960)

$$z_d = 0.04 \frac{U_o s^2}{(\eta/\rho)} \quad (6)$$

for  $s = 2.54 \times 10^{-2}$  m,  $U_o = 1$  m/sec,  $\eta/\rho = 1.5 \times 10^{-5}$  m<sup>2</sup>/sec,  $z_d = 1.7$  m.

Since the channel length is approximately 0.5m, at the position where the anemometer is inserted, the profile would still be rather flat there.

### 5.5.3 Measurements of Self-Precipitation of Charged Drops

If both charging bars are set at a certain d-c voltage, the drops produced are monocharged, and the current intercepted by the current probe is

$$I_p(z) = N(z)Qv(z)A_p \quad (7)$$

where  $A_p$  is the area of the probe. The drop concentration and velocity are averages across the channel. If the above equation is normalized to its value at some reference position  $z_r$  downstream, then

$$\frac{I_p(z)}{I_p(z_r)} = N(z)v(z)/N(z_r)v(z_r) \quad (8)$$

Figure 5.5.6 summarizes the measured spatial decay of the probe current for seven charging voltages. These currents have been normalized to their values near the entrance of the middle section. There the drops travel in twin sheets, and the probe collects all of the drops passing along its length. It is evident that diffusive effects play a dominant role in determining the loss of drops from the system at low voltages since for  $V_D < 20$  volts the curves overlap. For voltages greater than 50 volts, electrostatic precipitation becomes the more significant removal mechanism.

The low voltage decay characteristic can be used to obtain an estimate of  $\Delta U$ , the fluctuating velocity of the large scale eddies. Since the electrostatic effects are unimportant for these low charging levels, the drop loss can be accounted for by turbulent diffusion alone. If the region is assumed to be uniformly mixed, the drop conservation for an incremental length  $\Delta z$  and width  $w$  of the channel can be written, using Eq. (5.2.4) for the particle flux-density to the walls, as

$$Uws[N(z + \Delta z) - N(z)] = -2(N\Delta U)w\Delta z \quad (9)$$

In the limit  $\Delta z \rightarrow 0$ ,

$$\frac{dN}{dz} = - \frac{2}{s} \frac{\Delta U}{U} N \quad (10)$$

and

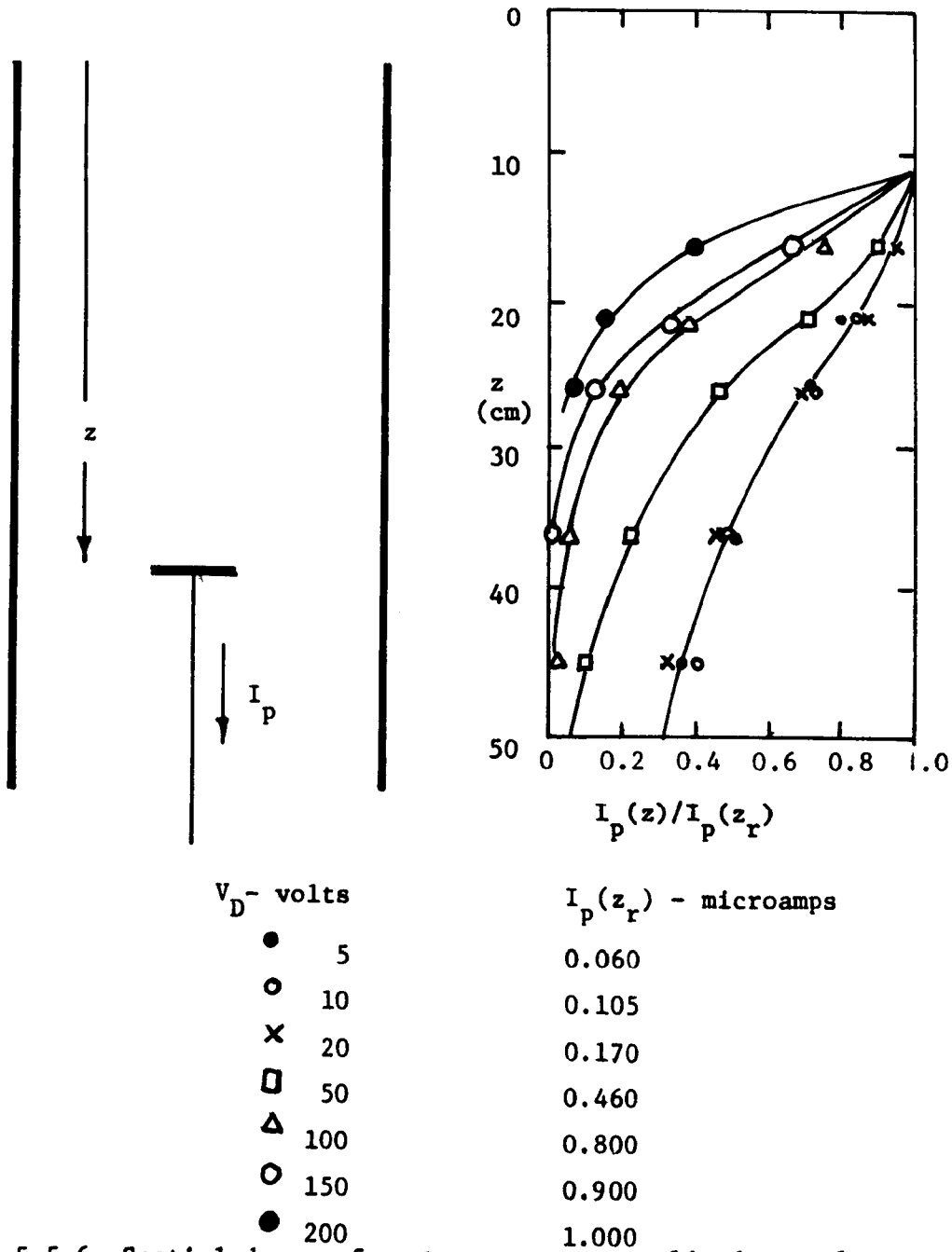


Fig. 5.5.6 Spatial decay of probe current normalized to value at  $z = z_r = 11\text{cm}$ , where  $z$  is the position of the probe relative to charging bars

$$\frac{N}{N_0} = e^{-z/\ell_T}; \quad \ell_T \equiv \frac{sU}{2\Delta U} \quad (11)$$

From the experiment

$$\ell_T \approx 30\text{cm} \rightarrow \Delta U \approx 15\text{cm/sec} \quad (12)$$

If the reference position is selected far enough downstream so that the drop velocity from that point onwards can be considered constant, the normalized current of Eq. (8) can be equated to the normalized particle concentration  $N(z)/N(z_r)$ . The evolution of monocharged drops entrained in a well-mixed channel flow is given by Eq. (5.2.11), which can be used to evaluate Eq. (8). Thus, the dependence of probe current on position is

$$\underline{I}(\underline{z}') = \underline{N}(\underline{z}') = \frac{1}{1 + \underline{z}'} \quad (13)$$

$$\underline{z}' = \frac{z - z_r}{\lambda_R(V, z_r)} ; \quad \lambda_R(V, z_r) = \frac{\epsilon_0 U}{N(z_r) Q(V) B(V)}$$

The droplet charge density at the reference position can be calculated from the probe current measured there. Since the velocity is known, and the mobility,  $B$ , determinable from the charging curve, all parameters necessary for the evaluation of the decay length for a given applied voltage are available.

If the reference position is taken as 16cm downstream of the bars, the decay lengths corresponding to a drop velocity of 4m/sec and the measured probe currents for the different charging voltages can be determined. These can then be used to find the normalized position,  $\underline{z}'$ , of each measuring point corresponding to the various voltages. If the measured values of the normalized current,  $\underline{I}_p$ , are plotted against their distance downstream of the reference point, normalized to the decay length appropriate for each charging voltage, and if electrical precipitation is the only removal process present, the data should lie on the curve given by Eq. (13) and shown as the solid curve in Fig. 5.5.7. Other removal processes will result in the droplet

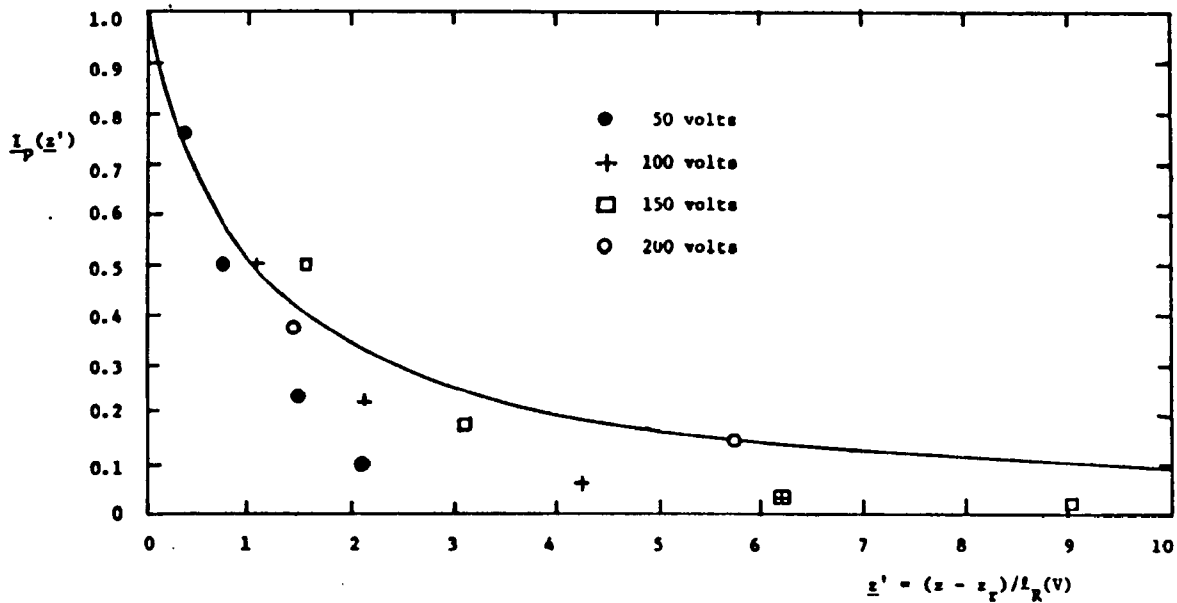


Fig. 5.5.7 Decay of current to probe normalized to value  $z_r = 16\text{cm}$  downstream of charging bars, beyond which drop velocity is constant (4m/sec). Downstream position  $z$  is normalized to decay length appropriate to particular charging voltage. Note that as voltage is raised decay rate approaches that predicted by theory assuming dominance of electric self-precipitation

concentration being attenuated more rapidly than the above relation would predict. From Fig. 5.5.7 it is evident that for voltages greater than 50 volts, the early portion of the decay corresponds to the purely electrostatic model. As expected, once the droplet population has been significantly diminished, diffusive effects become more important. Thus, at the positions further downstream, the droplet attenuation is greater than predicted for electrical self-precipitation alone. Agreement of the self-precipitation theory and measurements is quite good once the charging voltage exceeds 150 volts.

For diagnostic purposes using a fixed probe, it is useful to recognize the dependence of probe current on charging voltage that is implied by Eqs.

(7), (8) and (13). These combine to give

$$I_p = A_p UN(z_r) Q_R \frac{Q}{1 + Q^2} ; \quad Q \equiv \frac{Q}{Q_R} \quad (14)$$

where the characteristic charge

$$Q_R \equiv \sqrt{\frac{\epsilon_o U 6 \pi \eta R}{(z - z_r) N(z_r)}} \quad (15)$$

is the drop charge at which the probe current would peak if  $N(z_r)$  were maintained constant independent of  $Q$ . That is, at a fixed location  $z$ , the probe current  $I_p$  at first increases in proportion to the charging voltage, and then as the self-precipitation comes into play, peaks out and finally decreases in inverse proportion to the charging voltage. This characteristic is clearly evident in the measurements of probe current as a function of charging voltage shown in Fig. 5.5.8. Also as expected from Eqs. (14) and (15), the peak occurs at lower and lower values of  $V_D$  as the distance downstream is increased. Actually,  $N(z_r)$  is itself a function of the charging so that corrections should be made in evaluating Eq. (15) as a function of  $Q$ . But, taking as an average value  $N(z_r) = 5 \times 10^9 \text{ drops/m}^3$  inferred from the probe current measured at  $z_r = 11 \text{ cm}$  and with  $V_D = 100$  volts, the peaks in the curves of Fig. 5.5.8 are predicted by Eq. (15) (using the charging characteristic of Fig. 5.4.5 to relate  $V_D$  to  $Q_R$ ) to occur at 64, 51, 40 and 34 volts for the increasingly greater values of  $z$ . As would be expected, the agreement is good for the probe measurement taken furthest downstream.

## 5.6 Experimental Investigation of Self-Discharge of Bicharged Drops

One of the objectives in experimentally investigating the dynamics of systems of bicharged drops alone has been accomplished in Sec. 5.5.

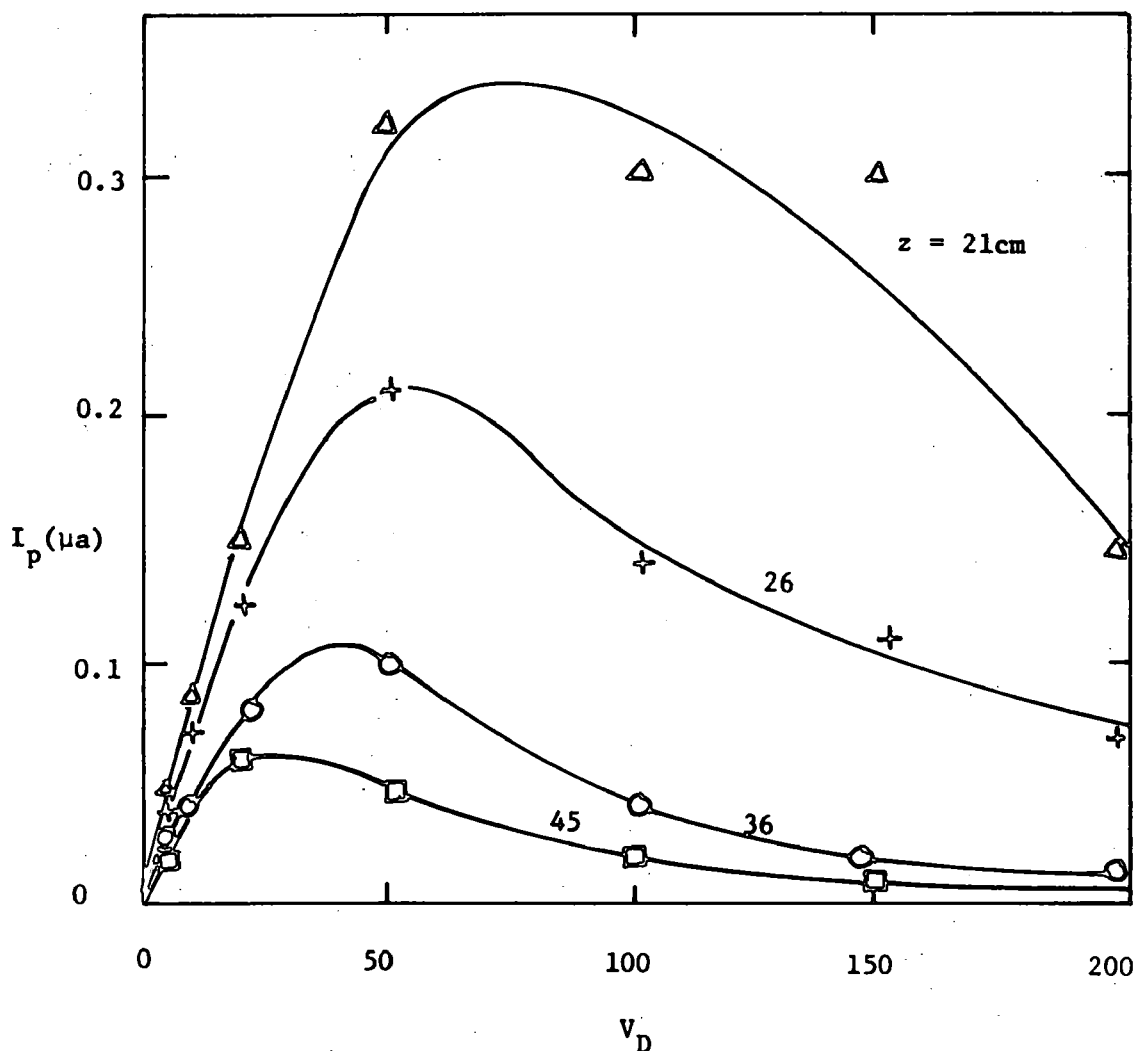


Fig. 5.5.8 Measured drop-probe current as function of  $V_D$  (which is proportional to the drop charge  $Q$ ) at four different positions  $z$  from charging bars

With bicharging, the development of the turbulent jet in the interaction channel of the system shown in Fig. 5.5.1 is much the same as with no charging. The spreading of the neutral bicharged beam is qualitatively independent of charging, and measurements of circulation velocity in the return channels indicate a gas velocity essentially independent of charging.



Hence, for the purposes of representing the fluid mechanics in the next chapter, the results of Sec. 5.5 are sufficient.

The second objective of establishing some confidence in the self-discharge theory discussed in Sec. 5.3 is pursued in the remainder of this section with the drop-jet injected into an essentially open region. This permits photographing the drops without the intervention of the wetted walls which make observation at best difficult in the enclosed system.

#### 5.6.1 Experimental Apparatus

The drop generator is again as described in Sec. 5.4.2 with the inducer bar voltages at opposite polarity and adjusted to produce drops of the same magnitude of charge. The drop stream is directed downward into an essentially open region, as shown in Fig. 5.6.1. To discern between the discharged drops and those that remain charged at a given distance  $z$  from the drop generator, a pair of electrodes are used as a precipitator to deflect the charged drops. For the potentials positive as shown in Fig. 5.6.1, positive drops are induced by the left bar, and if these remain charged upon reaching the analyzer at the position  $z$ , they are deflected to the right. The opposite is true of drops with charges induced by the right electrode. Of course, after about 20cm of travel, the initially sheet-like streams have developed into a turbulent jet and it is from this point on that interest is focused.

#### 5.6.2 Measurement of Drop Velocity

By making use of the analyzer electrodes as a field detector and exciting the inducer bars with 60Hz alternating voltage, it is easy to obtain a measure of the drop velocity as a function of distance from the drop generator. The system is as shown in Fig. 5.6.1 except that instead

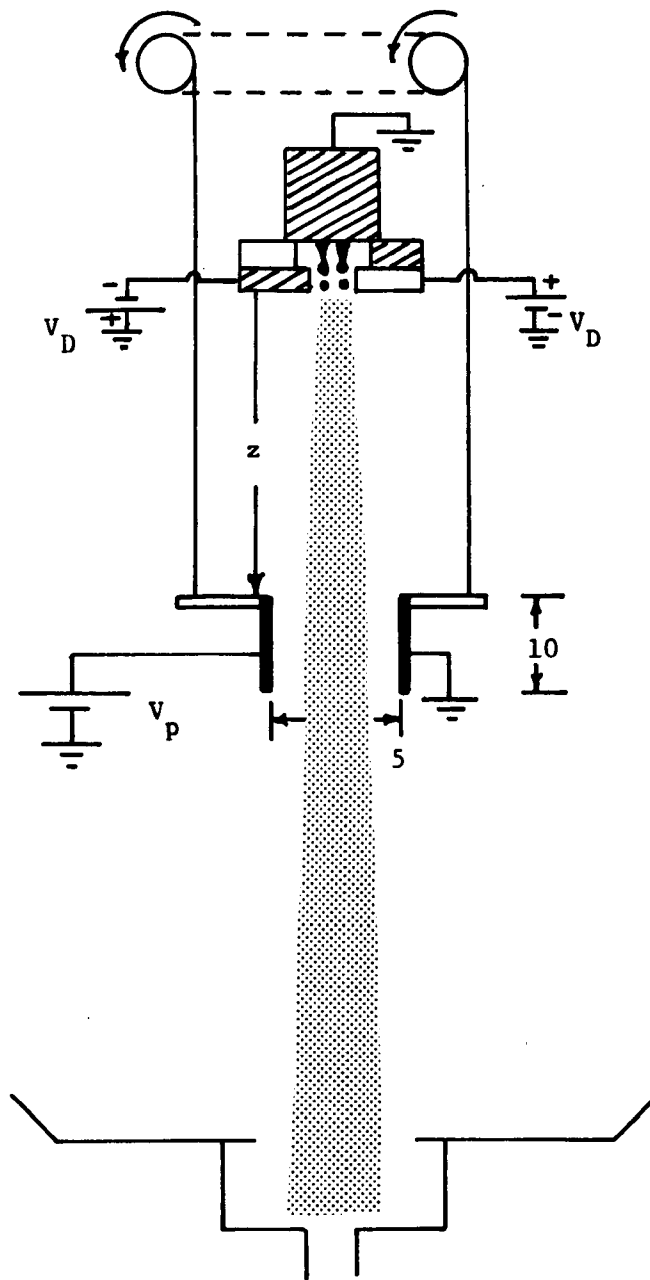
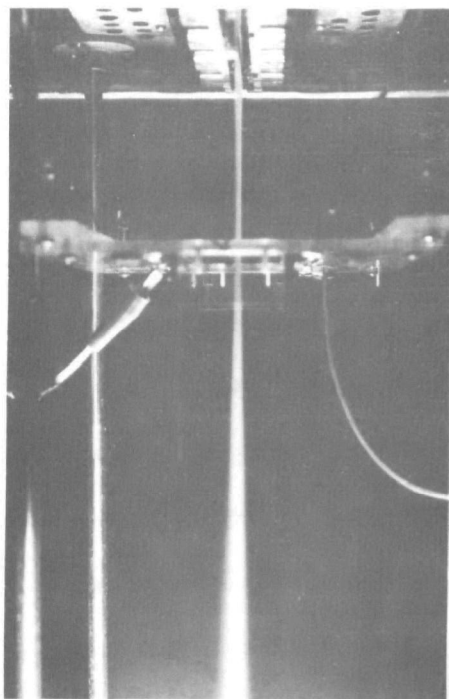
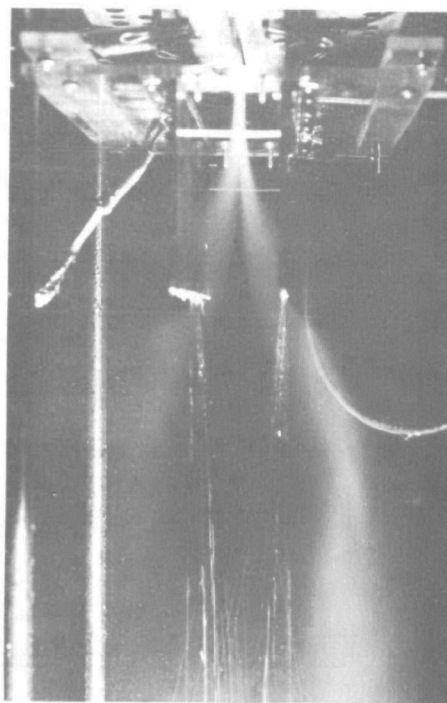


**Fig. 5.6.1** Bicharged drop stream with variable position analyzer to deflect drops that remain charged at a given position  $z$  Dimensions in cm.

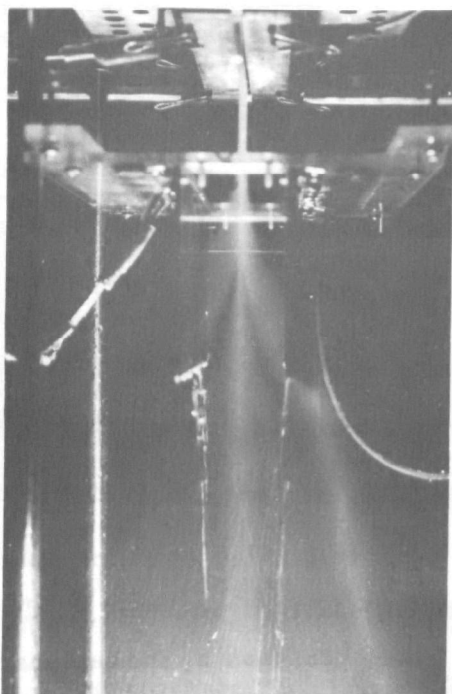
of the voltage source  $V_p$ , there is an oscilloscope. Also, the inducer bars are connected to the same a-c source so that the drop stream evolves as a traveling-wave of space charge. As this charge passes between the electrodes, charge induced on the left electrode results in a current which is measured



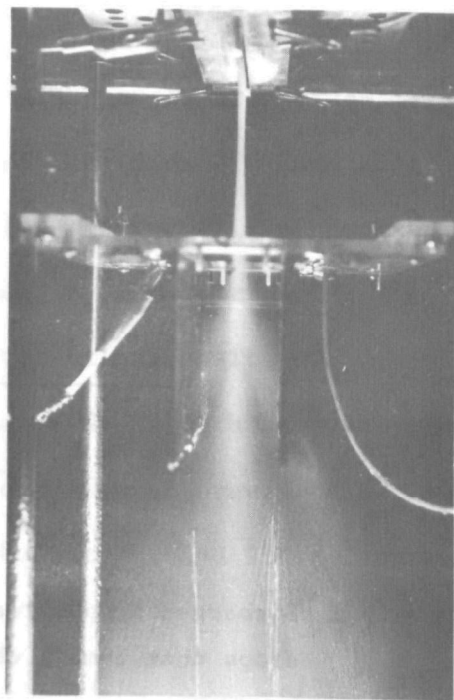
(a)



(b)



(c)



(d)

Fig. 5.6.2 Bicharged drop jet in configuration of Fig. 5.6.1. (a)  $V_D=0$  and  $V_p=0$ . With  $V_D=500V$  and  $V_p=6kV$ , (b)  $z = 3.5cm$ , (c)  $z = 7.25 cm$ , (d)  $z = 11 cm$ . Note increase in discharged drops as analyzer field is imposed increasingly further downstream.

by the oscilloscope. Measurement of positions  $z$  at which the signal changes its phase by  $180^\circ$  gives the half-wavelengths along the stream. Hence, the drop velocity at that position is  $v = f\lambda_d$ , where  $f = 60 \text{ Hz}$ . Typical drop velocities measured in this way for the unconfined drop-stream are shown in Table 5.6.1.

Table 5.6.1 Typical Drop Velocity as a Function of  $z$  as Measured by Observing Phase of Traveling Charge Wave

$z - \text{cm}$	$v - \text{m/sec}$
16	9.7
24	7.8
31	8.9
37	6.7
43	6.5

Hence, the drops are ejected at about 10m/sec, and in the unconfined configuration, continually transfer momentum to the surrounding air as they slow to 6.5m/sec near the bottom of the test range.

### 5.6.3 Drop Discharge Process

The jet of drops and entrained air is shown in Fig. 5.6.2. With no voltage  $V_p$  applied to the analyzer and no charge inducing voltage  $V_D$ , the drop jet appears as shown in Fig. 5.6.2a. At increasingly greater distances  $z$  from the inducer bars, the sequence of pictures then shows the effect of simultaneously charging the drops to  $V_D = 500$  volts and imposing an analyzer field with  $V_p = 6\text{kV}$ . The self-discharge of the two families of drops is evident from the photographs. At the first position, where the top edges

of the analyzer plates are 3.5cm below the inducer bars, essentially all of the drops remain charged, as is evident from their being deflected by the imposed analyzer field. By the time the drops reach the second position, where  $z = 7.25\text{cm}$ , a neutral beam is formed, which is undeflected by the analyzer. This beam has increased still more at the expense of the charged drops by the time drops reach the third position, where  $z = 11\text{cm}$ .

Over the length shown, the jet makes a transition over the first 5-10cm from a highly ordered pair of oppositely charged drop sheets to a turbulent jet. From the last two pictures, it is evident that the discharge process does in fact go forward in the turbulent flow region. Qualitatively, the discharge process occurs as expected. However, closer scrutiny shows that the discharge rate is slower than expected from Eq. (5.3.21) with  $K' = 2$ . Based on the width of the jet entering the analyzer in Fig. 5.6.2c, the total drop density is  $3 \times 10^{-9} \text{drops/m}^3$ . Using the charge and mobility extrapolated from Fig. 5.4.5,  $\tau_R = 5.5 \times 10^{-4} \text{sec}$  and  $\ell_R = 0.5\text{cm}$ . This is to be compared to  $\ell_R = 3-4\text{cm}$  inferred from the last two photographs and Eq. (5.3.21) by taking  $N/N_0 \approx 1/2$ ,  $z = (11-7.25)\text{cm}$  and  $N_0$  defined as the number density at  $z = 7.25\text{cm}$ . Thus, the experimental evidence is that in the turbulent jet, the drops discharge each other at a rate 6-8 times more slowly than would be expected from the model leading to Eq. (5.3.21).

Considered as a pair of oppositely charged sheets, so that the drops experience an essentially uniform electric field, but nevertheless are retarded by the viscous drag of an isolated sphere, the sheets would be attracted to each other within a distance of 0.2mm from the charging section. Considered as isolated pairs of drops having the initial spacing of 1.6mm between the sheets, the drops should neutralize each other within 3.7cm,

according to the two drop model of Sec. 5.3.1 ( $C = 4.7 \times 10^4$ ,  $\tau_R = 0.6$  sec,  $\tau_{sR} = 7 \times 10^{-3}$  sec). It is clear from the pictures that the drops survive retaining their initial charge, to a distance of several centimeters. Beyond this distance, the turbulent regime prevails.

The spreading of the deflected drops might be interpreted as an indication that the drops are not uniform in size or in charge. In fact, they are extremely uniform in both, and the spreading is a portent of the electrohydrodynamic instability that characterizes the transition from the highly ordered drop beam to the turbulent jet. A pair of charged sheets of drops are unstable, in the sense that the sheets tend to buckle, some drops moving inward and some outward under the influence of the self consistent self-fields. Ignoring the viscous drag, the rate of growth of this instability can be shown to be

$$\tau_{EH} = \sqrt{\frac{8\pi R^3 \rho \epsilon_0}{N_0^s Q^2 k}} \quad (1)$$

where  $N_0^s$  is the surface number density of drops in a sheet and  $k$  is the wavenumber of the instability wavelength in the  $z$  direction. Taking  $k = 2\pi/\lambda_s$  as the fastest growing wavelength where  $\lambda_s$  is the distance in the  $z$  direction between drops, (the shortest distance consistent with the continuum model used to derive Eq. (1)),  $N_0^s = 6 \times 10^{-11}$  drops/m<sup>2</sup> and  $Q$  and  $M$  consistent with the drop size and charging voltage, the rate of growth of this instability is predicted by Eq. (1) to e-fold in the distance 2.5mm. Noise initiated at the drop generator excites this instability, which then apparently amplifies into the distribution of particles seen when the analyzer field is applied.

## 6 Scrubbing and Precipitation of Charged Submicron Aerosols by Charged Supermicron Drops

### 6.1 Objectives

Three mechanisms for removal of submicron particulate by means of fields associated with charged drops are explored theoretically and experimentally in this chapter. In two of these, the CDS-I and CDS-II configurations, the particulate is collected by the drops. First, unipolar drops (of one sign) are used to collect submicron particles (of the opposite sign), and then bicharged drops, injected with net space charge neutrality, are used to collect charged particulate. In the third mechanism, the CDP configuration, drops and particulate are charged to the same sign, and hence the particulate is collected on the walls, much as in a conventional imposed field precipitator or in a space charge precipitator. The basic difference comes from the lifetime of the charged drops.

To develop a model for the CDS types of interactions it is first necessary to have a theory for the process through which the charged drops collect the charged particulate. To this end, Sec. 6.2 develops theories appropriate when the fields dominate in the collection process in two aerodynamic extremes, where the flow is laminar and where it is completely turbulent. For the most practical situations, these theories point at essentially the same collection rate. The remainder of the sections devoted to developing models, Secs. 6.3-6.6, combine the constituents of the three systems to obtain the cleaning performance as a function of basic parameters. Fundamentally, these systems involve five time constants: three times connected with the charged drops and particles,  $\tau_a$ ,  $\tau_R$  and  $\tau_c$ , which represent phenomena having an effect in accordance with their relation to two

more times, the gas residence time and the drop residence time. Experiments are correlated with these models in Secs. 6.7-6.9. The main products of this chapter are models, supported and qualified by experimental correlations, that can be used to scale and optimize the CDS-I, CDS-II and CDP configurations.

## 6.2 Models for Particle Collection on Isolated Drops

### 6.2.1 Laminar Theory of Whipple and Chalmers

Whipple and Chalmers (1944) use an imposed field and laminar flow model to predict the charging of water drops as they fall through positive, negative, and both positive and negative ions. Their theories cover the results given earlier by Pauthenier and Mme. Moreault-Hanot (1932). This latter work, which is the basis for the theory of impact (field) charging as used in precipitator design (see Sec. 5.4.4), did not include the aerodynamic effect of the streaming neutral gas. Because the particle inertia is ignored, the model developed here for collection of charged particles on a charged drop moving relative to a laminar gas is essentially the same as these ion-impact models.

A schematic view of the physical situation is depicted by Fig. 6.2.1 wherein the particle is viewed as fixed in the frame of reference, and hence the neutral gas streams relative to the drop with a velocity  $w_0$ . The imposed field, like the relative flow, is uniform at infinity with the amplitude  $E_0$  which is defined as positive if directed as shown in Fig. 6.2.1.

Objectives in the following derivations are to determine the rate of charging and hence particle collection of the drop, given its initial charge, and to find the final charge established. Regimes of charging are demarked by the critical charge



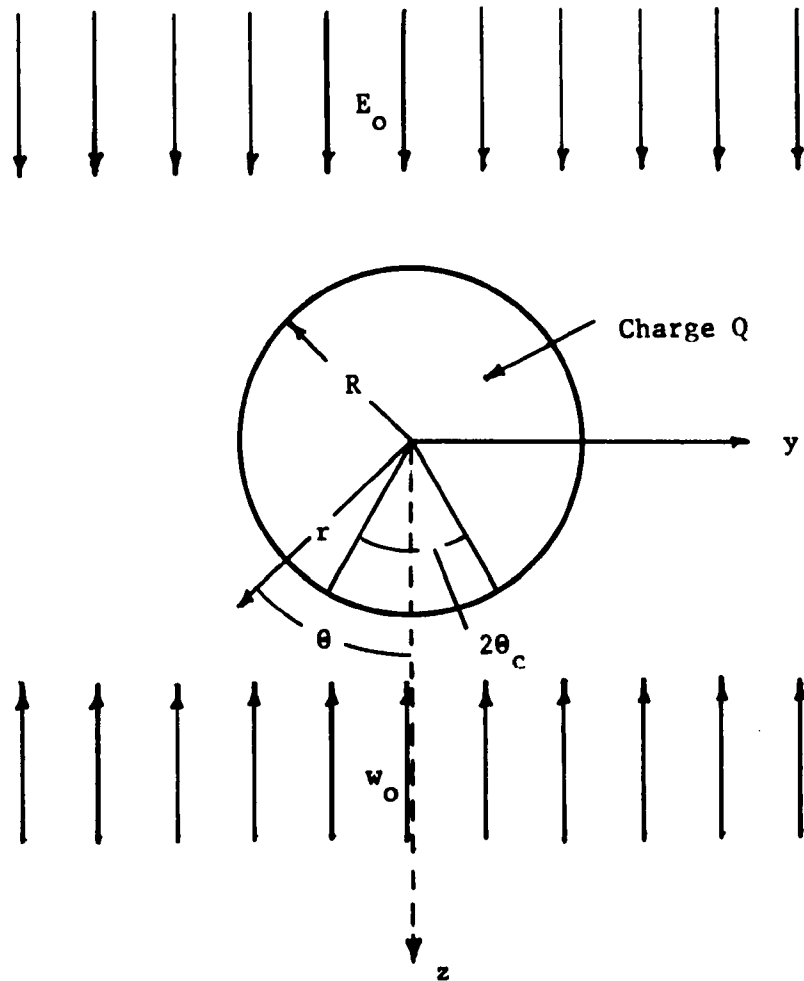


Fig. 6.2.1 Spherical conducting drop in imposed electric field  $E_0$  and relative flow  $w_0$  that are uniform at infinity.  $E_0$  and  $w_0$  are positive if directed as shown; in general, the electric field intensity  $E_0$  can be either positive or negative

$$Q_c = 12\pi\epsilon_0 R^2 E_0 \quad (1)$$

which can be positive or negative, depending on the sign of  $E_0$ . Rates of charging are characterized by the currents

$$I_{\pm} = \pi R^2 b_{\pm} \rho_{\pm} E_0 \quad (2)$$

also determined in sign by  $E_0$ . The magnitudes of the positive and

negative particle charge densities are  $n_{\pm} q_{\pm} \rho_{\pm}$  respectively, at infinity.

That the charging rate is to be calculated infers that the particle motions are not in the steady state. However, if transit times through several drop radii  $R$  are short compared to charging times of interest, then the drop charge,  $Q$ , and its associated field can be regarded as constant throughout the transit. The drop is well represented as perfectly conducting, hence the potential and electric field intensity follow from well known solutions (in spherical coordinates  $(r, \theta, \phi)$ .)

$$\bar{E} = -\nabla\phi = \{E_o(\frac{2R^3}{3} + 1) \cos\theta + \frac{Q}{4\pi\epsilon_o r^2}\} \bar{i}_r + \{E_o(\frac{R^3}{3} - 1) \sin\theta\} \bar{i}_\theta \quad (3)$$

Contributions to the field from the charge density of the particle are ignored. Because  $\nabla \cdot \epsilon_o \bar{E} \approx 0$ , a stream function for the electric field intensity can be defined as

$$\Sigma = -E_o R^2 [\frac{R}{r} + \frac{1}{2}(\frac{r}{R})^2] \sin^2\theta + \frac{Q \cos\theta}{4\pi \epsilon_o} \quad (4)$$

where

$$\bar{E} = -\nabla_{\mathbf{x}}[\bar{i}_\theta \frac{1}{r \sin\theta} \Sigma]$$

It will be evident shortly that the particular details of the velocity distribution are surprisingly unimportant. We could use potential flow, but here we follow Whipple and Chalmers (1944) and use low Reynolds number flow. Thus, it is possible to make both components of velocity at the spherical surface vanish. In terms of the stream function, the boundary condition at infinity is  $\psi = \frac{1}{2} w_o (r \sin\theta)^2$ . In fact, the stream function

is readily available in the literature.

$$\psi = \frac{w_o R^2}{2} \left[ \left(\frac{r}{R}\right)^2 - \frac{3}{2} \left(\frac{r}{R}\right) + \frac{1}{2} \frac{R}{r} \right] \sin^2 \theta \quad (5)$$

where

$$\bar{v} = - \nabla x \left[ i_\phi \frac{1}{r \sin \theta} \psi \right] \quad (6)$$

Equations 4.4.5 (with diffusion and space charge negligible) and 4.4.6 define the particle motions. They are equivalent to

$$dn_\pm = 0 \quad \text{on} \quad \frac{d\bar{r}}{dt} = \bar{v} \pm b_\pm \bar{E} \quad (7)$$

That is, the particle density of each species is constant along given force lines in  $(\bar{r}, t)$  space. If we are interested in determining the charge distribution within a volume enclosed by the surface  $S$ , then it is appropriate to impose boundary conditions on the  $i$ 'th species, wherever

$$\bar{n} \cdot (\bar{v} \pm b_\pm \bar{E}) < 0 \quad (8)$$

where  $\bar{n}$  is taken as positive if directed out of the volume of interest. At points on the surface other than those that satisfy Eq. (8), a boundary condition cannot be imposed. These observations, although seemingly obvious in the transient problem, are crucial to making sense out of quasi-steady motions.

With the stream functions given, the lines of constant charge density given by Eq. (7) take the form

$$\frac{d\bar{r}}{dt} = - \frac{1}{r^2 \sin \theta} \frac{\partial}{\partial \theta} (\pm b_\pm \Sigma + \psi) \quad (9)$$

$$r \frac{d\theta}{dt} = \frac{1}{r \sin\theta} \frac{\partial}{\partial r} (\pm b_{\pm} \Sigma + \Psi) \quad (10)$$

Multiplication of Eq. (10) by  $dr/d\theta$  and equating that expression to Eq. (9) multiplied by  $r$  gives the exact differential

$$d(\pm b \Sigma + \Psi) = 0 \quad (11)$$

provided  $\Sigma$  and  $\Psi$  are independent of time. Here, the fundamental assumption of quasi-steady particle motions must be invoked. To integrate particle equations of motion in this way particles must see essentially the same field and flow distribution throughout their motions through the volume of interest. But the particle transit times are likely to be brief compared to the time required for particles to charge the drop and hence change the electric field intensity significantly. Thus, over a longer time scale, the flow and field distribution, hence the stream functions, are functions of time. In summary, Eq. (11) shows that the charge density of a given species is constant along constant stream function lines

$$n_{\pm} = \text{constant on } \pm b_{\pm} \Sigma + \Psi = \text{constant} \quad (12)$$

Given Eqs. (4) and (5), the characteristic lines are determined by substituting into (11) to get

$$\begin{aligned} & \mp \left[ \frac{R}{r} + \frac{1}{2} \left( \frac{r}{R} \right)^2 \right] \sin^2 \theta \pm \frac{3Q}{Q_c} \cos \theta \\ & + \frac{1}{2} \frac{w_o}{b_{\pm} E_o} \left[ \left( \frac{r}{R} \right)^2 + \frac{1}{2} \left( \frac{R}{r} \right) - \frac{3}{2} \left( \frac{r}{R} \right) \right] \sin^2 \theta = C \end{aligned} \quad (13)$$

The upper and lower signs, respectively, refer to positive and negative particles and  $C$  is a constant which determines the particular characteristic line.

Just what constant charge density should be associated with each of these lines is determined by a single boundary condition imposed wherever the line "enters" the volume of interest at a point satisfying Eq. (8). Here,  $\bar{n}$  is outward at infinity and inward on the spherical surface of the drop.

In terms of parameters now introduced, the object is to obtain the net instantaneous electrical current to the drop  $i_{\pm}(Q, E_0, w_0, n_+q_+, n_-q_-)$ . With the imposed field, velocity and charge densities held fixed, this expression then serves to give the rate of drop charging as

$$\frac{dQ}{dt} = i_+(Q) + i_-(Q) \quad (14)$$

The rates of particle collection are then  $i_+/q_+$  and  $-i_-/q_-$  for the respective species. Permutations and combinations of flow velocity, imposed field, instantaneous drop charge, and sign of the incident particles are extremely large, so an orderly approach is required to sort out the possible collection regimes. These are conveniently pictured in the  $Q - bE_0$  plane: for positive particles Fig. 6.2.2, for negative ones Fig. 6.2.3. First, recognize the surfaces which satisfy the condition of Eq. (8), and hence impose boundary conditions. For positive particles (upper sign) the distribution of particle densities for particles entering at  $z \rightarrow -\infty$  is required if  $bE_0 > w_0$ . Otherwise, the charge density is imposed as  $z \rightarrow +\infty$  because the positive particles enter from below. Thus, the charge-imposed field plane divides into two regimes,  $b_+E_0 > 0$ .

Lines of force  $\bar{v} \pm b_{\pm}\bar{E}$  originating on the spherical surface carry zero charge density. At those points on the surface where the force lines are into the drop, there is the possibility of particle migration. At the drop surface, the velocity normal to the surface is zero, hence the force lines

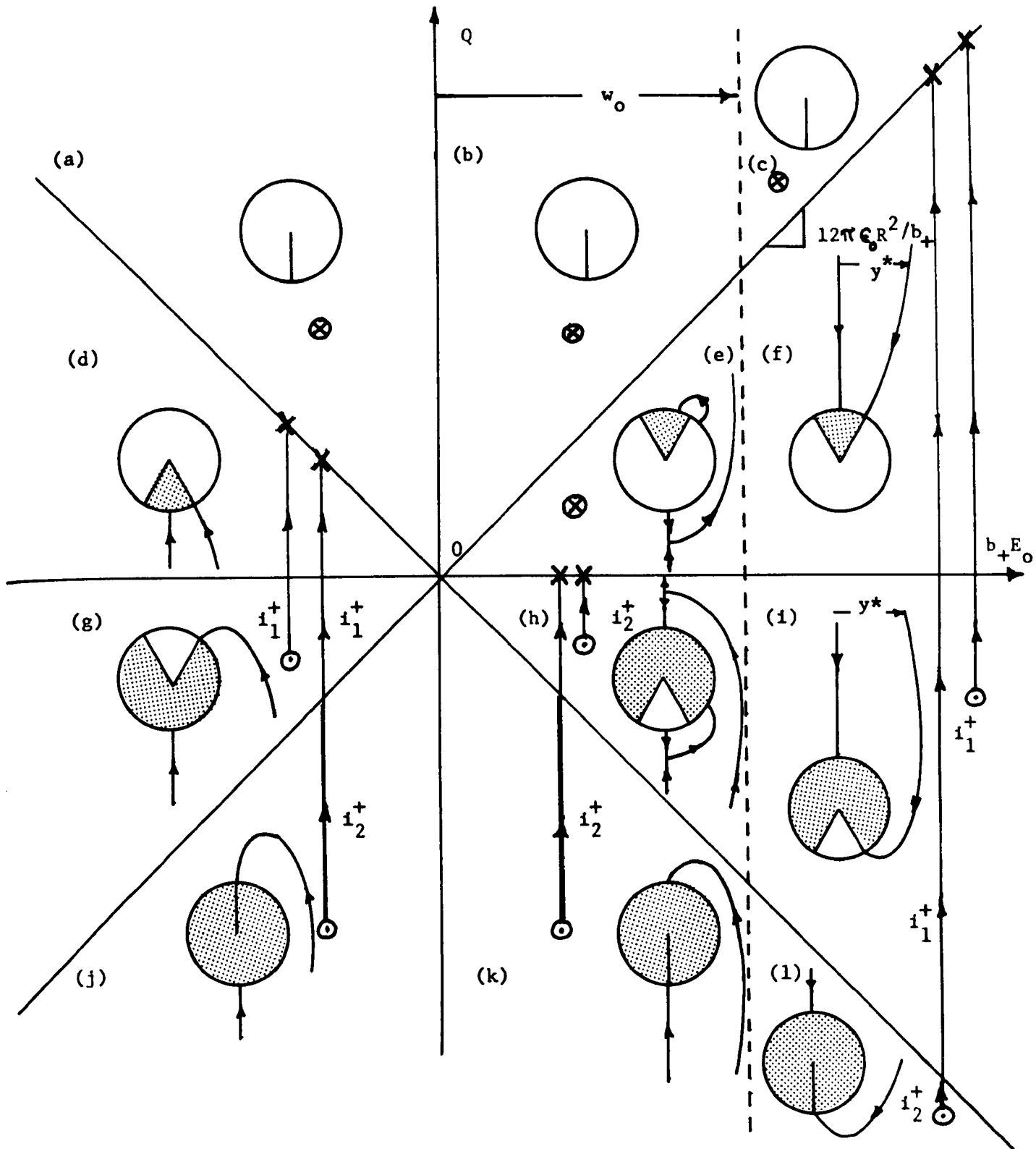


Fig. 6.2.2 Positive particle charging diagram. Charging regimes depicted in the plane of drop charge  $Q$  and mobility-field product  $b_+ E_0$ . With increasing fluid velocity, the vertical line of demarcation indicated by  $w_0$  moves to the right. Initial charges, indicated by  $\circ$ , follow the trajectories shown until they reach a final value given by  $\times$ . If there is no charging, the final and initial charges are identical, and indicated by  $\otimes$ . The inserted diagrams show the force lines  $\vec{v} \pm b_+ E_0$ .

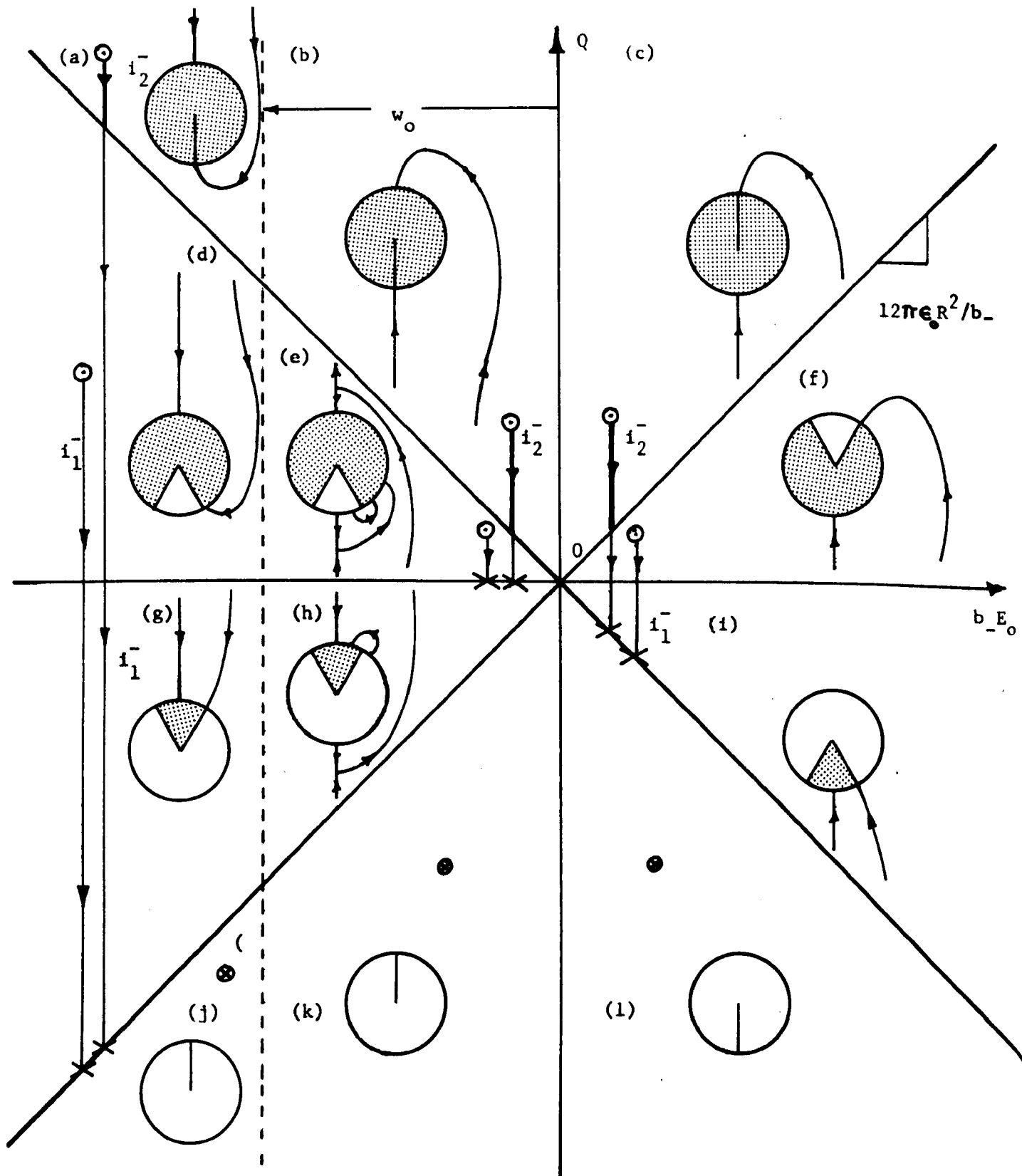


Fig. 6.2.3 Negative particle charging diagram. Conventions are as in the previous figure. With increasing fluid velocity, the line of demarcation indicated by  $w_0$  moves to the left

degenerate to  $\pm b_{\pm} \bar{E}$ . This greatly simplifies the charging process, because the electric field intensity given by Eq. (3) can be used to decide whether or not a given point on the particle surface can accept charge. Evaluation shows that force lines are directed into the particle surface wherever

$$E_o > 0 ; \theta_c < \theta < \pi ; \text{ positive particles} \quad (15)$$

$$E_o < 0 ; 0 < \theta < \theta_c ; \text{ negative particles} \quad (16)$$

The critical angle  $\theta_c$  demarking regions of inward and outward force lines follows from Eq. (3) as satisfying

$$\cos \theta_c = - \frac{Q}{Q_c} \quad (17)$$

where  $Q_c$  is defined by Eq. (1).

A graphical representation of what has been determined is given by the direction of incident force lines on the drop surfaces sketched in Figs.

6.2.2. and 6.2.3. Where directed inward, these force lines indicate a possible positive particle current. Whether or not the current is finite depends on whether the given force line originates on the boundary or at infinity. In any case, if the force lines is directed outward, there is no charging current to the particle, and so without further derivations, regimes (a), (b) and (c) for the positive particles and (j), (k) and (l) for the negative particles (Fig. 6.2.3) give no charging current; from Eq. (14) the particle charge remains at its initial value within that regime.



Regimes (f) and (i) for Positive Particles: (b) and (g) for Negative Particles To continue the characterization of each regime shown in Figs. 6.2.2 and 6.2.3, upper and lower signs respectively will be used to refer to the positive and negative particle cases.

The characteristic line terminating at the critical angle on the drop surface reaches the  $z \rightarrow -\infty$  surface at the radius  $y^*$  shown in the respective regimes in the figures. Particles entering within that radius strike the surface of the drop within the range of angles wherein the drop can accept particles. Hence, to compute the instantaneous drop charging current, simply find this radius  $y^*$  and compute the total current passing within that radius at  $z \rightarrow -\infty$ . The particular line is defined by Eq. (13) evaluated at the critical angle, and on the particle surface:  $\theta = \theta_c$ ,  $r = R$ . Thus, the constant is evaluated to be

$$C = \pm \frac{3}{2} \left[ 1 + \left( \frac{Q}{Q_c} \right)^2 \right] \quad (18)$$

To find  $y^*$ , take the limit of Eq. (13) using the constant of Eq. (18) to determine that

$$(y^*)^2 \left( 1 \mp \frac{w_o}{b_{\pm} E_o} \right) = 3R^2 \left[ 1 - \frac{Q}{Q_c} \right]^2 \quad (19)$$

The problem is particularly simple because the particle flux at infinity is uniform, so the current passing through the surface with radius  $y^*$  is simply the product of the current density and the circumscribed area

$$i_1^{\pm} = \pm n_{\pm} q_{\pm} (\pm b_{\pm} E_o - w_o) \pi (y^*)^2 \quad (20)$$

The combination of Eqs. (19) and (20) is

$$i_1^{\pm} = 3I_{\pm} \left( 1 - \frac{Q}{Q_c} \right)^2 = \pm 3 |I_{\pm}| \left( 1 \mp \frac{Q}{|Q_c|} \right)^2 \quad (21)$$

The second equality is written by recognizing the sign of  $E_0$  in the respective regimes.

In the positive particle regimes (f) and (i), the charging current is positive, tending to increase the particle charge until it reaches the limiting value  $Q = |Q_c|$ . Charging trajectories are shown in the figures, with  $i_1$  the rate of charging, whether the initial drop charge is within the respective regimes or the charge passes from another regime into one of these regimes, and then passes on to its final value,  $|Q_c|$ . For example, in the case of the positive particle charging, it will be shown that a particle charges at one rate in regime (l) and then, on reaching regime (i), assumes the charging rate given by Eq. (21), which it obeys until the charge reaches a final value on the boundary between regimes (f) and (c).

Also summarized in the charge field plots of Figs. 6.2.2 and 6.2.3 are the force line patterns, and the critical angles defining those portions of the drop over which conduction can occur. As a drop charges and then passes from regime (i) to (f), and finally to the boundary between regimes (f) and (c) in the positive particle case, the angle over which the drop can accept particles decreases from a maximum of  $2\pi$  to  $\pi$  at  $Q = 0$ , and finally to zero when  $Q = |Q_c|$ . It is the closing of this "window" through which charge can be accepted to the particle surface which is the essence of the collection process.

#### Regimes (d) and (g) for Positive Particles; (f) and (i) for Negative

Particles These regimes are analogous to the four just discussed except that the particles enter at  $z \rightarrow \infty$ , rather than at  $z \rightarrow -\infty$ . The derivation is therefore as just described except that the limiting form of (13) is taken as  $\theta \rightarrow 0$ , with  $C$  again given by Eq. (18) to obtain

$$(y^*)^2 \left(1 + \frac{w_o}{b_{\pm} E_o}\right) = 3R^2 \left(1 + \frac{Q}{Q_c}\right)^2 \quad (22)$$

Then, the particle currents can be evaluated as

$$i_1^{\pm} = -3I_{\pm} \left(1 + \frac{Q}{Q_c}\right)^2 = \pm 3|I_{\pm}| \left(1 + \frac{Q}{|Q_c|}\right)^2 \quad (23)$$

As would be expected on physical grounds, the positive particle case gives charging currents and final drop charges in regimes (d) and (g) which are the same as those in (f) and (i).

Regimes (j) and (k) for Positive Particles; (b) and (c) for Negative

Particles For these regimes, the total surface of the drop can accept particles. The radius for the circular cross section of particles reaching the surface of the drop from  $z \rightarrow \infty$  is determined by the line intersecting the drop surface at  $\theta = \pi$ . This line is defined by evaluating Eq. (13) at  $r = R$ ,  $\theta = \pi$  to obtain

$$C = + \frac{3Q}{Q_c} \quad (24)$$

Then, if the limit is taken  $r \rightarrow \infty$ ,  $\theta \rightarrow 0$  of Eq. (13),  $y^*$  is obtained and the current can be evaluated as

$$i_2^{\pm} = \pm n_{\pm} q_{\pm} (\pm b_{\pm} E_o + w_o) \pi (y^*)^2 = - \frac{12|I_{\pm}|}{|Q_c|} Q \quad (25)$$

Note that in the positive particle regimes,  $Q$  is negative, so the result indicates that the particle charges at this rate until it leaves the respective regimes when the charge  $Q = -|Q_c|$ .

Regime (l) for Positive Particles; (a) for Negative Particles The situation here is similar to that for the previous cases, except that

particles enter at  $z \rightarrow -\infty$ , so the appropriate constant for the critical characteristic lines given by Eq. (13) evaluated at  $r = R$ ,  $\theta = \pi$ , is the negative of Eq. (24). The limit of that equation given as  $r \rightarrow \infty$ ,  $\theta \rightarrow \pi$  gives  $y^*$  and evaluation of the current gives a value identical to that found with Eq. (25). In regime (1), for positive particles, where the initial charge is negative, the charging current is positive, and tends to reduce the magnitude of the drop charge until it enters regime (i), where its rate of charging shifts to  $i_1$  and it continues to acquire positive charge until it reaches the final value  $|Q_c|$  indicated on the diagram.

Regime (e), Positive Particles; Regime (h), Negative Particles In regimes (e) and (h) for either sign of particles, the window through which the drop can accept a particle flux is on the opposite side from the incident particles. Typical force lines are drawn in Fig. 6.2.4. Force lines terminating within the window through which the drop can accept particles can originate on the drop itself. In that case, the charge density on the characteristic line is zero, since the drop surface is incapable of providing particles.

To determine the particle charge that just prevents force lines originating at  $z \rightarrow \infty$  from terminating on the particle surface, follow a line from the  $z$ -axis where the drops enter at infinity back to the drop surface. That line has a constant determined by evaluating Eq. (13) with  $\theta = 0$

$$C = \pm \frac{3Q}{Q_c} \quad (26)$$

Now, if Eq. (13) is evaluated using this constant, and  $r = R$ , an expression is found for the angular position at which that characteristic line meets the drop surface

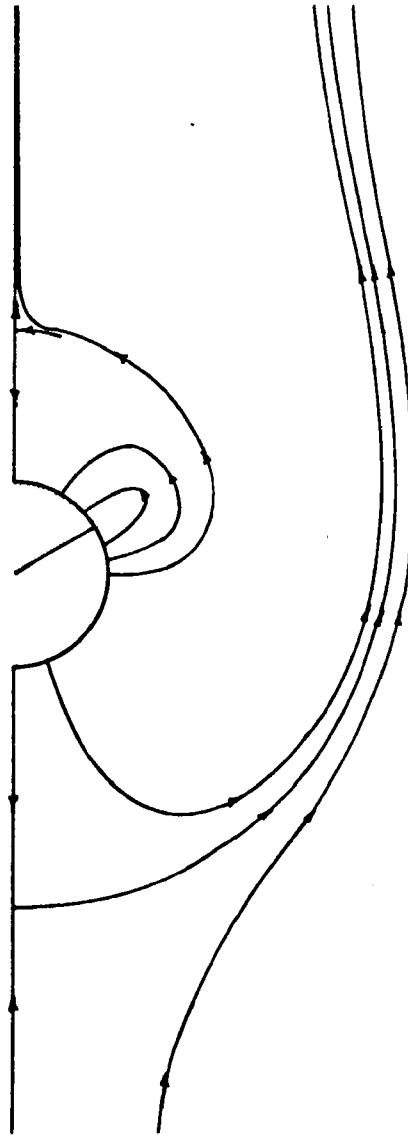


Fig. 6.2.4 Force lines in detail for regimes (e) for the positive ions and (h) for the negative ions. Here, all of the force lines terminating on the particle, also originate on the particle; hence, there is no charging. For the case shown,  $w_0 = \pm 2bE_0$ ,  $Q = \pm Q_c/2$

$$\frac{3}{2} \sin\theta = \frac{3Q}{Q_c} (\cos\theta - 1) \quad (27)$$

Note that the quantity on the right is always negative if  $Q/Q_c$  is positive, as it is in regimes (e) for the positive particles and (h) for the negative. Thus, in regime (e) for the positive particles and (h) for the negative, the rate of charging vanishes and the drop remains at its initial charge.

Regime (h) for Positive Particles; (e) for Negative Particles In these

regimes,  $Q/Q_c$  is negative and Eq. (27) gives an angle at which the characteristic line along the  $z$ -axis meets the particle surface. Typical force lines are shown in Fig. 6.2.5. To compute the rate of charging, the solution to this equation is not required because a circular area of incidence for particles at  $z \rightarrow \infty$  is then determined by the characteristic line reaching the drop at  $\theta = \pi$ . Actually, no new calculation is necessary because that radius is the same as that found for regime (k) for the positive particles and (b) for the negative. The charging current is  $i_2^\pm$ , as given by Eq. (25). Drops in these regimes discharge until they reach the charge zero. Moreover, if the initial drop charges place the drop in regimes (k) for the positive particles or (b) for the negative particles, the rate of discharge follows the same law through regimes (h) for the positive particles and (e) for the negative until the drop reaches zero charge.

Positive and Negative Particles Simultaneously If both positive and negative particles are present simultaneously, the drop charging is characterized by simply superimposing the results summarized with Figs. 6.2.2 and 6.2.3. The diagrams are especially helpful in this regard, in that the charging current for any given imposed field and drop charge is obtained as the superposition of the respective charging currents. Practically, the diagrams are superimposed with their origins (marked 0) coincident. A given point in either plane then specifies the charge and field experienced by both families of charges. This justifies merely superimposing the respective currents at the given point to find the total charging current.

#### 6.2.2 Collection With Complete Turbulent Mixing

The laminar flow picture of the collection process relates to the actual electromechanics of the particle migrations in a practical scrubber

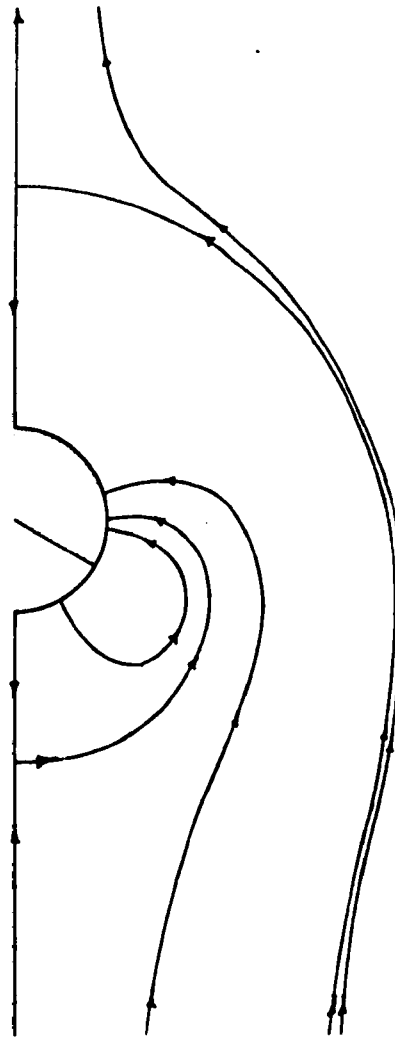


Fig. 6.2.5 Regimes (h) for the positive ion and (e) for the negative.  
Some of the force lines extend to where the charge enters.  
 $w_0 = \pm 2b_{\pm}E_0$ ,  $Q = \pm Q_c/2$

configuration in much the same way that laminar models for the conventional ESP represent the collection process in a real device. As in an industrial scale ESP, turbulent flow characterizes the fluid mechanics of the drops injected into the gas, and the resulting mixing dominates in determining the distribution of particles among the drops.

One way to see that the turbulent diffusion must have a dominant effect is to evaluate the characteristic time for the fine scale turbulent diffusion. From Eq. (5.3.2), this time is of the order

$$\tau_t \approx \frac{l^2}{D_t} = \frac{1}{\beta} \sqrt{\frac{\eta}{\gamma_T}} \quad (28)$$

where  $\beta$  is of order unity and the large scale energy dissipation density

$\gamma_T$  is given by Eq. (5.3.3). For the turbulent jet described in Chap. 5 and used in the experiments of Secs. 6.7-6.9,  $\gamma_T \sim 10^{-1}$ , and hence the characteristic time for turbulent diffusion is of the order  $10^{-2}$  secs.

This time is to be compared to the time typically required for particles to be collected on the drops. The results of this section support the simple model introduced in Sec. 2.4 which argues that this collection time is of the order

$$\tau_c = \frac{\epsilon_0}{NQb} \quad (29)$$

Typically,  $NQ \approx 10^{-4}$  coul/m<sup>3</sup> and  $b = 10^{-7}$  m/sec/V/m, and hence  $\tau_c \approx 1$  sec.

It can be inferred from the fact that  $\tau_t \ll \tau_c$  that until the particles are in the immediate vicinity of a drop, their density is essentially determined by the fluid mechanics. Locally, the turbulent diffusion tends to make the distribution of particles uniform between the drops.

By complete mixing, it is meant that the particle density over a surface very nearly coinciding with that of the drop is uniform. In this extreme, which represents the most optimistic picture of the electrically induced scrubbing, the rate of collection is easily calculated. The current normal to the drop surface has only an electrical component which is evaluated using Eq. (6.2.3) for  $E_r(r = R)$ . This calculation must be carried out taking care to recognize that there is a collection of positively charged particles only over that part of the drop surface where  $E_r < 0$ , and of negative particles where  $E_r > 0$ . The characterization of the possible collection regimes summarized by Figs. 6.2.2 and 6.2.3 is again helpful. Now however it is only necessary to distinguish three regimes. The first of these is  $Q < -|Q_c|$

$$i = - \oint n_+ q_+ b_+ \bar{E} \cdot \bar{n} da = -n_+ q_+ b_+ \oint \bar{E} \cdot \bar{n} da \quad (30)$$



From Gauss' Law, the integral over the surface enclosing the drop is  $Q/\epsilon_0$  and hence

$$i = -n_+ q_+ b_+ \frac{Q}{\epsilon_0} = i_2^+ ; G_1 = -n_+ b_+ \frac{Q}{\epsilon_0} \text{ for } Q < -|Q_c| \quad (31)$$

where  $G_1$  is the rate of particle collection per drop.

The second regime  $Q > |Q_c|$  is similar with negatively charged particulate rather than positively charged particulate collection.

$$i = -n_- q_- b_- \frac{Q}{\epsilon_0} = i_2^- ; G_1 = n_- b_- \frac{Q}{\epsilon_0} \text{ for } Q > |Q_c| \quad (32)$$

In the third regime where  $-|Q_c| < Q < |Q_c|$  both positive and negative particles contribute

$$i = i_1^+ + i_1^- = 3\{|I_+|(1 - \frac{Q}{|Q_c|})^2 - |I_-|(1 + \frac{Q}{|Q_c|})^2\} \text{ for } -|Q_c| < Q < |Q_c| \quad (33)$$

and the rate of particle collection is

$$G_2 = \frac{i_1^+}{q_+} - \frac{i_1^-}{q_-} = 3\pi R^2 E_0 \{b_+ n_+ (1 - \frac{Q}{|Q_c|})^2 + b_- n_- (1 + \frac{Q}{|Q_c|})^2\} \quad (34)$$

The charging trajectories are summarized by Fig. 6.2.6, where the possible evolutions of the charge are shown together with the appropriate charging current at a given position in the "state" space  $(Q, E_0)$ . For example, suppose that the drop initially has a negative charge exceeding in magnitude  $|Q_c|$ . Then, it acquires positive particles and its net charge changes at a rate  $i_2^+$  given by Eq. (31). The details of the temporal dependence

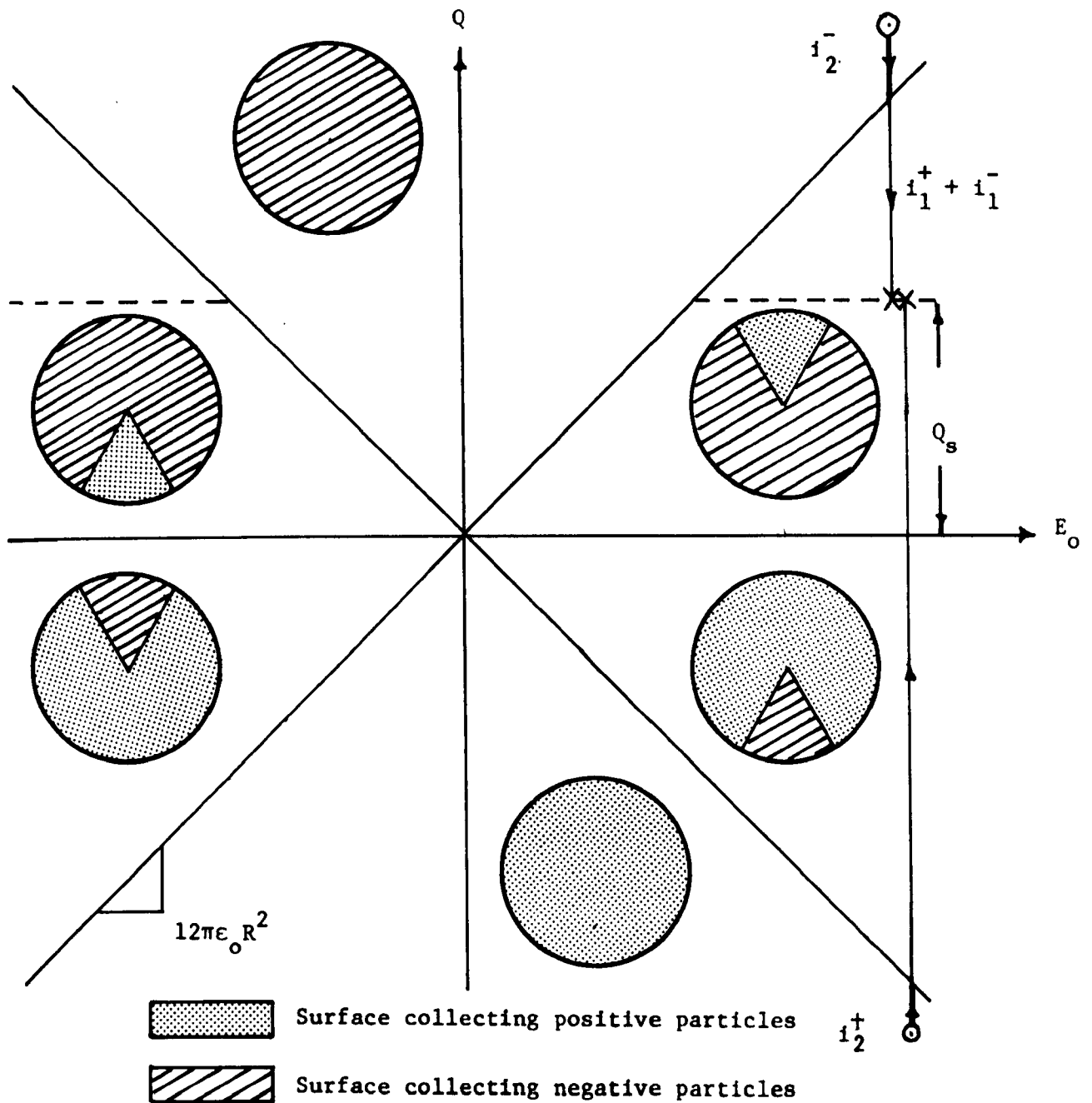


Fig. 6.2.6 Charging trajectories for a drop having total charge  $Q$  in an ambient field  $E_0$  as it collects positive and negative particles with complete mixing.  $\odot$  indicates initial charge while  $x$  indicates final state

of  $Q$  follow by solving Eq. (14) with  $i = i_2^+$ . When  $Q$  reaches  $-|Q_c|$ , the current shifts to Eq. (33) and the charging continues until  $Q$  reaches a value

such that  $i = 0$ . Solution of Eq. (33) shows that this happens when  $Q = Q_s$  where

$$Q_s = Q_c \frac{\sqrt{\frac{|I_+|}{|I_-|}} - 1}{\sqrt{\frac{|I_+|}{|I_-|}} + 1} \quad (35)$$

The largest possible value to which the drop can charge is therefore  $|Q_c|$ , and is obtained in the limit where there are no negative particles ( $I_- \rightarrow 0$ ). In the opposite limit of no positive particles, the drop never changes its original charge and the rate of particle collection is zero.

The difference between the laminar and turbulent models comes down to there being an effect of the mean relative velocity  $w_0$  for laminar flow, but not for the turbulent mixing model. As far as the charging currents are concerned, the combination of Figs. 6.2.2 and 6.2.3 to give a total charging diagram is in the limit  $w_0 \rightarrow 0$ , the same as Fig. 6.2.6. The turbulent mixing model is, by contrast with the laminar model, not restricted to having a colinear relative flow and ambient electric field.

### 6.3 Multipass Systems

Regardless of the specific geometry, the collection system involves a residence time for the gas that must be distinguished from that for the drops. The effective lifetime of the drops is necessarily on the order of  $\tau_R$ . For efficient cleaning, the gas residence time must be at least on the order of  $\tau_c$ . This means that the drop residence time must be made considerably shorter than the gas residence time.

If drops are simply sprayed into a cleaning volume through which the

particle laden gas is passed, it is clear that the gas must undergo internal circulation on one scale or another. Unless provision is made to control the flow pattern, the specific circulation pattern is likely to be extremely complex.

The system shown in Fig. 6.3.1 both illustrates what is involved in modeling the system as a whole and shows how relative control over the flow pattern is achieved in the experiments to be described in Secs. 6.7-6.9. The drop stream enters at the top and is removed by inertial impact at the bottom after passing down the center through the interaction channel. The aerosol is introduced at the top with volume rate of flow  $F_{in}$  and number density  $n_{in}$ . The drops entrain the gas carrying it down the center section. Because the gas residence time is much longer than that of the drops, most of the gas recirculates in the return sections with a volume rate of flow  $F_2$  essentially half that through the center section,  $F_1$ . Some gas is removed at the bottom entraining the particle density  $n_{out}$ . The mean gas velocities in the central and return section are respectively defined as  $U_{g1}$  and  $U_{g2}$  while the mean drop velocity is  $U$ .

In the interaction channel and in the return channels, there are one-pass particle removal efficiencies respectively defined as

$$\eta_1 = \frac{n_1(\ell)}{n_1(0)} \quad (1)$$

$$\eta_2 = \frac{n_2(\ell)}{n_2(0)} \quad (2)$$

Conservation of the gas in the volume where the gas is injected, the inter-

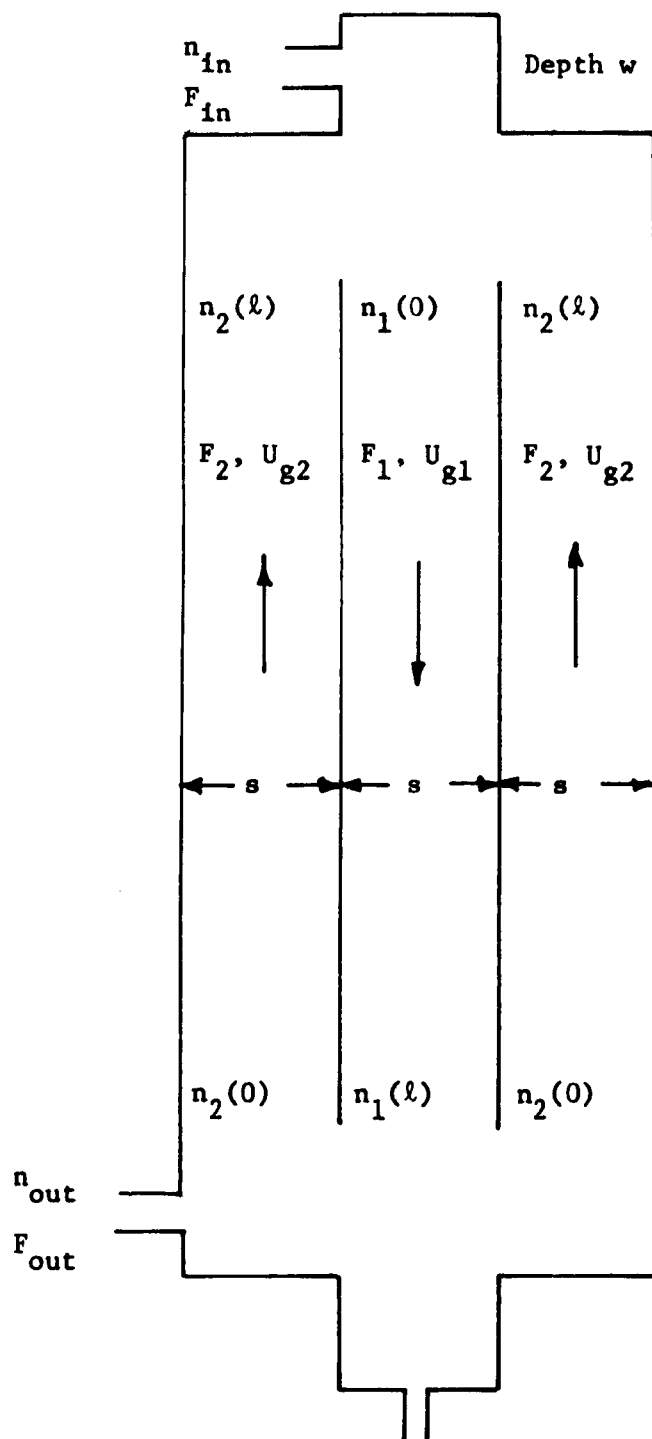


Fig. 6.3.1 Schematic cross-sectional view of cleaning volume. Drops are injected at top to form turbulent jet that drives gas downward in the central interaction region. Drops are removed by impaction at the bottom, while the baffles provide a controlled recirculation of gas and particles.

action channel originates and the return channels terminate requires that

$$F_1 = 2F_2 + F_{in} \quad (3)$$

Conservation of particles in this same region makes a further requirement on the system

$$n_{in}F_{in} + 2F_2n_2(l) = n_1(0)F_1 \quad (4)$$

Finally, under the assumption that complete mixing of the gas occurs at the outlet region,

$$n_1(l) = n_2(0) = n_{out} \quad (5)$$

Given the one-pass efficiencies and  $F_1 \gg F_{in}$ , these last three expressions combine to give the efficiency of the overall system.

$$\frac{n_{out}}{n_{in}} = \frac{F_{in}}{F_1} \left[ \frac{\eta_1}{1 - \eta_1\eta_2} \right] \quad (6)$$

In making quantitative use of this expression, remember that  $\eta_1$  and  $\eta_2$  are themselves somewhat dependent on the concentration level so that as written the expression is not explicit in  $n_{out}/n_{in}$ . In the form of Eq. (6), however, the one pass efficiency is clearly seen to be multiplied by  $F_{in}/F_1$ , which is the reciprocal of the number of times that the gas passes through the interaction channel during one gas residence time.

#### 6.4 Model for Scrubbing With Unipolar Drops and Particles of Opposite Sign (CDS-I)

The most important point to be made in writing the equations for the evolution of drops and particles as they pass through the interaction

channel is that over the entire volume the drop charge  $Q$  exceeds the critical charge  $Q_c$ . This can be established by using the induction charger model of Sec. 5.4.2 (Eq.(5.4.18)) to represent the charge at the point of injection

$$Q = \epsilon_o E_D \lambda_s h \quad (1)$$

where  $(\lambda_s h)$  is the effective area projected by one drop in the charging field  $E_D$ . If the drop charge is conserved, Gauss' Law requires that the electric field at the wall of the channel also be essentially  $E_D$ . It is at the outer periphery of the channel that the space charge field is greatest, and hence  $Q_c$  is greatest. So, at worst,

$$\frac{Q}{Q_c} > \frac{\lambda_s h}{12\pi R^2} \quad (2)$$

Using numbers  $\lambda_s = 1.84 \times 10^{-4}$ ,  $h = 4.96 \times 10^{-4}$  and  $R = 2.5 \times 10^{-5}$  from Sec. 5.4.2, it follows that  $Q/Q_c > 3.9$ . Self-precipitation of drops leads to a lesser electric field at the channel walls, and hence an even larger value of  $Q/Q_c$ . The tendency of the drops to be neutralized by the particles does decrease  $Q$ , but the space charge field and hence  $Q_c$  are proportionately decreased. Slowing of the drops tends to make the total charge/unit length in the channel about twice that in the charger section, but this is not sufficient to negate the inequality  $Q > Q_c$ .

This means that the rate at which the drop charge changes is given by  $i_2^+ = -n_{\pm} b_{\pm} q_{\pm} Q / \epsilon_o$  and the rate at which particles are collected by a drop is given by  $G_1 = \mp n_{\pm} b_{\pm} \frac{Q}{\epsilon_o}$  (Eqs. (6.2.31) and (6.2.32)). Note that these rates are predicted by either the laminar or the turbulent theory. The latter theory, however, is based on the more physical model and has the advantage of being strictly applicable to the case at hand where the ambient field and

mean relative flow are perpendicular.

With the drop-particle interaction terms so simply represented, determining the evolution through the channel is a matter of extending models tested in Chaps. 4 and 5. For convenience, take the drops as negative and particles as positive in the following. First, drop conservation is represented using the same model as in Sec. 5.2.2, but leaving the electric field at the wall,  $E_w$ , for the moment unspecified

$$\frac{dN}{dz} = \frac{NQ E_w u_{-1}(-E_w)}{6\pi\eta RU(s/2)} \quad (3)$$

Here  $U$  is the mean drop velocity. In recognition that there is no precipitation if the space charge of the particles dominates and  $E_w$  is in fact outward, the step function  $u_{-1}(-E_w)$  is unity if  $E_w < 0$  and is zero if  $E_w > 0$ .

Conservation of drop charge is represented by

$$\frac{dQ}{dt} = U \frac{dQ}{dz} = -nbq \frac{Q}{\epsilon_0} \quad (4)$$

That the particles acquired by the drops are lost from the particle continuum is now included in a conservation of particles equation similar to that developed in Sec. 6.2.2, with the addition of a loss term ( $G_1 N$ )

$$\frac{dn}{dz} = \frac{-nbQN}{\epsilon_0 U_g} - \frac{bnE_w u_{-1}(E_w)}{(s/2)U_g} \quad (5)$$

Here,  $U_g$  is the mean gas velocity. Finally, Gauss' Law requires that

$$E_w = (nq - NQ) \frac{s}{2\epsilon_0} \quad (6)$$

These last four equations, which involve the unknowns  $N, n, E_w$  and  $Q$ ,



determine the one-pass efficiency  $\eta_1$ . By setting  $Q = 0$ , Eqs. (5) and (6) determine the self-precipitation efficiency  $\eta_2$  in the return channels. Hence, the system efficiency of Eq. (6.3.6) is evaluated.

The solution of Eqs. (3) - (6) is easily carried out numerically. However, considerably more insight can be obtained by making two approximations that are likely to hold in any practical system, and give an adequate accuracy in interpreting experimental results in Sec. 6.7.

First, as can be seen by taking  $n$  as fixed in Eq. (4) and solving for the decay of  $Q$  with distance through the interaction channel, it is seen that drops tend to lose charge with a decay length  $\ell_a = \tau_a U$ , where  $\tau_a$  is based on  $n$  evaluated at the entrance to the interaction channel. This length is very long compared to  $\ell$ . Hence, the drop charge  $Q$  can be taken as essentially constant, and Eq. (4) ignored.

Second,  $NQ \gg nq$ , which is an approximation that is good once the drops are given a modest amount of charge, but is not true with no charging. The effect of this approximation is to relegate the self-precipitation to the return channels. In fact, at low charging levels there is some self-precipitation in the interaction channel. However, because the gas residence time in the return channels is twice that in the interaction channel, this approximation is acceptable.

Because  $E_w$  is determined by  $NQ$  alone, Eqs. (3) and (6) determine  $N(z)$ . The drop self-precipitation is not influenced by the particles and hence these equations reduce to Eq. (5.2.10) with a solution given by Eq. (5.2.11). This result makes it possible to in turn evaluate Eq. (5), which becomes

$$\frac{dn}{dz} = \frac{-nbQN(0)}{\epsilon_o U_g (1 + \frac{z}{\ell_R})} ; \quad \ell_R \equiv \frac{U\epsilon_o}{N(0)QB} \quad (7)$$

The solution of this equation, evaluated at  $z = l$ , gives the one-pass efficiency defined by Eq. (6.3.1);

$$\eta_1 = \left(1 + \frac{l}{l_R}\right)^{-\frac{l_R}{l_c}} \quad (8)$$

where

$$l_c \equiv \frac{\epsilon_o U g l}{N(0) Q b}$$

For a system that is prescribed in every way except the degree to which the drops are charged, it is now possible to ask what value of  $Q$  gives the best one-pass efficiency....gives the least value of  $\eta_1$ ? To this end Eq. (8) is written with  $Q$  expressed explicitly.

$$\eta_1 = \left[1 + \left(\frac{Q}{Q_R}\right)^2\right]^{-\frac{Q_d}{Q}} \quad (9)$$

where

$$Q_d \equiv 6\pi\eta R b \frac{U}{g l}$$

$$Q_R \equiv \sqrt{\frac{6\pi\eta R \epsilon_o U}{l N(0)}}$$

The minimum is then found with  $Q$

$$Q_{\text{opt}} \approx 2Q_R \quad (10)$$

and with that optimum charge the one-pass efficiency is

$$(\eta_1)_{\text{opt}} = 5^{-\frac{1}{2}} \left(\frac{Q_d}{Q_R}\right) \quad (11)$$

This result serves notice that the degree to which the drops are charged is not the primary limitation on a well designed system. In view of the peak in probe current shown in Fig. 5.5.8, that the  $(Q)_{\text{opt}}$  depends on the drops alone comes as no surprise. Using as numbers typical of Sec. 6.7,  $N(0) = 2 \times 10^9 \text{ drops/m}^3$ ,  $R = 2.5 \times 10^{-5} \text{ m}$  and  $\ell = 0.56 \text{ m}$  and  $Q_{\text{opt}} = 3 \times 10^{-14} \text{ coul.}$  This charge is obtained with an inducer bar voltage  $V_D \approx 75 \text{ volts}$  (Fig. 5.4.5). It is easily possible to raise the value of  $Q$  to at least 4 times this level with the induction system for charging described in Sec. 5.4.2.

The return channel one-pass efficiency  $\eta_2$ , defined by Eq. (6.3.2), follows by solving Eqs. (5) and (6) with  $Q = 0$ , to give

$$\eta_2 = [1 + \frac{\ell}{\ell_a}]^{-1} ; \quad \ell_a \equiv \frac{\epsilon_o U g^2}{b q n_2(0)} \quad (12)$$

Finally, Eqs. (9) and (12) can be used to evaluate the overall efficiency of the system, Eq. (6.3.6). With care taken to recognize that  $n_2(0) = n_{\text{out}}$ , it follows that

$$\frac{n_{\text{out}}}{n_{\text{in}}} = -B_f + \sqrt{(B_f)^2 + C_f} \quad (13)$$

where

$$B_f \equiv \frac{1}{2} \left[ \frac{\ell_{a1}}{\ell} (1 - \eta_1) - \frac{\eta_1 F_{1n}}{F_1} \right]$$

$$C_f \equiv \frac{\ell_{a1}}{\ell} \left( \frac{\eta_1 F_{1n}}{F_1} \right)$$

$$\ell_{a1} \equiv \frac{\epsilon_o U g^2}{n_{1n} b q}$$

The approximations implicit to Eq. (13) are most justified in the drop-charge range where the one-pass efficiency is optimal. Some error results at the charging extremes. If there is little charge on the drops, then the dominant particle removal mechanism in even the central region is self-precipitation. The expression for  $n_1$  should then be replaced by Eq. (12) with  $n_2(0) \rightarrow n_1(0)$ . This should have the effect of causing the measured particle concentration at low levels of drop charge to be lower than predicted by Eq. (13). For very high levels of drop charge, the drop self-precipitation distance  $l_R$  is small compared with the channel length  $l$ . Then, the self-field of the particles can again come into play. This would be a large effect in the experiments of Sec. 6.7 if it were not for the fact that the particle charge density in the interaction channel is essentially that at the outlet. Hence, because the system removes about 95% of the particles at high drop-charge levels, the effect tends to be small.

#### 6.5 Model for Scrubbing With Bicharged Drops and Charged Particles (CDS-II)

To avoid generation of space-charge fields by the drops, equal concentrations  $N(0)$  of positive and of negative drops are injected into the interaction channel. The charged particles can then be injected with unipolar charging of either polarity or bicharged. With bipolar charging, there is electrically induced scrubbing by only half of the drops and in addition the possibility of space charge precipitation due to the self-fields from the particles. With bicharged particles, space charge neutrality is preserved, and both drop species are active in the scrubbing. However, rather than a self-precipitation characterized by  $\tau_a$ , there is a self-agglomeration characterized by the same time constant. Instead of being a removal of the particles to the walls, the consequence is a discharge among the particles

that renders them inaccessible to the charged drop scrubbing.

A detailed model paralleling that represented by Eqs. (6.43)-(6.46) for the CDS-I interaction would recognize effects of the particle space charge, if any, and of the self discharge if the drops are bicharged. Because the particle density is suppressed to the point of being unappreciable on the time scale of the drop residence time, in this section it is assumed at the outset that these particle-field effects can be ignored. The drop densities of positive and negative species are defined as  $N_+$  and  $N_-$  respectively and are the same. Hence, each is represented by  $N_+ = N_- \equiv N$ . In the following, if  $N$  is taken as  $N_+$ , then  $n \equiv n_-$ . With fields from the particles ignored, the drops evolve in the same self-discharge process investigated in Sec. 5.3.2.

$$\frac{N}{N(0)} = \frac{1}{1 + \frac{z}{l_R}} ; \quad l_R \equiv \frac{\epsilon_o U}{K' N(0) Q B} \quad (1)$$

where  $K'$  is 2 if the drops are taken as behaving analogously to a system of bicharged particles, and is 3 according to the extension of the Harper model.

Unless fields induced by unipolar particle charging are extremely large (much larger than in the experiments of Sec. 6.8) the drop charge  $|Q| > |Q_c|$ , thus justifying representing the rate of collection of one sign of aerosol by the opposite sign of drops by  $NG_1$  (particles/ $m^3$ /sec), where  $G_1$  is given by Eq. (31) or (32). Thus, the decay of one species of particle is in accordance with

$$\frac{dn}{dz} = - \frac{nbQ N(0)}{\epsilon_o U_g (1 + \frac{z}{l_R})} \quad (2)$$

where Eq. (1) has been used for  $N(z)$ .

Equation (2) is the same as Eq. (6.4.7), found for the CDS-I interaction, except that  $K'$  appears in  $\ell_R$ , ( $U \rightarrow U/K'$  in  $\ell_R$ ). Because  $N$  is half of the total drop density injected, if  $K' = 2$ , it is evident that the only effect of changing from CDS-I to a CDS-II system is to increase  $\ell_c$  by a factor of two. If  $K' = 2$ , the effect on  $\ell_R$  of halving the drop density is exactly compensated by the factor  $K'$ . Hence, Eq. (6.4.13) evaluated using the CDS-I parameters predicts the particle collection for the system provided that  $\ell_c$  is doubled. According to this model, the collection is expected to peak-out at the same drop-charging voltage but the fraction of particles removed should be less than in the comparable CDS-I system.

#### 6.6 Model for Precipitation by Unipolar Drops and Particles of the Same Polarity (CDP)

The specific model of this section and the correlating experiment of Sec. 6.9 in which the drops and particles carry unipolar charge of the same polarity help to emphasize the ubiquity of the fundamental time constants. Now, the drops repel the particles, but collectively induce a sufficient space charge field to drive the particles to the walls. In practical systems, the walls are washed by the self-precipitating drops. Hence, the device has many of the features of a wet-wall precipitator.

As in Sec. 6.4, general equations for the evolution of drops and particles would include effects of particle space charge. For the present purposes, the approximation is made at the outset that  $|NQ| \gg nq$ , so that the drop dynamics are in essence determined without a coupling to the particles. Thus, the self-precipitation of the drops is described by Eq. (5.2.11), which gives  $N(z)$ .

The precipitation of particles in the field caused by the self-precipitating

drops is found by writing a conservation of particles equation for an incremental volume having length  $\Delta z$  and the cross-section of the channel.

With drops and particles both positive,

$$swU_{g1}[n(z + \Delta z) - n(z)] = -2nbE_w w\Delta z \quad (1)$$

Here, the field at the wall induced by the drops is

$$E_w = \frac{NQ(s/2)}{\epsilon_o} \quad (2)$$

so that in the limit  $\Delta z \rightarrow 0$  and with the substitution of Eq. (5.2.11) for  $N(z)$ ,

$$\frac{dn}{dz} = -\frac{nbQ}{U_{g1}\epsilon_o} \frac{N(0)}{1 + \frac{z}{l_R}} ; \quad l_R \equiv \frac{\epsilon_o U}{N(0)QB} \quad (3)$$

This expression for the particle density decay through the channel is the same as found in Sec. 6.4.2 for the CDS-I interaction, Eq. (6.4.7). Hence, for this physically very different system, the one-pass efficiency is the same as for the CDS-I systems and the collection for the total CDP system is as given by Eq. (6.4.13).

## 6.7 Experiments with Unipolar Drops and Particles of Opposite Sign

### 6.7.1 Experimental System

A schematic diagram of the complete system is given in Fig. 6.7.1. All components, except the channel, are described in previous chapters. The drops are injected from above, pass between the inducing bars, and then enter the central channel. The aerosol is injected through manifolds located beneath each bar. The drops are impacted at the bottom of the channel, hence experience just one pass through the system. The gas is

drawn off at the bottom at a rate slightly greater than is supplied with the aerosol. The balance is drawn in through leaks in the system in the vicinity of the plugs inserted between the charging bars and droplet generator. Corrections are made in correlating experiments with theories to account for this disparity between inflow and outflow.

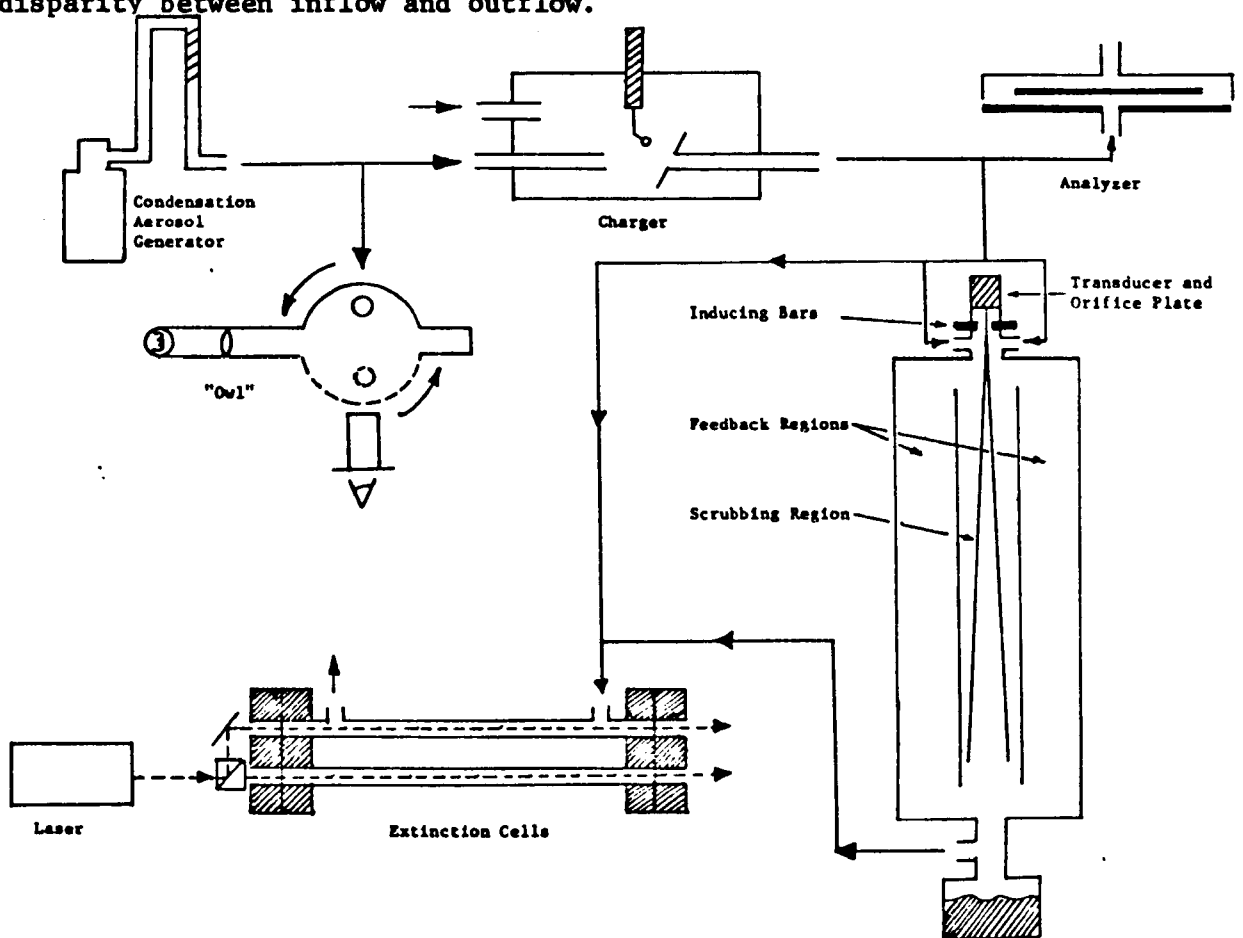


Fig. 6.7.1 Drop-particle interaction experiment showing system for controlled generation of charged particles and measurement of essential parameters

### 6.7.2 Experimental Diagnostics

The operating conditions for the experiment are summarized in Table 6.7.1. The angular positions of reds in the "Owl" are:  $\theta_{\text{red}} = 50^\circ, 103^\circ$ . Hence, from Fig. 4.5.2 the radius of the aerosol particles follows from  $\alpha = 2\pi a/\lambda = 3.2$ ,  $\lambda_{\text{red}} = 0.629\mu\text{m}$  to be  $a = 0.32\mu\text{m}$ .



Table 6.7.1 Operating conditions for drop-particle experiments

## Aerosol Generator:

- a. 5% DOP Solution
- b. Heating Tape Voltage - 70 volts
- c. Pressure of Prepurified Nitrogen - 15 psig
- Aerosol Flow Rate - 5.1 liters/min.

## Charger:

- a. Corona Voltage - +8 kV
- b. Corona Current - +3  $\mu$ A
- c. Accelerating Nitrogen Flow Rate - 1.3 liters/min

## Flows:

- a. Output Flow Rate Through Aspirator ( $F_{out}$ ) -  $1.37 \times 10^{-4} \text{ m}^3/\text{sec}$
- b. Input Flow Rate ( $F_{in}$ ) -  $1.08 \times 10^{-4} \text{ m}^3/\text{sec}$

## Droplet Generator:

- a. Pressure to Water Reservoir - 15 psig
- b. Frequency of Orifice Plate Transducer - 54 kHz
- c. Droplet Generation Rate -  $2.76 \times 10^7$  drops/sec

## Channel

- a. Length ( $l$ ) - 0.565 m
- b. Width ( $s$ ) -  $2.54 \times 10^{-2}$  m
- c. Drop Velocity ( $U$ ) - 4m/sec
- d. Gas Velocity ( $U_{g1}$ ) - 2m/sec
- e. Gas Velocity ( $U_{g2}$ ) - 1m/sec
- f.  $w = 15\text{cm}$

The self-precipitation and saturation currents measured using the analyzer of Sec. 4.7.2 determine the charge density and mobility to be  $b = 2.5 \times 10^{-7} \text{ m/sec/V/m}$  and  $nq = 0.67 \times 10^{-4} \text{ coul/m}^3$  respectively.

In order to evaluate the charge density that actually can be considered to enter the channel, this density must be corrected for impaction of the aerosol onto the droplets immediately below the point of injection and for the dilution that occurs because the flow drawn out by the aspirator exceeds that supplied with the aerosol. This is done by performing a measurement with the aerosol and the drops uncharged. In this case the ratio of output-to-input concentrations is found to be  $n_{\text{out}}/n_{\text{in}} = 0.59$ . Measurement of inlet and outlet gas volume rates of flow shows that 21% of the decrease in exit particle density is due to dilution and 25% is due to inertial impaction. Most of the leakage is at the inlet, justifying the correction of  $n_{\text{in}}$  to account for both effects. In all of the following discussion,  $n_{\text{in}}$  is taken as the corrected value.

Because the drops make a transition from a confined beam to a turbulent jet, there is some ambiguity in specifying  $N(0)$ . In the correlations of this chapter,  $N(0) = x/Uws = 1.77 \times 10^9 \text{ drops/m}^3$ , where  $x$ , the rate at which drops are produced by the generator, is the number of orifices multiplied by the acoustic frequency.

The particle concentrations  $n_{\text{in}}$  and  $n_{\text{out}}$  are obtained from extinction measurements performed on flows sampled from different points in the system. The approximate form of the extinction law, Eq. (4.5.5) is used, Although the amount of beam attenuation is sufficient to cause some error in its applications, this is considered to be less than that resulting from the application of Eq. (4.5.4)  $I(0) - I(L)$  and  $I(0)$  are measured directly.

To obtain  $I(L)$  would require subtraction of these quantities, one of which,  $I(0)$ , is known less accurately than the other.

### 6.7.3 Scrubbing Efficiency

A plot of Eq. (13) for these experimental conditions is shown in Fig. 6.7.2. The measurement at  $V_D = 0$ , which reflects the self-precipitation alone, confirms the particle self-precipitation model for the side channels. Although this process also occurs in the central section, the particle velocity is twice as large there. Thus, most of the period required for a particle to make a complete circuit is accounted for by the time it spends traveling up the sides. In addition, if the interval that a system of monocharged particles spends is sufficient to cause significant self-precipitation, then the increase in particle removal resulting from even a doubling of the residence time is relatively small. The drop voltage at which the collection process peaks (between 30 and 50 volts) corresponds with the expected range of  $Q_{opt}$  (Eq. (10)) and reflects the loss of drops through self-precipitation.

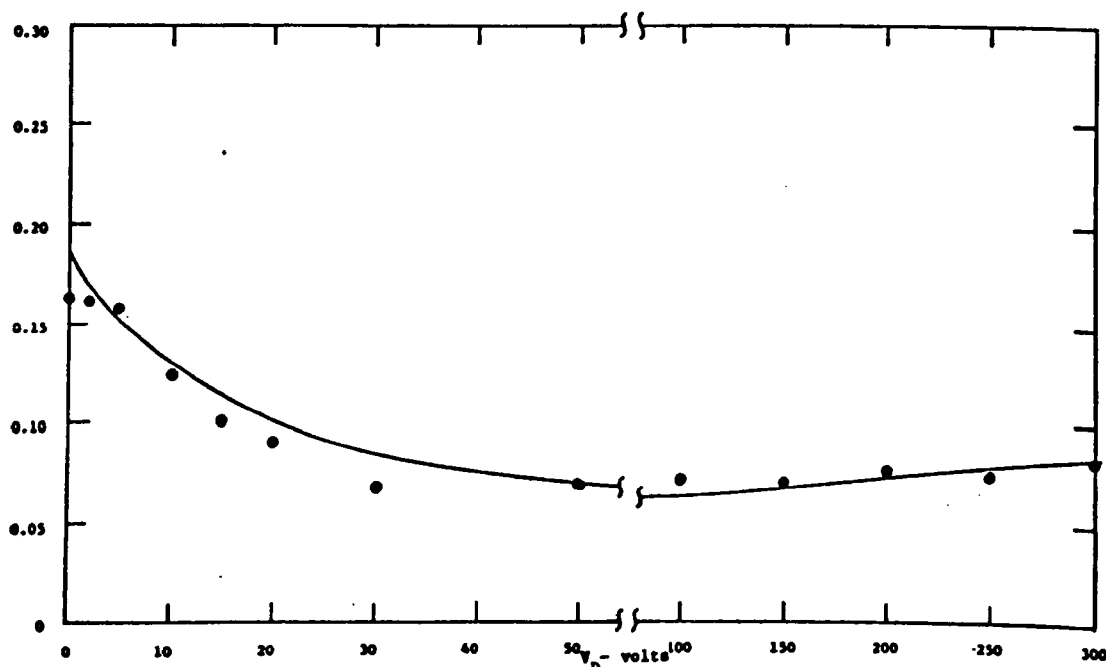


Fig. 6.7.2 Calculated and measured collection of positively charged aerosol particles upon negatively charged drops as a function of drop charging voltage

The smaller than expected rate at which  $n_{\text{out}}/n_{\text{in}}$  decreases at low levels of drop charge can be accounted for by the self-precipitation in that region. Until the charge density of the drops exceeds that of the particles, the increased collection by the drops tends to be counterbalanced by a loss of the particle self-precipitation mechanism.

### 6.8 Experiments With Bicharged Drops and Charged Particles

Experimentally, the alteration from a monocharged drop to a bicharged drop system is accomplished by applying a positive voltage to one charging bar and a negative voltage to the other. The variation of drop charge with voltage is assumed to be identical to that given in Fig. 5.4.4. In practice, the positive voltage is adjusted to the indicated value, and the negative one then increased until a probe inserted into the drop stream indicates no net current. Probably due to geometric asymmetry, the positive voltage tends to create more highly charged drops. For example, in order to achieve charge neutrality at  $v_a = +250$  V,  $V_b$  had to be adjusted to  $-190$  V. The theoretical predictions are based on the higher value of  $V_D$ . The structure of the bicharged drop beam differs considerably from the monocharged one. Whereas the spread of the beam in the latter case increases with drop charging, in the former case, the beam appears essentially similar to the uncharged one for voltages as high as  $\pm 300$  volts. (See Secs. 5.5 and 5.6). The operating conditions cited in Sec. 6.7 also apply to this experiment.

Equation(6.4.13), normalized, as described in Sec. 6.7 to the corrected inlet particle density, is plotted in Fig. 6.8.1. A comparison of the theoretical models for CDS-I and CDS-II interactions afforded from Figs. 6.7.2 and 6.8.1 shows the effect of doubling  $\ell_c$ . The fraction of particles removed as a result of charging the drops is reduced. According to the model, which

is based on taking  $K' = 2$ , the optimum charge level is the same as for the CDS-I interaction.

Of the three collection processes investigated experimentally in this chapter, the CDS-II collection, is the least well understood. The process does appear to be characterized by  $\ell_c$  and  $\ell_R$ . However, as a comparison of model and experimental results in Fig. 6.8.1 shows, the collection tends to increase less rapidly with voltage than predicted, and does not tend to peak out as expected, but rather tends toward an asymptote. This latter fact reflects the observation from Sec. 5.6 that the self-discharge process goes on more slowly than expected from a theoretical model which takes  $K' = 2$  (as is assumed in the model for Fig. 6.8.1).

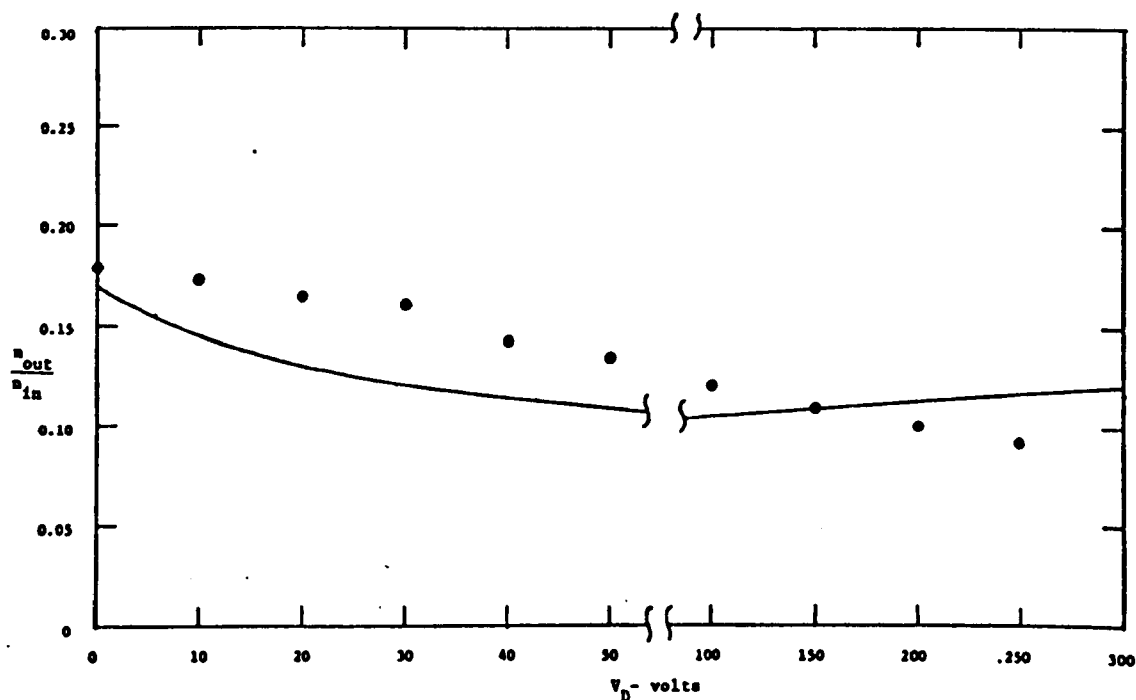


Fig. 6.8.1 For bicharged drops, calculated and measured efficiencies for collection of positively charged aerosol particles

## 6.9 Experiments With Unipolar Drops and Particles of the Same Polarity (CDP)

With the important modification of having drops and particles charged to the same polarity, the experiment of this section is much the same as the CDS-I experiment of Sec. 6.7. The theoretical curve shown in Fig. 6.9.1 is based on the results of Sec. 6.6, which show that collection is expected to be the same as in the CDS-I experiment. The differences between the theoretical curves shown in Figs. 6.9.1 and 6.7.2 reflect the experimental variations in measured parameters used as inputs to the calculations. The major uncertainty is in the measured correction factor. As described previously, this number is evaluated by measuring the efficiency of the system when both the drops and the particles are uncharged. The densities of the particles are sufficiently large to cause  $I(L)$  and  $I(0) - I(L)$  to be on the same order. Thus, the unapproximated extinction formula (Eq. (4.5.4)) is appropriate. However, evaluation of  $I(L)$  from the measurements requires subtraction of two close numbers, and, as is evidenced by the variation for otherwise identical systems, is a source of uncertainty.

Two observations can be made on the basis of these experiments and the interpretation afforded by the underlying model. The optimum collection occurs in essentially the same range as for the CDS-I configuration and in roughly the range expected from the theoretical model. The maximum removal is about the same as for the CDS-I configuration and essentially what is predicted using the simple model.

## 6.10 Summary of Measured Efficiencies

The experimental results of the last three sections are representative of several experimental runs in each of the classes of operation. The data presented accurately reflect the trends and magnitudes. Because each of the

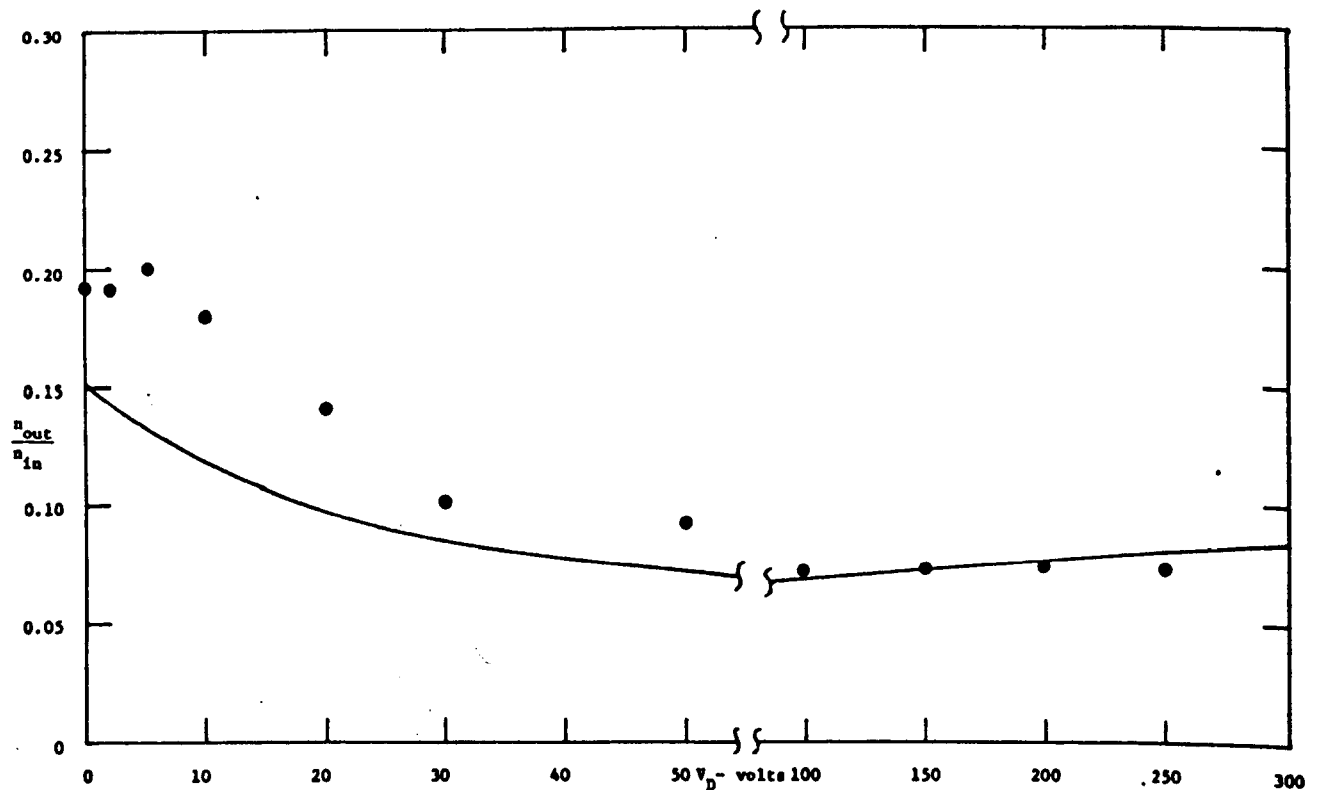


Fig. 6.9.1 Theoretical and measured particle collection for drop-precipitation of positively charged aerosol particles by positively charged drops as a function of drop charging voltage

runs involves re-establishing the flow and aerosol charging conditions there is some variation in the experimental conditions. This is reflected in parameters used in the calculation and accounts for the small differences between the theoretical and between the experimental  $V_D = 0$  collection in the respective curves of the preceding sections.

The block diagram of Fig. 6.10.1 helps in summarizing the performance of the overall system, considered as a collection device. The dilution of the gas at the inlet due to leakage must be removed from an efficiency ascribed to the device. Thus, the particle density  $n_{IN}$  at the inlet, where the volume rate of flow is  $F_{in}$ , is corrected to give the effective particle density  $n'_{IN}$  to the device as a whole

$$\frac{n'_{IN}}{n_{IN}} = \frac{F_{in}}{F_{in} + F_{dilution}} = \frac{F_{in}}{F_{out}} = 0.79 \quad (1)$$

The inertial scrubbing occurs primarily in the zone at the inlet of the experiment prior to entering the mixing zone at the entrance to the interaction channel. The collection attributed to inertial scrubbing is measured by determining  $n_{out}$  with  $q = 0$  and  $V_D = 0$  and is summarized in Table 6.10.1.

Table 6.10.1 Efficiency of System as a Whole

	CDS-I	CDS-II	CDP
$(q = 0, V_D = 0)$			
INS	25%	25%	25%
$(q, V_D = 0)$			
INS + SCP	87%	86.5%	85%
$(q, V_D)$			
INS + SCP + ( )	95%	92%	95%

The additional effect of charging the particles with the drops injected but with no charging is then represented by the efficiency

$$\text{Efficiency} = 1 - \frac{n_{out}}{n'_{IN}} = 1 - \frac{n_{out}}{n_{in}} \frac{n_{in}}{n'_{IN}} = 1 - 0.75 \frac{n_{out}}{n_{in}} \quad (2)$$

With  $n_{out}/n_{in}$  taken from Figs. 6.7.2, 6.8.1 and 6.9.1 respectively, the overall efficiencies found from Eq. (2) are as summarized in Table 6.10.1. Finally, with the drops charged, the overall efficiencies under optimal conditions are similarly computed from the data and Eq. (2), and are summarized in the table.

The electrical augmentation of the device is evident from the table.



In the absence of particle and drop charging, it functions as an inertial scrubber. The space charge precipitation mechanism accounting for the collection with  $V_D = 0$  would be absent in the limit of an infinitely dilute particle concentration. The collection mechanisms associated with the drop charging would then be dominant. The table emphasizes once again that the three charged drop configurations result in essentially the same efficiency.

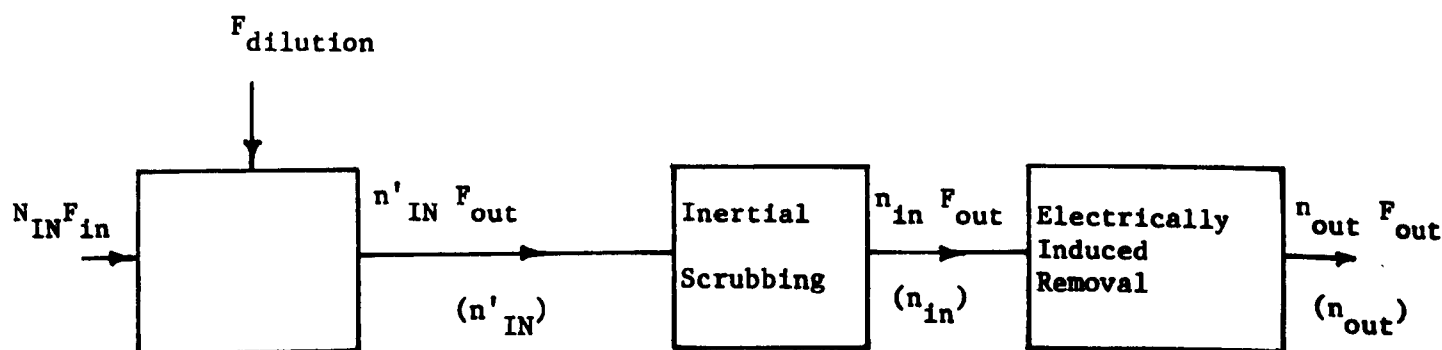


Fig. 6.10.1 Stages of concentration attenuation through system as a whole  
Efficiencies of Table 6.10.1 are  $(1 - n_{\text{out}}/n'_{\text{IN}})$  in percent

## 7 Summary

### 7.1 State of Fundamentals

The basic laws of collection for submicron particle control devices are developed in Chaps. 4-6 in a sequence of interrelated models and supporting experiments. What can be concluded with the hindsight of these chapters is that the overview of conventional, self-precipitation, self agglomeration and charged drop systems given in Chap. 2 does in fact place the alternative approaches in perspective. Thus, Chap. 2 should be regarded as part of this summary. The hierarchy of electromechanical time-constants  $\tau_a$ ,  $\tau_c$ ,  $\tau_R$  is clearly basic to models that predict the performance of the SCP, SAG, CDS-I, CDS-II and CDP configurations. In those situations where the drop charge  $Q$  exceeds in magnitude the critical charge  $Q_c$  (a condition that is most probable in a practical system in either the CDS-I or CDS-II configurations) experimental evidence supports the use of the simple rates deduced in Sec. 6.2.2 for electrically dominated collection. The role of turbulent mixing, which is basic to this model, should be incorporated into thinking about practical charged drop collection systems. That the way in which a given drop "sees" the surrounding sea of particles is poorly pictured in terms of deterministic laminar trajectories is perhaps best emphasized by simply observing that in the experiments of Chap. 6 the average slip velocity between drops and gas is 2m/sec, while even at the drop surface the velocity of a submicron particle is only of the order of 5cm/sec.

What is found in Chap. 5 concerning the self-discharge of bicharged drops taken together with the collection performance of the bicharged drop system found in Sec. 6.8 tends to support the view that the most poorly understood aspect of any of the systems is the self-discharge of the drops. This process

seems to go forward somewhat more slowly than expected. The characteristic time can be taken as perhaps  $4\tau_R$  rather than  $\tau_R$ . (The coefficient  $K' = 0.5$  rather than 2 or 3 in the model for the one-pass efficiency.) The observed reduced rate of self-discharge in the bicharged system gives some impetus to preferring the CDS-II configuration in practical applications and future developments.

On the basis of the experience obtained here, it is clear that a more refined picture of the drop-particle interactions could be obtained by suppressing the role of self-precipitation. In an improved experiment, the efficiency would be measured by more sensitive mass monitoring equipment which would permit operation at a reduced particle density  $n_{in}$ . Thus, the masking effects of the self-precipitation in the feedback loops would be largely eliminated. Effectively, this would mean that the particle removals shown in Figs. 6.7.2, 6.8.1 and 6.9.1 would start at unity when  $V_D = 0$  and approach the curves shown by the time  $V_D$  is on the order of 50 to 100 volts. Such experiments would be justified if a critical measure of the drop collection rate under actual flow and field conditions were called for.

By including effects of particle inertia, or "near-field" image forces and the like, it is possible to add tentative refinements of the electrical collection rate model emphasized here. Given a two-particle calculation that promises radical improvements in scrubbing efficiency if the drops and particles are oppositely charged, two facts supported by every finding in this work should be kept firmly in view. First, the effect of the field is extremely unlikely to be larger than the rate actually used in most of the modeling of Chap. 6

and corroborated by the experiments there as well. The turbulent mixing model pictures the drop as acting much like the electrode in an ESP, with the effective collection field at the surface of the drop where it is most intense, and the particle density supplied by the turbulent diffusion right up to that surface. Second, the collective interactions of the drops must be included, or the fundamental limitations on the device will not be perceived.

## 7.2 Charged Drop Devices Compared to Conventional Devices

The beauty of devices making use of charged drops is undoubtedly in the eyes of the user. When Penney did his early work he probably had in mind making a viable competitor for the conventional electrostatic precipitator. When he obtained particle removal efficiencies in the CDS-I configuration of less than 50% to him it was a disappointment. But from the point of view of wet-scrubber technology, Penny's findings were more impressive and Pilat's recent experiments in the CDS-I mode are even encouraging. He found an improvement in scrubber performance for  $1.05\mu\text{m}$  particles from 69% with no charging to 94% with charging. Are these experimental results consistent with the fundamentals developed here? Given that the scaling laws implied by these fundamentals are correct, is there a future for the charged drop family of devices?

Rough estimates of Pilat's experimental parameters can be made if it is assumed that the drops have an average velocity of 5m/sec through the active volume. The parameters shown in Table 7.2.1 are only rough averages, since both particles and drops are polydisperse, and flow parameters are not reported.

Table 7.2.1 Estimates of Average Parameters in Pilat's CDS-I Experiments

$a \sim 5 \times 10^{-7} \text{ m}$	$R \sim 2.5 \times 10^{-5} \text{ m}$
$n \sim 6.7 \times 10^{11} \text{ particles/m}^3$	$N \sim 10^9 \text{ drops/m}^3$
$q \sim 2.8 \times 10^{-17} \text{ coul/particle}$	$Q \sim 3.7 \times 10^{-14} \text{ coul/drop}$
$b \sim 1.5 \times 10^{-7} (\text{m/sec})/(\text{V/m})$	$B \sim 4 \times 10^{-6} (\text{m/sec})/(\text{V/m})$

It follows from these parameters that

$$\tau_a \sim 3.3 \text{ secs.} ; \tau_c \sim 1.6 \text{ sec} ; \tau_R = 6 \times 10^{-2} \text{ sec}$$

(1)

These times are to be compared to a gas residence time of 7 sec and a drop residence time of perhaps 1/4 sec. Thus, because the gas residence time is longer than  $\tau_a$ , appreciable space-charge precipitation is to be expected with the particles charged but the drops uncharged. Although not formally reported, this SCP contribution is confirmed by Pilat. The particle collection, characterized by  $\tau_c$  relative to the 7 sec gas residence time, is such that charging the drops should result in an additional increase in efficiency as indeed it did. Finally, the drop residence time is about 4 times  $\tau_R$ . This is corroborated by the observation that the drops appear to "stiffen" when they are charged. Insofar as experimental conditions can be pinned down, the results reported by Pilat are therefore in accord with the models developed here.

What is evident from all available studies is that drop and particle charging can dramatically improve the performance of the inertial scrubber in the submicron range. Improvements in performance summarized in Table 6.10.1 are from 25% for the inertial scrubbing alone to 95% with particles and drops charged.

That it makes little difference whether the drops and particles have opposite signs, the same signs, or there is a mixture of both positive and negative drops, points to the fact that "scrubber" is a misleading term for the charged drop devices. What is called a charged drop scrubber really has the same characteristics in the limit of electrically dominated collection as the charged drop precipitator. This fact makes it natural to return to Penny's original point of view. What is the position of the charged drop devices in a picture that includes the conventional electrostatic precipitator? The charged drop precipitator is, after all, an electrostatic precipitator with half the electrodes replaced by the mobile drops. Taken together, these observations make it clear that the charged drop devices are extremely unlikely to outperform the electrostatic precipitator in terms of residence time needed for gas cleaning.

Fundamentally, the only way that the gas residence time can be reduced is to increase the collection surface area per unit volume. Comparison of a drop system, having drops of radius  $R$  separated by an average distance of  $\alpha$  radii, to a conventional precipitator having circular cylindrical electrodes of radius  $r$ , shows that for the drop device to have the shorter residence time for cleaning (Eq. (2.5.12))

$$\alpha < \left(\frac{r}{R}\right)^{\frac{1}{3}} \quad (3)$$

With  $r = 10\text{cm}$  and  $R = 25\mu\text{m}$ , this means that the drops must be packed less than 16 radii between centers. In the experiments of Chap. 6, for comparison,  $\alpha \sim 30$ . By designing a counterflow of particles and drops it is possible to make a system having a greater drop density but not charge density. Here again is that limitation, represented by  $\tau_R$ , unique to the charged drop devices.

Given a packing satisfying Eq. (3), the drops might just as well be left uncharged and an ambient electric field used to induce charges of opposite sign over hemispheres of the collection sites, as in the EFB and EPB configurations discussed in Sec. 2.5. Then  $\tau_R$  is not a limiting time constant.

If the residence time is the dominant criterion for the viability of a submicron particle control system, then the EFB and EPB configurations have great promise. In these systems, the drops are most likely to be replaced by solid collection sites. As pointed out in Sec. 2.5, dramatic improvements can be made in the residence time for cleaning using this class of devices. Recent work confirms this prognosis and in fact corroborates the turbulent mixing collection model developed in Sec. 6.2 (Zahedi and Melcher, 1974).

### 7.3 Practical Application

The question of whether or not there is a practical position for devices making use of charged drops, and hence incentive for technical developments, is relatively easy to answer. If there is a practical place for wet inertial scrubbers, then there is one for the charged drop devices as well.

Valid applications for the charged drop devices tend to spring from domains in which the wet scrubber is viable. The wet-scrubber has a position in air pollution control because its use tends to be intensive in operating costs while relatively low in capital investment. This is by contrast with the typical industrial scale electrostatic precipitator. Certainly, if a wet scrubber is marginally competitive because it lacks desired performance in the submicron range, the electrical augmentation is highly attractive.

Hybrid scrubbers, designed to remove gaseous effluents as well as efficiently control submicron particulate, especially deserve development. What is obtained by charging the drops and particles is a class of devices with the capital investment and operating cost profile of the wet scrubber but a particle removal efficiency approaching that of the electrostatic precipitator.



#### 7.4 Summary of Calculations Estimating CDS-I, CDS-II and CDP Performance

The models developed in Secs. 6.3 through 6.6 are intended not only to support the experiments of Chap. 6, but to serve as a guide in scaling and designing practical devices. Summarized in this section is the procedure by which these results can be applied.

It is assumed that the system as a whole has the multipass configuration of Fig. 6.3.1 wherein

$n_{in}$  = the number density of particles to be removed ( $\#/m^3$ )

$F_{in}$  = the volume rate of flow of polluted gas ( $m^3/sec$ )

$l$  = the length of the region over which gas and drops interact (m)

To be practical, particles circulate with the gas through return paths also of length  $l$  so that the gas passes through the droplet jet region many times. To a first approximation the volume rate of gas flow in the interaction region,  $F_1$ , is the average drop velocity  $U$  multiplied by the drop-jet cross-sectional area. (In the system described in Chap. 6, the gas velocity  $U_{g1}$  is half the drop velocity.)

For optimal removal of particles in the interaction region, drops should be charged to the value (Eq. (10) of Sec. 6.4)

$$Q_{opt} = 2Q_R : Q_R = \frac{6\pi\eta R \epsilon_0 U}{lN(0)} \quad (4)$$

where

$\eta$  = viscosity of air ( $2 \times 10^{-5}$  nt-sec/ $m^2$  at room temperature)

$R$  = droplet radius (m)

$U$  = mean drop velocity (m/sec)

$N(0)$  = droplet number density at entrance to interaction region

Methods of charging the drops are discussed in Sec. 5.4. In terms of these parameters, the optimum particle removal in one pass is given by

$$\eta_1 \equiv \frac{n_1(\ell)}{n_1(0)} = 5^{-\frac{1}{2}} \left( \frac{Q_d}{Q_R} \right) \quad (5)$$

where

$$Q_d \equiv 6\pi\eta Rb \left( \frac{U}{U_{g1}} \right) \quad (6)$$

and  $b$  is the mobility of the particles entering with density  $n_{in}$ . These particles have been previously charged, probably by conventional ion impact in a corona discharge region as discussed in Sec. 5.4.4.

In the limit where the particle density  $n_{in}$  is low enough that self-precipitation is negligible, ( $\ell \ll \ell_{a1} \equiv \epsilon_0 U_{g2} / n_{in} bq$ ) the CDS-I, CDS-II and CDP devices then have the particle removal efficiency

$$\text{Efficiency} \equiv 1 - \frac{n_{out}}{n_{in}} = 1 - \frac{F_{in}}{F_1} \frac{(\eta_1)_{opt}}{1 - (\eta_1)_{opt}} \quad (7)$$

If self-precipitation effects cannot be ignored ( $\ell$  on the order of  $\ell_{a1}$ ), then Eq. (13) of Sec. 6.4 can be evaluated to determine  $n_{out}/n_{in}$  and hence the efficiency.

## REFERENCES

- Anonymous, 1970 "More Help for Solid Waste Disposability", Modern Plastics, 67-68.
- Brillouin, L., 1949 "The Scattering Cross-Section for Electromagnetic Waves", J. Appl. Phys. 20, 1110-1125.
- Brown, J.H., Cook, K.M., Ney, F.G. & Hatch, T., 1950 "Influence of Particle Size Upon the Retention of Particulate Matter in the Human Lung", Am. J. Public Health 20, 450-458.
- Browning, J.A., 1958 "Production and Measurement of Single Drops, Sprays, and Solid Suspensions", Advances in Chemistry Series #20, 136-154.
- Calvert, W., 1970 "Venturi and Other Atomizing Scrubbers Efficiency and Pressure Drop", AIChE Jrl. 16, #3, 392-396.
- Cobine, J.D., 1958 Gaseous Conductors, N.Y., Dover Pub., 99, 38.
- DallaValle, J.M., Orr, C. & Hinkle, B.L., 1954 "The Aggregation of Aerosols", Brit. J. Appl. Phys. Supp. 3, 5, S198-S208.
- Davies, C.N., 1966 "Deposition of Aerosols from Turbulent Flow Through Pipes", Proc. Roy. Soc. A289.
- Davis, M.H., 1964 "Two Charged Spherical Conductors in a Uniform Electric Field Forces and Field Strength", Quart. J. Mech. Appl. Math 17, 499-511.
- Devir, S.E., 1967 "On the Coagulation of Aerosols -- III. Effect of Weak Electric Charges on Rate", J. Colloid. Interface Sci. 21, 80-89.
- Drinker, P. & Hatch, T., 1954 Industrial Dust, N.Y., McGraw-Hill Book Co., Ch. 2.
- Dunskii, V.F. & Kitaev, A.V., 1960 "Precipitation of a Unipolarly Charged Aerosol in an Enclosed Space", Kolloidn. Zh. 22, 159-167.
- Dwight, H.B., 1961 Tables of Integrals and Other Mathematical Data, N.Y., MacMillan Co., 37.
- Eyraud, C., Joubert, J., Henry, C. & Morel, R., 1966 "Étude D'un Nouveau Type de Dépoussierneur à Pulvérisation Electrostatique D'Eau", C.R. Acad. Sci., Paris, t262, 1224-1226.
- Faith, L.E., Bustany, S.N., Hanson, D.N. & Wilke, C.R., 1967 "Particle Precipitation by Space-Charge in Tubular Flow", I & EC Fundamentals 6, 519-526.
- Foster, W.W., 1959 "Deposition of Unipolar Aerosol Particles by Mutual Repulsion", Brit. J. Appl. Phys. 10, 206-213.

- Fuchs, N.A., 1964 The Mechanics of Aerosols, N.Y., Pergamon Press and MacMillan Co.
- Fuchs, N.A. & Sutugin, A.G., 1966 "Generation and Use of Monodisperse Aerosols", Aerosol Science, Davies, C.N., Ed., Acad. Press.
- Gillespie, T., 1960 "Electric Charge Effects in Aerosol Particle Collision Phenomena", Aerodynamic Capture of Particles, N.Y. Pergamon Press, 44-49.
- Gillespie, T., 1953 "The Effect of the Electric Charge Distribution on the Aging of an Aerosol", Proc. of the Roy. Soc., A216.
- Gott, J.P., 1933 "On the Electric Charge Collected by Water Drops Falling Through Ionized Air in a Vertical Electric Field", Proc. Roy. Soc. A142, 248.
- Green, H.L. & Lane, W.R., 1965 Particulate Clouds -- Dusts, Smokes and Mists, London, E. and F.N. Spon Ltd., 42, 98.
- Gumprecht, R.O. & Sliepcevich, C.M., 1951 "Tables of Light-Scattering Functions for Spherical Particles", Special Publication, Tables, Ann Arbor, Michigan, Univ. of Michigan, Engineering Research Institute.
- Gunn, R., 1957 "The Electrification of Precipitation and Thunderstorms", Proc. of I.R.E., 1331-1358.
- Hanson, D.N. & Wilke, C.R., 1969 "Electrostatic Precipitator Analysis", I & EC Process Design and Development 8, 357-364.
- Harper, W.R., 1932 "On the Theory of the Recombination of Ions in Gases at High Pressures", Proc. Cambridge Phil Soc. 28, 219-233.
- Heller, W. & Tabibian, R., 1962 "Experimental Investigations on the Light Scattering of Colloidal Spheres. IV. Scattering Ratio", J. Phys. Chem. 66, 2059-2065.
- Herold, L., 1967 "Traveling-Wave Charged Particle Generation", M.S. Thesis, Dept. Electrical Engineering, M.I.T., Cambridge, MA.
- Hewitt, G.W., 1957 "The Charging of Small Particles for Electrostatic Precipitation", Trans. AIEE, 300-306.
- Hidy, G.M. & Brack, J.R., 1970 The Dynamics of Aerocolloidal Systems, 1, N.Y., Pergamon Press, 171, 300.
- Hurd, F.K. & Mullins, J.C., 1962 "Aerosol Size Distribution from Ion Mobility", J. Colloid Sci. 17, 91-100.
- Joubert, J., Henry, C. & Eyraud, C., 1964 "Étude des Trajectoires des Particules Sub-microniques dan les Champs Ionisés", Le J. de Phys. Appliqués,

Supplément An. #3, 25, 67A-72A.

Kitani, S., 1960 "Measurement of Particle Sizes by Higher Order Tyndall Spectra ( $\theta$ , Method)", J. Colloid Sci. 15, 287-293.

Kraemer, H.F. & Johnstone, H.F., 1955 "Collection of Aerosol Particles in Presence of Electrostatic Fields", Indus. and Eng. Chem. 47, 2426-2434.

Kunkel, W.B., 1950 "Charge Distribution in Coarse Aerosols as a Function of Time", J. App. Phys. 21, 833-837.

LaMer, V.K., Inn, E.C.Y. & Wilson, I.B., 1950 "The Methods of Forming, Detecting and Measuring the Size and Concentration of Liquid Aerosols in the Size Range of 0.01 to 0.25 Microns in Diameter", J. Colloid. Sci. 5, 471-496.

LaMer, V.K. & Sinclair, D., August 3, 1943 "A Portable Optical Instrument for the Measurement of Particle Sizes in Smokes, the "Owl"; and an Improved Homogeneous Aerosol Generator", OSRD Report No. 1668.

Langer, G., Pierrard, J. & Yamate, G., 1964 "Further Development of an Electrostatic Classifier for Submicron Airborne Particles", Intern. J. Air Water Poll. 8, 167-176.

Levich, V.G., 1962 Physicochemical Hydrodynamics, N.J., Prentice-Hall.

Liu, B.Y.H., Whitby, K.T. & Yu, H.H.S., 1966 "Condensation Aerosol Generator for Producing Monodispersed Aerosols in the Size Range 0.036 $\mu$  to 1.3 $\mu$ ", J. Recherches Atmospheriques 2, 397-406.

Lothian, G.F. & Chappel, F.P., 1951 "The Transmission of Light Through Suspensions", J. Appl. Chem. 1, 475-482.

Marks, A.M., 1971 "Charged Aerosols for Air Purification and Other Uses", paper presented at Symposium on Useful Electrical Field-Induced Phenomena in Physical and Chemical Operations, 69th National AIChE Meeting, Cincinnati, Ohio.

Maron, S.H., Elder, M.E. & Pierce, P.E., 1963 "Determination of Latex Size by Light Scattering V. Polarization Ratio at 90°", J. Colloid, and Interface Sci. 18, 107-118.

McCully, C.R. et al., 1956 "Scavenging Action of Rain on Air-borne Particulate Matter", Indus. and Eng. Chem. 48, #9, 1512-1516.

McDaniel, E.W., 1964 Collision Phenomena in Ionized Gases, N.Y., John Wiley and Sons, 693-700.

Melcher, J.R., 1963 Field Coupled Surface Waves, Cambridge, Massachusetts, The M.I.T. Press, 123.

- Melcher, J.R. & Woodson, H.H., 1968 Electromechanical Dynamics: Part II, Fields, Forces, and Motions, N.Y., John Wiley & Sons, 370.
- Müller, H., 1928 "Zur Theorie der Elektrischer Ladung und der Koagulation der Kolloide", Kolloidchemische Beihefte, 26, 257-311, 177.
- Natusch, D.R.S., January 15-18, 1974 "The Chemical Composition of Fly Ash", Proc. of Symposium on Control of Fine-Particulate Emissions from Industrial Sources, Environ. Prot. Agency.
- Nicolaon, G., Cooke, D.D., Dans, E.J., Kerker, M. & Matijevic, E., 1971 "A New Liquid Aerosol Generator, II: The Effect of Reheating and Studies on the Condensation Zone", J. Colloid and Interface Sci. 35, 490-501.
- Oglesby, S.J. et al., 1970 "A Manual of Electrostatic Precipitator Technology, Part I - Fundamentals", Report PB 196380, National Air Pollution Control Adm., 317.
- Overbeek, J. Th. G., 1952 "Kinetics of Flocculation", in Colloid Science, H.R. Kruyt, Ed., N.Y., Elsevier Pub. Co.
- Paluch, I.R., 1970 "Theoretical Collision Efficiencies of Charged Cloud Droplets", J. Geophys. Res. 75, #9, 1633-1640.
- Pauthenier, M.M. & Moreau-Hanot, M., 1932 "La Charge des Particules Spheriques Dans un Champ Ionisé", J. de Physique et le Radium, 3, 590-613.
- Penney, Gaylord, W., 1944 "Electrified Liquid Spray Dust Precipitators", U.S. Patent No. 2,357,354.
- Pilat, M.J., Jaasund, S.A. & Sparks, L.E., 1974 "Collection of Aerosol Particles by Electrostatic Droplet Spray Scrubbers", Environmental Sci. and Tech. 8, 360-362.
- Rapaport, E. & Weinstock, S.E., 1955 "A Generator for Homogeneous Aerosols", Experientia 9, 363-364.
- Rayleigh, Lord, 1882 "On the Equilibrium of Liquid Conducting Masses Charged with Electricity", Phil. Magazine 14, 184-186.
- Rouse, H., 1957 Elementary Mechanics of Fluids, N.Y., John Wiley & Sons.
- Sargent, G.D., 1969 "Dust Collection Equipment", Chemical Engineering.
- Sartor, J.D., 1960 "Some Electrostatic Cloud-Droplet Collision Efficiencies", J. Geophys. Res., 65, #7, 1953-1957.
- Schlichting, H., 1960 Boundary Layer Theory, N.Y., McGraw Hill Book Co., Inc., 231.

- Semonin, R.G. & Plumlee, H.R., 1966 "Collision Efficiency of Charged Cloud Droplets in Electric Fields", J. Geophys. Res. 71, #18, 4271-4278.
- Sinclair, D & LaMer, V.K., 1949 "Light Scattering as a Measure of Particle Sizes in Aerosols -- The Production of Monodisperse Aerosols", Chem. Rev. 44, 245-267.
- Smirnov, L.P. & Deryagin, B.V., 1967 "Inertialess Electrostatic Deposition of Aerosol Particles on a Sphere Surrounded by a Viscous Stream", Kolloidnyi Zhurnal 29, #3, 400-412.
- Sparks, L.E., 1971 "The Effect of Scrubber Operating and Design Parameters on the Collection of Particulate Air Pollutants", Ph.D. Dissertation, Univ. of Washington, Seattle, Wash.
- Tammet, H.F., 1970 The Aspiration Method for the Determination of Atmospheric-Ion Spectra, Israel Program for Scientific Translations, 32.
- Taylor, G.I., 1964 "Disintegration of Water Drops in an Electric Field", Proc. Roy. Soc., London, A280, 383-397.
- Thomson, J.J. & Thomson, G.P., 1969 Conduction of Electricity Through Gases, Vol. 1, N.Y., Dover Pub., 47.
- Tomaides, M., Liu, B.Y.H. & Whitby, K.T., 1971 "Evaluation of the Condensation Aerosol Generator for Producing Monodispersed Aerosols", Aerosol Science 2, 39-46.
- Van De Hulst, H.C., 1962 Light Scattering by Small Particles, N.Y., John Wiley & Sons.
- Walton, W.H. & Woolcock, A., 1960 "The Suppression of Airborne Dust by Water Spray", Int. Jrl. Air Poll. 3 129-153.
- Whipple, F.J.W. & Chalmers, J.A., 1944 "On Wilson's Theory of the Collection of Charge by Falling Drops", Quart. J. of the Roy. Met. Soc. 70, 103-119.
- Whitby, K.T. & Liu, B.Y.H., 1966 "The Electrical Behavior of Aerosols", Chap. III in Aerosol Science, ed. by Davies, C.N., N.Y., Academic Press.
- White, H.J., 1963 Industrial Electrostatic Precipitation, Reading, MA, Addison-Wesley Pub. Co., Chs. 5 & 6.
- Zahedi, K., 1974 "Measurement of Particle Size by Higher Order Tyndall Spectra", S.B. Thesis, M.I.T. Cambridge, MA.
- Zahedi, K. & Melcher, J.R., 1974 "Progress Report Electrostatically Induced Agglomeration Processes in the Control of Oil Ash Particulate" Report to Consolidated Edison Corp., N.Y., Contract # 2-44-090.
- Zebel, G., 1968 "Capture of Small Particles by Drops Falling in Electric Fields", J. Colloid & Interface Science 27, #2, 294-304.

## GLOSSARY OF SYMBOLS

$A$	gas flow cross-section
$A_b$	light beam area
$A_o$	radius of sphere of influence beyond which turbulent diffusion dominates electrical attraction
$A_p$	probe area
$A_{syst}$	overall cross-sectional area of device
$a$	radius of particle to be collected
$a_{db}$	Debye length
$a_o$	radius of sphere of influence beyond which diffusion dominates electrical attraction
$B$	drop mobility
$B'$	see Eq. (6.4.13)
$b, b_+, b_-$	particle mobility
$b_i$	ion mobility
$\underline{C}$	defined following Eq. (11) of Sec. 5.3.1
$C'$	see Eq. (6.4.13)
$C_a, C_b, C_m$	charging capacitances (see Eq. (17) of Sec. 5.4.2)
$C_c$	coefficient of contraction
$C_D$	coefficient of discharge
$c$	jet radius
$D$	defined with Eq. (22) of Sec. 4.3.2
$D_B, D_+, D_-$	Brownian diffusion coefficient
$D_T$	large scale turbulent diffusion coefficient
$D_t$	fine scale turbulent diffusion coefficient
$d$	spacing of drop sheet and charging bar



$d_o$	orifice diameter
$E_c$	charging electric field intensity
$E_o$	ambient electric field intensity
$\bar{E}_s, \bar{E}_o$	incident and scattered optical electric field intensity
$\bar{E}_T$	electric field intensity transverse to flow direction
$E_{tay}$	Taylor limit on electric field that an uncharged drop can sustain
$E_w$	electric field intensity at electrode or wall
$e$	$1.6 \times 10^{-19}$ coulomb (electronic charge)
$F$	volume rate of flow of gas
$F_{dilution}$	volume rate of flow of gas leakage
$F_1, F_2$	gas volume rates of flow in central and return sections
$F_{in}, F_{out}$	volume rates of flow into and out of device
$f$	frequency
$f_c$	frequency beyond which liquid jet is stable
$f_m$	frequency of maximum growth-rate on liquid jet
$G_+, G_-$	rate of particle collection by single particle
$h$	spacing of jets within drop sheet
$I_{\pm}$	see Eq. (2) of Sec. 6.2.1
$I, I_1, I_2$	light intensity
$I_p$	electrical drop current
$I_{sat}$	saturation current
$i, i_1, i_2$	electrical current
$j$	$\sqrt{-1}$
$K_s$	inertial impact parameter
$k$	Boltzman coefficient, $1.381 \times 10^{-23}$ m-nt/deg C
$k$	optical wave number $2\pi/\lambda_{\ell}$

$L$	length
$l$	length
$l_a$	particle self-precipitation length
$l_a$	particle self-discharge length
$l_R$	drop self-precipitation length
$l_T$	turbulent diffusion length for drops
$l_T$	large scale eddy size
$l_1$	Brownian diffusion length
$M$	total drop mass
$m$	mass
$N$	number density of drops
$n$	number density of particles
$n_i$	ion density
$n_{in}$	inlet particle density
$n'_{IN}$	effective particle density into device
$n_\ell$	index of refraction
$n_o$	initial particle density
$n_{out}$	outlet particle density
$Q_a, Q_b$	drop charge
$Q_c$	saturation charge by ion impact
$Q_d$	see Eq. (9) of Sec. 6.4
$Q_{opt}$	drop charge for achieving optimum efficiency
$Q_R$	see Eq. (15) of Sec. 5.5.3
$Q_{Ray}$	Rayleigh limit on charge of an isolated drop
$Q_{1/2}$	charge on hemisphere of polarized collection site
$q, q_+, q_-$	ion or particle charge
$R$	radius of drop
$R_y$	Reynolds number

$r$	radial position coordinate
$\bar{r}$	position of particle
$r_o$	mean spacing of particles
$S$	precipitation perimeter
$S_1, S_2$	scattering functions
$s$	electrode spacing
$T$	absolute temperature
$t$	time
$U$	mean gas velocity
$U_{g1}, U_{g2}$	mean gas flow in central and return sections of multi-pass system
$U_s$	jet velocity
$u_1( )$	step function, having value 0 and 1 for argument negative and positive respectively
$V$	applied voltage
$V$	active volume of collection device
$V_D$	voltage of charger bars
$V_{sat}$	voltage at which analyzer current saturates
$\bar{V}$	gas velocity
$v_a, v_b$	charging bar voltages
$w$	width of interaction volume
$w$	relative gas velocity
$w_o$	ambient relative gas velocity
$x$	coordinate
$y$	radius of collection cross-section
$z$	position coordinate
$z_d$	growth distance for laminar boundary layer

$\alpha$	mean distance between centers of spherical particles on drops normalized to particle or drop radius
$\alpha_\ell$	particle circumference normalized to wavelength of light
$\bar{\Gamma}$	particle current density
$\Gamma_E$	electrically induced particle flux
$\Gamma_T$	turbulent particle flux
$\gamma$	surface tension
$\gamma, \gamma_0$	total particle flux
$\gamma_T$	large-scale turbulent energy dissipation density
$\Delta U$	large-scale turbulent fluctuation velocity
$\delta$	spacial growth rate of sausage instability on liquid jet
$\delta_c$	see Eq. (6) of Sec. 5.4.2
$\epsilon$	permittivity
$\epsilon_0$	$8.854 \times 10^{-12}$ farads/meter
$\eta$	gas viscosity
$\eta_1, \eta_2$	single pass particle collection ratios
$\eta_c$	gas viscosity corrected by Cunningham factor
$\eta_s$	water viscosity
$\theta_c$	critical angle for charging (see Eq. (17) of Sec. 6.2.1)
$\theta_d$	acceptance angle of optical detector
$\theta_{red}$	angle of observation for red Tyndall spectra
$\lambda$	mean free path
$\lambda_d$	wavelength of charge-wave on drops
$\lambda_\ell, \lambda_r, \lambda_g$	wavelength of light
$\lambda_s$	wavelength of jet instability
$\xi$	relative distance between particles and drops
$\xi_a, \xi_R$	absolute positions of particles and drops

$\xi_0$	initial spacing of particles and drops
$\rho$	mass density of gas
$\rho_{\pm}$	particle charge densities
$\rho_a$	mass density of particle to be collected
$\rho_R$	mass density of drop
$\rho_s$	liquid jet mass density
$\Sigma$	"stream-function" for solenoidal electric field intensity
$\sigma$	ohmic electrical conductivity
$\tau$	collision time (general)
$\tau_a$	self-discharge on self-precipitation time of particles
$\tau_{bc}$	characteristic time for collection by particles polarized by ambient electric field (bed particles)
$\tau_c$	collection time of particles on oppositely charged drops or time for precipitation of particles due to space charge of drops
$\tau_{dc}$	typical particle collection time due to Brownian diffusion
$\tau_{EH}$	characteristic time for instability of drop sheet
$\tau_{pc}$	characteristic time for collection in electrostatic precipitator
$\tau_R$	drop self-discharge or self-precipitation time
$\tau_{Re}$	liquid charge relaxation time
$\tau_{res}$	average residence time of gas
$\tau_{sc}$	characteristic time for inertial impact scrubbing
$\tau_{sR}$	drop scrubbing lifetime
$\tau_T$	turbulent eddy characteristic time
$\tau_t$	fine scale turbulent diffusion time
$\phi, \theta$	angular coordinate
$\phi_+, \phi_-$	rate of particle collection per unit volume
$\Psi$	stream function for gas flow
$\omega$	angular frequency

**TECHNICAL REPORT DATA**  
(Please read instructions on the reverse before completing)

1. REPORT NO. <b>EPA-650/2-74-075</b>		2.		3. RECIPIENT'S ACCESSION NO.	
4. TITLE AND SUBTITLE <b>Charged Droplet Scrubbing of Submicron Particulate</b>				5. REPORT DATE <b>August 1974</b>	
				6. PERFORMING ORGANIZATION CODE	
7. AUTHOR(S) <b>J. R. Melcher and K. S. Sachar</b>				8. PERFORMING ORGANIZATION REPORT NO.	
9. PERFORMING ORGANIZATION NAME AND ADDRESS <b>Massachusetts Institute of Technology Department of Electrical Engineering Cambridge, Massachusetts 02139</b>				10. PROGRAM ELEMENT NO. <b>1AB012; ROAP 21ADL-003</b>	
				11. CONTRACT/GRANT NO. <b>68-02-0250</b>	
12. SPONSORING AGENCY NAME AND ADDRESS <b>EPA, Office of Research and Development NERC-RTP, Control Systems Laboratory Research Triangle Park, NC 27711</b>				13. TYPE OF REPORT AND PERIOD COVERED <b>Final</b>	
				14. SPONSORING AGENCY CODE	
15. SUPPLEMENTARY NOTES					
16. ABSTRACT The report gives results of an investigation of the collection of charged submicron particles, through a sequence of interrelated experiments and theoretical models: by oppositely charged supermicron drops; by bicharged drops; and by drops charged to the same polarity as the particles. It provides experimentally verified laws of collection for a system with different effective drop and gas residence times. The report shows, experimentally and through theoretical models, that all three of the above configurations have the same collection characteristics. Charging of the drops in any of these cases: results in dramatically improved efficiency, compared to inertial scrubbers; and approaches the efficiency of high-efficiency electrostatic precipitators. For example, in experiments typical of each configuration, inertial scrubbing by 50 $\mu$ m water drops of 0.6 $\mu$ m DOP aerosol particles gives 25% efficiency; self-precipitation of the particles with charging (but without charging of the drops) results in 85-87% efficiency; and drop and particle charging (regardless of configuration) results in 92-95% efficiency. Charged-drop scrubbers and precipitators have the operating cost and capital investment profiles of wet scrubbers, and submicron particle removal efficiencies approaching those of high-efficiency electrostatic precipitators.					
17. KEY WORDS AND DOCUMENT ANALYSIS					
a. DESCRIPTORS		b. IDENTIFIERS/OPEN ENDED TERMS		c. COSATI Field/Group	
Air Pollution Scrubbers Washing Charging Drops (Liquids) Experimentation		Mathematical Models Electrostatic Precipitators		Air Pollution Control Stationary Sources Charged Droplets Submicron Inertial Scrubbers Particulate	
				13B, 12A 07A 13H  07D 14B	
18. DISTRIBUTION STATEMENT  <b>Unlimited</b>		19. SECURITY CLASS (This Report) <b>Unclassified</b>		21. NO. OF PAGES <b>258</b>	
		20. SECURITY CLASS (This page) <b>Unclassified</b>		22. PRICE	